


November 2017

# POLYORGANOSILOXANES: MOLECULAR NANOPARTICLES, NANOCOMPOSITES AND INTERFACES

Daniel H. Flagg

Follow this and additional works at: [https://scholarworks.umass.edu/dissertations\\_2](https://scholarworks.umass.edu/dissertations_2)

 Part of the [Materials Chemistry Commons](#), [Polymer and Organic Materials Commons](#), and the [Polymer Chemistry Commons](#)

---

## Recommended Citation

Flagg, Daniel H., "POLYORGANOSILOXANES: MOLECULAR NANOPARTICLES, NANOCOMPOSITES AND INTERFACES" (2017). *Doctoral Dissertations*. 1080.  
[https://scholarworks.umass.edu/dissertations\\_2/1080](https://scholarworks.umass.edu/dissertations_2/1080)

This Open Access Dissertation is brought to you for free and open access by the Dissertations and Theses at ScholarWorks@UMass Amherst. It has been accepted for inclusion in Doctoral Dissertations by an authorized administrator of ScholarWorks@UMass Amherst. For more information, please contact [scholarworks@library.umass.edu](mailto:scholarworks@library.umass.edu).

**POLYORGANOSILOXANES: MOLECULAR NANOPARTICLES, NANOCOMPOSITES  
AND INTERFACES**

A Dissertation Presented

by

Daniel H. Flagg

Submitted to the Graduate School of the  
University of Massachusetts in partial fulfillment  
of the degree requirements for the degree of

DOCTOR OF PHILOSOPHY

September 2017

Polymer Science and Engineering

© Copyright by Daniel H. Flagg 2017

All Rights Reserved

**POLYORGANOSILOXANES: MOLECULAR NANOPARTICLES, NANOCOMPOSITES  
AND INTERFACES**

A Dissertation Presented

by

Daniel H. Flagg

Approved as to style and content by:

---

Thomas J. McCarthy, Chair

---

E. Bryan Coughlin, Member

---

John Klier, Member

---

E. Bryan Coughlin, Head, PS&E

To John Null

## ACKNOWLEDGEMENTS

There are countless individuals that I need to thank and acknowledge for getting me to where I am today. I could not have done it alone and would be a much different person if it were not for the support of my advisors, friends and family. Above all, I thank God for the blessings and direction he has provided me.

My academic career would not exist had it not been for numerous advisors along the way. Dr. Joseph Freeman (Virginia Tech), Dr. Tim Vance (Michelin), Dr. Steph Nesbitt (Michelin) and Dr. Doug Holmes (Virginia Tech). These are the people responsible for my pursuit of a doctoral degree.

There is too much to say about my experience with Dr. Tom McCarthy. He has been one of the best advisors I could ask for. Tom was always supportive and granted me the freedom to do the work that I wanted. Tom has not only been a great academic advisor but he has been an example of a great mentor and group leader. This is especially apparent in the relationships between Tom and group alumni. I must thank the past McCarthy group members for laying the foundation of the group culture and research. My coworkers in the McCarthy group (Yan Wang, Liming Wang, Minchao Zhang, Shota Fujii, Pei Bain, Ting Dong, and Yan Cong) have been an important part of my time with the group. Our discussions and collaboration were an important part of my work at UMass.

My committee, Dr. Bryan Coughlin and Dr. John Klier, were always available regardless of their busy schedules. They provided a different perspective and had valuable insights not only with my work but also in my job search. I want to thank them specifically for our discussions and their mentorship concerning career paths in industrial research and development.

Without the help of the Polymer Science and Engineering facilities and scientist my work could not have been done. Dr. Ribbe, Dr. Weiguo, Dr. Waldman, Jack Hirsch and

Dr. Eyles made sure that their facilities were always operating smoothly and provided expert training and advice. Students in PSE are also responsible for keeping facilities running and without Nick Posey (GPC), Rachel Letteri (GPC), Connor Evans (Thermal Lab), Brian Cromer (Rheometer), Steven Strassburg (Brookhaven LS) and many others, productive work in Conte would come to a halt. The PSE staff made my life much less complicated by taking care of all the administrative challenges. Lisa Groth, Lisa McNamara, Maria, Jessica and Alyssa all make sure that the students in PSE can focus on research.

Outside of PSE, I must thank Nanocomp Technologies Inc, Gelest and McMaster University. Trips and discussions at Nanocomp always inspired new work and stimulated new ideas. Without Gelest, my life as a silicone chemist would have been much more synthetically challenging and labor intensive. Not only do they provide thousands of silanes and silicones, but they also opened their doors to me so that I could make some special silicones in their labs. Barry, Jonathan, Annalesse, Ferdinand, Santi and Max were great friends and resources in the small world of silicone chemists. Dr. Mike Brook at McMaster University also opened his doors to me so that I could learn from his group's expertise. One week in his labs working with his students taught me how to run reactions using tris(pentafluorophenyl)borane. Mike is a great mentor and his group was a great host.

The friends and coworkers within PSE are too many to list. Whether it be discussions of science or time spent having fun outside of work, my relationships within PSE were a fundamental part of my time at UMass. Life in Amherst would not have been the same without my climbing friends, my lifting buddies and the Easthampton Barbell Club. I have to thank Pioneer Valley Crossfit for allowing me to coach weightlifting. Coaching provided communication and teaching skills that have been a huge part of my graduate career. Having things to do outside of work and having a diverse group of friends

enabled me to balance my life and appreciate that there is more to life than work. I must thank all my coaches (Coach Cannon, Coach Morris and Coach Rogers to name a few) for teaching me about hard work and perseverance.

Leah Hollrock has been especially important in helping me achieve balance and fulfillment outside of work. She has given me an appreciation for time spent exploring, trying new things and travelling to new places. Her enjoyment of the moment and sense of beauty in the world inspires me. I cannot thank her enough for putting up with me.

Last, I want to thank my family. My Mom (Mary Beth) and Dad (Rod) have been supportive of anything I have set off to do. They have shown me the importance of showing up early, working hard, taking pride in your work and being humble. They also demonstrate the importance of balance in life, work and family. My Brother (John) has been instrumental in my development into a man. I learned many lessons from him and am forever grateful. My family has always had my back and I am thankful for their love and honesty. Of course, my grandparents are responsible for who I am as well, and I have to specifically thank John and Marcella Null. I spent days as a child in John's woodshop or in Marcella's kitchen. It was there that I learned to "measure twice, cut once," that you can't push a rope and how to bake (which is basically chemistry).

There are too many people that I need to thank that have helped me become the scientist, weightlifter, climber and man that I am today, but at least that is a start.

"For from him and through him and for him are all things.

To him be the glory forever! Amen."

-Romans 11:36



## ABSTRACT

### **POLYORGANOSILOXANES: MOLECULAR NANOPARTICLES, NANOCOMPOSITES AND INTERFACES**

SEPTEMBER 2017

DANIEL H. FLAGG

B.S., VIRGINIA POLYTECHNIC INSTITUTE AND STATE UNIVERSITY

M.S., UNIVERSITY OF MASSACHUSETTS AMHERST

Ph.D., UNIVERSITY OF MASSACHUSETTS AMHERST

Directed by: Professor Thomas J. McCarthy

This dissertation presents research performed in the field of siloxane polymer science. Three research topics will be explored in five projects. The first topic involves the synthesis and interfacial activity of trimethylsiloxysilicate (MQ) copolymers. The second topic encompasses the fabrication and characterization of Silicone - Carbon Nanotube (CNT) composites. The last topic examines the modification of silica surfaces using tris(pentafluorophenyl)borane to catalyze the condensation of silanes and silanols, with a particular focus on the preparation and study of water-repellant siloxane polymer grafts.

The first chapter provides the reader a general introduction to silicones and their history. This chapter describes the invention of silicones and the properties of silicone polymers that sets them apart from carbon-based polymers. A general background on silicone chemistry and applications is provided. Characterization methods are discussed with particular attention paid to measurements of interfaces, an area where siloxane materials demonstrate remarkable performance.

Five research projects are then described. First, a reproducible, lab-scale synthesis of MQ silicone copolymers is presented. MQ copolymers are commercially important materials that have been ignored by the academic community. One possible reason for this is the difficulty of controlling and reproducing the preparative

copolymerizations that have been reported. A reproducible method for lab-scale preparation was developed that controls molecular weight by splitting the copolymerization into the discrete steps of sol growth from silicate precursor and end-capping by trimethylsiloxy groups. Characterization of MQ products implicates that they are composed of highly condensed, polycyclic structures.

The MQ copolymers prepared in the first project were observed to form tenacious emulsions and foams. This was an obvious indication of surface activity and led to further investigation. No open literature reports any measurements of MQ copolymers at interfaces. In this second project, selected MQ structures were studied at three interfaces: the air-water interface, the oil-water interface and the solid-air interface of supported MQ monolayers. The qualitative surface activity of MQ is confirmed and quantified. Residual silanols are found to be responsible for surfactancy in MQ copolymers.

The third and fourth projects encompass research in Silicone-CNT composites. The first part of this work describes the ease with which CNTs can be dispersed into silicone matrices. Changes in silicone chemistry can improve CNT dispersion resulting in improved conductivities and mechanical reinforcement at CNT loadings of only fractions of a weight percent. The second portion of work on nanocomposites involves the discovery and investigation of the dramatic increase in thermal stability of silicone elastomers containing CNTs. Thermogravimetric analysis and pyrolysis gas chromatography-mass spectrometry indicate that the CNT network constrains silicone polymer chains and alters the mechanisms of decomposition.

The last project uses the Piers-Rubinsztajn reaction to rapidly and cleanly modify silicon oxide surfaces. This reaction has been studied very little as a method to modify surfaces and there has yet to be any work that measures dynamic contact angles on smooth surfaces. Trialkylsilane and methylsiloxane monolayers were prepared and analyzed. Monolayer densities are low in this reaction and result in anomalously low

contact angle hysteresis for alkylsilane monolayers. Wetting properties in precise methylsiloxane polymer monolayers are shown to depend on graft structure. Dynamic contact lines from the liquid-like mobility of these grafts results in low contact angle hysteresis.

Lastly, conclusions are made regarding the future directions of silicone polymer science in the McCarthy group. Work on 'rediscovering' silicones has been insightful and informative. It is now time to move onto 'discovering' silicones.

## TABLE OF CONTENTS

	Page
ACKNOWLEDGEMENTS.....	iv
ABSTRACT.....	vii
LIST OF TABLES.....	xv
LIST OF FIGURES.....	xvii
CHAPTER	
1. SILICON, SILICA AND SILICONES.....	1
1.1. Silicon: The Element.....	1
1.2. Silica and Silicates: The oxides.....	3
1.3. Silicones: Organosiloxane Polymers.....	5
1.4. General Properties, Chemistry and Structure of Siloxane Polymers.....	10
1.5. Ignorance of Silicones.....	14
1.6. Important Reactions in Organosiloxane Polymer Science.....	15
1.6.1. Hydrolysis and Condensation.....	16
1.6.2. Ring Opening Polymerization.....	17
1.6.3. Pt-Catalyzed Hydrosilylation.....	19
1.6.4. Piers-Rubinsztajn.....	20
1.7. Silicones at Interfaces.....	22
1.7.1. PDMS at the Air-Water Interface.....	23
1.7.2. Silicone Surfactants at the Oil-Water Interface.....	26
1.7.3. Silane and Siloxane Monolayers: Wetting and Contact Angle Hysteresis.....	28
1.8. Rediscovering and Discovering Silicones.....	32
1.9. References.....	32
2. SYNTHESIS AND CHEMISTRY OF MQ COPOLYMERS.....	39

2.1. Introduction.....	39
2.1.1. Background.....	39
2.1.2. Objective.....	43
2.2. Experimental Section.....	44
2.2.1. Reagents.....	44
2.2.2. Preparation of MQ Silicone.....	44
2.2.3. Chemical Modifications of MQ Copolymers.....	48
2.2.4. Characterization.....	50
2.3. Results and Discussion.....	53
2.3.1. MQ Copolymer Synthesis.....	53
2.3.2. MQ Copolymer Characterization.....	64
2.3.3. MQ Copolymer Structure.....	71
2.3.4. MQ Copolymer Chemical Modification.....	78
2.4. Conclusions and Comments.....	83
2.5. References.....	83
3. SURFACE ACTIVITY IN MQ SILICONES.....	88
3.1. Introduction.....	88
3.1.1. Background.....	88
3.1.2. Objective.....	90
3.2. Experimental Section.....	91
3.2.1. Materials.....	91
3.2.2. Pendant Drop Tensiometry.....	91
3.2.3. Langmuir Monolayers and Blodgett Depositions.....	92
3.2.4. Surface Adsorption.....	93
3.3. Results and Discussion.....	93
3.3.1. MQ Copolymers at the Oil-Water Interface.....	94

3.3.2. MQ Copolymers at the Air-Water interface.....	98
3.3.3. MQ Copolymer surfaces.....	102
3.4. Conclusions.....	104
3.5. References.....	105
4. SILICONE-CARBON NANOTUBE COMPOSITES: TUNING DISPERSION AND PROPERTY WITH POLYSILOXANE BACKBONE CHEMISTRY.....	110
4.1. Introduction.....	110
4.1.1. Carbon Nanotubes.....	110
4.1.2. Challenges facing CNT polymer nanocomposites.....	111
4.1.3. Nanocomp Technologies, Inc.....	113
4.1.4. Siloxane-Carbon Nanotube Polymer Nanocomposites.....	115
4.1.5. Objective.....	116
4.2. Experimental Section.....	117
4.2.1. Materials and Abbreviations.....	117
4.2.2. Sample Preparation.....	118
4.2.3. Characterization.....	118
4.3. Results and Discussion.....	120
4.3.1. Polydimethylsiloxane ( $D_n$ ).....	120
4.3.2. Effect of siloxane polymer chemistry on CNT dispersion.....	127
4.3.3. Conductivity in Silicone-CNT Elastomer Composites.....	133
4.4. Conclusions.....	134
4.5. References.....	135
5. SILICONE-CARBON NANOTUBE COMPOSITES: THERMAL STABILITY ENHANCEMENTS AND DECOMPOSITION MECHANISM.....	139
5.1. Introduction.....	139
5.1.1. Background.....	139

5.1.2. Objective.....	141
5.2. Experimental Section.....	141
5.2.1. Materials.....	141
5.2.2. Sample Preparation.....	142
5.2.3. Characterization.....	142
5.3. Results and Discussion.....	144
5.3.1. Sample preparation and dispersion of MWCNTs in PDMS.....	144
5.3.2. Thermogravimetric Analysis.....	147
5.3.3. Pyrolysis Combustion Flow Calorimetry.....	152
5.3.4. Differential Scanning Calorimetry of Elastomer Composites.....	153
5.3.5. Decomposition Products in Elastomer Composites.....	155
5.3.6. Decomposition in Linear PDMS Models.....	156
5.3.7. Proposed Mechanism of Thermal Decomposition in PDMS-CNT Composites.....	158
5.3.8. Are Nanocomp CNTs Unique?.....	161
5.3.9. Is the Thermal Stabilization by CNTs Universal to All Silicones?.....	162
5.4. Conclusions.....	164
5.5. References.....	165
6. RAPID AND CLEAN COVALENT ATTACHMENT OF METHYLSILOXANE POLYMERS AND OLIGOMERS TO SILICA USING $B(C_6F_5)_3$ CATALYSIS.....	169
6.1. Introduction.....	169
6.1.1. Background.....	169
6.1.2. Objectives.....	175
6.2. Experimental Section.....	175
6.2.1. Materials.....	175
6.2.2. General Reaction Information.....	176

6.2.3. Characterization.....	178
6.3. Results and Discussion.....	178
6.3.1. Alkylsilane Monolayers.....	179
6.3.2. Model Methylsiloxane Monolayers.....	184
6.3.3. Covalently Attached Polymeric Methylsiloxane Monolayers.....	191
6.3.4. Mechanism of BCF Catalysis of Hydridosilanes on Silica.....	200
6.4. Conclusions.....	202
6.5. References.....	203
A6. Data Appendix.....	206
7. DISCOVERING SILICONES.....	222
7.1. MQ Silicones.....	222
7.2. Silicone-Carbon Nanotube Composites.....	225
7.3. Tris(pentafluorophenyl)borane-catalyzed modifications of silanols.....	226
7.4. Discovering Silicones.....	227
APPENDICES	
A. SULFOLANE-FUNCTIONALIZED SILICONES FOR LITHIUM ION CONDUCTION.....	228
B. CLIMBING OF SUPERHYDROPHOBIC MICROPARTICLES ON WATER WETTED SURFACES.....	244
BIBLIOGRAPHY.....	253



## LIST OF TABLES

Table	Page
1.1. Atomic Properties of Silicon, Oxygen, Carbon and Hydrogen.....	3
2.1. MQ Copolymer Molecular Weights and Compositions.....	61
2.2. Effect of H <sub>2</sub> SO <sub>4</sub> Concentration during sol growth on MQ product.....	62
2.3. Vinyl and Hydride MQ silicones.....	63
2.4. Estimated hydrodynamic radii (in nm) based on GPC, D-NMR and DLS.....	67
3.1: Molecular Weight and M:Q Ratios of MQ copolymers examined in this study.....	91
3.2 MQ surfaces prepared from Langmuir Blodgett transfer (5 mm/min, 20 mN/m) and adsorption from toluene solution (100 °C, 24 h).....	103
3.3. Surfaces prepared by solution adsorption (toluene, 100 °C, 24 h) of silanol-containing MQ (M <sub>42</sub> Q <sub>100</sub> (OH) <sub>10</sub> (OEt) <sub>1</sub> ) and trimethylsilyliodide-treated MQ (M <sub>51</sub> Q <sub>100</sub> (OH) <sub>1</sub> (OEt) <sub>1</sub> ).....	104
4.1. Surface Resistivity of Silicone-CNT Elastomers (Ω/□).....	133
5.1. Contributions of degradation processes calculated from Gaussian deconvolution for 0.5 wt% PDMS-MWCNT Composite.....	151
5.2. PCFC results for PDMS-MWCNT Composites.....	152
5.3. Glass Transition measurements from DSC of PDMS-MWCNT elastomers.....	154
5.4. DSC Glass Transition and Crystallization Data for 0.5 wt% MWCNT in PDMS Elastomer.....	154
5.5. Py GC-MS Results of Elastomers and Linear PDMS Model.....	156
6.1 Water Contact Angle and XPS Data (15° take-off angle) for Alkylsilane Monolayers (1 M Silane, anhydrous toluene, 0.5 mol% BCF).....	183
6.2. Water Contact Angle for Alkylsilane Monolayers Prepared from Chlorosilanes for Comparison.....	184
6.3. Contact Angle and Ellipsometric Thickness Values for the BCF-Catalyzed Reaction of Pentamethyldisiloxane with Si(100).....	186
6.4 Kinetics of BCF-catalyzed modification of Si(100) with D <sub>4</sub> <sup>H</sup> at indicated Si-H concentration. (toluene, 0.5 mol% BCF, room temperature).....	190
6.5. Thickness, Contact Angles and XPS (15° ToA) of Vinyltetramethyldisiloxane surfaces and derivates.....	190
6.6. Ellipsometric Thickness, Water Contact Angle and Angle-Dependent XPS Data for <sup>R</sup> MD <sub>n</sub> M <sup>H</sup> and <sup>H</sup> MD <sub>n</sub> M <sup>H</sup> - Derived Monolayers.....	192
6.7. Ellipsometric Thickness, Water Contact Angle and XPS Data for MD <sub>x</sub> D <sub>y</sub> M <sup>H</sup> - Derived Monolayers.....	199
A6.1. Pentamethyldisiloxane Kinetics- Order of Addition.....	210

A6.2. Pentamethyldisiloxane Kinetics- [BCF], 0.1 M Silane.....	210
A6.3. Pentamethyldisiloxane Kinetics- [Si-H] (0.1 mol% BCF).....	210
A6.4. Heptamethyltrisiloxane (MDM <sup>H</sup> ) Kinetics.....	211
A6.5. bis(trimethylsiloxy)methylsilane (MD <sup>H</sup> M) Kinetics.....	211
A6.6. tris(trimethylsiloxy)silane (M <sub>3</sub> T <sup>H</sup> ) Kinetics.....	211
A6.7. Heptamethylcyclotetrasiloxane (D <sub>4</sub> <sup>1H</sup> ) Kinetics.....	211
A6.8. <sup>H</sup> MD <sub>17</sub> M <sup>H</sup> (M <sub>n</sub> 1260).....	212
A6.9. <sup>Bu</sup> MD <sub>20</sub> M <sup>H</sup> (M <sub>n</sub> 1450).....	213
A6.10. Solvent effects.....	213
A6.11. Polydimethylsiloxane graft thicknesses (t) and graft density.....	214
A6.12. MD <sub>26</sub> D <sup>H</sup> <sub>1</sub> M kinetics.....	215
A6.13. MD <sub>25</sub> D <sup>H</sup> <sub>2</sub> M kinetics.....	215
A6.14. MD <sub>23</sub> D <sup>H</sup> <sub>4</sub> M kinetics.....	215
A6.15. MD <sub>18</sub> D <sup>H</sup> <sub>8</sub> M kinetics.....	216
A6.16. poly(hydridomethylsiloxane) (MD <sup>H</sup> <sub>27</sub> M) kinetics.....	216
A.1. Physical properties of sulfolane and four related, commonly used dipolar aprotic solvents.....	232

## LIST OF FIGURES

Figure	Page
1.1 SEM micrographs of silicas. (a) Silica gel used in column chromatography. (b) Fumed silica. (c) and (d) are Stöber particles of two diameters. (e) and (f) are images of a diatom shell that illustrate structural hierarchy.....	5
1.2. Rochow's methylsilicone resins. <sup>29-31</sup> His first experiments utilized Grignard preparations of methyl chloro- and bromo- silanes. Later experiments utilized methylchlorosilanes from the direct synthesis to similar effect.....	9
1.3. Structure of poly(dimethylsiloxane) (PDMS). Silicon atoms and the attached methyl groups can swing about the oxygen atom and even pass through bond angles of 180° due to the high rotational freedom of the 51% ionic siloxane bond. The longer bond lengths in comparison to carbon-based polymers spaces organic substituents further apart, aiding flexibility and rotational freedom. The electronegativity differences are responsible for many behaviors of siloxane polymers including chemical reactivity.....	11
1.4. Structural components of silicone polymers and shorthand GE nomenclature.....	14
1.5. Hydrolysis and condensation of a monofunctional silane to yield a disiloxane.....	16
1.6. Kinetic Ring Opening Polymerization of D <sub>3</sub> .....	18
1.7. Mechanism of Pt(0)-Catalyzed Hydrosilylation.....	20
1.8. Mechanism of Tris(pentafluorophenyl)borane (B(C <sub>6</sub> F <sub>5</sub> ) <sub>3</sub> ) – catalyzed siloxane bond formation between hydridosilane and alkoxy silane or silanol.....	21
1.9. PDMS at the Air-Water interface. <sup>79</sup> Each regime of the pressure-area isotherm is labeled and illustrated. At high areas, the siloxane chains diffuse freely at the water interface with methyl groups predominantly expressed at the surface. As area decreases, PDMS molecules impinge upon one another and a monolayer forms. In the monolayer, backbone oxygens adsorb to the air-water interface with one methyl oriented normal to the water surface and the other in the plane of the water surface. At a surface pressure of about 8 mN/m, the PDMS monolayer collapses by forming multi-layered structures. Further compression increases the number of collapsed layers.....	26
1.10. Drop tensiometry is one way to quantify surfactancy at oil-water interfaces. (a) An emulsion is observed during the aqueous rinse step in a work up procedure which suggests Oil-Water interface activity. (b) In a tensiometry experiment, a drop of water is suspended from a flat-tipped, cylindrical needle into an organic ambient solution which contains the surface active molecule being investigated. The drop is imaged and the profile of the drop is fitted and the Young-Laplace equation is used to calculate interfacial tension. (c) The interfacial tension is measured as a function of time. For a surface active molecule, the cartoon plot illustrates the drop in surface pressure as the molecules cover the interface to reduce interface tension. Kinetic (rate) and thermodynamic information can be gained from such experiments.....	28

1.11. Two-dimensional graphic depiction of a water drop on a surface with contact angle hysteresis. (a) The advancing contact angle of a water droplet is reached as its volume increases from the addition of water. Trace 1 shows the initial configuration of the droplet. Water condenses and the drop volume increases at constant contact area until the advancing contact angle is reached in Trace 2. As more water condenses the drop volume increases by increasing the contact area with constant contact angle (Traces 3 and 4). (b) The receding angle of a water droplet is reached as its volume decreases from the removal of water. Trace 5 shows the initial configuration of the droplet. Water evaporates and the drop volume decreases at constant contact area until the receding contact angle is reached in Trace 6. As more water evaporates the drop volume decreases by decreasing the contact area with constant contact angle (Traces 7 and 8). (c) A droplet on an inclined surface can slide when the leading edge reaches the advancing contact angle and the trailing edge reaches the receding angle.....	30
1.12. Surface <b>A</b> has no contact angle hysteresis and a drop will immediately slide off once the surface is tilted away from horizontal. Surface <b>B</b> has higher contact angles but significant hysteresis. The drop on Surface <b>B</b> will not slide off until the surface is tilted, the drop deforms, and the advancing and receding contact angles are reached.....	31
2.1. Nomenclature and examples of silicones.....	41
2.2. (a) GPC, (b) IR, (c) <sup>1</sup> H-NMR, (d) <sup>29</sup> Si-NMR, and (e) TGA data for Dow Corning MQ1600.....	55
2.3. (a) GPC, (b) IR, (c) <sup>1</sup> H-NMR, and (d) <sup>29</sup> Si-NMR data for a sample of MQ prepared using the Goodwin method.....	57
2.4. (a) GPC, (b) IR, (c) <sup>1</sup> H-NMR, and (d) <sup>29</sup> Si-NMR data for a sample of MQ prepared using the Magee method.....	57
2.5. (a) <sup>1</sup> H NMR, (b) <sup>29</sup> Si NMR and (c) IR spectra of M <sub>32</sub> Q <sub>64</sub> (top), <sup>V</sup> M <sub>28</sub> Q <sub>68</sub> (middle) and <sup>H</sup> M <sub>35</sub> Q <sub>100</sub> (bottom).....	62
2.6. (a,c) Infrared and (b,d) <sup>29</sup> Si NMR spectra of <sup>V</sup> MMQ and <sup>H</sup> MMQ silicones. Samples are names by the M functionality (hydride or vinyl) and the mol% of the functional M incorporated into the reaction.....	63
2.7. (a) <sup>1</sup> H and (b) <sup>29</sup> Si NMR of M <sub>32</sub> Q <sub>64</sub> . (c) IR and (d) <sup>29</sup> Si NMR Q region of M <sub>41</sub> Q <sub>100</sub> before (top) and after (bottom) reaction with trimethylsilyl iodide.....	65
2.8. GPC chromatographs of preparative samples and commercial MQ copolymers.....	67

2.9. (a) DLS correlation function of M <sub>32</sub> Q <sub>64</sub> in <i>o</i> -xylene at 15° with inset of correlation functions at increasing angles. The red line is a single exponential fit to the black data points. (b) DLS correlation function of M <sub>66</sub> Q <sub>164</sub> in <i>o</i> -xylene at 30° with inset of correlation functions at increased angle. The red line is a single exponential fit to the black data points. Diffusion coefficients for the MQ copolymers were determined by the linear fit of decay constants ( $\Gamma$ ) plotted against the square of the scattering vector ( $q^2$ ). (c) D-NMR diffusion decays for M <sub>17</sub> Q <sub>15</sub> (orange), M <sub>17</sub> Q <sub>29</sub> (blue), M <sub>32</sub> Q <sub>64</sub> (black) and M <sub>66</sub> Q <sub>164</sub> (red) in <i>d</i> -chloroform. For diffusion coefficients determined by DLS and D-NMR, the Stokes-Einstein relationship was used to estimate the hydrodynamic radius.....	68
2.10. Dark field TEM micrographs of M <sub>32</sub> Q <sub>64</sub> sample. Scale bar is 50 nm. (Image courtesy Dr. Alex Ribbe).....	70
2.11. TGA decomposition profiles of MQ copolymers under nitrogen.....	71
2.12. MQ copolymer structures.....	75
2.13. Formation of polycyclic structures during sol growth.....	77
2.14. Condensation of silanol residues on M <sub>14</sub> Q <sub>29</sub> using divinyltetramethyldisilazane. (a) <sup>1</sup> H NMR and (b) IR show incorporation of vinyl groups and loss of silanols.....	79
2.15. B(C <sub>6</sub> F <sub>5</sub> ) <sub>3</sub> -catalyzed condensation of residual silanols on MQ with pentamethyldisiloxane. (a) <sup>1</sup> H NMR spectrum shows a peak associated with D <sup>Me</sup> and (b) <sup>29</sup> Si NMR shows disappearance of Q <sup>3</sup> and appearance of D. (c) IR shows loss of silanols.....	79
2.16. B(C <sub>6</sub> F <sub>5</sub> ) <sub>3</sub> -catalyzed condensation of residual silanols on MQ with octadecyldimethylsilane. (a) <sup>1</sup> H NMR spectrum shows octadecyl peak and no residual Si-H. (b) IR shows loss of silanols.....	80
2.17. Pt-catalyzed hydrosilylation of <sup>1</sup> HMQ and allyl-PEO. (a) <sup>1</sup> H NMR shows disappearance of Si-H and allyl protons and appearance of ethyleneoxide protons. (b) IR confirms disappearance of Si-H and PEO addition. (c) GPC chromatographs and (d) 2D DNMR spectrum of <sup>1</sup> HMQ and allyl-PEO and <sup>1</sup> HMQ- <i>graft</i> -PEO. Due to dispersity of the MQ sample, grafting is not clear in GPC but DNMR provides evidence that both PEO and MQ diffuse simultaneously. Along with the disappearance of Si-H and allyl groups, this clearly shows that the grafting was successful.....	81
2.18. Pt-catalyzed hydrosilylation of <sup>1</sup> H <sub>18</sub> <sup>Me</sup> onto <sup>v</sup> MQ. (a) <sup>1</sup> H NMR shows the disappearance of Si-H and vinyl protons indicating complete reaction and clean product. (b) GPC and (c) D-NMR show increase in molecular weight/size from <sup>1</sup> H <sub>18</sub> <sup>Me</sup> and <sup>v</sup> MQ to <sup>v</sup> MQ- <i>graft</i> -D <sub>18</sub> <sup>Me</sup> .....	82
3.1. (A) Interfacial tension of water drops in MQ-toluene solutions (1 mg/mL) for M <sub>17</sub> Q <sub>15</sub> (orange), M <sub>16</sub> Q <sub>32</sub> (red), M <sub>32</sub> Q <sub>64</sub> (black) and M <sub>66</sub> Q <sub>164</sub> (blue). The interfacial tension of the clean water-toluene interface is 35 mN/m. (B) Interfacial tension of water drops in MQ-toluene solutions (1 mg/mL) for silanol-containing M <sub>42</sub> Q <sub>100</sub> (red) and trimethylsilyl iodide-treated M <sub>51</sub> Q <sub>100</sub> (black). (C) Images of pendant drops at the lowest measured interface tension. (from left to right: M <sub>17</sub> Q <sub>15</sub> , M <sub>16</sub> Q <sub>32</sub> , M <sub>32</sub> Q <sub>64</sub> , and M <sub>66</sub> Q <sub>164</sub> ).....	95

3.2. Impact of $[M_{32}Q_{64}]$ on interfacial tension reduction. $[M_{32}Q_{64}] = 0.005$ (purple), 0.0075 (red), 0.01 (orange), 0.05 (blue), 0.1 (pink), 0.5 (green), 1.0 (black), 5.0 (gray), 10.0 (cyan) mg/ml. The interfacial tension of a clean water-toluene interface is 35 mN/m.	97
3.3. (A) Pressure-area isotherms to minimum trough area at 5 mm/min and (B) pressure-area hysteresis loops (5 mm/min, 3 cycles from 2-20 mN/m) of $M_{17}Q_{15}$ (orange), $M_{16}Q_{32}$ (red), $M_{32}Q_{64}$ (black) and $M_{66}Q_{164}$ (blue) monolayers on water. (C) Photos of the elastic surface wrinkles that form during high pressure compression of $M_{32}Q_{64}$ . Wrinkles grow in compression and relax on expansion reversibly. The surface tension probe was removed to allow imaging so exact surface pressures in these images are unavailable, but it is in the range of 50 to 60 mN/m.	99
3.4 Pressure-area hysteresis loop (0-10 mN/m x1, 2-10-2 mN/m x2, 2-20-2 mN/m, 2-50-2 mN/m) for silanol-containing $M_{42}Q_{100}$ (red) and trimethylsilyliodide-treated $M_{51}Q_{100}$ (black).	101
3.5. AFM micrographs of MQ copolymer surfaces from Blodgett depositions and solution adsorption. Note differences in scale bars.	103
4.1. (a) Optical micrograph (20x) of 0.1 wt% - $D_{1570}$ composite. (b) Steady-state flow experiment of CNT- $D_{1570}$ composites and control showing dramatic shear thinning. (c) Thixotropic loops where filled symbols are for the increasing shear rate step (Up step) and crossed open symbols are for the decreasing shear rate step (Down step). For (b) squares and (c) circles: black = 1.0 wt% CNT, red = 0.5 wt% CNT, pink = 0.1 wt% CNT, 0.05 wt% = blue, control = black diamond. Note the hysteresis between up and down steps observed in (c) at higher loadings.	121
4.2. Alignment of CNTs during shear flow. The initially random CNT network aligns in the direction of flow as shearing forces are applied (Up step in thixotropic loop). At the highest shear rates the CNTs are aligned in the direction of flow and the viscosity of the fluid is low. On the Down step in the thixotropic loop, the CNTs are still roughly aligned in the direction of flow but they are able to interact as shear rate decreases, thus reinforcing the composite and raising viscosity.	122
4.3. Breakdown of elastic CNT network by shear alignment in CNT- $D_{1570}$ composites. (a) Oscillatory stress sweeps and (b) oscillatory frequency sweeps show reductions in elasticity after shear alignment was accomplished by a preshear conditioning step. Black symbols are $G'$ and red symbols are $\Delta$ . Unfilled controls are hollow circles. CNT loadings are 0, 0.01, 0.05, 0.1, 0.5 and 1 wt% and increase in the directions shown by the arrows. Generally $G'$ increases and $\Delta$ decreases with CNT loading. All experiments are run at room temperature. Frequency sweeps are run in the linear viscoelastic region.	123
4.4. (a) $D_{230}$ and (b) $D_{1570}$ linear silicone-CNT composite micrographs (20x). Numbers indicate wt% CNT in silicone.	124

4.5. Oscillatory frequency sweeps at room temperature of (a) D <sub>1570</sub> composites and (b) D <sub>230</sub> composites. Arrows indicate increasing CNT concentration. Unfilled control samples are unfilled circles. In (a) increasing color intensity corresponds to loadings of 0.01, 0.05, 0.1, 0.5, and 1.0 wt% CNT. In (b) increasing color intensity corresponds to loadings of 0.01, 0.025, 0.05 and 0.1 wt% CNT. In general, G' increases and delta decreases with CNT loading. All experiments were run in the linear viscoelastic region.....	125
4.6. Optical micrographs (20x) of linear siloxane homopolymer–CNT composites.....	128
4.7. Optical micrographs (20x) of linear dimethylsiloxane copolymer – CNT composites.....	129
4.8. Oscillatory frequency sweeps at room temperature of siloxane polymer – CNT composites. CNT loadings are 0, 0.01, 0.025, 0.05 and 0.1 wt%. Black symbols are G' and red symbols are phase shift (delta). Empty circles are unfilled controls. Color intensity indicates loading from lightest (0.01 wt%) to darkest (0.1 wt%). Generally, G' increases and delta decreases with CNT loading. All experiments were run in the linear viscoelastic region.....	130
4.9. (a) Steady state flow and (b) oscillatory frequency sweeps of siloxane-CNT composites. In (a) filled symbols are 0.1 wt% CNT composites and open symbols are unfilled controls. In (b) black, G', and red, delta, plots are for 0.1 wt% CNT samples. Symbol Key: D <sup>Ph-Me</sup> = Down Triangle, D <sup>Et</sup> = circle, DD <sup>Ph</sup> = star, DD <sup>Ph-Me</sup> = pentagon, D = square.....	132
4.10: Schematic representations of heterogeneous, homogeneous and intermediate CNT dispersions.....	135
5.1. Structure and mobility of PDMS (MD <sub>n</sub> M in GE nomenclature).....	140
5.2. (a) Photos of 1 cm x 1 cm x 1 mm PDMS-MWCNT elastomer samples with MWCNT loadings from left to right of 0, 0.01, 0.025, 0.05, 0.1, 0.25 and 0.5 wt%. (b) Optical micrographs of 0.01 wt% and 0.1 wt% MWCNTs dispersed in linear PDMS <sup>116k</sup> . (c) Steady flow and (d) oscillatory frequency sweeps of PDMS <sup>116k</sup> -MWCNT composite fluids. In (c) square symbols represent composite samples of 1.0, 0.5, 0.1 and 0.05 wt% MWCNTs from black to light gray. Black diamonds are the unfilled control. Shear thinning is observed by the large reduction in viscosity with increasing shear rate. In (d) black and maroon circles are for 1.0 wt% MWCNTs and black and red diamonds are the unfilled controls. Composites of 0.01, 0.05, 0.1 and 0.5 wt% are squares from light gray to dark gray and light red to red. G' increases with CNT loading and delta decreases. (e) Surface resistivity as a function of MWCNT loading. Measured using a DESCO surface conductivity meter.....	146
5.3. TGA (a) weight loss and (b) derivative weight loss of PDMS elastomer composites in nitrogen atmosphere. Results for unfilled control (solid black), 0.05 (light gray), 0.1 (gray), 0.25 (dark gray) and 0.5 wt% (dashed black) are shown. Peak degradation temperatures are labeled in (b).....	147

5.4. Decomposition kinetics studied by TGA. (a) Weight loss and (b) derivative weight loss curves of unfilled PDMS elastomer (Gelest OE41) at heating rates of 1 (black), 2.5 (dark gray), 5 (gray), 10 (light gray) and 20 (dashed black) °C/min. (c) Weight loss and (d) derivative weight loss curves of 0.5 wt% MWCNT in PDMS elastomer at heating rates of 1 (black), 2.5 (dark gray), 5 (gray), 10 (light gray) and 20 (dashed black) °C/min. (e) 300 °C isothermal weight loss of unfilled (solid line) and 0.5 wt% MWCNT filled (dashed line) PDMS elastomers. (f) Stepwise isothermal analysis of unfilled PDMS elastomer (solid lines) and 0.5 wt% MWCNT filled PDMS elastomer (dashed lines). Black curves are for weight loss and blue curves show the temperature profile of the experiment. ....	149
5.5. Derivative weight loss (black) and curve fit (red) from deconvolution into Gaussian functions for (a) 0.5 wt% MWCNT composite and (b) unfilled control at a heating rate of 10 °C/min. ....	151
5.6. PCFC HRR (reds) with TGA weight loss (blacks) results for unfilled control (solid) and 0.1 (light gray/pink), 0.25 (gray/maroon), and 0.5 wt% (dash) PDMS-MWCNT Composites. ....	153
5.7. DSC (exotherm up) of unfilled and 0.5 wt% MWCNT composite elastomers. Crystallization is observed in the cooling step (top curve) and melting is observed in the heating step (bottom curve). The glass transition is detected in the heating step (bottom curve) by the shift of the baseline indicating a change in heat capacity. ....	154
5.8. Intramolecular depolymerization of PMDS to cyclic trimer. ....	155
5.9. Pyrolysis GC-MS chromatograms of (a) unfilled PDMS elastomer and (b) 0.5 wt% CNT PDMS composite. Pyrolysis conducted at 900 °C in helium atmosphere. ....	156
5.10. TGA of (a) PDMS <sup>17k</sup> and (b) PDMS <sup>16k</sup> . Black lines are unfilled controls, dark gray are 0.1 wt% MWCNTs and light gray lines are 1 wt% MWCNTs. The dashed line in (a) is the MWCNT enriched PDMS <sup>17k</sup> sample prepared by pressing and draining the 1 wt% MWCNT-PDMS <sup>17k</sup> sample. Py GC chromatographs of (c) neat PDMS <sup>17k</sup> and (d) PDMS <sup>17k</sup> saturated MWCNTs. All pyrolysis experiments were conducted at 900 °C in helium atmosphere. ....	158
5.11. Intramolecular depolymerization of PDMS to cyclic pentamer (D <sub>5</sub> ) ....	160
5.12. Effect of nanocarbon fillers at 0.5 wt% on thermal stability of Gelest OE41 PDMS elastomer ....	161
5.13. Effect of Boron Nitride Nanotube (BNNT) and Boron Nanopowder fillers at 0.5 wt% on thermal stability of Gelest OE41 PDMS elastomer. Nanocomp MWCNTs and control provided as reference. ....	162
5.14. TGA of silicone elastomers and composites containing 0.5 wt% MWCNTs. Blue lines are unfilled controls and black lines are composites. Dashed curves for the HV22 elastomer are filled with an additional 15 wt% hexamethyldisilazane-treated silica. ....	163



5.15. TGA of linear model silicone composites of varied chemistry. Blue curves are control samples, black solid curves are 0.1 wt% CNT composites and black dashed curves are 1 wt% CNT composites.	164
6.1. Five reported <sup>15-19</sup> methods for the preparation of covalently attached monolayers of PDMS on silicon wafers along with ellipsometric thickness and water contact angle data.	174
6.2. Conditions for maximum bonding density for BCF-catalyzed reactions of Si(100) with model hydridomethylsiloxanes (toluene, room temperature, 0.1 M hydromethylsiloxane and 0.0005M BCF (0.5 mol%).	188
6.3: Log-Log plot of ellipsometric thickness versus the number of repeat units, N, of <sup>x</sup> MDM <sup>H</sup> polymer grafts from BCF catalysis on Si(100) surface. The slope of the fitted data indicates the scaling exponent for the relationship of thickness and N.	194
6.4. Graphic depictions of the average degree of stretching of individual grafted chains based on molecular weight and ellipsometric thickness values. The abbreviations are abridged in the figure, leaving out the terminal M groups, thus <sup>v</sup> D <sub>53</sub> <sup>H</sup> represents <sup>v</sup> M D <sub>53</sub> M <sup>H</sup>	195
6.5. Two explanations for why thicker (~10 nm) films of higher molecular weight) end-grafted PDMS exhibit greater contact angle hysteresis. In <b>a</b> , polymer chains spread onto the water drop and impede advancing and receding events. In <b>b</b> , the liquid PDMS interface distorts at the contact line forming a liquid/liquid/air interface that must restructure for advancing and receding events to occur.	198
6.6. Proposed mechanism (after Escorihuela <i>et al.</i> <sup>1</sup> ) for BCF-catalyzed reaction of Si(100) with hydride-terminated PDMS. OA and RE abbreviate oxidative addition and reductive elimination.	202
A6.1: MD <sub>12</sub> M <sup>H</sup> (M=880) (GPC: Very low signal intensity did not allow analysis)	206
A6.2: MD <sub>15</sub> M <sup>H</sup> (M=1070)	206
A6.3: MD <sub>28</sub> M <sup>H</sup> (M=2070)	207
A6.4: MD <sub>36</sub> M <sup>H</sup> (M=2664)	207
A6.5: MD <sub>68</sub> M <sup>H</sup> (M=5000)	207
A6.6: MD <sub>112</sub> M <sup>H</sup> (M=8280)	208
A6.7: MD <sub>423</sub> M <sup>H</sup> (M=31 300)	208
A6.8: Stacked IR spectra of poly(methylhydro-co-dimethyl)siloxane (MD <sub>x</sub> D <sup>H</sup> <sub>y</sub> M) random copolymers.	209
A6.9: Stacked IR spectra of MD <sub>x</sub> M <sup>H</sup>	209
A6.10. <sup>1</sup> H NMR Kinetics of D <sub>4</sub> <sup>H</sup> (0.1 M Si-H, 0.5 mol% BCF, anhydrous toluene-d <sub>8</sub> ). Hydride transfer oligomerization is evident by the broadening of the Si-CH <sub>3</sub> peaks ( $\delta$ ~0.4 ppm) and the appearance of the peaks at $\delta$ ~3.5 ppm corresponding to CH <sub>3</sub> SiH <sub>3</sub> byproduct.	212
A6.11. XPS Spectra of <sup>Me</sup> MD <sub>x</sub> M <sup>H</sup> grafts	217

A6.12. XPS Spectra of $^{B_u}MD_xM^H$ grafts.....	218
A6.13. XPS Spectra of $^HMD_xD^H$ grafts.....	219
A6.14. XPS Spectra of $^VMD_xM^H$ grafts.....	219
A6.15. XPS Spectra of poly(hydridomethyl-co-dimethyl)siloxane ( $MD_xD^H_y$ ) grafts.....	220
A6.16. XPS Spectra of Alkyldimethylsilane grafts.....	220
A6.17. XPS Spectra of vinyl surfaces and derivatives.....	221
A.1. Preparation and characterization of allyloxysulfolane.....	234
A.2. $^1H$ NMR and IR of $^HMM$ -AS Pt-catalyzed hydrosilylation product, $^{POS}MM$ .....	235
A.3. Target propoxysulfolane-methylsiloxane polymers.....	236
A.4. $^1H$ NMR of propoxysulfolane-terminated PDMS, $^{POS}MDM^{POS}$ .....	237
A.5. $^1H$ NMR, IR and GPC of AS- $MD_xD^H_yM$ Pt-catalyzed hydrosilylation products.....	238
A.6. $^1H$ NMR of crude and rinsed $MD_{25}D^H_2M$ -AS hydrosilylation. The conversion in this sample was 22% (2 EQ AS, 20 ppm Pt, 80 °C, 16 hours).....	238
A.7. $^1H$ NMR and IR of $D_4^1H$ -AS Pt-catalyzed hydrosilylation product, $D_4^{1POS}$ .....	239
B.1. 1 $\mu m$ PTFE powder that has been vigorously shaken with 5 mL water in a Fisher scintillation vial. The opaque particle film coats the wetted walls of the glass. This film exhibits elastic behavior and will climb the walls if it is rinsed down.....	245
B.2. SEM micrographs of 1 $\mu m$ PTFE particles. Increasing the magnification shows that the particles have structure on multiple length scales.....	246
B.3. Pressure-area isotherm (left) and hysteresis of 1 $\mu m$ PTFE particles are the air- water interface.....	248
B.4. Photograph and 20x optical micrograph of 1 $\mu m$ PTFE film isolated from the air- water interface of a Langmuir monolayer.....	248
B.5. Photograph and 20x optical micrograph of 1 $\mu m$ PTFE film isolated from the air- water interface within a scintillation vial.....	249
B.6. Surface pressure - driven climbing of hydrophobic particles. In the first image, the walls of the vessel are dry and no climbing will occur: there is no water surface for the excess particles to expand onto. In the second image, the walls of the vessel are wet and excess particles are trapped (this could be in the form of bubbles or agglomerates that form from the collapse of the high surface area of the water during shaking). In the final image, the excess particles are merging with the film, creating a surface excess of particles. This exerts a surface pressure that drives the film up the wet walls of the vessel. Climbing continues until all excess particles have merged, the entire water interface has been covered or the surface pressure cannot overcome the weight of the climbing film.....	251

## CHAPTER 1

### SILICON, SILICA AND SILICONES

*“Methyl silicone was so different in composition, in structure, and in physical and chemical properties that it was outside the ordinary day-to-day thinking of chemists and engineers fifty years ago.”*

- Eugene Rochow<sup>1</sup>

You’ve probably heard the word silicone and are familiar with silicone products. In the lab, you use silicone oil baths, silicone vacuum grease and perhaps you have even used “PDMS” (Dow Corning Sylgard 184). Outside the lab, you use silicone caulks, silicone bakeware, dimethicone-containing personal care products, silicone-containing contact lenses and silicone antifoaming agents that keep cooking oils from foaming and calm an upset stomach. In contrast, It is unlikely that you have seen silicones in the classroom. How can these ubiquitous polymers that fill so many roles simultaneously be ignored in our chemistry and materials science curricula? Organosiloxane polymers, the chemically correct name for silicones, are polymers based on the inorganic siloxane (Si-O-Si) bond. Organosiloxane polymers are technology-enabling materials that perform in places where no other polymer can. To appreciate these polymers, it is necessary to first explore their invention and history. After an historical introduction, the properties, structure and chemistry of silicones will be introduced.<sup>1-7</sup>

#### 1.1 Silicon: The Element

Silicon is the second most abundant element (25.7% by mass), behind oxygen (49.5%), found on terrestrial Earth. It exists naturally in the form of silica and silicates and typically is not found in its elemental form. In 1823, Berzelius was the first to isolate and study amorphous silicon which he formed by the potassium reduction of  $\text{SiF}_6$  at red heat.<sup>8</sup>

In 1854, Sainte-Claire Deville<sup>9</sup> was the first to report crystalline silicon obtained from impure aluminum. Since silicon is present only as an impurity in aluminum melts, this was not an efficient way to produce large quantities of silicon. It wasn't until 1895 that Henri Moisson<sup>10</sup> discovered an efficient method of producing silicon by reducing silica using an electric arc furnace with graphite electrodes. This is the same process used today in large-scale metallurgical-grade silicon production. While at the time of its discovery there were very few applications of pure silicon, it has proven to be irreplaceable in modern semiconductor technology where ultrapure forms are required.

The location of silicon below carbon on the periodic table suggests similar chemistry and many early researchers assumed this to be true. There were even scientists who proposed silicon-based life. Similar to carbon, silicon is typically tetravalent, bonding with four atoms in a tetrahedral arrangement. Unlike carbon, silicon can expand its valency to six due to the presence of empty d-orbitals, leading to cases of unique bonding and reactivity. Table 1.1 exhibits some of the atomic properties of silicon in comparison to carbon and other common atoms. Silicon has a larger atomic radius than carbon (117.6 pm versus 70 pm). Silicon has a Pauling electronegativity<sup>11</sup> of 1.8, so it is more electropositive than carbon with an electronegativity of 2.5. This has serious implications on the chemistry of its bonding: the electropositive nature of silicon means that bonds to halogens, oxygen and nitrogen are far more reactive than their organic counterparts. Perhaps the most dramatic difference in bonding can be demonstrated by the different reactivity of carbon-hydrogen bonds and silicon-hydrogen bonds. Carbon and hydrogen have similar electronegativities so they bond almost entirely covalently with a slight partial negative charge on carbon (carbon being slightly more electronegative). Carbon-hydrogen bonds are stable and we can intuit this by the almost infinite number of stable hydrocarbons. The opposite is true in the silicon-hydrogen bond; the hydrogen is

more electronegative and carries a partial negative charge. This means that a silicon-hydrogen bond behaves chemically as a metal hydride.<sup>12</sup> The reactivity of the hydrosilane is demonstrated by the instability of silanes, which ignite when exposed to air. That silicon behaves differently than carbon must be appreciated to understand silicates and siloxane polymers.

Table 1.1. Atomic Properties of Silicon, Oxygen, Carbon and Hydrogen

Atom	Atomic Number	Atomic Mass	Atomic Radius (pm)	Pauling Electronegativity, <sup>11</sup> $\chi_{\text{Pauling}}$
Si	14	28.0855	110	1.80
O	8	15.9994	60	3.50
C	6	12.0096	70	2.55
H	1	1.00794	25	2.20

## 1.2 Silica and Silicates: The Oxides<sup>13-15</sup>

As mentioned above, silicon is the second most abundant element in the Earth's crust and it is found almost exclusively bound to oxygen in the form of silica and silicates. In these materials each silicon atom bonds with four oxygen atoms to form a tetrahedron and these tetrahedra organize to form a network. The exact structure of the tetrahedral network varies and numerous silica structures exist including quartz, tridymite and cristobalite. Silicates are similar in structure to silica, but contain other metal atoms that replace silicon atoms in the network. Examples of silicates and their structures are: peridotite  $[\text{Mg}_2\text{SiO}_4]$  (isolated tetrahedron or orthosilicate), tourmaline  $[\text{XY}_3\text{Z}_6\text{B}_3\text{Si}_6(\text{O},\text{OH})_{30}(\text{OH},\text{F})]$  (ring silicate or metasilicate), spodumene  $[\text{LiAlSi}_2\text{O}_6]$  (single chain silicate or pyroxene), muscovite  $[\text{KAl}_3\text{Si}_3\text{O}_{10}(\text{OH})_2]$  (sheet silicate in the mica family), and albite  $[\text{NaAlSi}_3\text{O}_8]$  (framework silicate in the Feldspar family).

Human history has a close relationship with silica and silicates particularly through ceramic arts and science. The first tools were made of silicate flints. Clay pottery was

developed 25,000 years ago. Glass, an amorphous form of silica, was being produced by Egyptians 5000 years ago. To this day developments in concrete, cement, geopolymers and glass are important in construction and infrastructure technology.

Silica micro- and nanoparticles are a form of silica with countless uses ranging from inorganic fillers and filtration media, to biomedical imaging and drug delivery. Silica particles come in many forms that depend on how they are prepared and a few of these forms are illustrated in scanning electron microscope (SEM) micrographs in Figure 1.1. Fumed silica comes from the combustion of  $\text{SiCl}_4$  in an oxygen-rich environment and is commonly used after surface treatment as an additive in polymer composites. Silica gels and precipitated silicas are prepared from silicate sols, like sodium silicate. Chemists are familiar with silica gels as column packings and we find precipitated silicas in the household as an abrasive component in toothpastes. Another form of silica is Stöber silica, monodisperse silica particles prepared from alkoxy silanes, the size of which can be controlled.<sup>16</sup> Lastly, a variety of silicas are formed by organisms in nature.<sup>17</sup> Diatoms, algae that grow a hierarchical shell of silica, are one example that has attracted the attention of materials scientists and engineers.

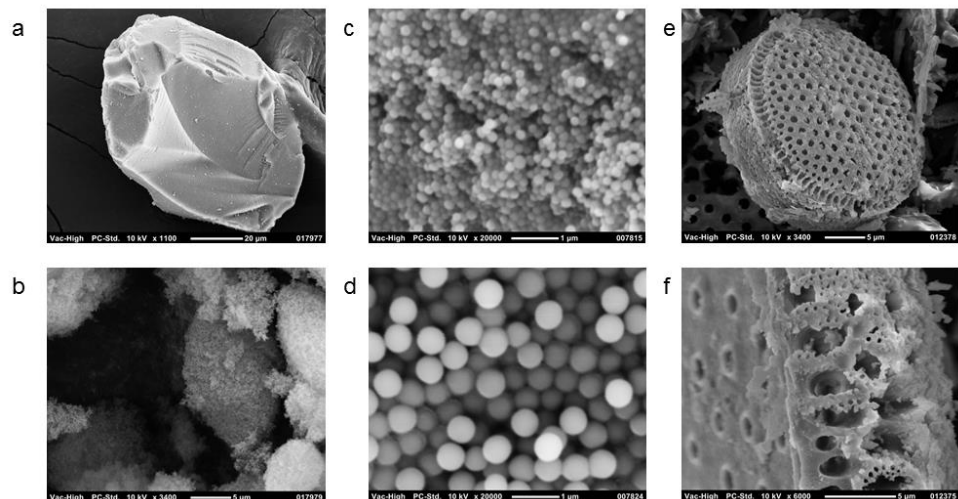


Figure 1.1. SEM micrographs of silicas. (a) Silica gel used in column chromatography. (b) Fumed silica. (c) and (d) are Stöber particles of two diameters. (e) and (f) are images of a diatom shell that illustrate structural hierarchy.

Silica can also be found as a native oxide on the surface of pure silicon. Our group and others have utilized the molecularly smooth silicon oxide layer as a platform to study surface science.<sup>18-21</sup> The smooth surface is a perfect model for the chemistry of wetting since surface topography does not contribute: liquid contact angles can be directly related to surface chemistry. Smooth silica substrates on silicon wafers also simplify characterization by ellipsometry and X-Ray Photoelectron Spectroscopy. The reactivity of the oxide is similar to that of other forms of silica, making it a great model system to develop and study the fundamental chemistry and properties of silica surface modifications. Our group has a long history in surface science and chemistry, and our current understanding of wetting would not have been possible without the availability of a flat, molecularly smooth, easily characterized and chemically reactive substrate.

### 1.3 Silicones: Organosiloxane Polymers

The history of organosiloxane polymers and “silicones” brings us back to Berzelius who was the first to isolate a reactive chlorosilane, silicon tetrachloride ( $\text{SiCl}_4$ ). From this

silicon tetrachloride, Friedel and Crafts in 1863 synthesized the first organosilicon compound, tetraethylsilane ( $\text{Si}(\text{C}_2\text{H}_5)_4$ ), using diethylzinc.<sup>22</sup> Friedel continued work on organosilicon chemistry with a coworker, Ladenburg, who in 1872 independently discovered the synthesis of diethyldichlorosilane ( $(\text{C}_2\text{H}_5)_2\text{SiCl}_2$ ). Hydrolysis of diethyldichlorosilane resulted in the first organosiloxane polymer.<sup>23</sup> Poly(diethylsiloxane) (or silicon diethyl oxide as Ladenburg called it) was described as a viscous, odorless syrup with high thermal stability. Ladenburg also prepared ethyltrichlorosilane ( $(\text{C}_2\text{H}_5)\text{SiCl}_3$ ) and triethylchlorosilane ( $(\text{C}_2\text{H}_5)_3\text{SiCl}$ ) and hydrolyzed these products into the first silicone 'T' resin and disiloxane. This work was the birth of organosilicon chemistry that led to the invention of organosiloxane polymers. But no discussion of organosilicon chemistry can be complete without mention of the "grandfather of silicone chemistry," Frederic Stanley Kipping.

Kipping's primary goal in organosilicon chemistry was to isolate a silicon stereocenter and isolate the optically active *D* and *L* isomers. Kipping synthesized hundreds organosilicon compounds primarily via Grignard chemistry and arduous separations. At this time, the reactivity of silicon was imagined to be much like that of carbon and during the course of his investigations Kipping proposed that he had prepared a silicon-oxygen double bond, a silicone in analogy to a ketone.<sup>24</sup> Kipping was incorrect, silicon does not form double bonds with oxygen, and the silicones did not have properties analogous to ketones; but, the name silicone has stuck to this day. Seyferth<sup>4</sup> comments in his review of the direct process that "Kipping's insistence on forcing organosilicon compounds - their properties and reactions - into the framework of organic chemistry was a bias that actually proved to be a handicap to his research in organosilicon chemistry." Nevertheless, Kipping prepared and isolated numerous silicon compounds that laid the groundwork for modern organosilicon chemistry.<sup>25</sup> It is worth noting that many of the



viscous byproducts he so abhorred were in fact going to be the future of organosilicon research that would eventually create a new industry.

Another important figure in the story of siloxane polymers is Alfred Stock. Stock was an inorganic chemist who synthesized and isolated silanes and organosilanes in strict air-free environments. During the course of his investigations, he prepared numerous siloxanes and identified them for what they truly were: Si-O bonds and not Si=O bonds as Kipping had proposed. His nomenclature for silanes and siloxanes was part of his universal systematic nomenclature that was later adopted by the International Union of Pure and Applied Chemistry. Of particular value and importance to the future of siloxane polymers was Stock's preparation and observation of polydimethylsiloxane in 1919.<sup>26</sup> Although less than 20 mg of product was obtained, it was enough to observe that the new material was a colorless, hydrophobic oil.

The academic interest in silicones had proven fruitful for synthetic chemists looking to make and isolate molecules, but in 1937 Kipping famously concluded that "most if not all the known types of organic derivatives of silicon have now been considered and it may be seen how few they are in comparison with those which are entirely organic; as moreover the few which are known are very limited in their reactions, the prospect of any immediate and important advance in this section of organic chemistry does not seem to be very hopeful."<sup>27</sup> With academic interest waning, the future of silicones lay in industry. The age of electricity had arrived and the new technology required new materials, particularly insulators for electrical wire and cable. The best performing insulators at the time were made from glass fibers in an organic polymer matrix, but their performance was limited by the organic binder that failed at elevated temperature and left conductive carbon residues. A new binder was needed that could withstand more extreme working

environments and optimally would be composed of less organic mass to minimize conductive degradation residues.

The first industrial player was Corning Glass Works, which wanted to sell more glass. They knew that selling glass fibers for electrical insulation was one way to do this and developing a high performance binder would create a greater market. Dr. James Franklin Hyde, a Corning researcher, tackled the problem by preparing ethyl-phenyl siloxane polymers using Kipping's Grignard methods.<sup>28</sup> These polymers could be oxidatively cured at elevated temperatures to make a resinous binder for glass fibers. New ethylphenylsilicone binders enabled glass fiber insulation to operate at temperatures of 180 °C, a 30 °C improvement over the current state-of-the-art. When Corning Glass Works decided to continue research on silicones and become a large scale producer, they joined forces with Dow Chemical Company. Dow had control over all magnesium production in the United States and using the Grignard method meant silicone production required large quantities of magnesium. The joint venture created Dow-Corning which remains one of the largest silicone manufacturers in the world.

When Corning had discovered the new silicone resins for electrical insulation, it approached the key large equipment manufactures in the United States to sell their new product. General Electric (GE) was among them. Corning invited GE to their labs to see the new silicone materials. Winton Patnode was a GE researcher present at the visit who had previous interest in silicone materials for insulation and now had a renewed interest in developing a silicone resin that would belong to GE. He approached Dr. Eugene Rochow and challenged him to develop the new polymer. Rochow, an inorganic chemist working in the ceramics department, decided that the optimal material would have the minimal organic content possible and thus focused his attention onto the preparation of

methylsilicones. His first preparations involved the use of Grignard reagents to make mixtures of chloro- and bromosilanes which he cohydrolyzed over ice water.<sup>29</sup> The ratio of CH<sub>3</sub> to Si could be determined analytically and he found ratios of 1.3 to 1.5 cured into horny resins with the best performance for insulation (Figure 1.2). The drawback of this method was that it required magnesium, that was now owned by Dow-Corning, for the preparation of Grignard reagents. This was not an industrially feasible route for GE. Rochow then developed perhaps the most important process in all of silicone chemistry: the direct process for the preparation of methylchlorosilanes.

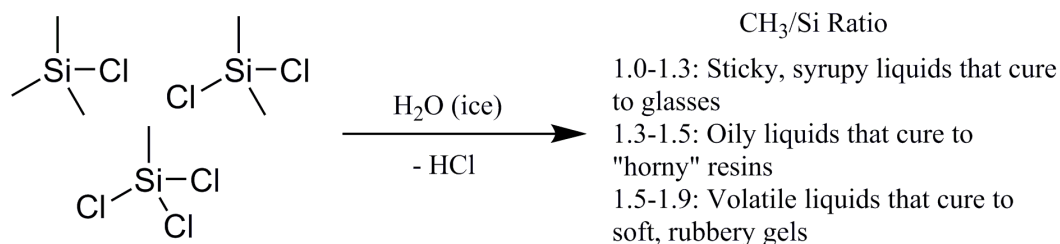
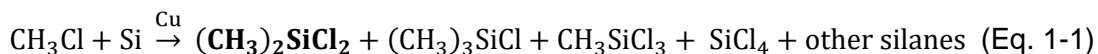


Figure 1.2. Rochow's methylsilicone resins.<sup>29-31</sup> His first experiments utilized Grignard preparations of methyl chloro- and bromo- silanes. Later experiments utilized methylchlorosilanes from the direct synthesis to similar effect.

In "the most important single experiment and the best single day's work in the history of the silicone industry,"<sup>3</sup> Rochow discovered the direct process.<sup>30,31</sup> In the direct process, a mixture of methylchlorosilanes (that can be separated by distillation) is produced by flowing chloromethane gas over Cu-Si alloy in a tube furnace (Eq. 1-1). Dimethyldichlorosilane is the major product, which is good news since it makes up the backbone of the most important methylsilicone, polydimethylsiloxane. In Germany, Richard Müller<sup>32</sup> independently discovered the direct process; because of their simultaneous discoveries the direct process is called the Müller-Rochow process. The methylchlorosilanes that result from the Müller-Rochow process are nothing short of

magic. They have created a new field of polymer science and opened the door to new technologies that would not be possible otherwise.



#### 1.4 General Properties, Chemistry and Structure of Siloxane Polymers

The new methylsiloxane polymers invented by Rochow had properties unlike any carbon-based polymers. Most important to General Electric was their high thermal stability, high dielectric strength, low dielectric power loss and non-conducting char. Methylsiloxane resins could be prepared directly from hydrolysis and condensation of chlorosilanes from the direct process. In the form of liquids these resins could be easily applied to glass fiber insulation and subsequently cured into solids at elevated temperature. Siloxane resins were developed that not only act as electrical insulation but also as protective, hydrophobic paints. While the resins have useful properties, the most well-known methylsiloxane polymer, polydimethylsiloxane (PDMS), has some of the most fascinating properties of any manmade material.<sup>33,34</sup>

Polydimethylsiloxane (PDMS) is the most widely recognized and studied silicone polymer. The structure, shown in Figure 1.3, consists of a linear siloxane backbone with two methyl groups on each silicon. PDMS has a  $T_g$  of  $-125\text{ }^\circ\text{C}$  and at room temperature is a viscoelastic liquid at all molecular weights. It is stable in air at  $150\text{ }^\circ\text{C}$  and in inert atmosphere to over  $300\text{ }^\circ\text{C}$ . Unique properties of PDMS are the small changes in viscosity with temperature, its high compressibility compared to hydrocarbon oils, its high dielectric strength, its gas permeability and its low cohesive energy density. These properties make PDMS irreplaceable in numerous applications, particularly those that require a wide service temperature window.

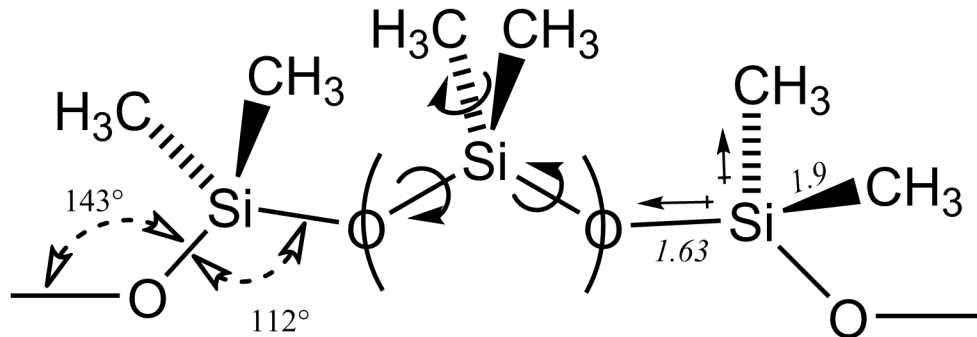


Figure 1.3. Structure of poly(dimethylsiloxane) (PDMS). Silicon atoms and the attached methyl groups can swing about the oxygen atom and even pass through bond angles of  $180^\circ$  due to the high rotational freedom of the 51% ionic siloxane bond. The longer bond lengths in comparison to carbon-based polymers spaces organic substituents further apart, aiding flexibility and rotational freedom. The electronegativity differences are responsible for many behaviors of siloxane polymers including chemical reactivity.

To make use of PDMS or other linear siloxanes as materials, siloxane networks need to be created. This is achieved by crosslinking linear siloxane polymers into elastomers. These elastomers are viscoelastic solids, but if they are not compounded with filler (most commonly silica) they will have the mechanical properties of tofu. This is due to the low cohesive energy of the siloxane chains. PDMS elastomers have physical and chemical properties similar to linear PDMS oils: low glass transition and high thermal stability enabling wide service temperature range, high gas permeability, hydrophobicity and great dielectric properties. Crosslinking chemistry in PDMS and other linear silicones is commonly accomplished using hydrolysis and condensation (RTV silicones), radicals (peroxide cured) or Pt-catalyzed hydrosilylation.

The performance and properties of silicones that makes them special comes from the siloxane bond that forms their skeleton. The siloxane bond is longer than the carbon-carbon bond ( $1.63 \text{ \AA}$  versus  $1.53 \text{ \AA}$ ) and has average bond angles of  $112^\circ$  (O-Si-O) and  $143^\circ$  (Si-O-Si) versus the  $109.5^\circ$  of carbon-carbon bonds. This places the organic

substituents on the siloxane backbone further apart than those on a carbon backbone, enabling greater rotational mobility. Most important is the fundamental difference in bonding that arises from the different electronegativity of silicon and oxygen. The siloxane bond is 51% ionic (based on Pauling electronegativity) and because of this has extreme conformational freedom (bond angles can pass through 180° and the bond rotates freely)<sup>33</sup>. The flexibility of the backbone gives siloxanes extreme dynamic mobility which grants linear silicone polymers the lowest glass transition temperatures of all polymers (-135 °C for polydiethylsiloxane). In the case of PDMS, Rochow described the mobility such that “the silicon atom and its associated pair of methyl groups swing as a unit, as though the silicon-oxygen bond were a ball and socket joint.”<sup>2</sup> The extreme dynamic mobility of the siloxane backbone and the widely spaced organic substituents creates high free volumes. The high free volume of silicones is responsible for their high compressibility, small change in viscosity with temperature, and large molar volumes. The freely rotating, low energy methyl groups result in low cohesive energy densities and low boiling points for methylsilicone molecules in comparison to hydrocarbons.

The high temperature stability of methylsiloxanes arises from the thermodynamic strength of the siloxane bond; however, the thermodynamic stability should not be confused with chemical stability. The polarity of the siloxane bond makes it susceptible to attack by acid, base and hydrolysis. This reactivity is evident in the use of acid and base catalysts for silicone synthesis and equilibration.<sup>35-37</sup> If not properly removed, these catalysts can have deleterious effects on thermal and dimensional stability of siloxane polymer products. Linear PDMS – containing materials are particularly susceptible to degradation by equilibration into cyclic oligomers and structural changes induced by chemical stress relaxation.<sup>38,39</sup>

There is an affinity of silicones for interfaces. Like many of the other properties of silicones, this too arises from the dynamic mobility of the siloxane backbone and organic substituents on the backbone. In PDMS, the freely rotating methyl groups minimize intermolecular interactions between neighboring chains as mentioned previously, but additionally minimize interactions with interfaces. The flexible backbone ensures that the methyl groups can be expressed at interfaces in low energy conformations. Together these two phenomena result in the low surface energies of PDMS. If branching is introduced the mobility of the PDMS is decreased and the surface tensions are observed to increase accordingly.<sup>3</sup>

General Electric developed a convenient shorthand<sup>40</sup> to describe the structure of silicone polymers that I think of as the silicone alphabet. The four letters of the silicone alphabet are shown in Figure 1.4 and represent the four building blocks that can be combined to form silicone polymers: M for monofunctional, D for difunctional, T for trifunctional and Q for tetrafunctional (or quatrafunctional since T is taken). Using this shorthand, PDMS is  $MD_nM$  where  $n$  is the degree of polymerization. Cyclic PDMS oligomers are written as  $D_3$ ,  $D_4$ ,  $D_5$ , and so on. The famous polyhedral oligomeric silsesquioxane (POSS) cube is simply  $T_8$ . Using these four building blocks, an infinite number of silicone skeletal structures can be imagined. Commercially important silicone copolymers include those of MQ, MT, DT and TQ. Chapters 2 and 3 of this thesis will focus on the preparation and properties of MQ copolymers.

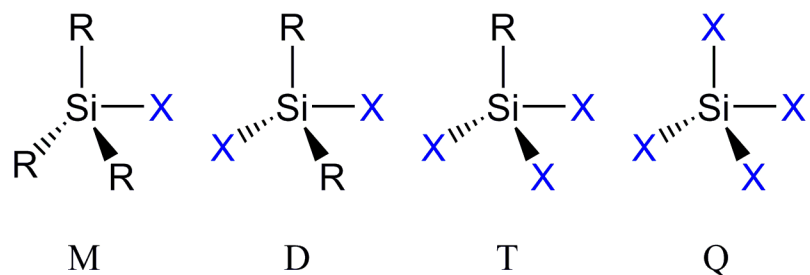


Figure 1.4. Structural components of silicone polymers and shorthand GE nomenclature.<sup>40</sup>

Beyond the diversity in physical structures that can be formed from M, D, T and Q there is even greater diversity in the chemical identity silicones can inherit from the organic substituents (denoted by R in Figure 1.4). Methyl groups are the most commonly encountered organic substituents but hydride, alkane, alkene, alkyne, perfluoroalkane, thiol, amine, phenyl, aryl, epoxy, ionic and zwitterionic functions can be incorporated. The versatility of silicones is infinite. Unfortunately, silicones are relatively unexplored in academic literature.

### 1.5 Ignorance of Silicones

Silicones are technology enabling materials that were invented to fulfill a practical need. Not only do they possess unique properties but they tell an impressive story of curiosity-driven academic research united with pragmatic, applied industrial research. How is it that silicones are not found in materials science or polymer science curricula? Why is this material ignored in the classroom? What keeps modern academic researchers from working in the field? The reasons lay in the historical context of the story of silicones and the very nature of siloxane polymers.

Silicones were invented by two competing industrial powers. This obviously led to trade secrets and limited the early literature concerning silicones to patents. To complicate



matters further, the development of silicones coincided with World War II. The remarkable new silicones, which enabled Allied aircraft to fly higher among other technological advantages, were a national security secret. This held the publication of any silicone related work back until after the war. On top of that, the silicone producers were mandated to work together to support wartime production and thus had temporary access to all silicone patents. After the war, patent lawsuits arose from these relationships that further delayed the release of silicone knowledge.

Even with the knowledge of silicones available, there was little academic interest in them or polymers in general. Materials science was, and in many cases still is, focused on metallurgy, ceramic and semiconductor technologies. Chemistry departments did not yet view polymers as an academic subject. Polymers eventually gained more ground in academic curricula but silicones did not. Carbon-based polymers neatly fit into organic chemistry, general polymer science and even biology curricula. Silicone polymers do not. The inorganic siloxane backbone and unorthodox reactivity excludes them from organic chemistry. The organic substituents exclude them from inorganic chemistry. The oddball properties and behaviors makes them hard to fit into a general polymer science education. So, in the end, silicones are generally ignored in academic curricula and research programs.

## 1.6 Important Reactions in Organosiloxane Polymer Chemistry

The following sections will provide a brief introduction to important chemistries in organosiloxane polymer science. This overview is by no means comprehensive and the interested reader can find additional depth in the provided references. Attention has been paid to chemistries utilized in this thesis to prepare silicone polymers.

### 1.6.1 Hydrolysis and Condensation<sup>2,6,7,14</sup>

The polarization of silicone-halogen bonds and silicon-oxygen bonds leaves the silicon atom susceptible to nucleophilic attack, often by water. Hydrolysis of these bonds results in silanols. Following hydrolysis, the silanols condense producing water and building the siloxane skeleton. The simplest hydrolysis and condensation reaction of an M silane to form MM disiloxane is illustrated in Figure 1.5. In the case of chlorosilanes, these reactions are spontaneous in the presence of water. Hydrolysis occurs rapidly for chlorosilanes and the HCl byproduct acts as a catalyst to speed up condensation. Alkoxysilanes hydrolyze much more slowly than chlorosilanes in the presence of water and are often, but not always, catalyzed by the addition of acid or base. The final products structure and properties will depend heavily on the catalyst used. For example, acid catalysis of tetraethoxysilane produces sols and fractal networks that can be used to produce aerogels, while base catalysis of tetraethoxysilane produces condensed Stöber particles. Hydrolysis and condensation are random processes that can be difficult to control precisely but are cornerstones of silicone preparation.

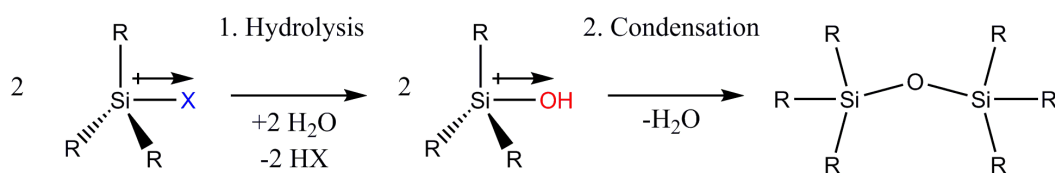


Figure 1.5. Hydrolysis and condensation of a monofunctional silane to yield disiloxane.

The most commonly encountered example of a silicone material prepared by hydrolysis and condensation is the family of one-part RTV silicones found in sealants and caulking. These products are formulated to bond specific materials and function in various working environments but have the same basic chemistry. The chemistry utilizes multifunctional acetoxysilane crosslinkers that hydrolyze and condense when atmospheric

moisture permeates into the silicone upon exposure to air. The byproduct of the hydrolysis, acetic acid, gives these silicones their unique odor upon application and curing.

In addition to the preparative importance of hydrolysis and condensation in silicone chemistry, the reactions are used to modify silica surfaces and are thus critical to surface chemistry. Chlorosilanes in particular are useful for the preparation of monolayers or multilayer from solution or the vapor phase. Fadeev and McCarthy<sup>20-21</sup> developed a thorough understanding of these reactions and the McCarthy group continues to use these reactions to develop new insights into wetting and surface science.

#### 1.6.2 Ring Opening Polymerization<sup>41-43</sup>

The synthesis of linear silicones is most commonly performed via ring opening polymerizations. These processes can be catalyzed by acid or base and can be run under kinetic or thermodynamic control.

Kinetic control grants monodisperse linear polymer of controlled molecular weight and end-group functionality.<sup>44</sup> Lithium reagents are commonly used as strong base initiators and the strained cyclic trimer (hexamethylcyclotrisiloxane, D<sub>3</sub>) must be used as monomer. The polymerization of D<sub>3</sub> with *n*-butyllithium initiator is exhibited in Figure 1.6. Initiation proceeds by the attack of a D<sub>3</sub> molecule by one molecule of lithium reagent which opens the ring and forms a linear lithium silanolate. The linear lithium silanolate trimer is then attacked by 2 more molecules of base to form three monomeric lithium silanolate initiator species.<sup>45</sup> Propagation and growth of the polymer proceeds by ring opening of cyclic trimer monomer. Termination is accomplished by addition of a monofunctional chlorosilane. Termination must be done before monomer is consumed to avoid backbiting

and chain scrambling reactions that lead to equilibrium products. This typically corresponds to 95% conversion.<sup>43,45</sup>

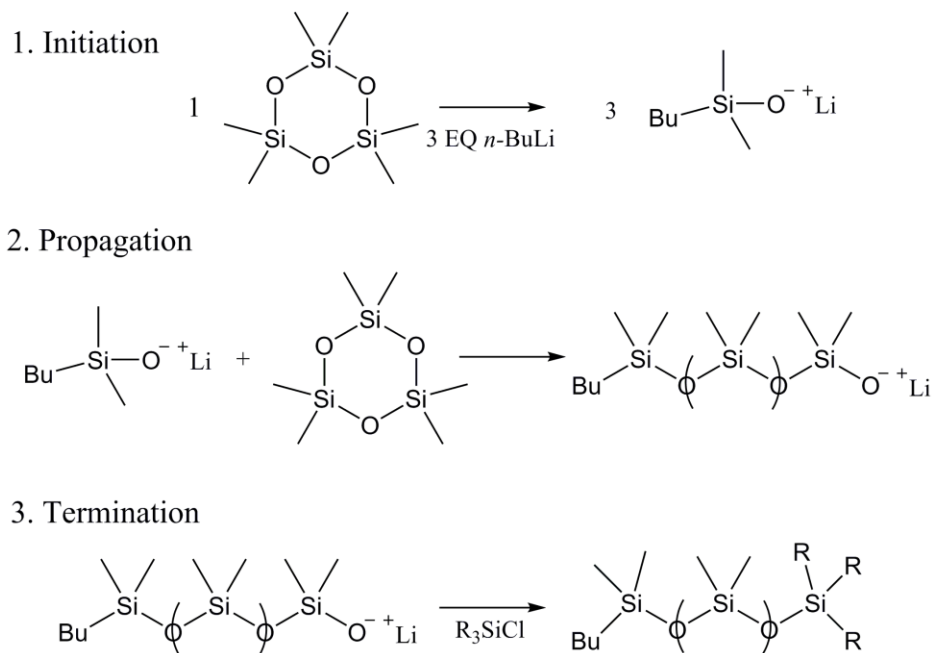


Figure 1.6. Kinetic Ring Opening Polymerization of  $D_3$

Thermodynamic ring opening is the most common and simplest method for preparing linear silicones. Under thermodynamic control the polymer product will have the most probable distribution ( $\bar{D} = 2$ ) and will contain about 18% cyclic oligomer. Acid or base initiators can be used. The inexpensive cyclic tetramer (octamethylcyclotetrasiloxane,  $D_4$ ) is the most common monomer. The polymerization of  $D_4$  into linear polymer is a unique case of an entropically driven polymerization.<sup>46</sup> There is no ring strain in  $D_4$  ( $\Delta H \sim 0$ ) but the increase in conformational entropy upon ring opening to linear polymer is able to drive the reaction ( $\Delta S = 6.7 \text{ J/mol}\cdot\text{K}$ ). End groups are incorporated through end-capping monomers, typically chlorosilanes or disiloxanes. If no end-capping monomer is used the final product will contain silanol end groups. Transient catalysts can be used to leave active end groups that are useful in the preparation of living networks.<sup>35-37</sup> Equilibration

reactions are also used to produce pure cyclic oligomers by 'cracking' of hydrolyzed mixtures of chlorosilanes.<sup>2</sup> The hydrolyzed silanes are mixed with a small amount of KOH catalyst and heated. Pure cyclic D<sub>n</sub> oligomers are separated by distillation from the equilibrating mixture.

### 1.6.3 Pt-catalyzed Hydrosilylation<sup>47</sup>

Hydrosilylation describes the addition of a hydrosilane to substrates containing carbon-carbon double bonds to yield an ethylene linkage between silicon and substrate. While it can be accomplished using radical initiators, the most efficient and commonly used method utilizes a Pt(0) complex, such as Karstedt's catalyst. The reaction requires only parts-per-million catalyst and is selective. This limits the presence of catalyst residues and unwanted byproducts from side reactions which can be problematic in radical hydrosilylation. Hydrosilylation has been used to produce a seemingly infinite number of organic-functional silanes and siloxanes by attaching allyl functional organic moieties to silicon hydrides. The chemistry is also at work in two-part RTV silicone materials.

The most commonly accepted mechanism was proposed in 1965 by Chalk and Harrod<sup>48</sup> and is illustrated in Figure 1.7. There is debate over the nature of the active species with catalytic activity reported for both heterogenous platinum colloids and homogeneous platinum complexes.<sup>49,50</sup>

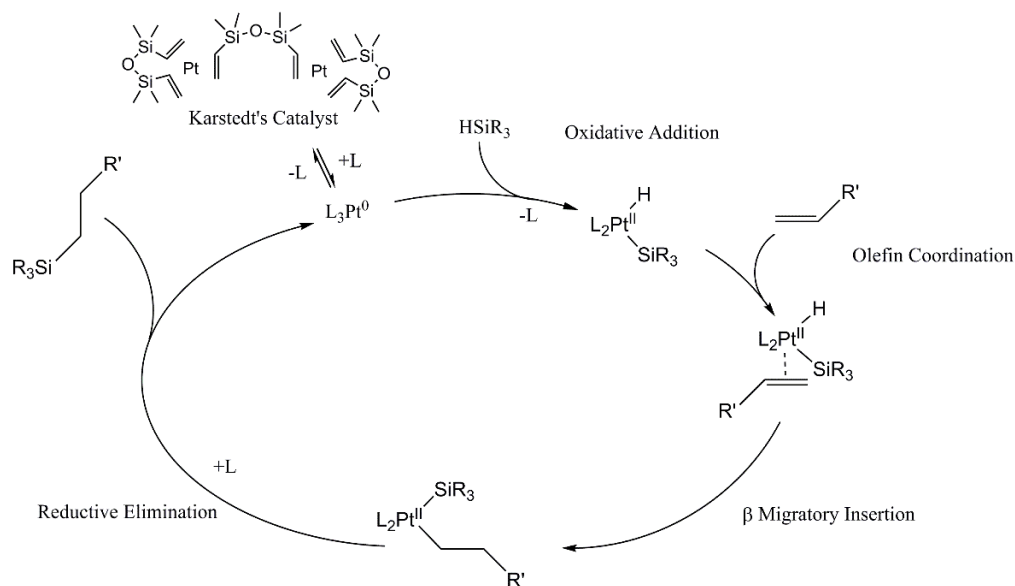


Figure 1.7. Mechanism of Pt(0)-Catalyzed Hydrosilylation.

#### 1.6.4 Piers-Rubinsztajn

The Piers-Rubinsztajn (P-R) reaction forms a siloxane bond from the reaction of silyl hydride and alkoxy silane or silanol using tris(pentafluorophenyl)borane ( $B(C_6F_5)_3$ , BCF) as catalyst. The reaction was named by Michael Brook after Warren E. Piers, who in 1996 reported the BCF-catalyzed hydrosilylation of aromatic aldehydes, ketones, and esters,<sup>51</sup> and Slawomir Rubinsztajn, who in 2005 reported the reaction as a new polycondensation method for preparing siloxane polymers.<sup>52</sup> Many aspects of the reaction are still under investigation and while it has yet to gain widespread popularity as a preparative reaction for making siloxane polymers, there are useful advantages that the reaction provides: rapid rates of reaction, low required catalyst concentrations, easily removable catalyst residues, and typically inert byproducts. Michael Brook has studied the details of and made extensive use of this reaction to prepare dendrimers, surfactants and networks.<sup>53-58</sup>

The mechanism of BCF-catalyzed hydrosilylation was studied in detail with organic substrates by Piers<sup>58,59</sup> and in alkoxy silane substrates by Rubinsztajn.<sup>60</sup> The mechanism discussed here and shown in Figure 1.8 reflects the work of Rubinsztajn, although most of the mechanistic details are the same. In a system containing silane ( $R_3SiH$ ) and alkoxy silane ( $R'_3SiOR''$ ), spectroscopic evidence and simulations have shown that BCF catalyst first forms a weak complex with the hydride atom of the silane ( $\phi^F_3B-H-SiR_3$ ). The silicon atom of the silane is now more positive and undergoes nucleophilic attack by silylether oxygen of the alkoxy silane. This forms an oxonium ion and  $H(B(C_6F_5)_3)$  which form a salt-like intermediate containing both reactants and catalyst. The hydride is then transferred to any of the three nearby electrophiles bound to the oxonium ion. This hydride transfer results in the formation of three products: regenerated starting substrates, silane metathesis, or disiloxane. In this reaction disiloxane formation is irreversible while the other routes are reversible so the final equilibrium product is disiloxane.

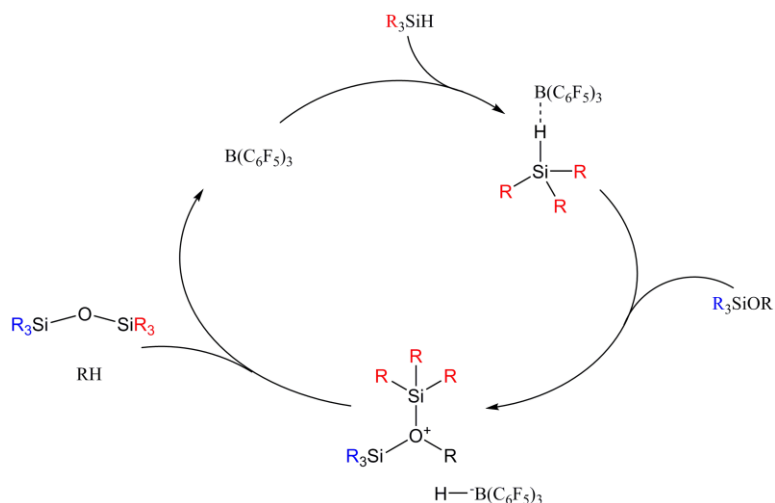


Figure 1.8. Mechanism of Tris(pentafluorophenyl)borane ( $B(C_6F_5)_3$ ) – catalyzed siloxane bond formation between hydrosilane and alkoxy silane or silanol.

Due to the strong Lewis acidity of BCF the reaction is not compatible with Lewis base-containing substrates and must be done in the absence of water. Grande *et.al.*<sup>53</sup> studied the reaction's tolerance to various functional alkoxy silanes. Amino groups

completely suppress any reaction with silane, epoxy rings are opened and thiols react competitively for reaction with alkoxy groups. Halogen-containing silanes and silanes containing unsaturation were found to be compatible with the P-R reaction.

The downside of the P-R reaction is the rapid rate at which it proceeds and produces gas byproducts. This results in vigorous bubbling of reaction mixtures which requires adequate outgassing capabilities. In the case of network formation this almost always results in foam formation with little control over pore size and distribution. Water sensitivity, metathesis reactions and hydride transfer oligomerization<sup>61,62</sup> reactions can lead to additional complications.

## 1.7 Silicones at Interfaces

Since their invention, organosiloxanes have been recognized for their interfacial activity. Stock observed that the 20 mg of PDMS he synthesized coated glass and was hydrophobic. Winton Patnode observed that paper products in the methylchlorosilane pilot plant became hydrophobic from exposure to methylchlorosilane vapors. Silicone residues were not only hydrophobic but were observed to destabilize foams and emulsions. What is most remarkable about siloxanes at interfaces is their ability to perform in seemingly contradictory roles: they are foam stabilizers and defoaming agents, emulsifiers and de-emulsifiers, release coatings and pressure sensitive adhesives. How a siloxane behaves will depend on its chemical structure, physical structure and the characteristics of the interface. Here we will consider three interfaces for which examples of silicone surface activity will be discussed: Air-Water, Oil-Water and Solid-Air.



### 1.7.1 PDMS at the Air-Water Interface

*“Insoluble monolayers are strange things.”*

- George L. Gaines Jr.<sup>63</sup>

The air-water interface is a specific example of a vapor-liquid interface. The air-water interface was first studied in a scientifically rigorous way by Irving Langmuir (see references 64-74 for a selection of Langmuir’s monumental work). Langmuir won the Nobel Prize in Chemistry in 1932 for his studies and investigations into surface chemistry, specifically on his work regarding fatty acid monolayers on water.<sup>64</sup> He hypothesized that water insoluble fatty acids adsorb to the water interface through their polar head groups to form molecular monolayers. This is in contrast to insoluble hydrocarbons that form a lens on water. Langmuir devised the Langmuir Trough to study these molecular monolayers at the air-water interface. Using his trough, Langmuir could compress monolayers to probe their structures, and by using simple geometric calculations could accurately predict molecular configurations before spectroscopy techniques were available. Langmuir also investigated the nature of chemical bonding and the dissociation of molecular hydrogen. Katherine Blodgett, Langmuir’s direct assistant, developed a technique to transfer monolayers from the air-water interface onto substrates.<sup>72-74</sup> The technique is now commonly referred to as Langmuir-Blodgett deposition. Besides their work on surface chemistry, Langmuir and Blodgett laid the foundations of plasma physics, developed anti-reflective coatings and worked on GE technologies to help the Allied forces during World War II. Blodgett, who was indispensable to Langmuir’s work, was not only the first female research scientist at the GE research lab but also the first female to be awarded a doctorate in physics from Cambridge University.

Typical measurements of monolayers using Langmuir troughs involve first spreading the adsorbate molecules from a dilute solution of volatile solvent onto a clean

water surface. Common spreading solvents are chloroform and hexanes. The molecules must be soluble in the spreading solvent and the solvent is typically immiscible with water. The choice of spreading solvent can affect monolayer formation and properties so it is common to experiment with solvent selection to achieve the best monolayer formation. Once adsorbate solution is spread, solvent is evaporated and the adsorbed monolayer is given time to equilibrate. Pressure-area isotherms are the most common experiment used to study the properties of monolayers. In these experiments, the monolayer is compressed at a constant rate by barriers at the water surface and the surface pressure is measured. Surface pressure is the difference between the surface tension of the clean water/liquid interface and the measured surface tension. Changes in surface pressure correspond to changes in the structure of the monolayer. In the early stages of the experiment, where the trough area is large, the molecules are in a two-dimensional gas phase and are capable of free diffusion on the water surface. In this region, the measured surface pressure is zero. As the area of the trough decreases during compression, the molecules will form a complete monolayer and the surface pressure will increase. With further compression, the surface pressure – area relationship will depend on the properties of the monolayer. Small molecule monolayers exhibit a rich two-dimensional phase space where crystallization and phase transitions can be observed in pressure-area data. In polymers, the behavior is simpler. Polymer monolayers are typically classified as condensed (rigid, sharp pressure rise) or expanded (fluid, gradual pressure rise). Collapse of polymer monolayers is observed when surface pressure plateaus or decreases during compression, and can correspond to multilayer formation or expulsion of polymer from the monolayer into the water subphase.<sup>63</sup>

The methods developed by Langmuir to study insoluble molecular monolayers adsorbed to the air-water interface have been extended to other vapor-liquid interfaces

and adsorbates. Not all molecules and polymers will adsorb to the air-water interface to form a monolayer. In the case of small molecules, they must be insoluble in the water subphase, have some attractive group to anchor them to the surface, be stable in air and nonvolatile. In polymers, if the monomers have a finite adsorption affinity for the interface, then it is possible to form monolayers even of water soluble polymers, like proteins. Water-insoluble polymers can form monolayers if there are sufficient attractive groups present in the chemical structure, similar to small molecules adsorbates. Perhaps unsurprisingly, silicone polymers, with all their strange behaviors, spread to form monolayers on the air-water interface.

The first studies of linear siloxane polymers at the air-water interface were reported by Zisman and coworkers.<sup>75</sup> PDMS in particular had interesting collapse behavior which was suggested to arise from the formation of a PDMS helix, similar to that of the PDMS crystalline phase, at the interface. These studies have been followed up by numerous researchers using a variety of techniques in an attempt to understand the molecular structure of PDMS at the air-water interface.<sup>76-80</sup> It is now generally agreed that PDMS undergoes a layering transition that results in its collapse behavior. Adsorption of PDMS to the air-water interface involves the attractive interaction of the polar siloxane backbone with the water subphase and the expression of low energy methyl groups at the interface to lower surface energy. When a complete PDMS monolayer is compressed, the chains rearrange so that the oxygen atoms of the backbone are adsorbed to the water surface and the freely rotating methyl groups are sticking out into the air. Further compression leads to the formation of odd numbered layers. This description is based on Vibrational Sum Frequency Spectroscopy and is illustrated in Figure 1.9.<sup>79</sup>

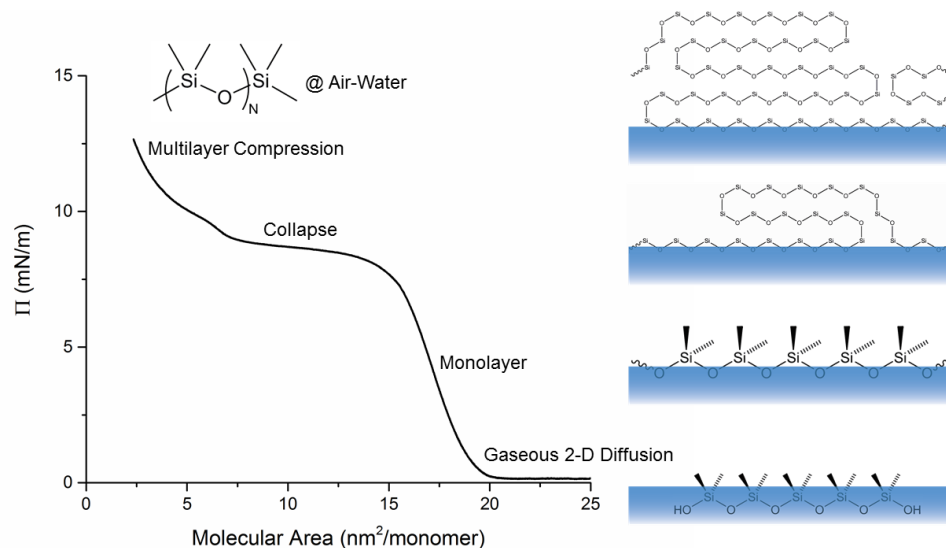


Figure 1.9. PDMS at the air-water interface.<sup>79</sup> Each regime of the pressure-area isotherm is labeled and illustrated. At high areas, the siloxane chains diffuse freely at the water interface with methyl groups predominantly expressed at the surface. As area decreases, PDMS molecules impinge upon one another and a monolayer forms. In the monolayer, backbone oxygens adsorb to the air-water interface with one methyl oriented normal to the water surface and the other in the plane of the water surface. At a surface pressure of about 8 mN/m, the PDMS monolayer collapses by forming multi-layered structures. Further compression increases the number of collapsed layers.

The adsorption of PDMS to the air-water, and to air-oil interfaces, is important in defoaming. PDMS migrates and adsorbs to the interface, dramatically lowering the surface tension so that foam bubbles collapse. Typical anti-foaming silicone formulations use linear PDMS polymers adsorbed to fumed particles. By adsorbing PDMS onto high surface area silica, the thin layer of PDMS can spread more rapidly than if it is deposited as a bulk liquid.

### 1.7.2 Silicone Surfactants at the Oil-Water Interface

Silicone surfactants<sup>81</sup> were first developed in the 1950's at Union Carbide for the stabilization of polyurethane foams. In silicone surfactants, the low surface energy, hydrophobic silicone is paired with a hydrophilic group. Although the hydrophilic-hydrophobic structure is similar to hydrocarbon surfactants, silicone surfactants generate

greater reductions in interfacial tensions and can stabilize organic dispersions. The first silicone surfactants were linear and branched PDMS-PEO block copolymers. PEO is still the most common hydrophile incorporated into silicone surfactants but ionic and zwitterionic hydrophiles are also available. The mechanism of action involves the strong adsorption affinity of siloxanes to interfaces to lower surface tension and the anchoring of the siloxane to the interface by hydrophilic groups. This anchoring is what sets silicone emulsifiers and foam stabilizers apart from defoaming agents. Without the anchoring groups present, PDMS chains will adsorb and spread on interfaces to lower the surface tension, as discussed in the previous section. The continued spreading of the PDMS at the interface destroys foams and emulsions.

Other special silicone surfactants are the trisiloxane superspreaders<sup>82,83</sup> and trisilanol-POSS.<sup>84</sup> Superspreaders are T siloxanes with PEO tails that enable the rapid spreading of aqueous solutions. They are commonly applied in agricultural applications to assist wetting of fertilizer and pesticide solutions onto plant leaves. Trisilanol-POSS is an amphiphilic POSS molecule. One corner of the  $T_8$  cube is removed to make  $T_7^{(OH)_3}$ . The localized hydrophilic silanols promote adsorption to water interfaces while the alkyl groups on each T corner provide hydrophobicity.

One way in which the action of surfactants is observed is in measurements of oil-water interfacial tension using drop tensiometry, as illustrated in Figure 1.10. In oil-water drop tensiometry, a water droplet is suspended in a stationary organic liquid phase (alternatively, an organic liquid drop can be suspended in a stationary water phase). A camera captures the images of the droplet and from the shape of the droplet (which is assumed to be axisymmetric), interfacial tension is calculated using the Young-Laplace

equation. To analyze kinetics of adsorption and the equilibrium surface tension reduction, the interfacial tension is measured as a function of time.

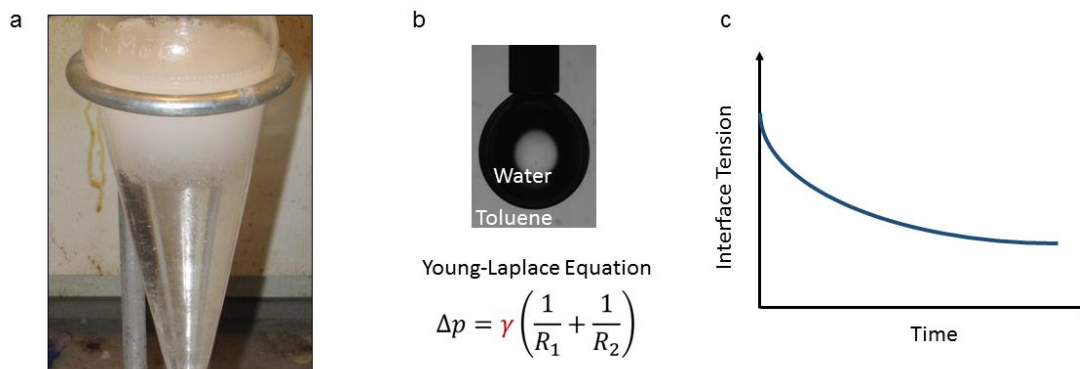


Figure 1.10. Drop tensiometry is one way to quantify surfactancy at oil-water interfaces. (a) An emulsion is observed during the aqueous rinse step in a work up procedure which suggests oil-water interface activity. (b) In a tensiometry experiment, a drop of water is suspended from a flat-tipped, cylindrical needle into an organic ambient solution which contains the surface active molecule being investigated. The drop is imaged, the profile of the drop is fitted by software and the Young-Laplace equation is used to calculate interfacial tension. (c) The interfacial tension is measured as a function of time. For a surface active molecule, the cartoon plot illustrates the drop in surface pressure as the molecules cover the interface to reduce interface tension. Kinetic (rate) and thermodynamic information can be gained from such experiments.

### 1.7.3 Silane and Siloxane Monolayers: Wetting and Contact Angle Hysteresis

The importance of silanes and silicones to surface science cannot be understated. Reactive alkylsilanes enable the preparation of self-assembled monolayers<sup>19</sup>, randomly-attached monolayers, vertically polymerized brushes and three-dimensionally polymerized networks.<sup>20,21</sup> Precise surfaces from these reagents has enabled surface science to flourish. The importance and behavior of smooth silane-derived surfaces is discussed in Chapter 6 and in the provided references. The focus for this introduction will be the hydrophobicity of silicone polymers, the properties of the siloxane bond that enable this behavior and how hydrophobicity is measured.

Before discussing hydrophobicity in silicone polymers, we must first define what 'hydrophobic' means.<sup>85-89</sup> This may seem simple at first: a hydrophobic surface isn't wet by water. But as emphasized by McCarthy and Gao, such 'simple' words and definitions can be confusing and even destructive.<sup>87</sup> A more appropriate perspective on hydrophobicity requires contact angle hysteresis. Contact angle hysteresis,  $\Delta$ , is the difference between the advancing,  $\theta_A$ , and receding,  $\theta_R$ , contact angle of a liquid on a surface. What are the advancing and receding angles? When water is added to a droplet resting on a surface, it will grow at a constant contact area until the three phase contact line reaches the advancing contact angle. Once the advancing contact angle is reached, the contact line will advance at a constant angle and the contact area will increase. The constant angle with which the droplet advances is the advancing contact angle. When water is removed from a liquid drop resting on a surface, it will shrink at a constant contact area until the receding contact angle is reached. Once the receding angle is reached, the contact line will recede at a constant angle and the contact area will decrease. The constant angle with which the droplet recedes is the receding contact angle. These processes are depicted in Figure 1.11. The difference between the advancing and receding contact angles, the contact angle hysteresis, truly indicates how 'hydrophobic' a surface is.

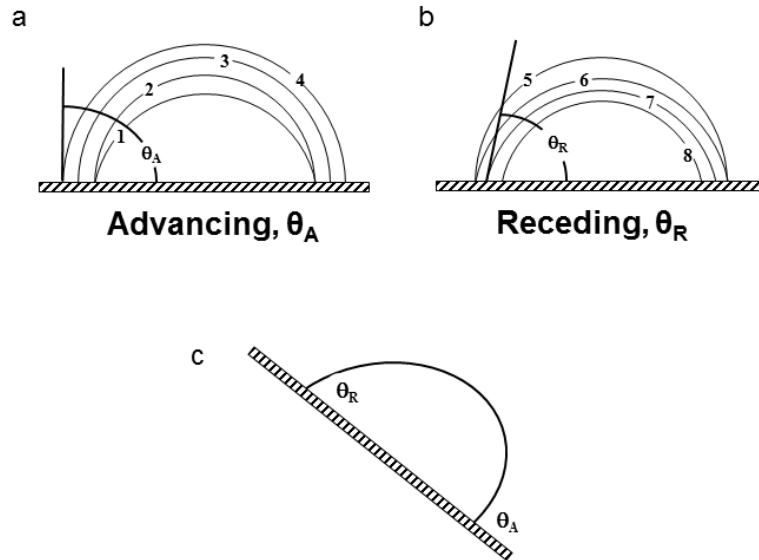


Figure 1.11. Two-dimensional graphic depiction of a water drop on a surface with contact angle hysteresis. (a) The advancing contact angle of a water droplet is reached as its volume increases from the addition of water. Trace 1 shows the initial configuration of the droplet. Water condenses and the drop volume increases at constant contact area until the advancing contact angle is reached in Trace 2. As more water condenses the drop volume increases by increasing the contact area with constant contact angle (Traces 3 and 4). (b) The receding angle of a water droplet is reached as its volume decreases from the removal of water. Trace 5 shows the initial configuration of the droplet. Water evaporates and the drop volume decreases at constant contact area until the receding contact angle is reached in Trace 6. As more water evaporates the drop volume decreases by decreasing the contact area with constant contact angle (Traces 7 and 8). (c) A droplet on an inclined surface can slide when the leading edge reaches the advancing contact angle and the trailing edge reaches the receding angle.

A simple thought experiment can help illustrate the importance of contact angle hysteresis. Imagine two surfaces **A** and **B** (Figure 1.12). Surface **A** has water contact angles of  $\theta_A/\theta_R = 80^\circ/80^\circ$ . Surface **B** water contact angles of  $\theta_A/\theta_R = 120^\circ/80^\circ$ . Now imagine that both surfaces are perfectly flat and a drop of water is placed on each. The *static* contact angle measured in this experiment will be  $80^\circ$  for Surface **A** and will be *anywhere* between  $80^\circ$  and  $120^\circ$  for Surface **B**. Let us assume its  $100^\circ$  for Surface **B**. At a glance, we may be tempted to say that Surface **B** is more hydrophobic as it has the higher contact angle. Now consider what happens when the surfaces are tilted  $1^\circ$ . The drop on Surface **B** will deform but stay pinned to the substrate while the droplet on Surface



**A** will immediately slide off because there is no contact angle hysteresis. If we continue to tilt the stage, the droplet on Surface **B** will be pinned and unable to move across the surface until the leading edge reaches the advancing angle of  $120^\circ$  and the trailing edge reached the receding angle of  $80^\circ$ . It is obvious that Surface **A** more easily expels water than Surface **B** although higher static angles can be measured on Surface **B**.

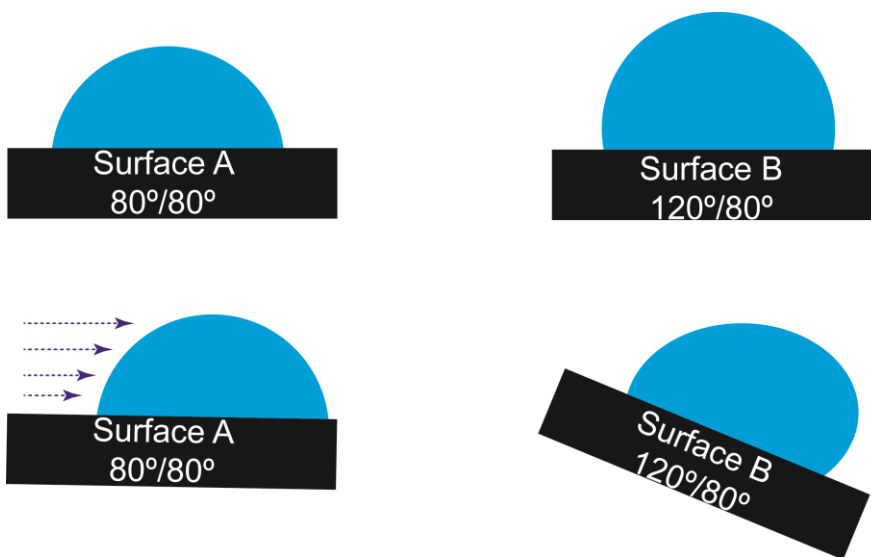


Figure 1.12. Surface **A** has no contact angle hysteresis and a drop will immediately slide off once the surface is tilted away from horizontal. Surface **B** has higher contact angles but significant hysteresis. The drop on Surface **B** will not slide off until the surface is tilted, the drop deforms, and the advancing and receding contact angles are reached.

Contact angle hysteresis is governed by motion of the contact line over a surface. It is sensitive to molecular scale roughness and surface defects. Minimization of contact angle hysteresis requires dynamic contact lines that easily transition from metastable advancing and receding events, and a contact line that is always simultaneously advancing and receding would have no hysteresis. Achieving such dynamic contact lines on smooth surfaces requires a surface with liquid-like molecular mobility. PDMS, due its extreme flexibility and conformational freedom, is able to achieve this. There are numerous examples of smooth PDMS grafts on smooth silicon wafers that exhibit

remarkably low contact angle hysteresis.<sup>90-96</sup> These will be discussed in more detail in Chapter 6.

## 1.8 Rediscovering and Discovering Silicones

Over the last decade, the McCarthy group has investigated the chemistry and properties of silicones. Much of this work has been a process of “rediscovering” silicones. Unearthing previous knowledge from patents and publications, but with an emphasis on addressing modern polymer materials science challenges. These goals have coincided with a goal of educating and inspiring the scientific community regarding the diversity and special behavior of silicone polymers. Work along the lines of rediscovering silicones is pursued in this thesis. These objectives have not only reminded the scientific community of silicones but have also provided the scientific community with new insights into silicones. However, it is also time to discover silicones. The process of discovery is certainly more challenging but the silicone alphabet offers an infinite number of possibilities. Creating a toolbox of silicones enables materials scientists to tackle challenges where carbon-based polymers and current silicone materials fail. The work in the following chapters aims to accomplish both of these tasks: rediscovery of MQ silicones, the discovery of a special synergy between carbon nanotubes and silicones, and the exploration of wetting of methylsilicone polymers using a newly discovered surface modification inspired by the Piers-Rubinsztajn reaction.

## 1.9 References

1. Clarson, S. J.; Semlyen, J. A. *Siloxane Polymers*. Prentice Hall: Englewood Cliffs, **1993**.
2. Rochow, E. G. *Silicon and Silicones*. Springer-Verlag: Berlin; New York, **1987**.
3. Liebhafsky, H. A. *Silicones Under the Monogram*. J. Wiley & Sons: New York, **1978**.

4. Seyferth D. Dimethyldichlorosilane and the Direct Synthesis of Methylchlorosilanes. The Key to the silicones Industry. *Organometallics* **2001**, *20*, 4978-4992.
5. Butts, M.; Cella, J.; Wood, C. D.; Gillette, G.; Kerboua, R.; Leman, J.; Lewis, L.; Rubinsztajn, S.; Schattenmann, F.; Stein, J.; Wicht, D.; Rajaraman, S.; Wengrovius, J. Silicones. In *Kirk-Othmer Encyclopedia of Chemical Technology*, Wiley & Sons: New York, 2006; Vol. 22, pp 547-626.
6. Noll W. *Chemistry and Technology of Silicones*. Academic Press: New York; London, **1968**.
7. Brook, M. A. *Silicon in Organic, Organometallic, and Polymer Chemistry*. Wiley-Interscience, John Wiley & Sons: New York, **2000**.
8. Berzelius, J. J. *Ann. Phys. Chem.* **1824**, *1*, 169.
9. Sainte-Claire Deville, H. E. *Compt. Rend. Acad. Sci.* **1854**, *39*, 321.
10. Moissan, H. *Bull. Soc. Chim. Fr.* **1895**, *13*, 972.
11. Pauling, L. The Nature of the Chemical Bond. IV. The Energy of Single Bonds and the Relative Electronegativity of Atoms. *J. Am. Chem. Soc.* **1932**, *54*, 3570-3582.
12. Fadeev, A. Y.; McCarthy, T. J. A New Route to Covalently Attached Monolayers: Reaction of Hydridosilanes with Titanium and Other Metal Surfaces. *J. Am. Chem. Soc.* **1999**, *121*, 12184-12185.
13. Carter, C. B.; Norton, M. G. *Ceramic Materials Science and Engineering*. Springer: New York. **2007**.
14. Iler, R. K. *The Chemistry of Silica*. John Wiley & Sons: New York, **1979**.
15. Brinker, C. J.; Scherer, G. W. *Sol-Gel Science: The Physics and Chemistry of Sol-Gel Processing*. Academic Press: Boston **1990**.
16. Stöber, W.; Fink, A. Controlled growth of monodisperse silica spheres in the micron size range. *J. Colloid Interface Sci.* **1968**, *26*, 62-69.
17. Hildebrand, M. Diatoms, Biomineralization Processes, and Genomics. *Chem. Rev.* **2008**, *108*, 4855-4874.
18. Plueddemann, E. P. *Silane Coupling Agents*, 2nd ed.; Plenum: New York, **1991**.
19. Ulman, A. Formation and Structure of Self-Assembled Monolayers. *Chem. Rev.* **1996**, *96*, 1533-1554.
20. Fadeev A. Y.; McCarthy, T. J. Trialkylsilane Monolayers Covalently Attached to Silicon Surfaces: Wettability Studies Indicating that Molecular Topography Contributes to Contact Angle Hysteresis. *Langmuir* **1999**, *15*, 3759-3766.
21. Fadeev, A. Y.; McCarthy, T. J. Self-Assembly Is Not the Only Reaction Possible between Alkyltrichlorosilanes and Surfaces: Monomolecular and Oligomeric Covalently Attached Layers of Dichloro- and Trichloroalkylsilanes on Silicon. *Langmuir* **2000**, *16*, 7268-7274.
22. Friedel, C.; Crafts, J. M. *Ann.* **1863**, *127*, 28.
23. Ladenburg, A. *Ann.* **1872**, *164*, 390.

24. Kipping, F. S.; Lloyd, L. L. *J. Chem. Soc.*, **1901**, 79, 449-459.
25. Post, H. W. *Silicones and Other Organosiloxane Compounds*. Reinhold: New York, **1949**.
26. Stock, A.; Somieski, C. *Ber. Dtsch. Chem. Ges.* **1919**, 52, 695.
27. Kipping, F. S. Organic Derivatives of Silicon. *Proc. R. Soc. (London)* **1937**, 159, 136-148.
28. Hyde J. F.; DeLong, R. C. Condensation Products of the Organo-silane Diols. *J. Am. Chem. Soc.* **1941**, 63, 1194-1196.
29. Rochow, E. G.; Gilliam, W. F. Polymeric Methyl Silicon Oxides. *J. Am. Chem. Soc.* **1941**, 63, 798-800.
30. Rochow, E. G. Preparation of Organosilicon Halides. US Pat. 2,380,995, Aug. 7, 1945.
31. Rochow, E. G. The Direct Synthesis of Organosilicon Compounds. *J. Am. Chem. Soc.* **1945**, 67, 963-965.
32. Müller, R. *Chem. Tech.* **1950**, 2, 41.
33. Mark, J. E. Some Interesting Things About Polysiloxanes. *Acc. Chem. Res.* **2004**, 37, 946-953.
34. Owen, M. J. Why Silicones Behave Funny. *Chemtech.* **1981**, 11, 288-292.
35. Kantor, S. W.; Grubb, W. T.; Osthoff, R. C. The Mechanism of the Acid- and Base-catalyzed equilibration of Siloxanes. *J. Am. Chem. Soc.* **1954**, 76, 5190-5197.
36. Gilbert, A. R.; Kantor, S. W. Transient catalysts for the polymerization of organosiloxanes. *J. Polym. Sci.* **1959**, 40, 35-58.
37. Zheng, P.; McCarthy T. J. A Surprise from 1954: Siloxane Equilibration is a Simple, Robust, and Obvious Polymer Self-Healing Mechanism. *J. Am. Chem. Soc.* **2012**, 134, 2024-2027.
38. Johnson, D. H.; McLoughlin, J. R.; Tobolsky, A. V. Chemorheology of some specially prepared silicone rubbers. *J. Phys. Chem.* **1954**, 58, 1073-1075.
39. Osthoff, R. C.; Bueche, A. M.; Grubb, W. T. Chemical stress-relaxation of polydimethylsiloxane elastomers. *J. Am. Chem. Soc.* **1954**, 76, 4659-4663.
40. Hurd, C. B. Studies on Siloxanes. I. The Specific Volume and Viscosity in Relation to Temperature and Constitution. *J. Am. Chem. Soc.* **1946**, 68, 364-370.
41. Chojnowski, J.; Cypryk, M. in *Silicon-containing polymers*, Jones, R. G.; Ando, W.; Chojnowski, J.; Kluwer Acad. Publ.: Dordrecht, **2000**.
42. Chojnowski, J. Ring-opening Polymerization of Cyclosiloxanes in *Silicon Compounds: Silanes and Silicones*. 3<sup>rd</sup> ed. Gelest, Inc.
43. Maschke, U.; Wagner, T. Synthesis of high-molecular-weight poly(dimethylsiloxane) of uniform size by anionic polymerization, 1. Initiation by a monofunctional lithium siloxanolate. *Makromol. Chem.* **1992**, 193, 2453-2466.

44. Goff, J.; Sulaiman, S.; Arkles, B.; Lewicki, J. P. Soft materials with recoverable shape factors from extreme distortion states. *Adv. Mater.* **2016**, *28*, 2393-2398.
45. Frye, C. L.; Salinger, R. M.; Fearon, F. W. G.; Klosowski, J. M.; DeYoung T. Reactions of Organolithium Reagents with Siloxane Substrates. *J. Org. Chem.* **1970**, *35*, 1308-1314.
46. Odian, G. *Principles of Polymerization*. Wiley-Interscience: Hoboken, **2004**.
47. Marciniac, B. *Hydrosilylation: A Comprehensive Review on Recent Advances*. Springer
48. Chalk, A. J.; Harrod, J. F. Homogeneous Catalysis. II. The Mechanism of the Hydrosilylation of Olefins Catalyzed by Group VIII Metal Complexes. *J. Am. Chem. Soc.* **1965**, *87*, 16-21.
49. Stein, J.; Lewis, L. N.; Gao, Y.; Scott, R. A. In Situ Determination of the Active Catalyst in Hydrosilylation Reactions Using Highly Reactive Pt(0) Catalyst Precursors. *J. Am. Chem. Soc.* **1999**, *121*, 3693-3703.
50. Galeandro-Diamont, T.; Zanota, M.; Sayah, R.; Veyre, L.; Nikitine, C.; Bellefon, C.; Marrot, S.; Meille, V.; Thieduleux, C. Platinum nanoparticles in suspension are as efficient as Karstedt's complex for alkene hydrosilylation. *Chem. Commun.* **2015**, *51*, 16194-16196.
51. Parks, D. J.; Piers, W. E. Tris(pentafluorophenyl)boron-Catalyzed Hydrosilylation of Aromatic Aldehydes, Ketones, and Esters. *J. Am. Chem. Soc.* **1996**, *118*, 9440-9441.
52. Rubinsztajn, S.; Cella, J. A. A New Polycondensation Process for the Preparation of Polysiloxane Copolymers. *Macromolecules* **2005**, *38*, 1061-1063.
53. Grande, J. B.; Thompson, D. B.; Gonzaga, F.; Brook, M. A. Testing the functional tolerance of the Piers-Rubinsztajn reaction: a new strategy for functional silicones. *Chem. Commun.* **2010**, *46*, 4988-4990.
54. Grande, G. B.; Gonzaga, F.; Brook, M. A. Rapid assembly of explicit, functional silicones. *Dalton Trans.* **2010**, *39*, 9369-9378.
55. Grande, G. B.; Urlich, T.; Dickie, T.; Brook, M. A. Silicone dendrons and dendrimers from orthogonal SiH coupling reactions. *Polym. Chem.* **2014**, *5*, 6728-6739.
56. Zhang, J.; Chen, Y.; Brook, M. A. Reductive Degradation of Lignin and Model Compounds by Hydrosilanes. *ACS Sustainable Chem. Eng.* **2014**, *2*, 1983-1991.
57. Zhang, J.; Chen, Y.; Sewell, P.; Brook, M. A. Utilization of softwood lignin as both crosslinker and reinforcing agent in silicone elastomers. *Green Chem.* **2015**, *17*, 1811-1819.
58. Chadwick, R. C.; Grande, J. B.; Brook, M. A.; Adronov, A. Functionalization of Single-Walled Carbon Nanotubes via the Piers-Rubinsztajn Reaction. *Macromolecules* **2014**, *47*, 6527-6530.
59. Parks, D. J.; Blackwell J. M.; Piers W. A. Studies on the Mechanism of B(C<sub>6</sub>F<sub>5</sub>)<sub>3</sub>-Catalyzed Hydrosilylation of Carbonyl Functions. *J. Org. Chem.* **2000**, *65*, 3090-3098.

60. Piers, W. E.; Marwitz, A. J. V.; Mercier, L. G. Mechanistic Aspects of Bond Activation with Perfluoroarylboranes. *Inorg. Chem.* **2011**, *50*, 12252-12262.
61. Chojnowski, J.; Rubinsztajn, S.; Cella, J. A.; Fortuniak, W.; Cypriak, M.; Kurjata, J.; Kaźmierski, K. Mechanism of the  $B(C_6F_5)_3$ -Catalyzed Reaction of Silyl Hydrides with Alkoxysilanes. Kinetic and Spectroscopic Studies. *Organometallics* **2005**, *24*, 6077-6084.
62. Chojnowski, J.; Fortuniak, W.; Kurjata, J. Oligomerization of Hydrosiloxanes in the Presence of Tris(pentafluorophenyl)borane. *Macromolecules* **2006**, *39*, 3802-3807.
63. Chojnowski J.; Kurjata J.; Fortuniak W.; Rubinsztajn S.; Trzebicka B. Hydride Transfer Ring-Opening Polymerization of a Cyclic Oligomethylhydrosiloxane. Route to a Polymer of Closed Multicyclic Structure. *Macromolecules* **2012**, *45*, 2654-2661.
64. Gaines, G. L. Insoluble Monolayers at Liquid-Gas Interfaces. Interscience Publishers: New York, **1966**.
65. Langmuir, I. *Surface Chemistry*. Nobel Lecture. **1932**.
66. Langmuir, I. Constitution and fundamental properties of solids and liquids. Part I. Solids. *J. Am. Chem. Soc.* **1916**, *38*, 2221-2295.
67. Langmuir, I. Constitution and fundamental properties of solids and liquids. Part II. Liquids. *J. Am. Chem. Soc.* **1917**, *39*, 1848-1906.
68. Langmuir, I. The adsorption of gases on plane surfaces of glass, mica, and platinum. *J. Am. Chem. Soc.* **1918**, *40*, 1361-1403.
69. Langmuir, I. Surface Chemistry. *Chem. Rev.* **1933**, *13*, 147-191.
70. Langmuir, I.; Langmuir, D. B. The Effect of Monomolecular Films on the Evaporation of Ether Solutions. *J. Phys. Chem.* **1927**, *31*, 1719-1731.
71. Langmuir, I. Oil Lenses on water and the nature of monomolecular expanded films. *J. Chem. Phys.* **1933**, *1*, 756-776.
72. Langmuir, I. Composition of fatty acid films on water containing calcium or barium salts. *J. Am. Chem. Soc.* **1936**, *58*, 284-287.
73. Blodgett, K. B. Monomolecular films of fatty acids on glass. *J. Am. Chem. Soc.* **1934**, *56*, 495-495.
74. Blodgett, K. B. Films built by depositing successive monomolecular layers on a solid surface. *J. Am. Chem. Soc.* **1935**, *57*, 1007-1022.
75. Blodgett, K. B.; Langmuir, I. Built-up films of barium stearate and their optical properties. *Phys. Rev.* **1937**, *51*, 0964-0982.
76. Fox, H. W.; Taylor, P. W.; Zisman, W. A. Polyorganosiloxanes....Surface Active Properties. *Ind. Eng. Chem.* **1947**, *39*, 1401-1409.
77. Mann, E. K.; Langevin D. Poly(dimethylsiloxane) Molecular Layers at the Surface of Water and of Aqueous Surfactant Solutions. *Langmuir* **1991**, *7*, 1112-1117.

78. Hahn, T. D.; Hsu, S. L.; Stidham, H. D. Reflectance Infrared Spectroscopic Analysis of Polymers at the Air-Water Interface. 4. Microstructure of Poly(dimethylsiloxane). *Macromolecules* **1997**, *30*, 87–92.
79. Kim, C.; Gurau, M. C.; Cremer, P. S.; Yu, H. Chain Conformation of Poly(dimethyl siloxane) at the Air/Water Interface by Sum Frequency Generation. *Langmuir* **2008**, *24*, 10155–10160.
80. Bernardini, C.; Stoyanov, S. D.; Cohen Stuart, M. A.; Arnaudov, L. N.; Leermakers, F. A. M. PMMA Highlights the Layering Transition of PDMS in Langmuir Films. *Langmuir* **2011**, *27*, 2501–2508.
81. Lenk, T. J.; Lee, D. H. T.; Koberstein, J. T. End Group Effects on Monolayers of Functionally-Terminated Poly(dimethylsiloxanes) at the Air-Water Interface. *Langmuir* **1994**, *10*, 1857–1864.
82. Petroff, L.; Snow, S. A. Silicone Surfactants in *Silicone Surface Science*. Springer: Dordrecht, **2012**.
83. Stoebe, T.; Lin, Z.; Hill, R. M.; Ward, M. D.; Ted David H. Surfactant-Enhanced Spreading. *Langmuir* **1996**, *12*, 337-344.
84. Churaev, N. V.; Esipova, N. E.; Hill, R. M.; Sobolev V. D.; Starov, V. M.; Zorin Z. M. The Suprespreading Effect of Trisiloxane Surfactant Solutions. *Langmuir* **2001**, *17*, 1338-1348.
85. Deng, J.; Polidan, J. T.; Hottle, J. R.; Farmer-Creely, C. E.; Viers, B. D.; Esker, A. R. Polyhedral Oligomeric Silsesquioxanes: A New Class of Amphiphiles at the Air/Water Interface. *J. Am. Chem. Soc.* **2002**, *124*, 15194–15195.
86. Chen, W.; Fadeev A. Y.; Hsieh, M. C.; Öner, D.; Youngblood, J.; McCarthy, T. J. Ultrahydrophobic and Ultralyophobic Surfaces: Some Comments and Examples. *Langmuir* **1999**, *15*, 3395-3399.
87. Gao, L.; McCarthy, T. J. Contact Angle Hysteresis Explained. *Langmuir* **2006**, *22*, 6234-6237.
88. Gao, L.; McCarthy, T. J. Teflon is Hydrophilic. Comments on Definitions of Hydrophobic, Shear versus Tensile Hydrophobicity, and Wettability Characterization. *Langmuir* **2008**, *24*, 9183-9188.
89. Gao, L.; McCarthy, T. J. Wetting 101°. *Langmuir* **2009**, *25*, 14105-14115.
90. Hunter, M. J.; Gordon, M. S.; Barry, A. J.; Hyde, J. F.; Heidenreich, R. D. Properties of Organopolysiloxanes on Glass. *Ind. Eng. Chem.* **1947**, *39*, 1389-1395.
91. Chae, S. S.; Oh, J. Y.; Park, J. H.; Choi, W. J.; Han, J. H.; Lee, J.-O.; Baik, H. K.; Lee, T. I. Strong Hydrophobizer: Laterally Chemisorbed Low-Molecular-Weight Polydimethylsiloxane. *Chem. Commun.* **2015**, *51*, 5844-5847.
92. Krumpfer, J. W.; McCarthy, T. J. Rediscovering Silicones: “Unreactive” Silicones React with Inorganic Surfaces. *Langmuir* **2011**, *27*, 11514-11519.
93. Lin, Y.; Wang, L. Krumpfer, J. W.; McCarthy, T. J. Hydrophobization of Inorganic Oxide Surfaces Using Dimethylsilanediol. *Langmuir* **2013**, *29*, 1329-1332.

94. Wang, L.; McCarthy, T. J. Covalently Attached Liquids: Instant Omniphobic Surfaces with Unprecedented Repellency. *Angew. Chem. Int. Ed.* **2016**, *55*, 244-248.
95. Cheng, D. F.; Urata, C.; Yagihashi, M.; Hozumi, A. A Statically Oleophilic but Dynamically Oleophobic Smooth Nonperfluorinated Surface. *Angew. Chem. Int. Ed.* **2012**, *51*, 2956-2959.
96. Cheng, D. F.; Urata C.; Masheder B.; Hozumi A. A Physical Approach To Specifically Improve the Mobility of Alkane Liquid Drops. *J. Am. Chem. Soc.* **2012**, *134*, 10191-10199.



## CHAPTER 2

### SYNTHESIS AND CHEMISTRY OF MQ SILICONES

#### 2.1 Introduction

##### 2.1.1 Background

MQ silicone copolymers<sup>1-3</sup> are commercially significant materials that have been largely ignored by the academic materials research community. In stark contrast to the widely used and well-recognized abbreviation for dimethylsiloxane polymers, "PDMS," and in somewhat less contrast to the abbreviation for polycyclic silsesquioxane oligomers, "POSS," the abbreviation, "MQ" is generally recognized only by specialists who use these copolymers. MQ copolymers are, however, commodity materials that uniquely enable a number of technologies, are manufactured on large scale by multiple companies and are widely used to formulate silicone elastomers, coatings, adhesives, sunscreens and cosmetics. They are useful as reinforcing fillers in some applications because of their silica content and particle-like physical structure. Their molecular characteristics and notably their solubility, make them useful in other applications that require film formation and homogeneity. Our group has published two papers<sup>4,5</sup> with titles that begin with the words, "Rediscovering Silicones," and another<sup>6</sup> with a title that begins with "A Surprise from 1954." These papers and Chapter 1 point out reasons for the neglect of silicones in academics. Work in these papers and our group has tried to emphasize and take advantage of the special reactivity and properties of silicones that set them apart from polymers with carbon-based backbones. This chapter highlights another aspect of this neglect and focuses on the synthetic approach to MQ copolymers. Although MQ materials were developed in the 1950s and have become increasingly present in our daily lives, I contend that they should be more widely appreciated than they are, particularly in the context of molecules that can help address today's materials science needs.

Silicones were invented in the 1940s largely by researchers at the General Electric (GE) and Corning/Dow Corning companies and methylsilicones were identified as particularly useful.<sup>7-10</sup> The widely-adopted GE nomenclature<sup>11</sup> (MDTQ) is reviewed in Figure 2.1 that also shows examples of methylsilicones comprised of their 4 different chemical structural components. The structures MD<sub>72</sub>M and T<sub>8</sub> are examples of the well-studied PDMS (liquid) and POSS (crystalline solid) materials. M(M<sub>2</sub>Q)<sub>24</sub>M is an isomer of MD<sub>72</sub>M and, were it to exist,<sup>12</sup> would also be a liquid with properties similar to those of MD<sub>72</sub>M. The parentheses are deliberately drawn through the oxygen atoms to represent the Si-O<sub>1/2</sub> structure that is necessary for correct MDTQ stoichiometry. M<sub>8</sub>Q<sub>8</sub> is a crystalline<sup>13</sup> polycyclic co-oligomer of M and Q with the same topology as the octameric silsesquioxane, T<sub>8</sub>. These examples demonstrate the flexibility of the 4 methylsilicone building blocks and emphasize that MQ materials can be isomeric with T-based, D-based or TD copolymeric materials and can exhibit similar properties. In fact, MQ-based silicones compete with, complement and are compounded with T-based silicones in multiple cosmetics applications.<sup>14</sup>

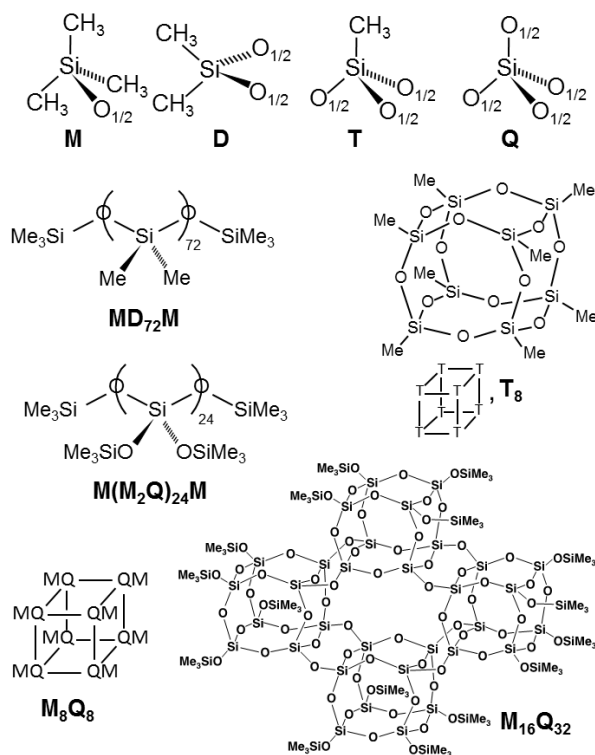


Figure 2.1. Nomenclature and examples of silicones.

The polycyclic structure  $M_{16}Q_{32}$  in Figure 2.1 is an overly symmetrical, low molecular weight representative of the MQ copolymers reported here as well as commercial MQ resins. Three points need to be made in regard to this structure and these molecules. First, there is no similar chemical structure for these compounds in the literature<sup>15-19</sup> and there is an absence of any discussion concerning their variable polycyclic structural features. There is a depiction of a computer-generated space-filling model of the "molecular structure of a typical MQ resin,  $[M_{0.62} Q^{OH}_{0.17} Q_{0.83}]_{32}$ " in both encyclopedia articles cited here.<sup>1,2</sup> This was presented by J. Wengrovius at the 10th International Symposium on Organosilicon Chemistry.<sup>15</sup> Reproductions of this structure appear in the Gelest catalog,<sup>16</sup> two articles,<sup>17,18</sup> a monograph,<sup>19</sup> and a color reproduction appears on the issue cover of reference 17. The space-filling model represents  $M_{20}Q_{32}$  as

4 octameric silicate cubes linearly linked by 3 siloxane bonds with 20 trimethylsilyl groups and 6 residual silanols. Despite this depiction, there remains no "graphic image" that comes to mind for MQ in the way the  $T_8$  cube does when POSS or silsesquioxane are discussed. The absence of this image is perhaps because the rather non-molecular term "resin" rather than "copolymer" or "molecule" generally follows MQ, perhaps because of the neglect of silicones<sup>4-6</sup> mentioned above, perhaps because of the difficulties in making these materials in an academic setting or perhaps because of all 3 of these reasons. Second, these copolymers are prepared by step-growth condensation of tetrafunctional silicic acid,  $Si(OH)_4$ , and termination (end-capping) by monofunctional trimethylsilanol,  $Me_3SiOH$ . The products are polydisperse in molecular weight, topology (branching and polycyclic structure), M:Q ratio, and residual silanol content (end-capping reaction yield). They are, however, mixtures of discrete molecules and  $M_{16}Q_{32}$  in Figure 2.1, were it to be prepared, would be one component of a polydisperse mixture, most of which would be comprised of much less symmetrical structures that contain silanols from incomplete end-capping. Third, the Q content (silica content) can be high (~70 mol%, M:Q ~ 0.4) yet the compounds readily dissolve in hydrocarbon solvents (most commercially available MQ resins are sold as hydrocarbon solutions) and, as well, in PDMS (one of their principal uses). This solubility, which has been referred<sup>1,2</sup> to as their "most unique and perhaps most useful characteristic," is counterintuitive to chemists and suggests that wetting and dispersion of nanoparticles by solvents and adsorption of PDMS chains to surfaces are better perspectives than solubility to rationalize the compatibility of these molecules with low surface energy media. These solid, white, free-flowing powders, however, are comprised of discrete molecules with molecular formulas and should be regarded as solutes when dispersed as molecules. MQ resins have been called nanoparticles,<sup>20</sup> "small silica-like particles,"<sup>21</sup> and "organic-solvent-soluble silicate particles,"<sup>22</sup> but they are in fact

molecules that exhibit nanoparticle-like properties when compounded with silicone polymers.

There is an enormous patent literature concerning MQ resin preparations<sup>23</sup> that is derivative of the 1950s reports of Daudt and Taylor<sup>24</sup> and Goodwin.<sup>25</sup> The Daudt/Taylor method involves preparing a silica sol by acidifying sodium silicate and reacting it with trimethylchlorosilane. Goodwin prepared MQ resins by co-hydrolysis of alkyl silicates and reactive trimethylsilyl compounds. More recent patents<sup>26-28</sup> illustrate that MQ resins are prepared using continuous processes and that precise control of resin properties is possible with proper engineering controls. Processing steps involve equipment such as jet mixers and spray dryers that are not available in typical academic laboratories. Several academic groups<sup>20,22,29-40</sup> have attempted to follow the Goodwin and Daudt/Taylor methods, with each group publishing different preparative procedures and reporting different products. The variations in reported properties illustrate the sensitivity of MQ resins to reaction conditions. None of the reports illustrate control of final product structure and there are no guidelines for designing a synthesis to prepare a specific molecular weight, M:Q ratio or other structural feature. In general, there is a lack of understanding of the reactions taking place to form these molecules and how they can be controlled.

### 2.1.2 Objective

In this chapter, a straight-forward and convenient laboratory scale synthesis of MQ copolymers is developed where the sol growth and end-capping reactions are separated. This method is reproducible with certain qualifications. Using this method, numerous MQ copolymers of different molecular weights and chemical functionalities are prepared. Characterization of the chemistry and composition of these MQ copolymers allows conjectures to be made concerning their structure. Structural control is demonstrated by

rationally varying molecular weight and chemical versatility is exhibited by preparing controlled composition hydridodimethyl-M and vinyl dimethyl-M derivatives. These derivatives allow MQ to be utilized as a molecular nanoparticle substrate for further chemical modification. These materials can be considered models for commercial MQ resins.

## 2.2 Experimental Section

### 2.2.1 Reagents

Absolute ethanol, toluene and sulfuric acid (18M) were obtained from Fisher. Tetraethoxysilane (TEOS), hexamethyldisiloxane, divinyltetramethyldisiloxane, and tetramethyldisiloxane were obtained from Gelest. All chemicals were used as received. House purified water (reverse osmosis) was further purified using a Millipore Milli-Q system (18.2 M $\Omega$ ).

### 2.2.2 Preparation of MQ silicone

1 equiv of TEOS (Q) is added to a round bottom flask containing a stirred mixture of 10 equiv water and 5 equiv ethanol that is acidified with H<sub>2</sub>SO<sub>4</sub> (3.75 mM). This mixture is held at 50 °C for the desired sol growth duration (under these conditions, the gel time is roughly 50 hours), at which time 0.5 equiv of hexamethyldisiloxane (MM), toluene and additional H<sub>2</sub>SO<sub>4</sub> (0.375 M to initial water-ethanol mixture) are added. The temperature of the mixture is increased to 60 °C for 1 hour, 70 °C for 1 hour and 80 °C for 2 hours. The organic phase is rinsed with water, neutralized with sodium bicarbonate solution and optionally rinsed with brine. After neutralization and separation, the organic phase is dried over magnesium sulfate and filtered. Solvent is removed using a rotary evaporator.

The preparation of M<sub>14</sub>Q<sub>29</sub> (Table 1) is provided as an example: In a two-neck round bottom flask fitted with a condenser and PTFE stopper, 17.8 g water (0.98 mol) and

23 g ethanol (0.5 mol) is heated to 50 °C with stirring. 10 µL of 18M H<sub>2</sub>SO<sub>4</sub> is added to the stirred mixture. 20.1 g TEOS (0.097 mol) is then added. The mixture is stirred at 50 °C for 4 hours, at which time 8.12 g hexamethyldisiloxane (0.05 mol) in 30 mL of toluene is rapidly added forming an emulsion. 1 mL of 18M H<sub>2</sub>SO<sub>4</sub> is then added dropwise to the stirred emulsion. The temperature is increased to 60 °C for 1 hour, 70 °C for 1 hour and 80 °C for 2 hours. The reaction mixture is transferred to a separatory funnel, rinsed with water, rinsed with sodium bicarbonate and finally rinsed with brine. Once separated, the organic phase is dried over magnesium sulfate and filtered. Upon removal of solvent, 9.3 g of white powder is obtained.  $M_n = 2900$ ,  $M_w = 4400$ ; M:Q = 0.48 (<sup>1</sup>H NMR with cyclohexane internal standard). The yield is 94% based on TEOS and the determined M:Q ratio.

Vinyl and hydride functional MQ copolymers are prepared using the same procedure with addition of divinyltetramethyldisiloxane or tetramethyldisiloxane end-capping monomers.

*MQ via Goodwin<sup>25</sup> Method.* The Goodwin method is based on a patent for MQ copolymers used in pressure sensitive adhesives. The product of this reaction has been noted in our lab for its tackiness, emulsifying behavior, and sensitivity to reaction conditions. To prepare MQ, TEOS and trialkylsilane in the desired M:Q ratio are dissolved in toluene. This mixture is added to stirring 60 °C water (with acid catalyst if necessary) in a round bottom flask. Stirring conditions and temperature control were found to be crucial to the success of this reaction. Following one hour of reaction at 60 °C, the temperature was incrementally increased to 80 °C and held for two hours. The reaction mixture is carefully rinsed with water, neutralized with sodium bicarbonate and dried over magnesium sulfate. Toluene is then removed using a rotary evaporator and an additional

24 hours under vacuum. This reaction produces a soluble solid MQ resin with few residual alkoxy or silanol groups that is stable in solution for months.

Example of the Goodwin preparation: 22.5 g water (1.25 mol, 5 EQ to TEOS) and 1.125 mL sulfuric acid (5 vol% to water) are mixed in a round bottom flask and heated to 60 °C. 52 g TEOS (0.25 mol) is mixed with 55 mL toluene and 16 g (0.2 mol M, 0.8 EQ to TEOS) hexamethyldisiloxane. The silane-toluene solution is poured into the stirring aqueous acid. The reaction is held at 60 °C for 1 hour, 70 °C for one hour and 80 °C for 2 hours. MQ is isolated by repeated (3x) rinsing of the organic phase with water, one rinse with aqueous sodium bicarbonate, drying of the organic phase with magnesium sulfate, filtration and rotary evaporation. The product is an organic solvent – soluble white powder.

*MQ via Magee<sup>42</sup> Method.* Magee and coworkers disclose a method of making MQ resins from poly(ethylsilicates). This method uses partially hydrolyzed TEOS as a precursor to MQ. In comparison to the one-pot methods used elsewhere, this is a two-step reaction involving the formation of a stable poly(ethylsilicate) followed by end-capping with trialkylsilane. To form the poly(ethylsilicate) prepolymer, ethanol and 1 EQ TEOS are mixed with hydrochloric acid and phosphonitrilic chloride catalysts. This mixture is heated to 70 °C and a substoichiometric volume of water is added (up to 1.8 EQ). This mixture is stirred for 2 hours and the temperature is slowly increased to 140 °C where volatiles are collected by distillation. The product of this reaction is a clear, viscous fluid. An example of prepolymer preparation follows: 52 g (0.25 mol) TEOS is mixed with 12 g (0.25 mol) ethanol and acidified with 12  $\mu$ L 37% HCl (~0.01 mmol) in a round bottom flask with magnetic stirring. 6.3 g (0.35 mol) water (MilliQ, 18.2 M $\Omega$ ), and 6.5 mg (0.02 mmol) phosphonitrilic chloride trimer is added to the flask and the stirring mixture is heated to 80 °C. The temperature is held at 80 °C for 2 hours then heated to 100 °C for 1 hour, 120 °C



for one hour and finally 140 °C for one hour. After stirring at 140 °C for one hour, 40 mL of volatiles were distilled off at  $T_{\text{vap}} = 78$  °C (ethanol). Distillation was carried out until  $T_{\text{vap}}$  reached 80 °C, at which point vapor condensation and collection had slowed dramatically. The product was a clear viscous oil.

Sulfuric acid was also tested as catalyst in place of HCl and phosphonitrilic chloride trimer and similar results were obtained. For example, 104 g (0.5 mol) TEOS was stirred in a round bottom flask with 56 mL reagent alcohol and 40  $\mu\text{L}$  sulfuric acid ( $\sim 0.8$  mmol). The mixture was heated to 80 °C and 12.6 g (0.7 mol) water was added. The mixture was held at 80 °C for one hour, 100 °C for one hour, 120 °C for one hour and 140 °C for one hour. 100 mL was distilled at  $T_{\text{vap}} = 78$  °C. 73 mL of clear, viscous prepolymer was collected. Characteristics of the prepolymers prepared with sulfuric acid were similar to those prepared with phosphonitrilic chloride trimer. Sulfuric acid therefore became the preferred catalyst.

To prepare MQ resin, the prepolymer is diluted in ethanol and catalytic acid is added. The remaining water for hydrolysis is added and the mixture is refluxed for two hours. Toluene and hexamethyldisiloxane for the desired M:Q ratio are then added. The end-capping reaction is carried out for 2 hours at 80 °C. At this point volatiles can be removed by distillation or the mixture can be worked up by rinsing with water, neutralization with sodium bicarbonate, drying over magnesium sulfate and finally solvent removal. As an example, an MQ copolymer was prepared by the dropwise addition of 42 mL prepolymer (formed from 0.25 mol TEOS) to an 80 °C stirring mixture of 42 mL toluene, 22.5 g water (5 EQ), 17 g hexamethyldisiloxane (0.8 EQ M) and 2 g sulfuric acid (.08 EQ). Following addition of prepolymer, the reaction mixture was held at 80 °C for 2 hours. MQ copolymer was isolated by repeated (3x) rinsing of the organic phase with water, one rinse

with aqueous sodium bicarbonate, drying of the organic phase over magnesium sulfate, filtration and rotary evaporation. The MQ product is an organic solvent – soluble, white powder.

This reaction proved difficult to control in the benchtop batch scales we worked with. Reproducible production of a poly(ethylsilicate) was a challenge. Additionally, gelation and formation of insoluble solids often limited yields. The reaction was found to be sensitive to stirring, temperature, concentration, and method of reagent addition. Soluble MQ resins obtained by this method contained a large amount of residual alkoxy groups visible in IR and NMR spectra. Although the patent claims GPC MW peaks of 34600, the highest obtained in our lab was 9300.

### 2.2.3 MQ Copolymer Chemical Modification

Condensation reactions on silanol-containing MQ copolymers were conducted using trimethylsilyliodide (TMSI) and divinyltetramethyldisilazane (DVTMDZ). For both reactions, MQ copolymer was dissolved in anhydrous toluene in a nitrogen-purged round bottom flask. In TMSI reactions, excess TMSI (~1 mmol per gram MQ) is added by syringe. The reaction proceeds rapidly at room temperature and is complete in under 2 hours. In DVTMDZ reactions, excess DVTMDZ is added by syringe. DVTMDZ requires elevated temperatures (80 °C) and longer times (4 hours) for reaction completion. Both reactions are worked up by aqueous rinsing, neutralization with sodium bicarbonate, isolation of the organic phase, drying with magnesium sulfate and solvent stripping. Any excess silane is removed during stripping.

Piers-Rubinsztajn reactions of MQ silanols with silicon hydrides (silanes and hydride-containing methylsilicones) were conducted in anhydrous toluene. MQ is

dissolved in anhydrous toluene and excess silane reagent is added. 0.1 mol% (to Si-H) tris(pentafluorophenyl)borane catalyst (40 mg/mL in toluene) is added. Sufficient air flow should be allowed for the rapid evolution of H<sub>2</sub> associated with this reaction! Typically, there is a brief induction period before rapid bubbling is observed. Reactions are complete after 1 hour at room temperature. Reactions are worked up by stirring over alumina, followed by filtration and solvent stripping. For volatile low molecular weight silanes, any excess silane is stripped under reduced pressure. Due to the difficulty of separating non-volatile silanes or siloxane polymers from MQ, such reagents are typically used below 1 EQ.

Hydrosilylation reactions are run in anhydrous toluene solutions of vinyl or hydride containing MQ. The desired silane or unsaturated modifying reagent is added and dissolved followed by the addition of 20 ppm Karstedt's catalyst (2% Pt in xylenes, Gelest). Reactions are run at 80 °C for 4 to 16 hours. Reactions are worked up by stirring over activated charcoal and filtration of the solution through a column of diatomaceous earth. MQ is isolated after solvent stripping.

I must emphasize here that modifications reactions were not optimized. Numerous reactions were run to demonstrate that MQ can be useful as a substrate but reaction conditions and work up procedures were not optimized. I suspect that each method of modifying MQ will have unique challenges. Perhaps the most difficult of these challenges will be isolating MQ product and separating reagents. For this reason, most MQ modifications were run with volatile reagents that could be removed in a vacuum oven or with excess MQ so that excess reagent would not be present.

#### 2.2.4 Characterization

*Size exclusion chromatography* was conducted on an Agilent 1260 GPC equipped with two PLgel Mixed-C and one PLgel Mixed-D columns (Polymer Laboratories) and a refractive index detector. Tetrahydrofuran (THF) at a flow rate of 1 mL/min was the mobile phase. Linear poly(methylmethacrylate) (PMMA) standards were used to assign relative molecular weights from which estimates of hydrodynamic radii were calculated using literature<sup>41</sup> Mark-Houwink parameters.

*Attenuated Total Reflection-Infrared* spectra (FT ATR-IR) were recorded using a PerkinElmer Spectrum 100 spectrometer. NMR studies were performed on a Bruker Avance III HD 500 MHz spectrometer in CDCl<sub>3</sub>. 0.02M Cr(acac)<sub>3</sub> was used as a relaxation agent for <sup>29</sup>Si spectra and a Hahn pulse echo program was used to minimize background signals from glass NMR tubes. After optimization of the pulse echo program to remove the background of the NMR tube, we still observed a persistent Q region background signal. <sup>1</sup>H NMR spectra were recorded in CDCl<sub>3</sub> solutions of samples containing a measured mass of MQ and known concentration of cyclohexane as an internal standard. M:Q ratios were calculated using integrations of the cyclohexane and trimethylsilyl peaks to determine the organic mass fraction of a known mass of MQ. The M:Q ratio is determined from the organic mass %.<sup>34</sup>

*Diffusion NMR* was conducted using 32 or 64 magnetic gradient scans from 2% to 95% with quadratic distribution. The intensity difference between the 2% and 95% gradient spectra was optimized to between 1% and 5% for all samples by controlling gradient pulse duration and the delay time between pulses. For M<sub>32</sub>Q<sub>64</sub>, concentrations from 0.5 to 20 wt/vol CDCl<sub>3</sub> were tested. Decay curves show the same behavior for each concentration indicating that no aggregation is occurring and only diffusion of single MQ molecules is

being observed. 10 wt/vol concentrations were chosen for all other MQ samples since this concentration provided adequate signal without aggregation.

Diffusion NMR is particularly useful for analysis of MQ chemical modifications. Measuring the change in diffusion behavior of a grafted MQ species indicates successful grafting. This requires separate measurements of (1) the MQ substrate, (2) the species to be grafted and (3) the grafted MQ product. Each species will have its own diffusion behavior and it is most useful to plot the grafted species in two-dimensions (chemical shift vs diffusion coefficient). By plotting in two dimensions, grafted and ungrafted/unreacted species can be separated by their chemical shift and diffusion behavior. Successful grafting and clean work-up is indicated when one diffusing species is measured in DNMR.

*Dynamic light scattering* was conducted using a Brookhaven 637 nm laser with a TurboCorr digital correlator. Correlation functions were collected for angles from 15-75°. A 100 µm aperture was used with sampling times ranging from 10-30 min. Dust free samples were prepared using a thorough washing and filtering procedure: sample vials are rinsed with 3-5 times with water (MilliQ, 18.2 MΩ), 3 times with clean acetone, dried upside down in a clean oven and sample solutions are added to vials through syringe filters in a clean fume hood. M<sub>32</sub>Q<sub>64</sub> was examined at concentrations from 5-30 mg/ml. All correlation functions demonstrated monomodal exponential decays and decay constants did not change with concentration. The 30 mg/mL sample provided acceptable correlation intensities with no apparent aggregate formation. We acknowledge that this cannot be considered a dilute solution and that multiple scattering is expected to lead to an underestimation in size, but are comfortable using these results for estimation. For the smaller MQ copolymers the same 30 mg/ml concentration was chosen, however the smaller size of the molecules and lower contrast decreased the intensity of the correlation

functions, decreasing our confidence in the data. Thus, the size of the smaller MQs appears to approach the limitations of our scattering system. Scattering of the largest MQs was possible at lower concentrations due to improved contrast and slower diffusion. Concentrations of <5 mg/ml were found to be appropriate. Our assessment of light scattering techniques for MQ silicones is that it is difficult due to the size of the molecules and the low contrast. Even after experimenting with multiple solvents under a variety of experimental conditions, it was found to be difficult if not impossible to obtain reliable data.

*Determination of hydrodynamic radius (DLS, D-NMR, and GPC).* Correlation functions for dust free DLS experiments were fit with a single exponential decay function using OriginPro 9.0 software. The decay constants ( $\Gamma$ ) were plotted against the square of the scattering vector,  $q^2$  (eq. 1). The slope of the linear fit to this data provides the diffusion coefficient,  $D$ . The hydrodynamic radius can be calculated using the Stokes-Einstein equation (eq. 2).

$$q = \frac{4\pi}{\lambda} \sin \frac{\theta}{2} \quad (1)$$

$$R_h = \frac{kT}{6\pi\eta D_0} \quad (2)$$

For D-NMR the diffusion coefficient is extracted from the slope of  $\ln(I/I_0)$  vs  $g^2\gamma^2\delta^2(\Delta-\delta/3)$  plots (eq. 3), where  $g$  is the magnetic gradient,  $\gamma$  is the gyromagnetic ratio,  $\delta$  is the length of the gradient pulse, and  $\Delta$  is the length between pulses. Again the Stokes-Einstein equation is used to determine a hydrodynamic radius.

$$I = I_0 e^{-D\gamma^2 g^2 \delta^2 (\Delta - \delta/3)} \quad (3)$$

For GPC, Mark-Houwink parameters can be used to estimate the intrinsic viscosity (eq. 4) from which the hydrodynamic radius can be estimated using the Einstein viscosity relation for an equivalent sphere (eq. 5).

$$[\eta] = KM^a \quad (4)$$

$$[\eta] = \frac{2.5NV_e}{M} \quad (5)$$

*Thermogravimetric analysis (TGA)* was performed under nitrogen using a TA Q80 TGA. Temperature ramps were from 25 °C to 900 °C at a rate of 10 °C/min. Residual mass content was used to gain insight into the inorganic composition of the MQ copolymers. Differential scanning calorimetry (DSC) was conducted on a TA Q200 DSC with liquid nitrogen cooling. Samples were prepared in hermetically sealed aluminum pans and were heated to between 150 and 350 °C (depending on sample degradation temperature) at 10 °C/min, then cooled to -150 °C at 10 °C/min, and finally heated to 150-350 °C at 10 °C/min. Softening points were observed using a Stanford Research Instruments Optimelt MPA100. Samples were heated from room temperature to 400 °C at a rate of 10 °C/min. The softening point was defined as the point at which the sample became transparent or began to flow.

*Transmission electron microscopy* samples were prepared by placing a drop of water onto a copper-supported carbon film grid (Electron Microscopy Sciences, CF400-Cu) and dipping this into a 1 mg/ml solution of MQ copolymer in toluene. After being immersed in the MQ solution for 60 seconds, the grid was removed and dried at room temperature. The sample was imaged at 200kV on a JEOL JEM-2200FS transmission electron microscope.

## 2.3 Results and Discussion

### 2.3.1 MQ Copolymer Synthesis

Some comments that detail the complexity of MQ copolymer synthesis are in order and are made in the next paragraph. This complexity was not recognized at the onset of these studies but became readily apparent in short time. Although product could be

prepared in good yield rather easily, the same material could not be made consistently - often not twice in a row. There are dozens of reported procedures and we tried many of them (changing and trying to tune variables with combinatorial methods) at small scale in 20 mL scintillation vials using a temperature-controlled 63-cell shaken reaction block. None of these data are reported here; there was zero success in scaling up the most promising methods. Stirring reaction mixtures gave very different results than did shaking them and we did not want to develop reactions that needed to be "shaken, not stirred." Even the shape of the reaction vessels was important, likely due to differences in agitation. Work up procedures impacted product structure: solids could be prepared by rapid removal of solvent from solutions that would render oils by slower solvent removal. Oils could be converted to solids by freeze-drying cyclohexane solutions, but these solids would sometimes (inconsistently) revert to oils. It became clear that the literature reports of MQ resins are not useful preparative guides and that product structure is sensitive to slight changes in reaction conditions. One report<sup>29</sup> in particular demonstrates the sensitivity of MQ properties to reaction conditions. Six resins are reported to have been prepared with the same composition using 6 different synthetic methods. Structural differences, inherent from the syntheses, resulted in distinct differences in rheological behavior for all 6. At this point, I realized that I would not be able to compare the materials I was preparing with any in the literature and that a readily (commercially) available "model" MQ resin was needed to compare, contrast and calibrate my MQ copolymers against. Dow Corning MQ-1600 was chosen and characterized (Figure 2.2); the logic used in making this choice is discussed below.



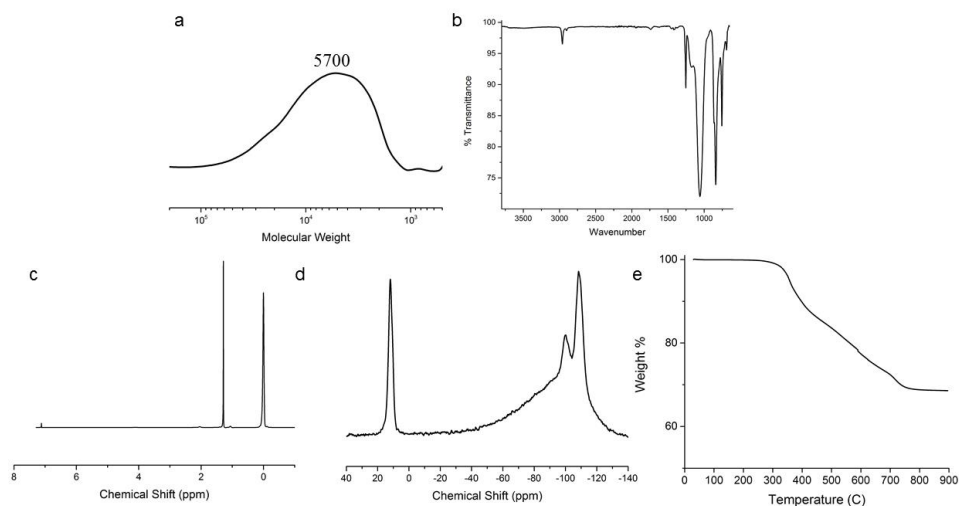


Figure 2.2. (a) GPC, (b) IR, (c)  $^1\text{H-NMR}$ , (d)  $^{29}\text{Si-NMR}$ , and (e) TGA data for Dow Corning MQ1600.

It must be emphasized that the patent literature dwarfs the reviewed literature on the topic of MQ copolymer synthesis and that all of the reports can be considered derivatives of two 1950s patents.<sup>24,25</sup> One of these approaches involves hydrolysis of  $\text{Me}_3\text{SiOH}$  (M) precursors ( $\text{Me}_3\text{SiCl}$ ,  $\text{Me}_3\text{SiOSiMe}_3$ ,  $\text{Me}_3\text{SiNHSiMe}_3$ ) in the presence of a silica (Q) sol (acidified aqueous sodium silicate, water glass) and subsequent co-condensation. The other involves co-hydrolysis and co-condensation of M precursors and the Q precursor,  $\text{Si}(\text{OEt})_4$  (TEOS). Both approaches involve heterogeneous 2-phase reactions, the rates of which depend on, in addition to concentrations, catalyst, and temperature, the mixing of organic and aqueous phases (most often water and toluene or xylene). The end-capping condensation (M-Q bond formation) is competitive with the growth of the sol (Q-Q bond formation) and both of these reactions are, in principle, reversible. Intermediates in the reaction (as well as the products) are surfactants and emulsions are formed. The structure of these surfactants and emulsions evolve with the extent of reaction as well as vary with changes in agitation. Both types of reactions are of

the "sol-gel" type and procedures require careful temperature control and termination to avoid gelation. The difficulties in gaining control over and reproducibility with these complex systems is apparent.

In my first attempts to prepare MQ, I became successful in reproducibly replicating a procedure based on the Goodwin patent<sup>25</sup> and prepared dozens of MQ copolymers using this method. This approach was abandoned, however, because at least in my hands, there was no molecular weight control and most samples had very high polydispersity indices. The method of Magee<sup>42</sup> (derivative of Goodwin) appeared promising and I prepared dozens of samples; however, this line of research was also abandoned because of the high, variable and uncontrollable content of residual ethoxy groups. It appeared that incomplete hydrolysis or re-esterification was a recurring issue. These procedures and data for samples prepared by these methods are described in the experimental section and Figures 2.3 and 2.4. Both of these synthetic approaches are convenient methods to prepare materials that may be useful. The Goodwin approach yields materials that are tacky and exhibit strong emulsifying behavior. The Magee approach gives products with much lower polydispersity indices and high residual ethoxy content, which may find utility as a reactive handle for chemical modification.

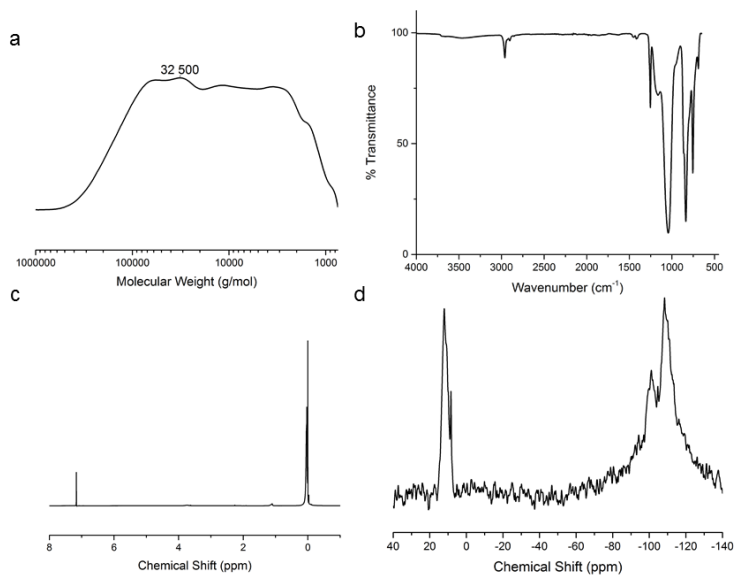


Figure 2.3. (a) GPC, (b) IR, (c) <sup>1</sup>H-NMR, and (d) <sup>29</sup>Si-NMR data for a sample of MQ prepared using the Goodwin method.

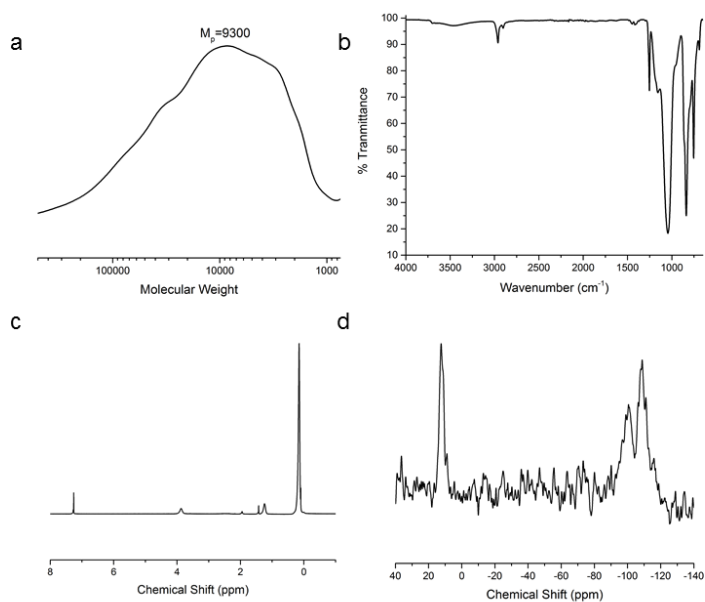


Figure 2.4. (a) GPC, (b) IR, (c) <sup>1</sup>H-NMR, and (d) <sup>29</sup>Si-NMR data for a sample of MQ prepared using the Magee method.

The method that is reported here is a derivative of the Goodwin method and my approach was to separate, as much as possible, the copolymerization of M and Q into distinct steps: (1) initial condensation of silicic acid (Q,  $\text{Si}(\text{OH})_4$ ), to form a silica sol, (2) subsequent end-capping the nascent sol with M (trimethylsilylation). The polymerization of silicic acid is extremely well documented and there is abundant evidence that the sol growth rate can be controlled using solvent ratios, water concentration and catalyst choice, and that the gelation time can be controlled (delayed) under appropriate conditions.<sup>43-45</sup> My strategy was to arrest the sol growth at various times in the polymerization reaction before it reached the gel state. The alkoxysilane method over the silica sol approach (Daudt/Tyler) was chosen somewhat arbitrarily, but mostly because previous experiments and initial studies determined it to be more controllable and easier to work with.

Table 2.1 shows GPC relative molecular weight and M:Q ratio data for a number of MQ copolymer samples that were prepared by the method detailed in the Experimental Section. Briefly, after adding TEOS to a stirred solution of water, ethanol and sulfuric acid at 50 °C and heating at this temperature for specific times, excess hexamethyldisiloxane in toluene and additional sulfuric acid are added. The temperature is increased to and maintained at 60 °C for 1 hour, then 70 °C for 1 hour, and then 80 °C for 2 hours. This procedure was arrived at (optimized) based on dozens of reactions with many variations. Table 2.1 permits several general observations concerning the reaction: (1) The yields of the reactions, based on TEOS, are "good" and 0.1 mole of TEOS generally yields >8 g of isolated MQ product. This not the case for the samples abbreviated in Table as  $\text{M}_{66}\text{Q}_{164}$ ,  $\text{M}_{52}\text{Q}_{178}$  and  $\text{M}_{46}\text{Q}_{121}$  (the samples prepared with a 48 h sol reaction); these were recovered in yields of 0.5-2 g. I did not try to optimize yields with fastidious work up procedures, as the reactions are easy to run and adequate amounts were readily prepared. (2) The second aliquot of acid and the staged temperature rise are important and were found to

minimize gelation and maximize the end-capping yield. (3) The  $\text{H}_2\text{SO}_4$  concentration in the first step (sol formation) affects the M:Q ratio in the product, however this was not studied methodically and data are not included in Table 2.1. The acid concentration was increased 10-fold and 100-fold and decreasing M:Q ratios were observed with increasing  $\text{H}_2\text{SO}_4$  concentration. This is in line with what would be predicted from more condensed sols. Molecular weight and composition data indicating this trend are presented in Table 2.2 and are not discussed further. If controlling M:Q ratio at constant molecular weight were an objective, changing the Q precursor and/or the catalyst may have been effective.

(4) At the relatively low  $\text{H}_2\text{SO}_4$  concentration that was used for all of the samples described in Table 2.1, the M:Q ratio in the product was independent of the amount of disiloxane M-precursor added. An M:Q feed ratio of 1 was generally used, but it was possible to produce MQ copolymers with ratios as low as 0.6 with no obvious loss in yield. If, however, ratios lower than 0.6 are used, sol growth and gel formation compete with end-capping, limiting yield and making the work up more difficult.  $\text{M}_{17}\text{Q}_{15}$  and  $\text{M}_{16}\text{Q}_{13}$  were prepared using conditions deliberately chosen to form low molecular weight, liquid MQ copolymer. The sol reaction was quenched very early and required an M:Q feed ratio of 2 to efficiently end-cap the large number of silanols. All of the other copolymers in Table 2.1 are solids.

(5) The highest molecular weight samples reported in Table 2.1,  $\text{M}_{66}\text{Q}_{164}$ ,  $\text{M}_{52}\text{Q}_{178}$  and  $\text{M}_{46}\text{Q}_{121}$  can be prepared with the reproducibility indicated, but gelation competes, rendering insoluble products and significantly lower amounts of toluene-soluble materials than the other reactions reported. The time of 48 h is very close to the "gelation time" for these reaction conditions. Higher molecular weights than those reported can be obtained, but at yields that would not be considered adequate for practical use. One reaction yielded a sample of several hundred milligrams that exhibited  $M_n = 10\,300$ ,  $M_w = 78\,000$ ,  $M_p = 86\,200$  (peak molecular weight), an M:Q ratio of 0.38, and a stoichiometry of  $\text{M}_{46}\text{Q}_{121}$ .

(6) There is a certain amount of "art" to this reaction and no doubt the conditions that are

reported are specific to our reaction set up and temperature control. I hesitate to use the word "reproducible," but point to the 4 samples prepared using 4 h sol gel reactions, 9 samples prepared at 16 and 18 h and the 3 samples prepared at 48 h sol reaction time in regard to this description. In addition to samples I have prepared, the reaction has been run by two other group members with similar results. Samples clearly vary, but there is an obvious reproducibility that is qualified by the variance in these data. An additional practical issue of note is that if the TEOS used is from a new, "fresh" bottle, a longer sol reaction is required to replicate the molecular weight of a sample prepared from old (likely partially hydrolyzed) TEOS. The sample labeled  $M_{32}Q_{64}$  was prepared from new TEOS with a sol reaction time of 18 h. It had molecular weight characteristics in line with those products prepared from older TEOS using 16 h sol reactions.

Figure 2.5 shows infrared,  $^1\text{H-NMR}$  and  $^{29}\text{Si-NMR}$  spectra for  $^{\text{V}}M_{28}Q_{68}$  and  $^{\text{H}}M_{35}Q_{100}$  and  $M_{32}Q_{64}$ .  $^{\text{V}}M_{28}Q_{68}$  and  $^{\text{H}}M_{35}Q_{100}$  are samples (Table 2.1) prepared using divinyltetramethyldisiloxane and tetramethyldisiloxane as capping agents (M precursors) and contain only vinyl dimethylsilyl- ( $^{\text{V}}\text{M}$ ) and hydridodimethylsilyl- ( $^{\text{H}}\text{M}$ ) M units, respectively, thus their spectra show strong absorbance and resonance signals from vinyl and hydride functional groups. Using only  $^{\text{V}}\text{M}$  or  $^{\text{H}}\text{M}$  precursors leads to MQ copolymers with high functional densities. If specific functional density is desired, it can be easily adjusted by substituting trimethylsilyl groups in this procedure, demonstrating that this preparative method is chemically versatile. We prepared a series of both  $^{\text{V}}\text{MMQ}$  and  $^{\text{H}}\text{MMQ}$  copolymers with varying ratios of  $^{\text{V}}\text{M}:\text{M}$  and  $^{\text{H}}\text{M}:\text{M}$  and these materials are described in Table 2.3 and Figure 2.6. The spectra (Figure 2.5 and Figure 2.6) permit quantitative analysis of end-capping reactivity and MQ product functional density. It was observed that  $^{\text{V}}\text{M}$  is incorporated at about the same rate as M in competitive reactions;  $^{\text{H}}\text{M}$  reacts slightly faster than M. MQ resins with these mixtures of functional groups, which

are useful in hydrosilylation reactions, are important commercial products and useful substrates for further modification.

Table 2.1. MQ Copolymer Molecular Weights and Compositions

sample	sol rxn time <sup>a</sup>	M <sub>n</sub> <sup>b</sup>	M <sub>w</sub> <sup>b</sup>	M <sub>w</sub> /M <sub>n</sub>	M:Q <sup>c</sup>
M <sub>17</sub> Q <sub>15</sub>	5 min <sup>2.0</sup>	2300	3000	1.30	1.1
M <sub>16</sub> Q <sub>13</sub>	5 min <sup>2.0</sup>	2100	2800	1.33	1.2
M <sub>14</sub> Q <sub>31</sub>	4 h <sup>1.0</sup>	3000	4300	1.43	0.45
M <sub>14</sub> Q <sub>29</sub>	4 h <sup>1.0</sup>	2900	4400	1.52	0.48
M <sub>17</sub> Q <sub>32</sub>	4 h <sup>1.0</sup>	3200	4300	1.34	0.52
M <sub>16</sub> Q <sub>32</sub>	4 h <sup>0.8</sup>	3100	4200	1.35	0.50
M <sub>32</sub> Q <sub>64</sub>	18 h <sup>1.0</sup>	6500	12 300	1.89	0.49
M <sub>42</sub> Q <sub>100</sub>	16 h <sup>1.0</sup>	8600	16 800	1.95	0.42
M <sub>37</sub> Q <sub>91</sub>	16 h <sup>1.0</sup>	8500	15 900	1.87	0.41
M <sub>30</sub> Q <sub>60</sub>	16 h <sup>0.8</sup>	6000	12 600	2.10	0.49
M <sub>30</sub> Q <sub>100</sub>	16 h <sup>0.8</sup>	8400	19 900	2.37	0.30
M <sub>31</sub> Q <sub>78</sub>	16 h <sup>0.8</sup>	7200	14 700	2.04	0.40
M <sub>27</sub> Q <sub>67</sub>	16 h <sup>0.6</sup>	6200	14 700	2.37	0.40
M <sub>66</sub> Q <sub>164</sub>	48 h <sup>1.0</sup>	15 100	39 800	2.64	0.38
M <sub>52</sub> Q <sub>178</sub>	48 h <sup>0.8</sup>	14 900	51 200	3.44	0.29
M <sub>46</sub> Q <sub>121</sub>	48 h <sup>1.0</sup>	10 300	78 000	7.57	0.38
<sup>v</sup> M <sub>28</sub> Q <sub>68</sub>	16 h <sup>1.0</sup>	6500	16 000	2.46	0.40
<sup>H</sup> M <sub>35</sub> Q <sub>100</sub>	16 h <sup>1.0</sup>	8300	21 000	2.53	0.35
MQ-1600		5700	10 700	1.87	0.63

<sup>a</sup>the superscript indicates the equivalents of M added. <sup>b</sup>relative molecular weight based on linear PMMA standards in THF <sup>c</sup>determined by <sup>1</sup>H-NMR

Table 2.2. Effect of H<sub>2</sub>SO<sub>4</sub> Concentration during sol growth on MQ product

	sol rxn time <sup>a</sup>	[H <sub>2</sub> SO <sub>4</sub> ] mM	M <sub>n</sub>	M <sub>w</sub>	D	M:Q <sup>b</sup>
M <sub>33</sub> Q <sub>47</sub>	3 h <sup>1.0</sup>	-	5500	19700	3.55	0.71
M <sub>32</sub> Q <sub>64</sub>	18 h <sup>1.0</sup>	3.75	6500	12300	1.89	0.49
M <sub>26</sub> Q <sub>61</sub>	20 h <sup>1.0</sup>	37.5	5800	10000	1.72	0.43
M <sub>31</sub> Q <sub>79</sub>	14 h <sup>1.0</sup>	375	7200	13600	1.89	0.39

<sup>a</sup>the superscript indicates the equivalents of M added. <sup>b</sup>determined by <sup>1</sup>H-NMR.

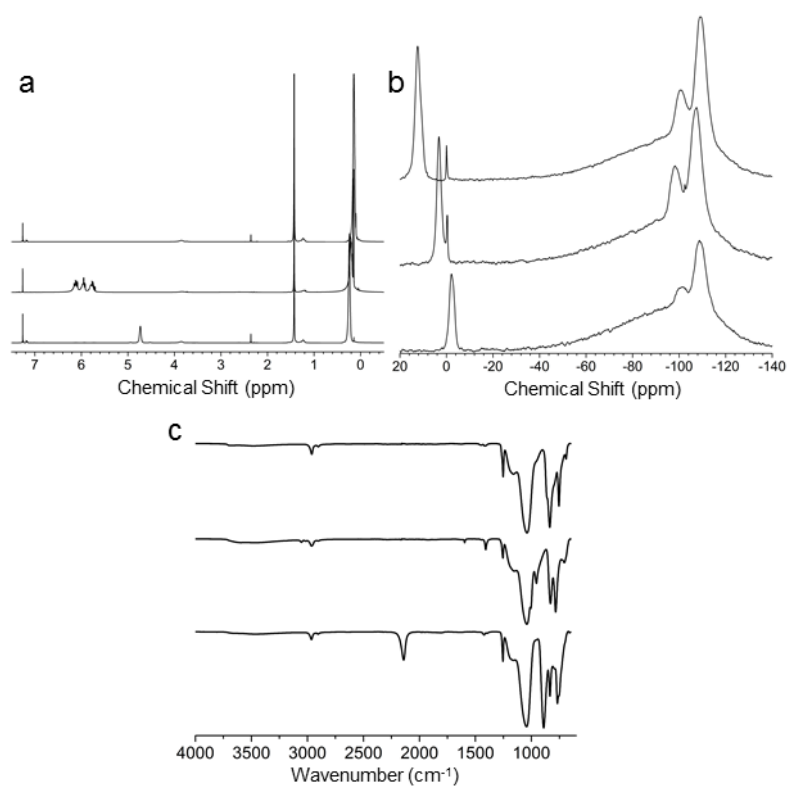


Figure 2.5. (a) <sup>1</sup>H NMR, (b) <sup>29</sup>Si NMR and (c) IR spectra of M<sub>32</sub>Q<sub>64</sub> (top), <sup>V</sup>M<sub>28</sub>Q<sub>68</sub> (middle) and <sup>H</sup>M<sub>35</sub>Q<sub>100</sub> (bottom).



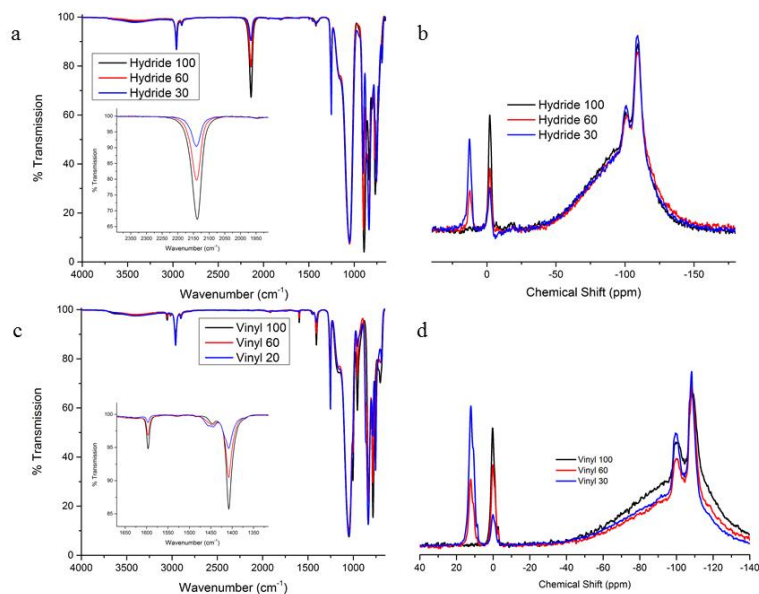


Figure 2.6. (a,c) Infrared and (b,d) <sup>29</sup>Si NMR spectra of <sup>V</sup>MMQ and <sup>H</sup>MMQ silicones. Samples are names by the M functionality (hydride or vinyl) and the mol% of the functional M incorporated into the reaction

Table 2.3. Vinyl and Hydride MQ silicones

<sup>a</sup> mol% <sup>x</sup> M	Form	M <sub>n</sub>	M <sub>w</sub>	<sup>x</sup> M Content (EQ/g) <sup>b</sup>	fraction <sup>x</sup> M <sup>b</sup>	fraction <sup>x</sup> M <sup>c</sup>
<sup>V</sup> 100	Solid	6500	16000	1.10E-01	1	1
<sup>V</sup> 50	Solid	4500	8700	4.54E-02	0.21	0.44
<sup>V</sup> 25	Solid	5200	8800	3.69E-02	0.08	0.2
<sup>V</sup> 12.5	Solid	7200	13000	8.95E-03	0.03	0.1
<sup>V</sup> 100	Liquid			1.10E-01	1	1
<sup>V</sup> 60	Liquid			5.32E-02	0.30	0.52
<sup>V</sup> 20	Liquid			3.95E-02	0.07	0.15
<sup>H</sup> 100	Solid	8286	20988	7.55E-03	1.00	1
<sup>H</sup> 60	Solid	7041	12900	4.45E-03	0.73	0.61
<sup>H</sup> 30	Solid	5100	13800	2.02E-03	0.49	0.32
<sup>H</sup> 100	Liquid			6.14E-03	1.00	1
<sup>H</sup> 60	Liquid			3.93E-03	0.69	0.52
<sup>H</sup> 30	Liquid			1.70E-03	0.41	0.27

<sup>a</sup>mol% <sup>x</sup>M in feed <sup>b</sup>determined by <sup>1</sup>H NMR <sup>c</sup>determined by <sup>29</sup>Si NMR

### 2.3.2 MQ Copolymer Characterization

Figure 2.7a-c exhibits infrared,  $^1\text{H-NMR}$  and  $^{29}\text{Si-NMR}$  spectra for one MQ copolymer,  $\text{M}_{32}\text{Q}_{64}$ . The spectra of all of these samples, including those of MQ-1600 are nearly indistinguishable and almost identical spectra of very similar materials have been published many times.<sup>29-35,46</sup> Thus the spectra in Figure 2.7 are representative of all of the methyl MQ samples listed in Table 2.1. Spectra for MQ-1600 and MQ copolymers prepared using the Goodwin and Magee methods are included in Figures 2.2, 2.3 and 2.4. The  $^1\text{H-NMR}$  spectrum (Figure 2.7a) shows a singlet for trimethylsilyloxy (M) groups at  $\delta = 0.1$  and a sharp singlet at  $\delta = 1.43$  for cyclohexane, an internal standard added to the  $\text{CDCl}_3$  ( $\delta = 7.26$  - 1H impurity). The small peaks at  $\delta = 1.2$  and  $\delta = 3.9$  are due to residual ethoxy groups and the signals at  $\delta = 2.36$  and  $\delta = 7.17/7.25$  are due to toluene. The silanol proton is not apparent. The  $^{29}\text{Si-NMR}$  spectrum (Figure 2.7b) shows a peak for M groups at  $\delta = 12.4$ , a  $\text{Q}_3$  region (silicon with three siloxane bonds and containing one silanol or one residual ethoxy group) centered at  $\delta \sim -100$  and a  $\text{Q}_4$  region (silicon with 4 siloxane bonds) centered at  $\delta \sim -110$ . There is also a very broad background signal from  $\delta \sim -40$  to  $-130$  from the glass NMR tube that could not be completely removed using a Hahn pulse echo technique. I chose not to manually baseline correct the spectra shown in the Figures; this data was not used for quantitative analysis. The infrared spectrum for  $\text{M}_{32}\text{Q}_{64}$  shows a strong siloxane stretching vibration ( $\sim 1050 \text{ cm}^{-1}$ ),  $\text{CH}_3$  stretching ( $2904, 2950 \text{ cm}^{-1}$ ) and bending ( $1250 \text{ cm}^{-1}$ ) vibrations, as well as a broad peak due to residual Si-OH stretching ( $\sim 3100\text{-}3800 \text{ cm}^{-1}$ ).

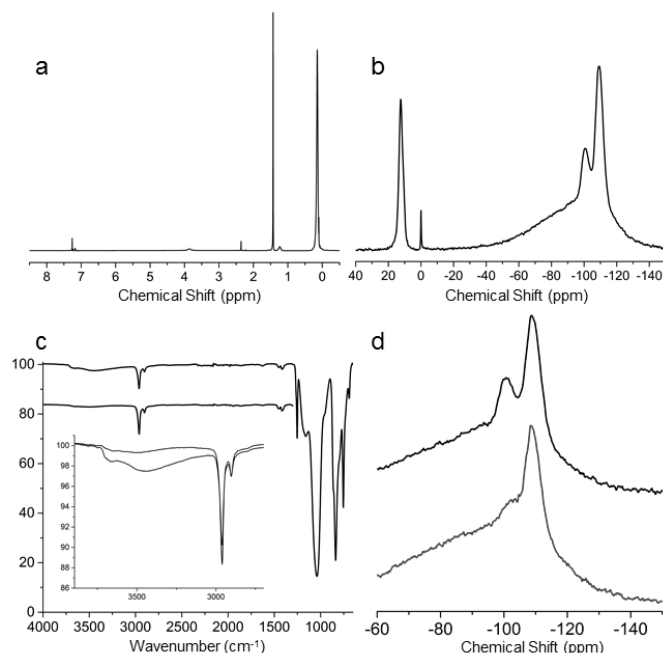


Figure 2.7. (a)  $^1\text{H}$  and (b)  $^{29}\text{Si}$  NMR of  $\text{M}_{32}\text{Q}_{64}$ . (c) IR and (d)  $^{29}\text{Si}$  NMR Q region of  $\text{M}_{42}\text{Q}_{100}$  before (top) and after (bottom) reaction with trimethylsilyl iodide.

Also shown in Figure 2.7c are infrared data for the product of the reaction of  $\text{M}_{42}\text{Q}_{100}$  with excess trimethylsilyl iodide. This is a more reactive trimethylsilylating reagent than hexamethyldisiloxane. The intensity of the broad Si-OH stretching peak ( $\sim 3700\text{-}3000\text{ cm}^{-1}$ ) is significantly reduced (inset of Figure 2.7c). Figure 2.7d shows the Q region of the  $^{29}\text{Si}$ -NMR spectra for  $\text{M}_{42}\text{Q}_{100}$  before and after reaction with excess trimethylsilyl iodide. The signal for  $\text{Q}_3$  is significantly reduced (from  $\text{Q}_3:\text{Q}_4 \sim 0.30$  to  $\text{Q}_3:\text{Q}_4 \sim 0.05$ ) from its initial intensity indicating that the reaction of residual silanols with trimethylsilyl iodide proceeds in good yield. Residual ethoxy groups, which also contribute to the  $\text{Q}_3$  signal do not react with this reagent, as evidenced by  $^1\text{H}$ -NMR spectra. By  $^1\text{H}$  NMR the M:Q ratio increases from 0.42 to 0.51.

Figure 2.8 shows GPC data for 4 of the preparative samples and the commercial sample, MQ-1600. These chromatograms are representative of those for all of the MQ

copolymers described in Table 2.1. The molecular weights assigned to MQ copolymers in Table 2.1 are based on linear PMMA standards in THF. I am aware that these are relative values that cannot be used to assign an absolute molecular weight; however, the data clearly show that this preparative procedure permits fairly good control of average molecular weight, that the molecular weight characteristics of the commercial sample, MQ-1600, are bracketed by samples prepared with 4 h and 16 h sol reaction times and that much higher molecular weight polymers can be prepared, albeit with lower yield, at 48 h sol reaction times. All of these samples exhibit high polydispersity indices and these values increase with increasing molecular weight.  $M_{66}Q_{164}$  contains molecules with molecular weight values over 300 000 g/mole.  $M_{46}Q_{121}$  has a component with molecular weight over  $10^6$  g/mole! In addition to GPC, diffusion NMR<sup>47</sup> (D-NMR) and dynamic light scattering (DLS) experiments were carried out to study the size of MQ silicones. The hydrodynamic radii measured using these methods and a calculated value based on GPC data are shown in Table 2.4. The value determined from GPC is based on each sample's peak molecular weight,  $M_p$  relative to linear PMMA in THF<sup>41</sup>, thus providing an estimate of the hydrodynamic radius of the most abundant species in solution. DLS is biased toward the largest diffusing species and D-NMR is biased toward the smallest diffusing species in solution. Figure 2.9 contains DLS correlation functions and D-NMR decay curves measured for MQ copolymer samples.

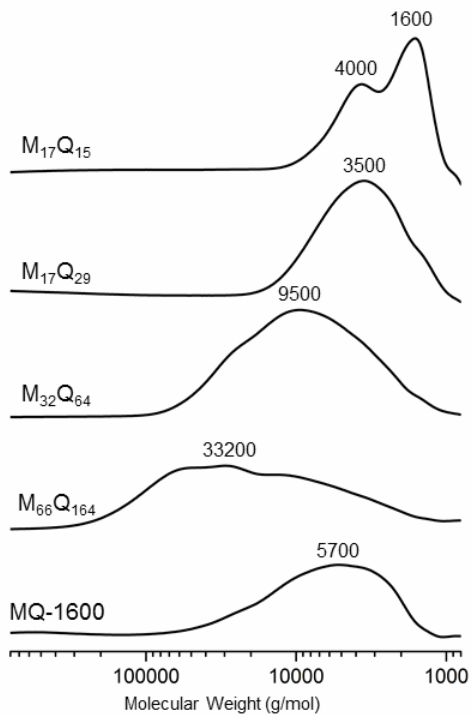


Figure 2.8. GPC chromatographs of preparative samples and commercial MQ copolymers.

Table 2.4. Estimated hydrodynamic radii (in nm) based on GPC, D-NMR and DLS

sample	GPC	D-NMR	DLS
	( $M_p$ , THF)	(d-chloroform)	( <i>o</i> -xylene)
M <sub>17</sub> Q <sub>15</sub>	1.02	0.55	-
M <sub>17</sub> Q <sub>29</sub>	1.48	0.94	-
M <sub>32</sub> Q <sub>64</sub>	2.35	1.72	3.45
M <sub>66</sub> Q <sub>164</sub>	4.22	2.53	33.5

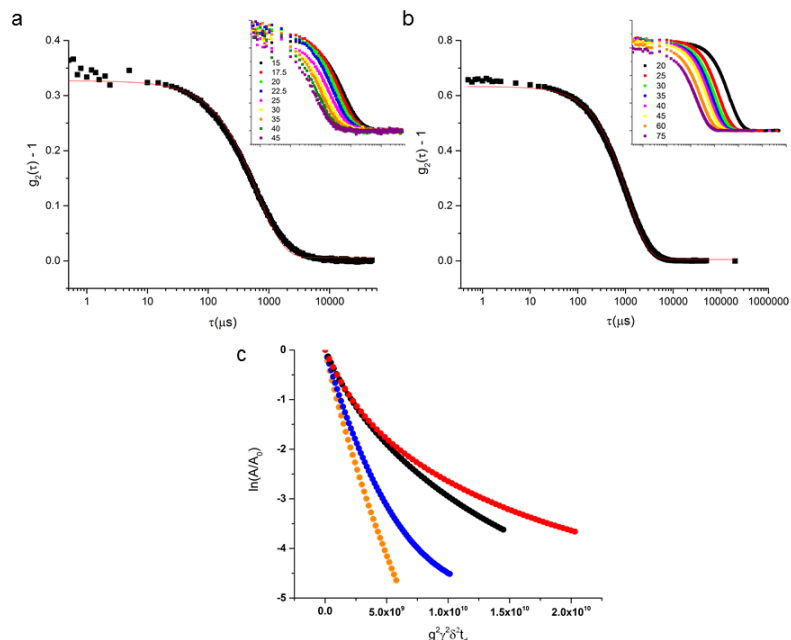


Figure 2.9. (a) DLS correlation function of  $M_{32}Q_{64}$  in *o*-xylene at  $15^\circ$  with inset of correlation functions at increasing angles. The red line is a single exponential fit to the black data points. (b) DLS correlation function of  $M_{66}Q_{164}$  in *o*-xylene at  $30^\circ$  with inset of correlation functions at increased angle. The red line is a single exponential fit to the black data points. Diffusion coefficients for the MQ copolymers were determined by the linear fit of decay constants ( $\Gamma$ ) plotted against the square of the scattering vector ( $q^2$ ). (c) D-NMR diffusion decays for  $M_{17}Q_{15}$  (orange),  $M_{17}Q_{29}$  (blue),  $M_{32}Q_{64}$  (black) and  $M_{66}Q_{164}$  (red) in *d*-chloroform. For diffusion coefficients determined by DLS and D-NMR, the Stokes-Einstein relationship was used to estimate the hydrodynamic radius.

In the dynamic light scattering experiments, correlation functions at multiple angles were fitted to single exponential decay functions to obtain a diffusion coefficient in *o*-xylene from which a hydrodynamic radius was calculated. Multiple concentrations were tested to ensure that individual molecules and not aggregates were being observed. There are challenges regarding characterization of MQ copolymers using light scattering techniques. Low scattering contrast gave weak correlation functions and required long scattering times at low angles. The contrast was too low to obtain meaningful data for  $M_{17}Q_{15}$  and  $M_{17}Q_{29}$ . High concentrations of  $M_{32}Q_{64}$  were required for adequate contrast which can lead to multiple scattering, resulting in a faster apparent decay time and an underestimation of hydrodynamic radius.  $M_{66}Q_{164}$  provided better contrast but the high polydispersity and

multimodal distribution (Figure 2.8) led to greater error in the exponential fitting. Additionally, DLS measurements are sensitive to the largest molecules in solution (scattering intensity being proportional to the sixth power of the radius). This is apparent for  $M_{66}Q_{164}$  where the estimated radius corresponds to the front shoulder of the GPC data and not the number average or peak estimate. Static light scattering (SLS) and multi-angle light scattering (MALS) were also attempted in hopes of determining the radius of gyration, the second virial coefficient and absolute molecular weight, but proved ineffective. The size and low  $dn/dc$  values of the MQ copolymers provided insufficient contrast at the low concentrations required for accurate, meaningful data. Multiple solvents were tested but none provided adequate contrast. Only careful solvent selection and testing made dynamic light scattering of the higher molecular weight MQ copolymer samples possible. Addition of high refractive index moieties onto MQ resins would be a method to increase scattering contrast that we did not pursue.

D-NMR proved to be a useful tool in characterizing MQ copolymers in solution. The slope of the decay curves for each copolymer in Figure 2.9 represents a diffusion coefficient of a species in chloroform. The shape of the decay curves is an indication of the dispersity of the sample. The lower molecular weight MQ copolymers have the steepest slopes, the fastest diffusion, and the lowest polydispersity (as supported by GPC). The largest MQ copolymer exhibits slower diffusion and the curvature indicates high polydispersity. From the diffusion coefficient, a hydrodynamic radius can be estimated using the Stokes-Einstein equation. D-NMR appears to be most sensitive to the smallest molecules in solution as shown by the data in Table 2.4.

Transmission electron microscopy is likely a very useful technique to study MQ copolymers. With the help of Dr. Alex Ribbe, sufficient data was obtained to make this

statement but I did not follow through on more careful studies. My interest was to focus on these materials as molecules and I consciously abandoned microscopy, largely to my lack of skill in this technique. Figure 2.10 shows one of several TEM micrographs of  $M_{32}Q_{64}$  that were obtained by dipping a wet (water) TEM grid into a toluene solution of  $M_{32}Q_{64}$  and drying. The contrast clearly shows the particle-like structure of these molecules. The diameters of 100 imaged molecules were measured to be  $4.15 \pm 2.12$  nm.

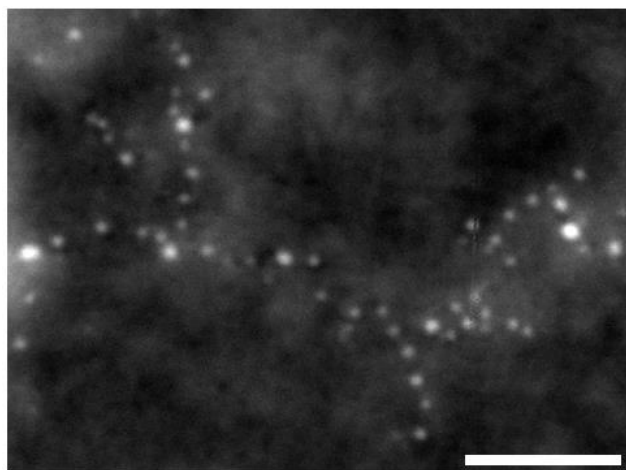


Figure 2.10. Dark field TEM micrographs of  $M_{32}Q_{64}$  sample. Scale bar is 50 nm. (Image courtesy Dr. Alex Ribbe)

The thermal stability and degradation behavior of MQ copolymers was studied using TGA. MQ copolymers were heated to 900 °C in a nitrogen atmosphere at a rate of 10 °C/min. As seen in Figure 2.11, there is a notable molecular weight - dependent thermal stability for the lower molecular weight samples.  $M_{17}Q_{15}$  contains a significant volatile component and exhibits almost 60% mass loss below 300 °C.  $M_{17}Q_{29}$  degrades at temperatures and rates that are similar to MQ-1600.  $M_{32}Q_{64}$  and  $M_{66}Q_{164}$  exhibit greater thermal stability than the commercial sample. Residual mass values for the solid copolymers at 900 °C increase with increasing Q content. Differential scanning calorimetry was performed to determine any thermal transitions in MQ copolymers. No



thermal transitions were observed for M<sub>17</sub>Q<sub>29</sub>, M<sub>32</sub>Q<sub>64</sub>, M<sub>66</sub>Q<sub>164</sub>, or MQ-1600; M<sub>17</sub>Q<sub>15</sub> exhibits a T<sub>g</sub> at -109 °C. Although there was no measurable glass transition observed for M<sub>17</sub>Q<sub>29</sub> or MQ-1600, "softening points" were observed at ~100 °C and ~300 °C respectively using a melting point apparatus; M<sub>32</sub>Q<sub>64</sub> and M<sub>66</sub>Q<sub>164</sub> did not show softening points.

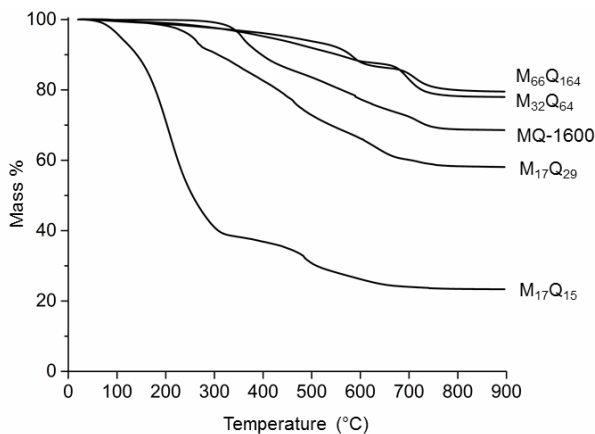


Figure 2.11. TGA decomposition profiles of MQ copolymers under nitrogen.

### 2.3.3 MQ Copolymer Structure

The data described in the previous section can be interpreted to yield chemical structural information concerning these molecules. These interpretations, in some ways, are unambiguous and give rather lucid insight into MQ copolymer structure. In other ways ambiguity is unavoidable. These materials are polydisperse in molecular weight and this is obvious from the data presented in Table 2.1 and Figure 2.8. They are also polydisperse in M:Q ratio, branching and polycyclic ring structure (topology), as well as in residual silanol content. Although it is possible to interpret the data and draw consistent chemical structures, the preparative difficulties described above spawn obvious challenges in comparing these samples and structures with materials reported from other labs. I use a commercial sample, Dow Corning MQ-1600, to calibrate my MQ copolymers against and

some comments are warranted concerning this choice. There is no standard MQ resin. Numerous companies market these materials. Dow Corning offers MQ-1600 as an isolated solid resin in addition to many silicone formulations containing MQ resins, Momentive Performance Products offers SX1000 as a solid resin, Wacker produces an MQ resin powder 803TF, Shin-Etsu markets MQ resins as components of emulsifiers, BlueStar sells numerous MQ resins as powders or dissolved in organic solvents, SilTech has a library of MQ resins which range from viscous liquids to solids and come pure or in solvent, and Gelest sells vinyl and hydride functional MQ resins. Literature reports describe samples obtained primarily from Dow Corning,<sup>48-53</sup> but also from Wuhan Green Chemical Technology<sup>54</sup>, Shandong Dayi Chemical<sup>55</sup>, Shanghai Ai Shi Bo Silicon Material<sup>56</sup>, Shenzhen Haili Chemical<sup>57</sup>, Runhe Chemical Industry<sup>58</sup> and GuangZhou Gigantic Silicon Material<sup>59</sup>. MQ-1600 stands out among these possible choices. It is mentioned by name (and product number) in over 100 patents as a component in the formulation of cosmetics, sunscreens, adhesives and elastomers. It is sold as "solid 100% trimethylsilylsilicate resin." Dow Corning compares their other products with it in marketing literature and provides free samples. It is likely prepared using a modern continuous version of the Daudt/Tyler procedure.

The composition of the MQ copolymers (M:Q ratio) was determined from the <sup>1</sup>H-NMR data using the mass of the MQ copolymer sample and the concentration of the internal standard, cyclohexane. These data (Table 2.1) are precise and the analytical method is much more accurate and reproducible than the synthesis. Of 7 samples prepared with sol reactions of 16 or 18 h, four had M:Q ratios of 0.40-0.42, but two had 0.49 and one had 0.30. The four samples prepared with 4 h sol reactions had M:Q ratios of 0.45-0.52 and the three samples prepared with 48 h sol reactions had M:Q ratios of

0.29-0.38. There is a clear trend of decreasing M:Q ratio with increasing molecular weight and sol reaction time.

I have not measured an absolute molecular weight for any of the MQ copolymers and note that freezing point depression (cyclohexane) did not give reproducible results and that no meaningful data were obtained from attempts at static light scattering or MALDI-TOF mass spectrometry. I would expect higher absolute molecular weight values than what we measure using GPC molecular weights relative to linear PMMA due to the dense, polycyclic structure and this has in fact been observed by other researchers measuring low molecular weight MQ copolymers.<sup>32</sup> That said, I am very comfortable with the GPC relative molecular weight data reported in Table 2.1. All of the reported samples are so polydisperse that a precise absolute value would give no better insight into the structure of these polymers. The D-NMR and dynamic light scattering experiments are consistent with the GPC data. Figure 2.8 shows graphically that molecular weight can clearly be controlled and MQ copolymers can be prepared with peak molecular weights ( $M_p$ ) of ~3500, ~9500 and ~33 000 g/mol by controlling the sol reaction time. The polydispersity index ( $M_w/M_n$ ) increases with increasing molecular weight, a characteristic of sol gel reactions. Samples are labeled as  $M_{XX}Q_{YY}$  based on the  $M_n$  value and the M:Q ratio.

All of the MQ copolymers contain residual silanols and a small amount of residual ethoxy groups. The  $Q_3:Q_4$  ratio, as assessed by  $^{29}\text{Si}$  NMR, is strikingly similar (~1:10) for all samples including the commercial sample, MQ-1600 (Figure 2.2). The reaction of  $M_{42}Q_{100}$  with trimethylsilyl iodide converts ~90% of the  $Q_3$  silicon to  $Q_4$  and the O-H absorbance in the infrared spectrum is similarly attenuated (Figure 2.7).  $^1\text{H}$  NMR reveals that the M:Q ratio increases from 0.42 to 0.51 upon reaction, that the ratio of ethoxy groups

to trimethylsilyl (M) groups is ~1:40 (before reaction) and that ethoxy groups are not removed by reaction with Me<sub>3</sub>SiI. These data allow the structure M<sub>42</sub>Q<sub>100</sub>(OH)<sub>10</sub>(OEt)<sub>1</sub> to be formulated for the MQ molecule that reacts with trimethylsilyl iodide to form M<sub>51</sub>Q<sub>100</sub>(OH)<sub>1</sub>(OEt)<sub>1</sub>. Molecular weights for M<sub>42</sub>Q<sub>100</sub>(OH)<sub>10</sub>(OEt)<sub>1</sub> and M<sub>51</sub>Q<sub>100</sub>(OH)<sub>1</sub>(OEt)<sub>1</sub> are 9617 and 10 193 g/mol. This sample is polydisperse and contains molecules ranging from ~1300 to ~106 000 g/mol.

A hypothetical symmetrical structure for M<sub>16</sub>Q<sub>32</sub> is shown in Figure 2.1 that does not indicate the residual silanols or ethoxy groups that are present in the actual sample. This is depicted again as "M<sub>16</sub>Q<sub>32</sub>" in Figure 2.12 using a line drawing scheme in which the intersections indicate tetra-coordinate Q units that contain attached M units (not shown) in remaining valence sites. Also shown are chemical structures that are consistent with the spectroscopic and molecular weight data for M<sub>16</sub>Q<sub>32</sub> and M<sub>42</sub>Q<sub>100</sub>. A different isomer for M<sub>16</sub>Q<sub>32</sub> that contains 4 silanols is shown and labeled M<sub>16</sub>Q<sub>32</sub>(OH)<sub>4</sub>. M<sub>42</sub>Q<sub>100</sub>(OH)<sub>10</sub>(OEt)<sub>1</sub> is a structure consistent with the data discussed above.

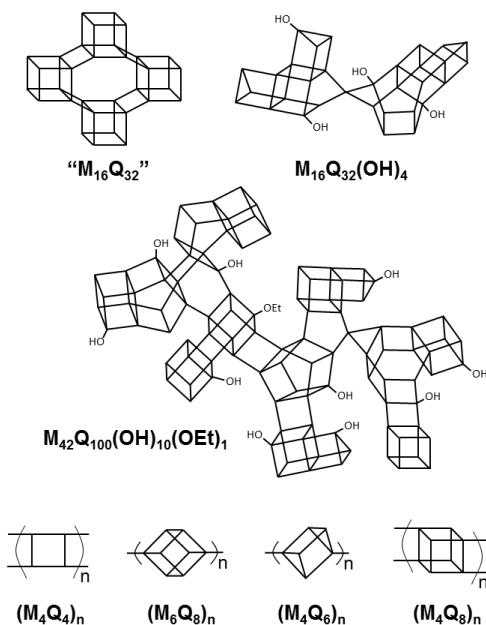


Figure 2.12. MQ copolymer structures

The "fabricated" cage-like structures labeled  $M_{16}Q_{32}(OH)_4$  and  $M_{42}Q_{100}(OH)_{10}(OEt)_1$  in Figure 2.12 are presented with no direct evidence that any of the specific components exist as drawn. However, these structures are useful as graphic depictions of a particular molecular weight component of the MQ copolymers and the specific components drawn are representative of the features present in these molecules. In fact, the analytical data put rather severe restrictions on and dictate the molecular structure of the components present. In particular, the low M:Q ratios for these copolymers (0.29 - 0.52) prescribe large numbers of rings, thus dense polycyclic ring systems are required to be present to account for the stoichiometry. For example, any structure for  $M_{42}Q_{100}(OH)_{10}(OEt)_1$  must contain 70 rings. Copolymers with lower M:Q ratios contain greater ring density. The pentacyclic  $Q_8$  motif is favored in the drawn structures for several reasons: cyclic tetramer rings form more readily and are less strained than cyclic trimer rings in silicic acid polymerization,<sup>43</sup>  $M_8Q_8$  can be prepared in good yield,<sup>13</sup> and this

structure ( $T_8$ ) is the major oligomeric component in equilibrated silsesquioxanes.<sup>60</sup> The structures drawn at the bottom of Figure 2.12 with repeat unit structures  $M_4Q_4$ ,  $M_6Q_8$ ,  $M_4Q_6$  and  $M_4Q_8$  have M:Q ratios of 1.0, 0.75, 0.67 and 0.5. The low observed M:Q ratios dictate that these structural elements cannot be prevalent in these MQ materials.

It must be reiterated that these copolymers are polydisperse in molecular weight and M:Q ratio.  $M_{42}Q_{100}$  contains, in addition to the  $M \sim 10\,000$  g/mol component shown in Figure 2.12, portions with  $M_n \sim 2\,000$  g/mol and  $M_n \sim 100\,000$  g/mol. Lower molecular weight fractions have less condensed Q skeletons and higher M:Q ratios (fewer rings) whereas higher molecular weight fractions have more condensed Q skeletons and lower M:Q ratios (more rings). This trend in molecular weight - dependent composition (and structure) is observed in Table 2.1 for samples prepared with controlled sol reaction time and is expected as a consequence of separating the sol reaction and the end-capping reaction in order to control molecular weight. The sol becomes more condensed as it grows in size under conditions designed to delay gelation. A schematic representation of this process is shown in Figure 2.13, which depicts silicic acid polymerizing in a fashion which the density of cyclic structures increases with extent of reaction and which explains the trends in M:Q ratios that are observed. That intramolecular (non-random) cyclization is favored in acid-catalyzed TEOS hydrolysis/condensation (sol-gel reactions) has been addressed<sup>45</sup> and the repeat unit structure,  $M_4Q_6$  (Figure 2.12), is used by these authors to explain delayed gelation. The analytical data reported here (low M:Q ratios) indicates that the non-random cyclization trend described<sup>45</sup> is more extensive than indicated.

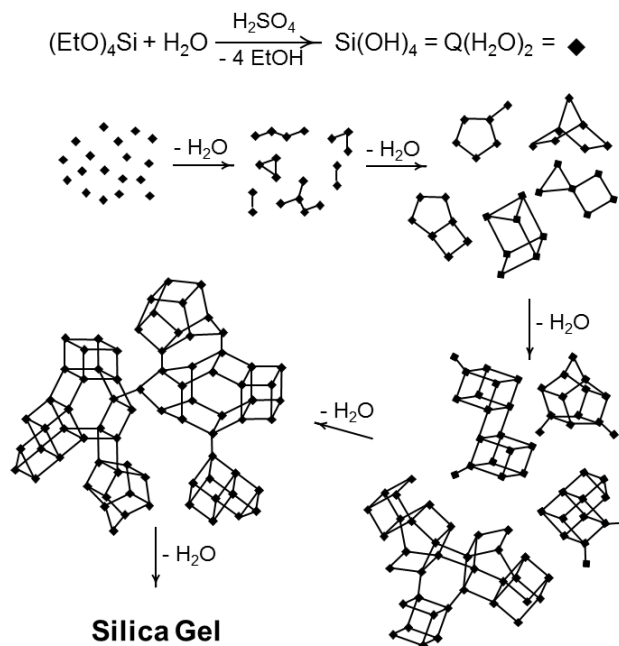


Figure 2.13. Formation of polycyclic structures during sol growth.

The MQ copolymers that are reported (Table 2.1) are different than those prepared by the Goodwin and the Magee methods and different also than those reported in other publications. The low M:Q ratios of these samples, with the retention of solubility, sets them apart from other reported MQ copolymers. This is likely due to the separation of the sol and end-capping reactions. These MQ copolymers have significantly lower M:Q ratios than the commercial sample, Dow Corning MQ-1600 (M:Q = 0.63), but can be prepared with similar molecular weight. The composition of MQ-1600 is  $\text{M}_{32}\text{Q}_{51}$  based on its  $M_n$  value and  $^1\text{H-NMR}$  data. This suggests that a denser silica core is grown when the end-capping reaction no longer competes with growth. The inorganic core and organic shell in these MQ copolymers makes them particle-like hybrid molecules.<sup>33</sup>

#### 2.3.4 MQ Copolymer Chemical Modification

Having developed a reproducible method of preparing MQ copolymers and exploring their physical structure, the final objective of this work involved investigating the chemistry of MQ copolymers. I believe that MQ copolymers are ideal candidates for chemical modification for expansion of both academic study and practical applications. Advantages of MQ over other nanoparticle platforms include its solubility, synthetic control of molecular weight and the synthetic control of chemical functionality. As prepared, MQ copolymers contain functional silanols (Figure 2.7) but there is limited control over the functional density afforded in the synthetic method presented here. Controllable levels of functionality can be incorporated using functional M silanes (Figure 2.6). Three modification methods of MQ are presented to demonstrate versatility as a synthetic platform: (1) reaction through silanols, (2) reaction through silicon hydrides and (3) reactions through vinyl groups.

Silanol-containing MQ affords two modification methods common to siloxane chemistry: condensation reactions and the Piers-Rubinsztajn reaction. The condensation of silanol residues has already been demonstrated above using trimethylsilyliodide (Figure 2.7). Additionally, condensation reactions using disilazanes are commonly utilized in patents to incorporate vinyl groups into MQ and proved effective as shown in Figure 2.14. Tris(pentafluorophenyl)borane ( $B(C_6F_5)_3$ ) catalyzed condensation of silanols with hydridosilanes (the Piers-Rubinsztajn reaction) was very effective on MQ substrates. Two reactions are demonstrated: (1) a model reaction with pentamethyldisiloxane (Figure 2.15) and (2) the addition of octadecyldimethylsilane to MQ (Figure 2.16). Yields for these reactions are high based on the nearly complete removal of silanols as evidenced in  $^{29}\text{Si}$  NMR and IR spectra. In addition to these modifications that result in discrete MQ molecules, BCF catalyst can also be used to form MQ-PDMS elastomers via condensation



of MQ silanols and hydride-terminated PDMS. This was confirmed in a handful of experiments but not investigated.

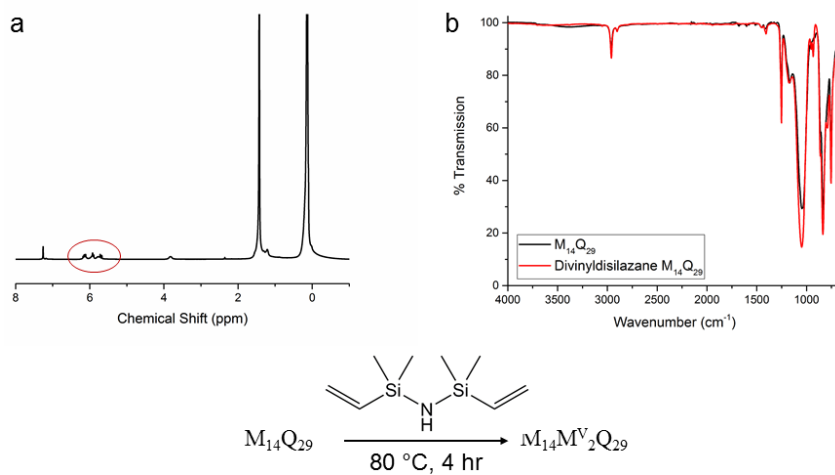


Figure 2.14. Condensation of silanol residues on  $M_{14}Q_{29}$  using divinyltetramethyldisilazane. (a)  $^1\text{H}$  NMR and (b) IR show incorporation of vinyl groups and loss of silanols.

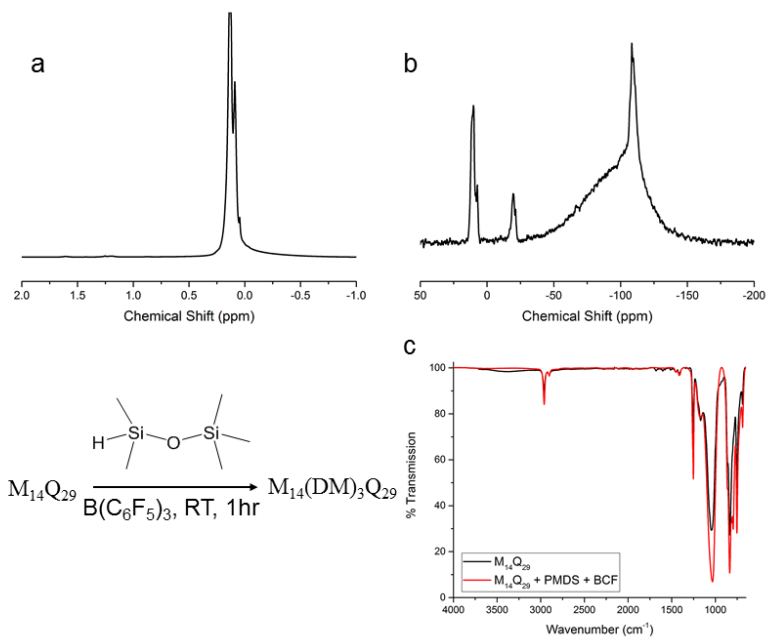


Figure 2.15.  $\text{B}(\text{C}_6\text{F}_5)_3$ -catalyzed condensation of residual silanols on MQ with pentamethyldisiloxane. (a)  $^1\text{H}$  NMR spectrum shows a peak associated with  $\text{D}^{\text{Me}}$  and (b)  $^{29}\text{Si}$  NMR shows disappearance of  $\text{Q}^3$  and appearance of D. (c) IR shows loss of silanols.

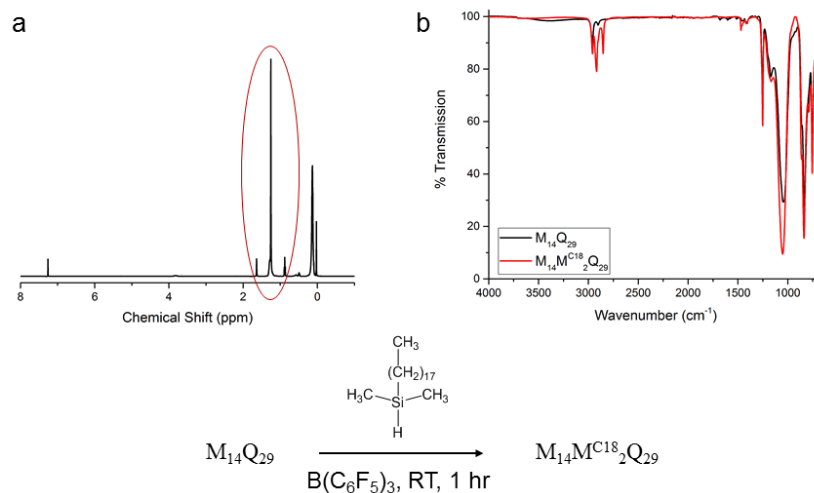


Figure 2.16.  $B(C_6F_5)_3$ -catalyzed condensation of residual silanols on MQ with octadecyldimethylsilane. (a)  $^1H$  NMR spectrum shows octadecyl peak and no residual Si-H. (b) IR shows loss of silanols.

MQ copolymers prepared using tetramethyldisiloxane ( $^HMM^H$ ) and divinyltetramethyldisiloxane ( $^VM^V$ ) lend themselves to hydrosilylation. Networks were prepared using  $^HMQ$  and  $^VD$  or  $^VMQ$  and  $^HD$ , however these materials were not investigated in detail. Two hydrosilylation-catalyzed grafting reactions of MQ are shown in Figure 2.17 and Figure 2.18. Grafting of allyl-poly(ethyleneoxide) (Gelest, ENEA0260,  $M_n = 480$ ) onto  $^HMQ$ , shown in Figure 2.17, results in a water dispersible MQ.  $^HD_{18}^{Me}$  (Gelest MCR-H11) was grafted to  $^VMQ$ , shown in Figure 2.18 by diffusion NMR and GPC. Grafting of molecules and macromolecules onto MQ copolymers changes the physical and chemical properties of the MQ in ways which expand its utility.

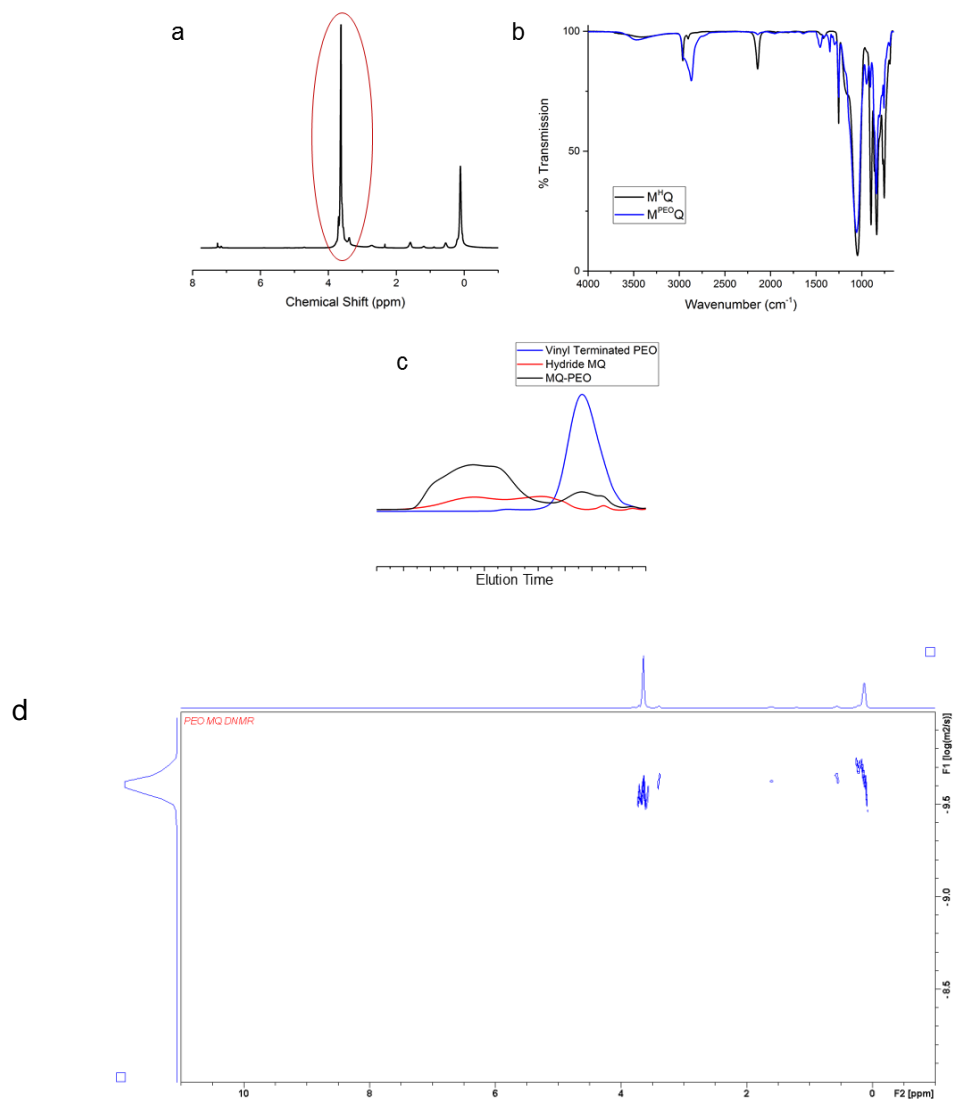


Figure 2.17. Pt-catalyzed hydrosilylation of  ${}^1\text{HMQ}$  and allyl-PEO. (a)  ${}^1\text{H}$  NMR shows disappearance of Si-H and allyl protons and appearance of ethyleneoxide protons. (b) IR confirms disappearance of Si-H and PEO addition. (c) GPC chromatographs and (d) 2D DNMR spectrum of  ${}^1\text{HMQ}$  and allyl-PEO and  ${}^1\text{HMQ-graft-PEO}$ . Due to dispersity of the MQ sample, grafting is not clear in GPC but DNMR provides evidence that both PEO and MQ peaks diffuse simultaneously. Along with the disappearance of Si-H and allyl groups, this clearly shows that the grafting was successful.

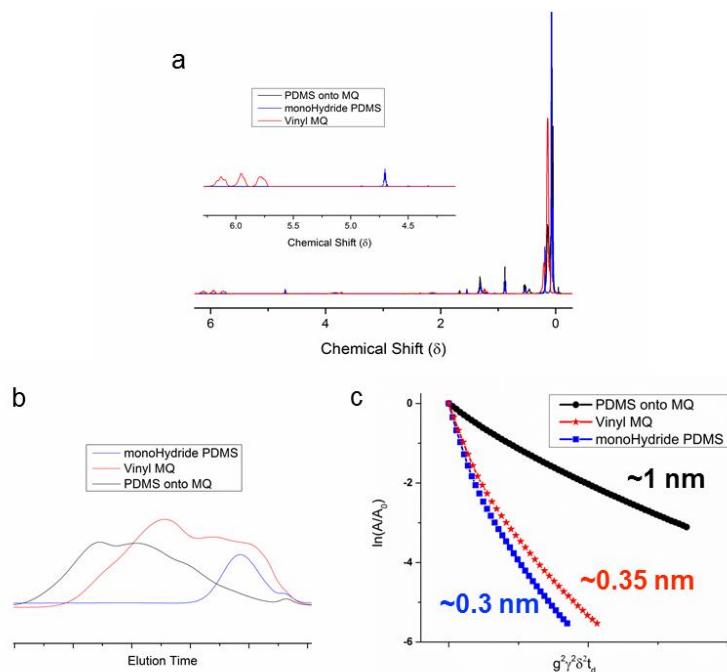


Figure 2.18. Pt-catalyzed hydrosilylation of  ${}^{\text{H}}\text{D}_{18}{}^{\text{Me}}$  onto  ${}^{\text{V}}\text{MQ}$ . (a)  ${}^1\text{H}$  NMR shows disappearance of Si-H and vinyl protons indicating complete reaction and clean product. (b) GPC and (c) D-NMR show increase in molecular weight/size from  ${}^{\text{H}}\text{D}_{18}{}^{\text{Me}}$  and  ${}^{\text{V}}\text{MQ}$  to  ${}^{\text{V}}\text{MQ-graft-}{}^{\text{H}}\text{D}_{18}{}^{\text{Me}}$ .

I must emphasize again that modifications reactions were not optimized. The reactions presented above and numerous other reactions have been run as illustrative examples of MQ's utility as a substrate. The conditions for the various reactions were not optimized for yield or efficiency. No precise kinetics were carried out. I suspect that each method of modifying MQ will have unique challenges: perhaps the most difficult being the purification MQ product. For this reason, most MQ modifications were run with volatile reagents that could be removed in a vacuum oven or with excess MQ so that excess reagent would not be present. There is much to be explored in the domain of functional MQ copolymers that involves optimizing functional densities, characterizing novel MQ properties and understanding if and how the unique structure of MQ can act synergistically with new chemistries.

## 2.4 Conclusions and Comments

MQ copolymers are important commodity materials that we believe should have broader impact than they currently do. I want to encourage chemists, engineers and scientists to explore the versatility of MQ copolymers to address the challenges of modern materials science. These unusual molecules are structurally similar to silica nanoparticles, yet 'dissolve' in organic solvents. These copolymers can be described as *phantom nanoparticles* due to the unique position they occupy between solid particle and soluble macromolecule. The method reported here allows MQ copolymers to be reproducibly synthesized in the form of viscous liquids (liquid nanoparticles) or solid organic-soluble powders. The incorporation and utilization of functional handles permits derivatization for specific physical properties and chemical reactivity. Characterization of these MQ silicones highlights their polycyclic silica-like structure; however, further investigations into the physical structure of MQ remains an open challenge. There is an art to the reproducible synthesis of MQ copolymers, but I believe the method developed in this research makes it possible for academic labs to create their own designer MQ silicones and I highly encourage these pursuits.

## 2.5 References

1. Butts, M.; Cella, J.; Wood, C. D.; Gillette, G.; Kerboua, R.; Leman, J.; Lewis, L.; Rubinsztajn, S.; Schattenmann, F.; Stein, J.; Wicht, D.; Rajaraman, S.; Wengrovius, J. Silicones. In *Encyclopedia of Polymer Science and Technology*, 2nd ed.; Wiley & Sons: New York, 2003, vol. 11, pp. 765-841.
2. Butts, M.; Cella, J.; Wood, C. D.; Gillette, G.; Kerboua, R.; Leman, J.; Lewis, L.; Rubinsztajn, S.; Schattenmann, F.; Stein, J.; Wicht, D.; Rajaraman, S.; Wengrovius, J. Silicones. In *Kirk-Othmer Encyclopedia of Chemical Technology*, Wiley & Sons: New York, 2006, vol. 22, pp. 547-626.

3. Lewis, L. N.; Wengrovius, J. H.; Burnell, T. B.; Rich, J. D. Powdered MQ Resin - Platinum Complexes and Their Use as Silicone-Soluble Hydrosilylation Cure Catalysts. *Chem. Mater.* **1997**, *9*, 761-765.
4. Zheng, P.; McCarthy, T. J. Rediscovering Silicones: Molecularly Smooth, Low Surface Energy, Unfilled, UV/Vis-Transparent, Extremely Cross-Linked, Thermally Stable, Hard, Elastic PDMS. *Langmuir* **2010**, *26*, 18585-18590.
5. Krumpfer, J. W.; McCarthy, T. J. Rediscovering Silicones: "Unreactive" Silicones React with Inorganic Surfaces, *Langmuir* **2011**, *27*, 181514-11519.
6. Zheng, P.; McCarthy, T. J. A Surprise from 1954: Siloxane Equilibration Is a Simple, Robust, and Obvious Polymer Self-Healing Mechanism. *J. Am. Chem. Soc.* **2012**, *134*, 2024-2027.
7. Rochow, E. G. Methyl Silicones and Related Products. U.S. Patent 2,258,218, October 7, 1941.
8. Rochow, E. G.; Gilliam, W. F. Polymeric Methyl Silicon Oxides. *J. Am. Chem. Soc.* **1941**, *63*, 798-800.
9. Hyde, J. F.; DeLong, R. C. Condensation Products of the Organo-silane Diols. *J. Am. Chem. Soc.* **1941**, *63*, 1194-1196.
10. McGregor, R. R.; Warrick, E. L. Organo-Silicon Polymers and Methods of Making Them. U.S. Patent 2,375,998, May 15, 1945.
11. Hurd, C. B. Studies on Siloxanes. I. The Specific Volume and Viscosity in Relation to Temperature and Constitution. *J. Am. Chem. Soc.* **1946**, *68*, 364-370.
12. This structure as a theoretical possibility was drawn in: Kuroda, K.; Kato, C. Synthesis of Polyorganosiloxane retaining SiO<sub>4</sub> Framework from Inosilicate Mineral by Trimethylsilylation. *Polymer* **1978**, *19*, 1300-1302.
13. Gromilov, S. A.; Basova, T. V.; Emel'yanov, D. Y.; Kuzmin, V.; Prokhorova, S. Layer Arrangement in the Structure of Octakis(trimethylsiloxy)octasilsesquioxane and Dodecakis(trimethylsiloxy)cyclohexasiloxane. *J. Structural Chem.* **2004**, *45*, 471-475.
14. The Dow Corning product, MQ-1640 is a blend of methyl-MQ and propyl-T resins.
15. Wengrovius, J. H.; Burnell T. B.; Zumburum M. A. 10th *International Symposium on Organosilicon Chemistry*, Poznan, Poland, August 1993.
16. Arkles, B.; Larson, G. L. *Silicon Compounds: Silanes and Silicones*, 3rd Edition; Gelest, Inc.: Morrisville, PA., 2013, p. 535.
17. Arkles, B. Future Developments in Silicon Chemistry - An Industrial Perspective. *Main Group Chem. News*, **1994**, *2(2)*, 4-10.
18. Griswold, R. M.; Krencieski, M.; Wengrovius, J. Designing Silicone PSAs. *Adhesives Age* **2002**, *45(9)*, 35-40.
19. Marciniak, B.; Chojnowski, J. *Progress in Organosilicon Chemistry*; Overseas Publishers Association: Amsterdam, 1995, p. 575.

20. Yoshii, K.; Yamashita, T.; Machida, S.; Horie, K.; Itoh, M.; Nishida, F.; Morino, S. Photo-probe study of siloxane polymers. I. Local free volume of an MQ-type silicone resin containing crosslinked nanoparticles probed by photoisomerization of azobenzene. *J. Non-Crystal. Solids* **1999**, *246*, 90-103.
21. Amouroux, N.; Petit, J.; Léger, L. Role of Interfacial Resistance to Shear Stress on Adhesive Peel Strength. *Langmuir* **2011**, *17*, 6510-6517.
22. Langley, N. R.; Mbah, G. C.; Freeman, H. A.; Huang, H.-H.; Siochi, E. J.; Ward, T. C.; Wilkes, G. Physical Structure of Polysilicate Particles in Organic Media. *J. Coll. Interfac. Sci.* **1991**, *143*, 309-317.
23. We note that MQ surface coatings that were prepared by vapor phase reactions of the  $\text{SiCl}_4/\text{Me}_3\text{SiCl}$  azeotrope were reported earlier: Norton, F. J. Production of Water-Repellent Materials. U.S. Patent 2,412,470, Dec. 10, 1946.
24. Daudt, W. H.; Tyler, L. J. Copolymeric Siloxanes and Methods of Preparing Them. U.S. Patent 2,676,182, Apr. 20, 1954.
25. Goodwin, J. T. Organopolysiloxane Compositions Having Pressure-Sensitive Adhesive Properties. U.S. Patent 2,857,356, Oct. 21, 1958.
26. Wengrovius, J. H.; Burnell T. B.; Zumbum M. A. Method for Making Substantially Silanol-Free Silicone Resin Powder, Product and Use. U.S. Patent 5,319,040, Jun. 7, 1994.
27. Wengrovius, J. H.; Green R. W.; Capuano, C. F. Continuous process for producing a silicon resin. European Patent 1,113,036, Dec. 21, 2005.
28. Ramdani, K.; Bossy H.; Lomel, S.; Durand N. Process for Preparing a Silicone Resin. U.S. Patent 7,951,895, May 31, 2011.
29. Mironova, M. V.; Tatarinova, E. A.; Meshkov, I. B.; Muzafarov, A. M.; Kulichikhin, V. G. Rheological and Relaxation Properties of MQ Copolymers. *Polym. Sci., Ser. A* **2012**, *54*, 177–186.
30. Huang, W. E. I.; Huang, Y.; Yu, Y. Synthesis of MQ Silicone Resins through Hydrolytic Condensation of Ethyl Polysilicate and Hexamethyldisiloxane. *J. Appl. Polym. Sci.* **1998**, *70*, 1753–1757.
31. Huang, W.; Huang, Y.; Yu, Y. The effect of the acid catalyst on the preparation of MQ silicone resins. *Chinese J. Polym. Sci.* **1999**, *17*, 429–433.
32. Ganicz, T.; Pakula, T.; Stańczyk, W. A. Novel liquid crystalline resins based on MQ siloxanes. *J. Organomet. Chem.* **2006**, *691*, 5052–5055.
33. Voronina, N. V.; Meshkov, I. B.; Myakushev, V. D.; Laptinskaya, T. V.; Papkov, V. S.; Buzin, M. I.; Il'ina, M. N.; Ozerin, A. N.; Muzafarov, A. M. Hybrid organo-inorganic globular nanospecies: Transitions from Macromolecule to Particle. *J. Polym. Sci., Part A: Polym. Chem.* **2010**, *48*, 4310–4322.
34. Xu, X.; Wu, C.; Zhang, B.; Dong, H. Preparation, structure characterization, and thermal performance of phenyl-modified MQ silicone resins. *J. Appl. Polym. Sci.* **2013**, *128*, 4189–4200.

35. Kuo, C. F. J.; Chen, J. B.; Shih, C. Y.; Huang, C. Y. Silicone resin synthesized by tetraethoxysilane and chlorotrimethylsilane through hydrolysis-condensation reaction. *J. Appl. Polym. Sci.* **2014**, *131*, 1–8.
36. Lin, S.B. Addition-Cured Silicone Adhesive Technology: Vinyl Silicone Crosslinker. *J. Appl. Polym. Sci.* **1994**, *54*, 2134-2145.
37. Zhan, H.; Lu, X.; Cao J. New Application and Technology of Silicone Pressure Sensitive Adhesives. *J. Polym. Eng.* **1997**, *17*, 339-344.
38. Min, H.; Qiuyu Z.; Jiying G. Synthesis and characterization of silicone based pressure sensitive adhesive. *Adv. Mtls. Res.* **2011**, *306*, 1773-1778.
39. Sun F.; Hu Y.; Du H. Synthesis and Characterization of MQ Silicone Resins. *J. Appl. Polym. Sci.* **2012**, *125*, 3532-3536.
40. Xiang H.; Ge J.; Cheng S.; Han H.; Cui S. Synthesis and characterization of titania/MQ silicone resin hybrid nanocomposite via sol-gel process. *J. Sol-Gel Sci. Technol.* **2011**, *59*, 635-639.
41. Wagner, H. L. The Mark–Houwink–Sakurada relation for poly(methyl methacrylate). *J. Phys. Chem. Ref. Data.* **1987**, *16*, 165-173.
42. Magee W. L.; Emerson A. W.; Joslyn W. G.; Odneal R. S. MQ resins from stable ethylsilicate polymer polymers. U.S. Patent Appl. 2011/0184142 A1, Jul. 28, 2011.
43. Iler, R. K. *The Chemistry of Silica*; Wiley: New York, 1979.
44. Brinker, C. J.; Scherer, G. W. *Sol-Gel Science: The Physics and Chemistry of Sol-Gel Processing*; Academic Press: Boston, 1990.
45. Ng, L. V.; Thompson, P.; Sanchez, J. Macosko, C. W.; McCormick, A. V. Formation of Cagelike Intermediates from Nonrandom Cyclization during Acid-Catalyzed Sol-Gel Polymerization of Tetraethyl Orthosilicate. *Macromolecules* **1995**, *28*, 6471-6476.
46. Vasil'ev S. G.; Volkov V. I.; Tatarinova E. A.; Muzafarov A. M. A Solid-State NMR Investigation of MQ Silicone Copolymers. *Appl. Magn. Reson.* **2013**, *44*, 1015-1025.
47. Vasil'ev S. G.; Volkov V. I.; Tatarinova E. A.; Muzafarov A. M. Study of Self-Diffusion of Silicone MQ Resins in Chloroform Solutions by Pulsed Field-Gradient NMR Spectroscopy. *Appl. Magn. Reson.* **2014**, *45*, 315-328.
48. Li H.; Ujihira Y.; Yoshino T.; Yoshii K.; Yamishita T.; Horie K. Free volumes and their distribution in crosslinked polysiloxanes probed by positron annihilation lifetime technique. *Polymer* **1998**, *39*, 17, 4075-4079.
49. Roberts C.; Cosgrove T.; Schmidt R.G.; Gordon G.V. Diffusion of Poly(dimethylsiloxane) Mixtures with Silicate Nanoparticles. *Macromolecules* **2001**, *34*, 538-543.
50. Cosgrove T.; Roberts C.; Choi Y.; Schmidt R. G.; Gordon G. V.; Goodwin A. J.; Kretschmer A. Relaxation Studies of High Molecular Weight Poly(dimethylsiloxane)s Blended with Polysilicate Nanoparticles. *Langmuir* **2002**, *18*, 10075-10079.



51. Cosgrove T.; Roberts C.; Garasanin T.; Schmidt R. G.; Gordon G. V. NMR Spin-Spin Relaxation Studied of Silicate-Filled Low Molecular Weight Poly(dimethylsiloxane)s. *Langmuir* **2002**, *18*, 10080-10085.
52. Gordon G. V.; Schmidt R. G.; Quintero M.; Benton N. J.; Cosgrove T.; Krukonis V. J.; Williams K.; Wetmore P. M. Impact of Polymer Molecular Weight on the Dynamics of Poly(dimethylsiloxane)-Polysilicate Nanocomposites. *Macromolecules* **2010**, *43*, 10132-10142.
53. Schmidt R. G.; Gordon G. V.; Dreiss C.A.; Cosgrove T.; Krukonis V. J.; Williams K.; Wetmore P. M. A Critical Size Ratio for Viscosity Reduction in Poly(dimethylsiloxane)-Polysilicate Nanocomposites. *Macromolecules* **2010**, *43*, 10143-10151.
54. Chen D.; Chen F.; Hu X.; Zhang H.; Yin X.; Zhou. Thermal stability, mechanical and optical properties of novel addition cured PDMS composites with nano-silica sol and MQ silicone resin. *Compos. Sci. Technol.* **2015**, *117*, 307-314.
55. Shi X.; Chen Z.; Yang Y. Toughening of Poly(L-lactide) with Methyl MQ Silicone Resin. *Eur. Polym. J.* **2014**, *50*, 243-248.
56. Di. M.; He S.; Li R.; Yang D. Radiation effect of 150 keV protons on methyl silicone rubber reinforced with MQ silicone resin. *Nucl. Instrum. Methods. Phys. Res., Sect. B.* **2006**, *248*, 31-36.
57. Li Y.; Wang J.; Fan L.; Chen D. Feasible Fabrication of a Durable Superhydrophobic Coating on Polyester Fabrics for Oil-Water Separation. *Acta Phys.-Chim. Sin.* **2016**, *32*, 990-996.
58. Yin, Y.; Chen X.; Lu J.; Liu Z.; Chen X. Influence of molar ratio of Si-H to Si-CH=CH<sub>2</sub> on mechanical and optical properties of silicone rubber. *J. Elastomers Plast.* **2016**, *48*, 206-216.
59. Zhan, X.; Zhang J.; Cheng J.; Shi L.; Lin X. Synthesis, characterization, and cure kinetics analysis of high refractive index copolysiloxanes. *J. Therm. Anal. Calorim.* **2014**, *117*, 875-883.
60. Itoh, M; Oka F.; Suto M.; Cook S.; Auner N. Characterization and Some Insights into the Reaction Chemistry of Polymethylsilsesquioxane or Methyl Silicone Resins. *Int. J. Polym. Sci.* **2012**.

## CHAPTER 3

### SURFACE ACTIVITY OF MQ SILICONES

#### 3.1 Introduction

##### 3.1.1 Background

MQ silicone copolymers<sup>1,2</sup> are commercially important materials that are used as reinforcing fillers<sup>3-6</sup>, tackifiers<sup>7-11</sup> and surfactants,<sup>12-17</sup> but have been generally ignored by academic research. A handful of open literature reports have investigated the reinforcing effects of MQ<sup>3-6</sup> and the performance of MQ in pressure sensitive adhesives<sup>9-11</sup>, but no study has quantified the properties of MQ at interfaces. This is peculiar due to the obvious surface activity of MQ to anyone who is familiar with its preparation: either through reviewing the patent literature<sup>7,8,17</sup> where emulsions are commonly described, or from direct experience of MQ emulsions formed during the reaction and work up procedures. How can it be that, to my knowledge, no open literature exists that quantifies the behavior of MQ copolymers at interfaces. Perhaps this is due to the perspective of MQ copolymers as organic solvent-soluble nanosilicate particles rather than viewing them as molecules which is the perspective of Chapter 2 and our recent publication.<sup>18</sup> By limiting the view of MQ copolymers to that of a chemically homogenous particle, its fascinating molecular structure and properties are overlooked.

Considering the family of silicones of which MQ is a member, its surface activity should not come as a surprise. Siloxane polymers and molecules have been recognized for their unique surface properties since their invention in the 1930's.<sup>19,20</sup> Poly(dimethylsiloxane) (PDMS) and other linear siloxanes were immediately recognized for their abilities to hydrophobize<sup>21,22</sup> and destabilize foams.<sup>23</sup> The ability of PDMS to generate hydrophobic, low hysteresis, covalently attached liquid surfaces has been studied and applied by numerous researchers.<sup>24-30</sup> Zisman and coworkers<sup>31</sup> were the first

to study PDMS at the air-water interface and numerous researchers have continued to probe the structure of these PDMS monolayers.<sup>32-38</sup> Polyhedral oligomeric silsesquioxane (POSS) materials have been investigated as omniphobic surface treatments<sup>39</sup> and in Langmuir monolayers.<sup>40-46</sup> A special class of trisiloxane surfactants are infamous as superspreaders.<sup>47-49</sup> In addition to silicone polymers, silica particles have long been used as models to investigate the surface activity of particles.<sup>50-55</sup> Silica particles at the air-water interface have been studied with regard to their behavior in Langmuir monolayers and these studies show that the hydrophobicity of silanized silica is important for monolayer stability and collapse mechanisms.<sup>53,54</sup> Recently silica particles were studied at the oil-water interface using drop tensiometry to show that silanized particles adsorb to the interface to reduce interfacial tension.<sup>55</sup> MQ copolymers are hybrid molecules that can not only utilize the chemical versatility of silicone polymers but can have a variety of physical structures: from oligomeric and cage-like to condensed and silica-like. Tuning the chemistry and structure of MQ provides routes to an infinite number of materials which may exhibit unique interfacial behavior, yet there is no literature regarding MQ copolymers at interfaces. The contrast between the literature on its silicone and silica relatives is quite stark. Having previously developed a synthetic technique to prepare MQ with control over size and silanol content, the goal in this work was to explore how the physical and chemical structures of MQ affect its interfacial activity.

Even without open literature regarding the interfacial properties of MQ, surface activity is obvious based on patent literature and personal experiences. Patent and marketing literature indicates that the surface activity of MQ is leveraged in emulsion formation, foam stabilization and hydrophobic surface coatings.<sup>56</sup> In fact, the first MQ material was a superhydrophobic coating produced using the vapor phase of the azeotrope of silicon tetrachloride and trimethylchlorosilane.<sup>57</sup> In personal experience,

developing synthetic procedures for preparing MQ copolymers, strong emulsions were commonly encountered that did not separate with prolonged rest or with the addition of brine solutions. These tenacious emulsions resulted in losses in product until proper rinsing procedures were developed. With patent suggestions and after experiencing the MQ emulsions firsthand, it was clear that these molecules were surface active. Qualitative observations of MQ surface activity indicated apparent differences in the characteristics of MQ interfaces that were dependent on molecular weight and chemical composition. Again, it must be stressed that unlike other silicones and silica, there is no open literature that quantifies MQ silicone interfacial behavior. It is clear that these are important characteristics of these polymers that should be measured. In particular, the behavior of MQ at interfaces highlights that MQ silicones need to be regarded as molecules with both a chemical and physical identity. When MQ is approached solely from a nanoparticle perspective, we miss out on the full picture of its surface activity. In this work, it is shown that the size of MQ affects surface activity; however, it is discovered that MQ is only surface active when it contains silanols from incomplete end-capping.

### 3.1.2 Objective

The objectives of this work involved three studies of MQ interfaces: (1) MQ at the oil-water interface using drop tensiometry, (2) MQ at the air-water interface using Langmuir monolayers and (3) MQ surface modifications on smooth silicon wafers via Blodgett depositions and adsorption from solution. Using the synthetic preparation described previously<sup>18</sup>, MQ copolymers of various apparent average molecular weights are compared and an effect of MQ size is determined. The importance of silanol residues in surface activity is examined by comparing the behavior of silanol-containing and fully trimethylsilylated MQ. These findings emphasize the importance of MQ molecular

structure, both chemical and physical, to its macroscopic properties at interfaces and suggests routes to tune the surface activity of MQ systems.

## 3.2 Experimental Section

### 3.2.1 Materials

Four MQ copolymers were prepared with number average molecular weights (GPC, PMMA Standards in THF) from 2300 to 15100 g/mol. In addition to MQ copolymers of various molecular weight, a trimethylsilylated MQ copolymer was prepared using trimethylsilyl iodide. These resins are discussed in Chapter 2 and reported.<sup>18</sup> Their properties are reproduced in Table 3.1.

Table 3.1: Molecular Weight and M:Q Ratios of MQ copolymers examined in this study

sample	$M_n$	$M_w$	$M_w/M_n$	M:Q <sup>a</sup>
M <sub>17</sub> Q <sub>15</sub>	2300	3000	1.30	1.1
M <sub>16</sub> Q <sub>32</sub>	3100	4200	1.35	0.50
M <sub>32</sub> Q <sub>64</sub>	6500	12 300	1.89	0.49
M <sub>42</sub> Q <sub>100</sub> /M <sub>51</sub> Q <sub>100</sub> <sup>b</sup>	8600	16 800	1.95	0.42/0.51 <sup>b</sup>
M <sub>66</sub> Q <sub>164</sub>	15 100	39 800	2.64	0.38

a) M:Q Ratio determined by <sup>1</sup>H NMR w/ cyclohexane reference

b) Trimethylsilyl iodide-treated

### 3.2.2 Pendant Drop Tensiometry

A Dataphysics OCA 20 pendant drop tensiometer was used to measure interfacial tension of water drops (Milli-Q, 18.2 MΩ) in toluene and MQ-toluene solutions. 1 mg/mL MQ solutions were prepared using 99.9% Toluene (ARCOS) and were filtered through PTFE syringe filters into quartz cuvettes. Deionized water drops were rapidly dispensed

and suspended from a flat 1.65 mm diameter needle tip. Interfacial tension was measured as a function of time, the initial time corresponding to the moment the drop was dispensed.

### 3.2.3 Langmuir Monolayers and Blodgett depositions

Chloroform was used as spreading solvent for the deposition of MQ at the water-air interface. 1 mg/ml solutions of MQ copolymer were prepared and deposited using a 10  $\mu$ L Hamilton syringe.

Langmuir monolayers were prepared on deionized water (Milli-Q, 18.2 M $\Omega$ ) in a Kibron MicroTrough XS. Before every experiment, the trough was thoroughly cleaned with ethanol and water and dried with nitrogen. After filling the trough with water, the surface was cleaned by repeated compression and suction cycles until the change in surface pressure was less than 0.1 mN/m for an entire compression-expansion cycle. The MQ solution was deposited by touching drops from the needle tip onto the water surface. A minimum evaporation period of 30 minutes was allowed before compression. For all experiments the compression rate was 5 mm/min. Compression isotherms were carried out to the instrument's minimum trough area. Hysteresis experiments involved compressed monolayers from 0 mN/m to 20 mN/m, returning to 2 mN/m then compressing to 20 mN/m for three cycles.

MQ Langmuir monolayers were transferred onto O<sub>2</sub> plasma-cleaned silicon wafer sections by Blodgett deposition. Each MQ monolayer was compressed and held at a constant surface pressure of 20 mN/m. Dry substrates were lowered into the trough until submerged and MQ deposited during retraction (substrate immersion and retraction speed was 5 mm/min). Wet substrates were lowered onto the water surface and upon contact an MQ monolayer spread on the wetted substrate. Surfaces from both methods were

indistinguishable, but dipping and retraction of dry substrates provided more reproducible surfaces. Multiple layers could be deposited by repeated deposition steps. Following deposition, wafer sections were dried at room temperature under reduced pressure.

#### 3.2.4 Surface Adsorption

Smooth silicon wafers were diced into 1 cm x 1 cm sections. Sections were rinsed (toluene, acetone, ethanol, water) and dried under a stream of nitrogen before O<sub>2</sub> plasma treatment for 15 minutes (Harrick Plasma Cleaner, 250 mtorr O<sub>2</sub>, 30 W).

Adsorption of MQ copolymers onto silicon wafers was achieved by incubating cleaned silicon wafer sections in 10 mg/mL solutions of MQ in toluene at 100 °C for 24 hours. Following this treatment, wafers were rinsed with toluene, acetone, ethanol and water and dried with a stream of nitrogen.

Dynamic water contact angle was measured with a Ramé-Hart goniometer. Surface thickness was measured using a Gaertner LSE Stokes Ellipsometer. Atomic force microscopy (AFM) imaging was carried out on a Bruker MultiMode Scanning Probe Microscope in tapping mode. Tip fouling was common and micrographs required cropping to isolate clean images. Adequate AFM images for the lowest molecular weight MQ samples (M<sub>17</sub>Q<sub>15</sub>) and trimethylsilylated MQ samples could not be obtained. Tip fouling and resolution were a problem with M<sub>17</sub>Q<sub>15</sub>, while tip fouling and surface heterogeneities were problematic for trimethylsilylated MQ.

### 3.3 Results and Discussion

Studies of MQ copolymers at interfaces were catalyzed by observations and frustrations with water-toluene emulsions that formed during work-up procedures of MQ

synthesis. When preparing the lowest molecular weight copolymers, the emulsions that formed were weak and the aqueous and organic phases would separate after resting. However, at higher molecular weights, the emulsions became tenacious; they would not separate over time or with brine. Without careful rinsing procedures, large amounts of the product or entire reactions would be lost. In addition to these observations regarding the physical size of the MQ copolymers, it was also observed that trimethylsilyl iodide-treated MQ, in which all silanol residues has been trimethylsilylated did not form emulsions. These qualitative observations led to the study of MQ at the Oil-Water interface by pendant drop tensiometry.

### 3.3.1 MQ Copolymers at the Oil-Water Interface

Pendant drop tensiometry measurements confirmed our observations of MQ oil-water interface activity, with significant decreases in water-toluene interfacial tension in 1 mg/mL MQ solutions as shown in Figure 3.1. The lowest molecular weight MQ copolymer only slightly reduced the interfacial tension from 35 mN/m to 33.2 mN/m. The higher molecular weight copolymers led to reductions from 35 mN/m to  $27.4 \pm 0.1$  mN/m,  $25.5 \pm 0.5$  mN/m and  $26.5 \pm 0.6$  mN/m for  $M_{66}Q_{164}$ ,  $M_{32}Q_{64}$  and  $M_{16}Q_{32}$  respectively. Due to the limited number of samples, no comment on the statistical significance of these differences can be made, however the effect of nanoparticle size on surface tension reduction has been predicted and observed.<sup>58-62</sup> In a second set of experiments,  $M_{42}Q_{100}$  was treated with trimethylsilyl iodide to trimethylsilylate residual silanols and yield  $M_{51}Q_{100}$ . The silanol-containing  $M_{42}Q_{100}$  reduced the interfacial tension to 25.4 mN/m. Removing the silanol residues led to a complete loss of surface activity with no reduction in surface tension.



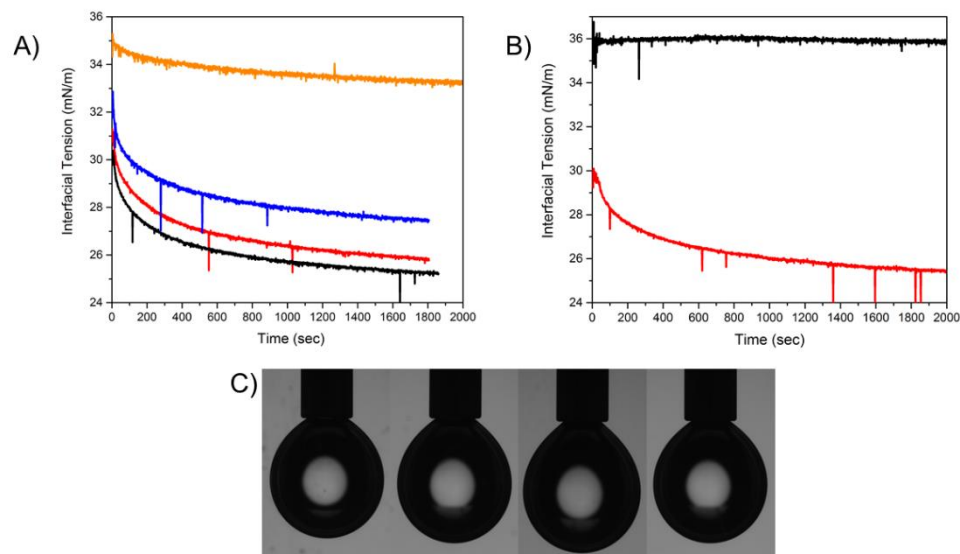


Figure 3.1. (A) Interfacial tension of water drops in MQ-toluene solutions (1 mg/mL) for  $M_{17}Q_{15}$  (orange),  $M_{16}Q_{32}$  (red),  $M_{32}Q_{64}$  (black) and  $M_{66}Q_{164}$  (blue). The interfacial tension of the clean water-toluene interface is 35 mN/m. (B) Interfacial tension of water drops in MQ-toluene solutions (1 mg/mL) for silanol-containing  $M_{42}Q_{100}$  (red) and trimethylsilyl iodide-treated  $M_{51}Q_{100}$  (black). (C) Images of pendant drops at the lowest measured interface tension. (from left to right:  $M_{17}Q_{15}$ ,  $M_{16}Q_{32}$ ,  $M_{32}Q_{64}$ , and  $M_{66}Q_{164}$ ).

The molecular weight, dispersity and chemistry of MQ affect the kinetics and equilibrium structure of their assembly at the toluene-water interface. Most importantly, the presence or absence of silanols dictates if MQ can adsorb to the interface. Silanols act as hydrophilic spots on the hydrophobic methyl MQ granting amphiphilic surfactant-like character. The observed behavior of silanol-containing MQ suggests that assembly of MQ at the toluene-water interface is driven by the favorable wetting and adsorption that results from these hydrophilic silanol defects. If we consider only the particle-like physical structure of MQ, we lose this perspective. The particle-like nature of trimethylsilylated MQ may still lend itself to adsorption similar to other nanoparticles; however, either due to intrinsic wettability or molecular size, it readily desorbs and thus cannot assemble to lower the interfacial tension. If the silanol-containing MQ strongly favors adsorption to the interface, it is possible to explain the effects of molecular weight and dispersity. In the case

of M<sub>17</sub>Q<sub>15</sub>, the lowest molecular weight MQ, there are two possible reasons for its low surface activity: (1) there are fewer residual silanols per molecule leading to reduced amphiphilicity and (2) the small size means that its adsorption strength is below that of thermal fluctuations ( $kT$ ) so that it cannot permanently adsorb. As molecular weight increases, the ability of MQ to assemble at the interface will be dictated by physical properties, such as diffusion and packing efficiency, and chemical properties, such as the number of silanols and trimethylsilyl capping efficiency, which will be further complicated by dispersity. Small molecules diffuse faster ( $D \sim r^{-1}$ ), can pack more efficiently, but will adsorb more weakly ( $\Delta E_{\text{ads}} \sim r^2$ ). Larger molecules diffuse more slowly, pack less efficiently, but adsorb with greater strength. As dispersity increases the competition between small and large molecules comes into play and the packing efficiency increases. Chemically, if we assume the same silanol density for all MQ copolymers, small molecules will have fewer silanols available to adsorb and so will adsorb more weakly than large molecules which contain a greater number of silanols. Since the MQ copolymers we report and studied are polydisperse mixtures both physically and chemically, the situation is complex. Regardless of the complexity, it is obvious that MQ is an effective surfactant and presents interesting opportunities for tuning surface activity for specific goals.

The critical concentration required for interface saturation was determined for the M<sub>32</sub>Q<sub>64</sub> copolymer. This particular sample was chosen for further study because: (1) it showed the greatest decrease in interfacial tension at 1 mg/ml and (2) it is the most similar to a commercially available MQ silicone (Dow Corning MQ1600) that we use as our 'standard MQ.' Concentrations from 0.005 mg/mL to 10 mg/mL were tested and presented in Figure 3.2. Interfacial tension reduction begins at concentrations as low as 0.0075 mg/mL (7.5  $\mu\text{g/mL}$ ) and the interfacial tension reduction saturates between 1 and 5 mg/ml. For complete coverage of a drop with surface area equal to 40 mm<sup>2</sup> (the average

measured drop surface area in these experiments), 0.1  $\mu\text{g}$  of  $\text{M}_{32}\text{Q}_{64}$  is required to form a monolayer (an estimation based on a thickness of 2.5 nm and specific gravity of 1). In these experiments, drops were deposited in about 1 mL of MQ-toluene solution which means there is from 50 to  $10^5$  excesses of MQ in 0.005 to 10 mg/mL solutions, respectively. Based on this estimation of monolayer surface coverage and the mass of MQ in solution, it is apparent that a large excess of MQ is required in the solution for surface tension reduction. Additionally, the adsorption kinetics and equilibrium interfacial tension reduction show a strong dependence on concentration: as concentration increases the equilibrium interfacial tension decreases and is reached faster. These results indicate (1) a partitioning of MQ between the interface and the solution, (2) an adsorption-desorption equilibrium occurs at the interface and (3) that multilayer formation may be important for maximum interfacial tension reduction based on the large excess of MQ in solution. The initial tension at  $t = 0$  decreases with increasing concentration, suggesting a rapid initial adsorption that is dependent on  $[\text{MQ}]$  followed by slower reversible equilibration. Although it has not been tested, it is expected that each MQ copolymer will have a unique critical concentration and maximal surface tension reduction that will depend on molecular weight, dispersity and chemical structure.

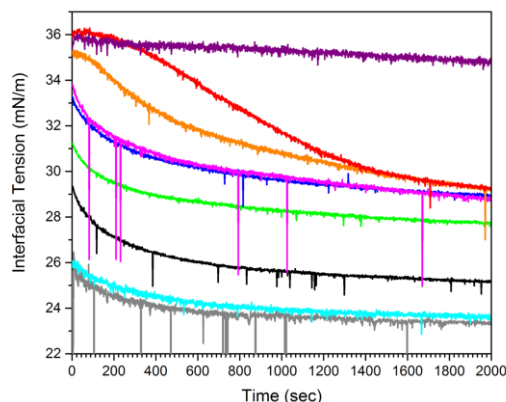


Figure 3.2. Impact of  $[\text{M}_{32}\text{Q}_{64}]$  on interfacial tension reduction.  $[\text{M}_{32}\text{Q}_{64}] = 0.005$  (purple), 0.0075 (red), 0.01 (orange), 0.05 (blue), 0.1 (pink), 0.5 (green), 1.0 (black), 5.0 (gray), 10.0 (cyan) mg/ml. The interfacial tension of a clean water-toluene interface is 35 mN/m.

### 3.3.2 MQ Copolymers at the Air-Water interface

Since the first observations of PDMS surface activity by Zisman and coworkers<sup>31</sup> there have been numerous studies of linear silicones<sup>33-38</sup> and polyhedral oligomeric silsesquioxane (POSS)<sup>40-46</sup> at the air-water interface using Langmuir monolayers. I discovered that MQ copolymers can also be deposited onto a water surface from chloroform to form Langmuir monolayers. Pressure-area isotherms of these monolayers are shown in Figure 3.3. Surface concentrations are reported in mg/m<sup>2</sup> and not area per repeat unit or per molecule because a repeat unit for MQ cannot be defined, an absolute molecular weight for MQ had not been measured, and because of the dispersity of each MQ copolymer. The lift-off concentration and collapse behavior of MQ monolayers has a strong dependence on molecular weight. As molecular weight increases, lift-off concentration increases, collapse pressure increases and surface rigidity increases. The lift-off concentration can be used to make a rough estimate of the initial monolayer thickness; if we assume that MQ has a density of 1, the estimated thickness is close to that of a true monolayer of MQ based on estimates of  $R_H$  from size exclusion chromatography, diffusion NMR and dynamic light scattering.<sup>18</sup> A spectrum of behaviors is observed starting from the  $M_{17}Q_{15}$  to  $M_{66}Q_{164}$  that ranges from a PDMS-like collapse-plateau to solid-like rigidity with high maximum surface pressures.

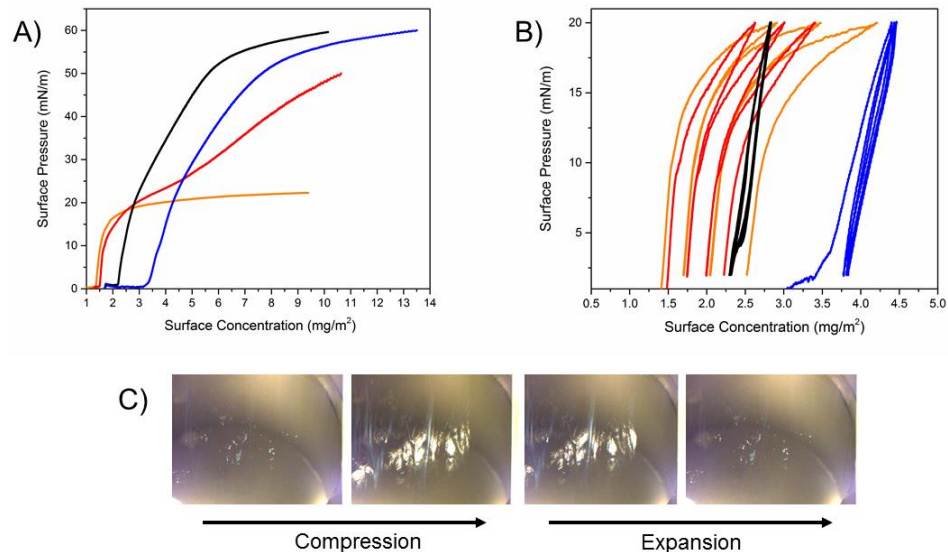


Figure 3.3. (A) Pressure-area isotherms to minimum trough area at 5 mm/min and (B) pressure-area hysteresis loops (5 mm/min, 3 cycles from 2-20 mN/m) of M<sub>17</sub>Q<sub>15</sub> (orange), M<sub>16</sub>Q<sub>32</sub> (red), M<sub>32</sub>Q<sub>64</sub> (black) and M<sub>66</sub>Q<sub>164</sub> (blue) monolayers on water. (C) Photos of the elastic surface wrinkles that form during high pressure compression of M<sub>32</sub>Q<sub>64</sub>. Wrinkles grow in compression and relax on expansion reversibly. The surface tension probe was removed to allow imaging so exact surface pressures in these images is unavailable but it is in the range of 50 to 60 mN/m.

M<sub>17</sub>Q<sub>15</sub> shows a single collapse at ~16 mN/m that plateaus and reaches a maximum pressure of 22 mN/m. M<sub>16</sub>Q<sub>32</sub> has more complex behavior. Surface pressure initially rises sharply, but the rate of pressure increase begins to decrease at ~15 mN/m. Unlike M<sub>17</sub>Q<sub>15</sub> which reaches a plateau in surface pressure, the M<sub>16</sub>Q<sub>32</sub> monolayer can sustain higher surface pressures as it rearranges during compression and reaches a maximum pressure of 50 mN/m. Due to the limited size of the trough it is not possible to further compress the M<sub>16</sub>Q<sub>32</sub> monolayer further while still capturing the lift-off behavior. It is possible that the monolayer can sustain still higher pressures by continued rearrangement although this has not been confirmed. M<sub>32</sub>Q<sub>64</sub> and M<sub>66</sub>Q<sub>164</sub> form more rigid, elastic monolayers than the two smaller MQ copolymers and have near identical behavior apart from their lift-off concentrations. Both rise sharply following lift-off and have a slight

change in slope  $\sim 25$  mN/m until  $\sim 55$  mN/m where collapse is observed and with maximum pressure of 60 mN/m being reached at the minimal trough areas. The hysteresis experiments demonstrate the irreversible collapse of  $M_{17}Q_{15}$  and  $M_{16}Q_{32}$  monolayers at surface pressures of 20 mN/m while  $M_{32}Q_{64}$  and  $M_{66}Q_{164}$  remain elastic in this region of pressures, although they do show some evidence of rearrangement following the first compression cycle. At very high pressures, the compressed MQ monolayers were observed to reversibly wrinkle into structures observable by eye. The structures initially appear as faint threads that run parallel to the barriers compressing the sample and eventually grow in number and brightness. The structures form reversibly although it could not be determined with the available instrumentation and methods if or how the structures change during repeated cycling.

The transition from soft, collapsible monolayers at low molecular weights to rigid, elastic monolayers at high molecular weights indicates that the physical and chemical structures of MQ copolymers affect adsorption to the air-water interface in a manner similar to MQ at the oil-water interface. At low molecular weights, adsorption is weakest and monolayers collapse irreversibly because of their less condensed, more open structure and lower silanol content per molecule. At higher molecular weights, adsorption is stronger and monolayers are elastic because of the condensed, silica-like structure and greater silanol content per molecule. The transition from less condensed, branched structures to condensed, polycyclic structures can be inferred from M:Q ratios as discussed in Chapter 2 and published work.<sup>18</sup> This dependence of Langmuir monolayer behavior on molecular weight provides insight into the physical structure of MQ molecules that supports the understanding of MQ based on M:Q ratios. The transition from soft to rigid corresponds to a transition from less to more condensed silica-like structures.

The role of silanol residues on MQ was determined by preparing monolayers from  $M_{42}Q_{100}$  and the trimethylsilylated derivative. Comparisons were made using a modified hysteresis experiment in which monolayers were compressed from liftoff to 10 mN/m then cycled between 2 and 10 mN/m for 2 cycles, 2 and 20 mN/m for 1 cycle and 2 and 50 mN/m for 1 cycle. Figure 3.4 shows that the TMS-treated MQ forms an inelastic monolayer that irreversibly collapses with each compression cycle whereas the silanol-containing MQ shows elastic behavior with very little permanent collapse even after compression to 50 mN/m. The lift-off pressures are similar since both molecules are the same size. The importance of silanols in the strong adsorption of MQ to the air-water interface is clear. The stability of the silanol-containing MQ monolayers arises from the adsorption of the hydrophilic sites to the water interface. Without the hydrophilic silanols the MQ irreversibly collapses under pressure, preferring to stick to itself in the collapsed aggregated structure. The differences in lift-off pressure can also be attributed to the silanols, since the TMS derivative monolayer is likely to have a greater number of aggregated structures before compression.

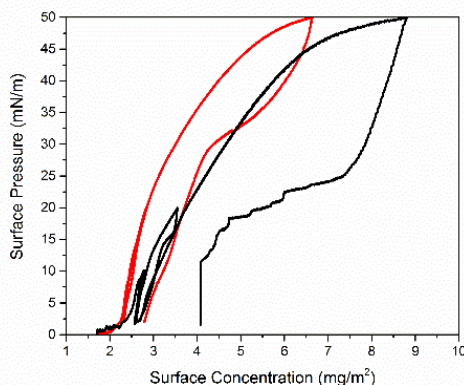


Figure 3.4 Pressure-area hysteresis loop (0-10 mN/m x1, 2-10-2 mN/m x2, 2-20-2 mN/m, 2-50-2 mN/m) for silanol-containing  $M_{42}Q_{100}$  (red) and trimethylsilyliodide-treated  $M_{51}Q_{100}$  (black).

### 3.3.3 MQ copolymer surfaces

The structure of the air-water monolayers under moderate compressions was studied by Blodgett deposition onto cleaned silicon wafer substrates. Deposition of MQ occurs two ways: (1) for dry substrates, deposition occurs on the withdraw step only or (2) for wet substrates, the first deposition occurs upon contact with the water surface, with surface pressure driving the first monolayer onto the wet substrate area. In both cases, subsequent deposition only occurs during the withdraw step of an immersed substrate. Table 3.2 presents the properties of the MQ surfaces prepared by Langmuir-Blodgett deposition from the air-water interface. Thickness by ellipsometry matches the estimated thicknesses of a monolayer from lift-off pressures and  $R_H$  measurements. Advancing water contact angles are consistent with a disordered methyl surface while receding contact angles demonstrate both chemical and topological heterogeneities. The high contact angle hysteresis is the result of contact line pinning that arises from (1) exposed surface silanols, (2) silanols on the MQ copolymer molecules and (3) molecular roughness of the MQ monolayer. AFM, presented in Figure 3.5, confirms that the surfaces are rough on a length scale comparable to that of the MQ molecules. The surfaces are also heterogenous, showing clusters of MQ molecules. In the case of  $M_{17}Q_{15}$ , adequate AFM data could not be collected due to severe tip fouling.



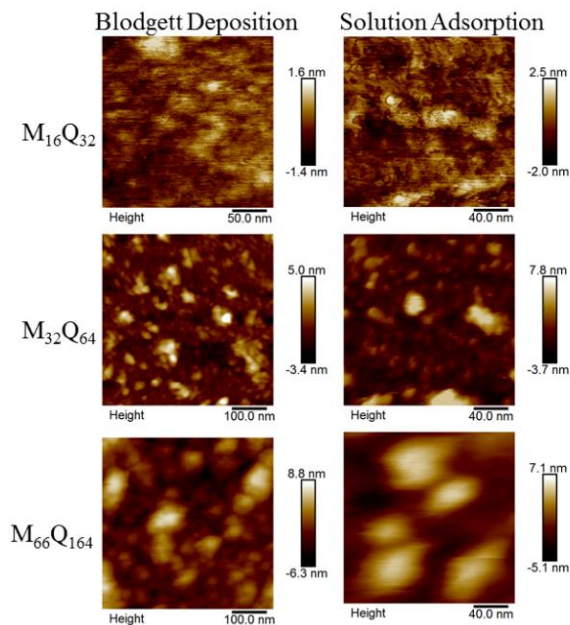


Figure 3.5. AFM micrographs of MQ copolymer surfaces from Blodgett depositions and solution adsorption. Note differences in scale bars.

Table 3.2 MQ surfaces prepared from Langmuir Blodgett transfer (5 mm/min, 20 mN/m) and adsorption from toluene solution (100 °C, 24 h)

MQ		Thickness (nm)	RMS Roughness (nm)	Advancing CA, $\theta_a$	Receding CA, $\theta_r$	Hysteresis
M <sub>17</sub> Q <sub>15</sub>	L-B	1.0	-	99	77	22
	Soln.	1.3	-	99	91	18
M <sub>16</sub> Q <sub>32</sub>	L-B	1.3	0.4	103	85	18
	Soln.	1.8	0.6	100	81	19
M <sub>32</sub> Q <sub>64</sub>	L-B	2.2	1.1	103	77	26
	Soln.	2.5	2.2	102	77	25
M <sub>66</sub> Q <sub>164</sub>	L-B	2.8	2.2	103	77	26
	Soln.	3.7	3.0	102	75	27

Surfaces of MQ were also prepared by adsorption from solution using a method similar to that reported by our group for the preparation of PDMS grafts.<sup>22,23</sup> The surfaces prepared this way have similar characteristics to those prepared from Blodgett deposition. Data for these surfaces is also exhibited in Table 3.2. Thickness, advancing contact angles, contact angle hysteresis, and roughness increase with molecular weight. While

ellipsometric thicknesses were close to that of a monolayer, AFM (Figure 3.5) showed clustering and multilayer formation. Again, In the case of  $M_{17}Q_{15}$ , adequate AFM data could not be collected. A comparison of silanol-containing  $M_{42}Q_{100}$  to trimethylsilylated  $M_{51}Q_{100}$  is presented in Table 3.3. The trimethylsilylated derivative has lower contact angles, higher contact angle hysteresis and is very heterogeneous as observed by variance in ellipsometry and stick-slip contact line motion.

Table 3.3. Surfaces prepared by solution adsorption (toluene, 100 °C, 24 h) of silanol-containing MQ ( $M_{42}Q_{100}(OH)_{10}(OEt)_1$ ) and trimethylsilyliodide-treated MQ ( $M_{51}Q_{100}(OH)_1(OEt)_1$ )

MQ	Thickness (nm)	Advancing CA ( $\theta_a$ )	Receding CA ( $\theta_r$ )	Hysteresis
$M_{42}Q_{100}(OH)_{10}(OEt)_1$	2.1	105	80	25
$M_{51}Q_{100}(OH)_1(OEt)_1$	2.6 (Large Variance)	88	48	40

These surfaces provide useful insight into the physical structure of MQ. The particle-like structure can be directly observed with AFM and the contact angle data indicate that the molecules are hydrophobic, but contain numerous defects as a result of silanols and molecular topography. Like the observations of other interfaces, the presence of silanols plays an important role in the ability of MQ copolymers to adsorb. Weak physisorption of trimethylsilylated MQ is indicated by the wettability and heterogeneity of the surfaces while silanol-containing MQ appears to chemisorb to the silicon surface.

### 3.4 Conclusions

For the first time, the properties of MQ silicone copolymers at interfaces has been quantified. These silicone copolymers exhibit unique surface activity that highlights their position between molecule and particle. Examinations of MQ at toluene-water, air-water

and on smooth solid substrates provides insight into the role of physical and chemical structure of MQ copolymers on interfacial behavior and surface activity. It has been shown that the apparent molecular weight of silanol-containing MQ copolymers is important but that the silanols are the critical component that enables MQ surface activity. Without the silanol residues MQ no longer demonstrates robust surface activity. I suspect that the characteristics of MQ silicones at interfaces could be precisely tuned by controlling molecular weight and silanol content. Future investigations in MQ surface activity could develop more precise structure-property relationships by fractionation of MQ samples into well-defined populations. The current conclusions are limited by the use of polydisperse samples that complicate the picture of MQ behavior. Characterization of precise MQ fractions would enable a more complete understanding of the relationship between molecular weight and surface activity.

The unique behavior of MQ silicones at various interfaces is leveraged in numerous commercial applications, but has been ignored by the academic community. The synthetic versatility of MQ as a platform and its unique properties beg for further, widespread investigation.

### 3.5 References

1. Butts, M.; Cella, J.; Wood, C. D.; Gillette, G.; Kerboua, R.; Leman, J.; Lewis, L.; Rubinsztajn, S.; Schattenmann, F.; Stein, J.; Wicht, D.; Rajaraman, S.; Wengrovius, J. Silicones. In *Kirk-Othmer Encyclopedia of Chemical Technology*, Wiley & Sons: New York, 2006; Vol. 22, pp 547-626.
2. Butts, M.; Cella, J.; Wood, C. D.; Gillette, G.; Kerboua, R.; Leman, J.; Lewis, L.; Rubinsztajn, S.; Schattenmann, F.; Stein, J.; Wicht, D.; Rajaraman, S.; Wengrovius, J. Silicones. In *Encyclopedia of Polymer Science and Technology*, 2<sup>nd</sup> ed.; Wiley & Sons: New York, 2003; Vol. 11, pp 765-841.
3. Lewis, L. N.; Wengrovius, J. H.; Burnell, T. B.; Rich, J. D. *Chem. Mater.* **1997**, *9*, 761-765.

4. Gordon, G. V.; Schmidt, R. G.; Quintero, M.; Benton, N. J.; Cosgrove, T.; Krukoniš, V. J.; Williams, K.; Wetmore, P. M. Impact of Polymer Molecular Weight on the Dynamics of Poly(dimethylsiloxane)-Polysilicate Nanocomposites. *Macromolecules* **2010**, *43*, 10132–10142.
5. Schmidt, R. G.; Gordon, G. V.; Dreiss, C. A.; Cosgrove, T.; Krukoniš, V. J.; Williams, K.; Wetmore, P. M. A Critical Size Ratio for Viscosity Reduction in Poly(dimethylsiloxane)-Polysilicate Nanocomposites. *Macromolecules* **2010**, *43*, 10143–10151.
6. Roberts, C.; Cosgrove, T.; Schmidt, R. G.; Gordon, G. V. Diffusion of Poly(dimethylsiloxane) Mixtures with Silicate Nanoparticles. *Macromolecules* **2001**, *34*, 538–543.
7. Goodwin, J. T. Organopolysiloxane compositions having pressure-sensitive adhesive properties. US Patent. 2,857,356, Oct. 21, 1958.
8. Currie, C. C.; Kell, J. W. Organopolysiloxane Adhesive and Pressure-Sensitive Adhesive Tape Containing Same. US Pat. 2,814,601, Nov. 26, 1957.
9. Min, H.; Qiuyu, Z.; Jiying, G. Synthesis and characterization of silicon based Pressure sensitive adhesive. *Adv. Mater. Res.* **2011**, *306*, 1773–1778.
10. Sun, F.; Hu, Y.; Du, H. Synthesis and Characterization of MQ Silicone Resins. *J. Appl. Polym. Sci.* **2012**, *125*, 3532-3536.
11. Kuo, C. J.; Chen, J.; Shih, C.; Huang, C. Silicone Resin Synthesized by Tetraethoxysilane and Chlorotrimethylsilane Through Hydrolysis-Condensation Reaction. *J. Appl. Polym. Sci.* **2014**, *131*, 40317.
12. Juen, D. R.; Zhong B.; Diaz M.; Johnson T. Foam Control Compositions having Resin-Fillers. US Pat. 6,207,722 B1 Mar. 27, 2001.
13. Araud, C. Polydimethylsiloxane/MQ resin antifoaming compositions. US Pat. 5,082,590 Jan. 21, 1992.
14. Liu, Y. Silicone MQ resin reinforced silicone elastomer emulsions. US Pat. 8,012,544 B2 Sept. 6, 2011.
15. Liu, Y. Method of Making Silicone Resin Emulsions. US Pat. 6,737,444 B1 May 18, 2004.
16. Liu, J. J.; Wu, P.; Feng, B.; Ylitalo, D. A. Silicone Compositions and Related Methods. US Pat. 2015/0259495 A1 Sep. 17, 2015.
17. Daudt, W. H.; Tyler, L. J. Copolymeric Siloxanes and Methods of preparing them. US Pat. 2,676,182 Apr. 20, 1954.
18. Flagg, D. H.; McCarthy, T. J. Rediscovering Silicones: MQ Copolymers *Macromolecules* **2016**, *49*, 8581–8592.
19. Rochow, E. G. Silicon and Silicones. Springer-Verlag: Berlin, 1987.
20. Liebhafsky, H. A. Silicones Under the Monogram. John Wiley & Sons: New York, 1978.

21. Patnode, W. I. Method of Rendering Materials Water Repellent. US Pat. 2,306,222 Dec. 22, 1942.
22. Norton, F. J. Waterproofing Treatment of Materials. US Pat. 2,386,259 Dec. 10 1946.
23. Larsen, R. G.; Diamond, H. Antifoaming Composition. US Pat. 2,375,007 May 1, 1945.
24. Krumpfer, J. W.; McCarthy, T. J. Rediscovering Silicones: “Unreactive” Silicones React with Inorganic Surfaces. *Langmuir* **2011**, *27*, 11514–11519.
25. Krumpfer, J. W.; McCarthy, T. J. Contact angle hysteresis: a different view and a trivial recipe for low hysteresis hydrophobic surfaces. *Faraday Discuss.* **2010**, *146*, 103-111.
26. Wang, L.; McCarthy, T. J. Covalently Attached Liquids: Instant Omniphobic Surfaces with Unprecedented Repellency. *Angew. Chemie Int. Ed.* **2016**, *55*, 244–248.
27. Cheng, D. F.; Urata, C.; Yagihashi, M.; Hozumi, A. A Statically Oleophilic but Dynamically Oleophobic Smooth Nonperfluorinated Surface. *Angew. Chemie Int. Ed.* **2012**, *51*, 2956-2959.
28. Cheng, D. F.; Urata, C.; Masheder, B.; Hozumi, A. A Physical Approach to Specifically Improve the Mobility of Alkane Liquid Drops. *J. Am. Chem. Soc.* **2012**, *134*, 10191-10199.
29. Chen, W.; Fadeev, A. Y.; Hsieh, M. C.; Didem, O.; Youngblood, J.; McCarthy, T. J. Ultrahydrophobic and Ultralyophobic Surfaces: Some Comments and Examples. *Langmuir* **1999**, *15*, 3395–3399.
30. Fadeev, A. Y.; McCarthy, T. J. Self-Assembly Is Not the Only Reaction Possible between Alkyltrichlorosilanes and Surfaces: Monomolecular and Oligomeric Covalently Attached Layers of Dichloro- and Trichloroalkylsilanes on Silicon. *Langmuir*, **2000**, *16*, 7268-7274.
31. Fox, H. W.; Taylor, P. W.; Zisman, W. A. Polyorganosiloxanes....Surface Active Properties. *Ind. Eng. Chem.* **1947**, *39*, 1401–1409.
32. Gaines, G. L. Insoluble Monolayers at Liquid-Gas Interfaces. Interscience Publishers, John Wiley & Sons: New York, 1966.
33. Mann, E. K.; Langevin D. Poly(dimethylsiloxane) Molecular Layers at the Surface of Water and of Aqueous Surfactant Solutions. *Langmuir* **1991**, *7*, 1112-1117.
34. Hahn, T. D.; Hsu, S. L.; Stidham, H. D. Reflectance Infrared Spectroscopic Analysis of Polymers at the Air-Water Interface. 4. Microstructure of Poly(dimethylsiloxane). *Macromolecules* **1997**, *30*, 87–92.
35. Kim, C.; Gurau, M. C.; Cremer, P. S.; Yu, H. Chain Conformation of Poly(dimethyl siloxane) at the Air/Water Interface by Sum Frequency Generation. *Langmuir* **2008**, *24*, 10155–10160.
36. Bernardini, C.; Stoyanov, S. D.; Cohen Stuart, M. A.; Arnaudov, L. N.; Leermakers, F. A. M. PMMA Highlights the Layering Transition of PDMS in Langmuir Films. *Langmuir* **2011**, *27*, 2501–2508.

37. Lenk, T. J.; Lee, D. H. T.; Koberstein, J. T. End Group Effects on Monolayers of Functionally-Terminated Poly(dimethylsiloxanes) at the Air-Water Interface. *Langmuir* **1994**, *10*, 1857–1864.
38. Mansuri, E.; Zepeda-Velazquez, L.; Schmidt, R.; Brook, M. A.; DeWolf, C. E. Surface Behavior of Boronic Acid-Terminated Silicones. *Langmuir*, **2015**, *31*, 9331-9339.
39. Tuteja, A.; Mabry, J. M. The Design of Non-wetting Surfaces with FluoroPOSS. In *Silicone Surface Science*; Springer: New York; **2012**; pp 179–193.
40. Deng, J.; Polidan, J. T.; Hottle, J. R.; Farmer-Creely, C. E.; Viers, B. D.; Esker, A. R. Polyhedral Oligomeric Silsesquioxanes: A New Class of Amphiphiles at the Air/Water Interface. *J. Am. Chem. Soc.* **2002**, *124*, 15194–15195.
41. Hottle, J. R.; Kim, H. J.; Deng, J.; Farmer-Creely, C. E.; Viers, B. D.; Esker, A. R. Blends of Amphiphilic PDMS and Trisilanolisobutyl-POSS at the Air/Water Interface. *Macromolecules* **2004**, *37*, 4900–4908.
42. Hottle, J. R.; Deng, J.; Kim, H. J.; Farmer-Creely, C. E.; Viers, B. D.; Esker, A. R. Blends of Amphiphilic Poly(dimethylsiloxane) and Nonamphiphilic Octaisobutyl-POSS at the Air/Water Interface. *Langmuir* **2005**, *21*, 2250–2259.
43. Deng, J.; Viers, B. D.; Esker, A. R.; Anseth, J. W.; Fuller, G. G. Phase Behavior and Viscoelastic Properties of Trisilanolcyclohexyl-POSS at the Air/Water Interface. *Langmuir* **2005**, *21*, 2375–2385.
44. Mitsuishi, M.; Zhao, F.; Kim, Y.; Watanabe, A.; Miyashita, T. Preparation of Ultrathin Silsesquioxane Nanofilms via Polymer Langmuir-Blodgett Films. *Chem. Mater.* **2008**, *20*, 4310-4316.
45. Yin, W.; Deng, J.; Esker, A. R. Surface Rheology of Trisilanolisobutyl-POSS at the Air/Water Interface. *Langmuir*, **2009**, *25*, 7181-7184.
46. Paczesny, J.; Binkiewicz, I.; Janczuk, M.; Wybrańska, K.; Richter, Ł.; Hołyst, R. Langmuir and Langmuir-Blodgett Films of Unsymmetrical and Fully Condensed Polyhedral Oligomeric Silsesquioxanes (POSS). *J. Phys. Chem. C* **2015**, *119*, 27007–27017.
47. Churaev, N. V.; Esipova, N. E.; Hill, R. M.; Sobolev V. D.; Starov, V. M.; Zorin Z. M. The Superspreading Effect of Trisiloxane Surfactant Solutions. *Langmuir* **2001**, *17*, 1338-1348.
48. Theodorakis, P. E.; Müller, E. A.; Craster, R. V.; Mater, O. K. Insights into surfactant-assisted superspreading. *Curr. Opin. Colloid Interface Sci.* **2014**, *19*, 283-289.
49. Nikolov, A.; Wasan, D. Current opinion in superspreading mechanisms. *Adv. Colloid Interface Sci.* **2015**, *222*, 517–529.
50. Aveyard, R.; Binks, B. P.; Clint, J. H. Emulsions stabilized solely by colloidal particles. *Adv. Colloid Interface Sci.* **2003**, *100*, 503-546.
51. Binks, B. P.; Whitby, C. P. Silica Particle-Stabilized Emulsions of Silicone Oil and Water: Aspects of Emulsification. *Langmuir* **2004**, *20*, 1130–1137.
52. Binks, B. P. Particles as Surfactants-Similarities and Differences. *Curr. Opin. Colloid Interface Sci.* **2002**, *7*, 21–41.

53. Razavi, S.; Cao, K. D.; Lin, B.; Lee, K. Y. C.; Tu, R. S.; Kretzschmar, I. Collapse of Particle-Laden Interfaces under Compression: Buckling vs Particle Expulsion. *Langmuir* **2015**, *31*, 7764–7775.
54. Bordács, S.; Agod, A.; Hórvölgyi, Z. Compression of Langmuir Films Composed of Fine Particles: Collapse Mechanism and Wettability. *Langmuir* **2006**, *22*, 6944–6950.
55. Zhang, Y.; Wang, S.; Zhou, J.; Zhao, R.; Benz, G., Tcheimou, S.; Meredith, J. C.; Behrens, S. H. Interfacial Activity of Nonamphiphilic Particles in Fluid-Fluid Interfaces. *Langmuir* **2017**, *33*, 4511–4519.
56. Shea, T. M. Durable Hydrophobic Surface Coatings using Silicone Resins. US Pat. 7,344,783 B2, Mar. 18, 2008.
57. Norton, F. J. Production of Water-Repellent Materials. US Pat. 2,412,470, Dec. 10, 1946.
58. Kutuzov, S.; He, J.; Tangirala, R.; Emrick, T.; Russell, T. P.; Boker, A. On the kinetics of nanoparticle self-assembly at liquid/liquid interfaces. *Phys. Chem. Chem. Phys.* **2007**, *9*, 6351–6358.
59. Lin, Y.; Boker, A.; Skaff, H.; Cookson, D.; Dinsmore, A. D.; Emrick, T.; Russell, T. P. Nanoparticle Assembly at Fluid Interfaces: Structure and Dynamics. *Langmuir* **2005**, *21*, 191–194.
60. Du, K.; Glogowski, E.; Emrick, T.; Russell, T. P.; Dinsmore, A. D. Adsorption Energy of Nano- and Microparticles at Liquid-Liquid Interfaces. *Langmuir* **2010**, *26*, 12518–12522.
61. Boker, A.; He, J.; Emrick, T.; Russell, T. P. Self-assembly of nanoparticles at interfaces. *Soft Matter* **2007**, *3*, 1231–1248.
62. Hua, X.; Bevan, M. A.; Frechette, J. Reversible Partitioning of Nanoparticles at an Oil-Water Interface. *Langmuir* **2016**, *32*, 11341–11352.

## CHAPTER 4

### SILICONE-CARBON NANOTUBE COMPOSITES: TUNING DISPERSIONS AND PROPERTIES WITH POLYSILOXANE BACKBONE CHEMISTRY

#### 4.1 Introduction

##### 4.1.1 Carbon Nanotubes

Nanomaterials have been proposed as the future of materials science. Applications of newly discovered nanomaterials cover the spectrum of sensing, imaging, electronics, catalysis, drug delivery and strong lightweight composites. One application of nanomaterials is in polymer nanocomposites where a nanomaterial is incorporated into a polymer matrix for enhanced properties; as a historical example, carbon black has been used to reinforce rubbers for over a century.<sup>1,2</sup> Of the numerous nanomaterials that are being explored today, few have generated the buzz and hype of carbon nanotubes (CNTs).<sup>3,4</sup> Since their discovery in 1987<sup>5</sup> and first open literature report in 1991,<sup>6</sup> few materials have matched the level of excitement that surrounds CNTs. However, realizing the promise of CNTs has been elusive and research into their practical utilization has hit numerous roadblocks. Nanotubes are not living up to their expectations. Despite the frustrating challenges they have posed to researchers and industry, work continues in hope that CNTs will one day be a solution to problems in materials science.

What are Carbon Nanotubes? It depends: CNTs come in an array of flavors.<sup>7, 8</sup> There are single-walled (SWCNT) and multi-walled (MWCNT), capped and uncapped and various chiral forms. The simplest way to think about the structure of a nanotube is to imagine wrapping a sheet of graphene (a one atom thick, hexagonally bonded, 2D carbon sheet) into a tube. SWCNTs can have diameters between 0.8 and 2 nm while MWCNTs are between 5 and 20 nm. Nanotubes have extraordinary properties: individual nanotubes can have metallic conductivity, thermal conductivities greater than diamond and elastic



modulus approaching 1 TPa with ultimate strength of 100 GPa. The length of a CNT depends on how it is prepared and ranges from below 100 nm to many millimeters. The high aspect ratio of CNTs allows them to achieve electrically and mechanically percolated networks at very low loadings in polymer composite applications.<sup>9-11</sup> With such properties, it is obvious that nanotubes have attracted a great deal of attention; however practical application of nanotubes faces numerous challenges, including a range of fundamental scientific, economic, health and safety, and practical issues.<sup>3,12,13</sup>

Although CNTs have experienced growing pains and no CNT space elevator is in the works, they have found niche applications in polymer composites<sup>9-17</sup> and energy storage/management.<sup>12,13,16</sup> Critical to their practical utilization in polymer composites is that they provide a significant advantage over conventional fillers at lower filler loadings. When this is achieved, materials scientists can begin to use them in commercial applications. Currently, the production of CNTs is far greater than the demand,<sup>2</sup> but as scientists and engineers understand more regarding nanotube processing/chemistry-structure-property relationships, more and novel applications will appear.

#### 4.1.2 Challenges facing CNT polymer nanocomposites

Aside from the challenges facing CNTs in general, there are some specific, relevant challenges to the utilization of CNTs in polymer nanocomposites. The largest of these challenges involves the dispersion of nanotubes in polymer matrices.<sup>9-17,19-22</sup> Like all nanomaterials, CNTs have a very high surface area to volume ratio. This makes interfacial interactions crucial in nanocomposites. Attractive nanotube-nanotube van der Waals interactions means that CNTs tend to aggregate and agglomerate. To overcome the aggregation of CNTs, polymer-nanotube interactions must be favored. This may seem like a simple task but finding solvents or polymers that can solubilize nanotubes has

challenged researchers for decades. To make things more difficult, the extreme aspect ratios of CNTs makes it almost impossible for them to reach true equilibrium states, resulting in kinetically trapped aggregates even if a preferable solvent is used.

Why does the dispersion or structure of CNTs in a polymer matrix matter? Performance and cost. CNTs are expensive and for them to compete with traditional fillers they must not only offer an advantage in performance, but also be comparable in cost. For CNTs to become a feasible technology, they must realize performance at ultra-low loadings so that their high cost is offset by low volume. In principle, the homogeneous dispersion of CNTs should lead to dramatic improvements in composite properties at filler loadings orders of magnitude lower than conventional macroscopic fillers. Dispersing CNTs and understanding structure-property relationships in CNT-polymer nanocomposites has therefore been a significant thrust in research.<sup>23-31</sup> Much of the work has been focused on creating homogenous dispersions and the results indicate that improving the dispersion of CNTs, either via processing or chemical modification, improves the performance of composites and uses the CNTs more efficiently. Heterogenous structuring<sup>32</sup> of CNTs in polymers has been observed to introduce anisotropy and in some cases can improve properties in composites. Having control over the formation of such CNT structures is desired because in uncontrolled cases, heterogenous dispersions act as defects which have a negative impact on composite properties.

There are numerous reviews on methods used to disperse nanotubes into polymer matrices and a few are cited in the references.<sup>19,20,22</sup> Current mechanical processing methods used to achieve homogeneous dispersions involve prolonged shear melt mixing or high powered sonication. These methods alone do not normally result in good quality

dispersions. Additionally, if the sonication power is too high, CNTs break thus reducing the aspect ratio that we aim to take advantage of. Chemical processes have been developed that significantly aid dispersion. These processes involve the use of cosolvents<sup>33</sup> and surfactants<sup>34</sup> as processing aides and the chemical modification of the nanotube surface.<sup>8,35,36</sup> The downside to these methods are the introduction of solvent or surfactant which must be removed from the final product and the possible degradation of nanotubes that results from chemical modification. This adds additional steps to CNT manufacturing that raises cost, especially in the case of chemical modifications. Optimally, dispersions of nanotubes would be achieved by simply dropping them into a polymer matrix and mixing, like what is done with carbon black.

In addition to the challenges in achieving dispersion, direct measurements of global dispersion can be difficult to carry out and to interpret.<sup>30</sup> Microscopy is a great tool to gain local information. Rheology<sup>23-31</sup>, conductivity<sup>28,29</sup>, scattering<sup>32</sup> and nuclear magnetic resonance<sup>37,38</sup> are typically used to analyze global information. The only way to truly understand the dispersion and performance of a polymer nanocomposite is by combining these techniques in a way that fits the desired application. One technique alone will provide limited information while a combination can begin to uncover the whole picture.

#### 4.1.3 Nanocomp Technologies, Inc.

A fundamental scientific challenge regarding the study and application of nanotubes is nanotube variability.<sup>2,3</sup> There are numerous preparative methods for CNTs and each yields CNTs with different structural characteristics (such as SWCNT vs MWCNT or capped vs uncapped).<sup>7,8</sup> In addition to the characteristics inherent to the method, nanotube structure is sensitive to minute changes in preparative conditions, so that different batches from the same method tend to suffer from high variability. On top of

this, commercial CNTs are often 'dirty.' Catalyst residues are present and processes used to remove the catalyst introduce chemical and structural defects that vary depending on the process. How the nanotubes are treated, or not treated, to remove catalyst particles will be important to their properties. Nanotubes in commercial samples are also 'dirty' in the sense that they are polydisperse in size and aspect ratio, something especially important in electronic applications. Given the above circumstances, it is nearly impossible to compare research results which (1) use different sources of nanotubes, since each preparative and post-preparative process will yield different chemical and physical structures, and (2) use different batches of nanotubes if production methods are not adequately controlled. The challenge of variability has limited large scale production and utilization of CNTs, thus limiting availability and raising costs. Luckily for us, we have collaborators at Nanocomp Technologies, Inc., a New Hampshire based producer of MWCNTs. Nanocomp has achieved process controls so that each batch of nanotube product we receive is comparable to those we have used before, something that cannot be said of other suppliers. This is critical in overcoming the problems of batch variability, allowing us to reproduce our results and make definitive conclusions regarding our CNT composites. The collaboration between our lab and Nanocomp is advantageous for both parties. For us, we get an ample supply of free, consistent CNT products. For Nanocomp, we are developing processing methods and investigating applications of their product.

Before shifting the attention to silicone-CNT nanocomposites, a few words about the CNT materials that we will be using are warranted. Nanocomp Technologies, Inc. produces MWCNTs from a continuous chemical vapor deposition (CVD) process from carbon fuel gasses onto iron nanoparticles. The process used by Nanocomp has been engineered to limit variability and can produce CNTs at rates of grams per hour. The CNTs are 10's of nanometers in diameter and have been measured to be millimeters in length.

This extreme aspect ratio is a unique outcome of this production method and maintaining this aspect ratio in subsequent processing is important in order to make effective use of this product. In the Nanocomp CVD preparation, nanotubes grow from the iron catalyst in a furnace and form an entangled mass that is collected onto a rotating drum. The final product is a sheet of entangled nanotubes with partial alignment along the circumference of the collection drum. This sheet can then be further densified by solvents. CNT powders are made by vigorous mechanical mixing and chopping of a CNT sheet with solvents or surfactants. There are a few open publications available which use Nanocomp CNTs in composites.<sup>38-41</sup>

#### 4.1.4 Siloxane-Carbon Nanotube Polymer Nanocomposites

We work on silicones and we believe that siloxane polymers are a special matrix material for CNT composites. The flexibility and conformational freedom of siloxanes allows them to adsorb and maximize polymer-nanotube interactions unlike any carbon-based polymer. The additional chemical versatility allows the adsorption strength to be tuned by the choice of functional group attached to the backbone. That methylsilicones are capable of dispersing CNTs have been reported and utilized.<sup>42-49</sup> Leveraging the unique properties of silicones and CNTs would open the door to specialty composites for use in flexible electronics, thermal management and flame retardants.

Besides applications in composites, siloxane polymers offer a convenient platform with which to study fundamental properties of CNT dispersions in polymer melts. Most studies regarding the structure-property relationships of CNT dispersions in polymer melts use carbon-based polymers and/or use different processing methods to achieve different dispersion states. Due to the higher glass transition temperatures of the polymers that have been studied, these experiments must be run at elevated temperatures for flow and

rheological observations. Silicones can be studied at room temperature, which is not only easier but mitigates any problems that may arise from degradation at high temperatures. Silicones also grant chemical versatility that allows adsorption behavior to be tuned. This allows silicone CNT nanocomposites to be prepared of varying dispersion quality with polymers of the same backbone using the same processing conditions. More direct comparisons can then be made between the properties of dispersion states allowing structure-property relationships to be formulated. This is not the case when CNTs are dispersed using different processing methods because improved dispersions are achieved in a manner that introduces solvent, surfactants, changes in nanotube chemistry or nanotube defects.

There are numerous studies on siloxane based CNT nanocomposites; however, the majority of them use Sylgard 184 as 'PDMS'.<sup>27,43,48</sup> This can be misleading since Sylgard 184 contains filler and is not strictly polydimethylsiloxane. Others have used various RTV formulations<sup>45-47</sup> and only one has used a phenyl containing siloxane as a dispersion agent.<sup>44</sup> The ability of silicones to disperse CNTs and investigations into the properties of various dispersion states in silicones remains unexplored.

#### 4.1.5 Objective

The objective of this work was to formulate relationships between CNT dispersion states and properties of silicone-CNT nanocomposites. Dispersion states were qualitatively observed using optical microscopy. Quantitative analysis was accomplished using melt rheology and surface resistivity of silicone-CNT nanocomposites. The development of processing methods and chemistry-structure-property relationships in silicone-CNT composites has improved our fundamental understanding of these material systems and has enabled us to engineer composite properties for specific applications.

## 4.2 Experimental Section

### 4.2.1 Materials and Abbreviations

Multi-walled carbon nanotubes (MWCNTs/CNTs) were provided by Nanocomp Technologies, Inc. A powder/pulp form of CNTs was used in these studies to prepare isotropic polymer composites. To prepare the powder/pulp product, a CNT sheet was 'chopped' in a mechanical mixer with the aid of a cosolvent and dried.

The linear silicone polymers studied are trimethylsilyl-terminated. For simplicity, the GE nomenclature<sup>49</sup> is used to refer to the silicone polymers. Low viscosity, low molecular weight silicone fluids ( $\eta \sim 500$  cSt /  $0.5$  Pa\*s): polydimethylsiloxane (M~17 500, Gelest DMS-T25,  $D_{230}$ ), polydiethylsiloxane (M~2000, Gelest DES-T23,  $D^{Et}_{20}$ ), poly(phenylmethyl)siloxane (M~2700, Gelest PMM-0025,  $D^{Ph-Me}_{20}$ ), poly(phenylmethyl-co-dimethyl)siloxane (M~10 000, 10 mol% phenylmethyl, Gelest PMM-1025,  $D_{112}D^{Ph-Me}_{13}$ ) and poly(diphenyl-co-dimethyl)siloxane (M~2400, 20 mol% diphenyl, Gelest PDM-1922,  $D_{19}D^{Ph}_5$ ). High viscosity, high molecular weight silicone fluid ( $\eta \sim 60$  000 cSt /  $60$  Pa\*s): polydimethylsiloxane (M~116 500, Gelest DMS-T46,  $D_{1570}$ ). All the above silicones were purchased from Gelest and used as received.

Elastomers were prepared with vinyl-terminated silicone fluids and hydridomethyl-dimethyl copolymers using Karstedt's catalyst (2% Pt solution in xylene, Gelest). Vinyl terminated silicone fluids purchased from Gelest were: polydimethylsiloxane (M~17 200, Gelest DMS-V25,  ${}^VD_{230}$  and M~28 000, Gelest DMS-V31,  ${}^VD_{380}$ ), poly(dimethyl-co-diethyl)siloxane (M~10 000, 20 mol% diethyl, Gelest EDV-2022,  ${}^VD_{100}D^{Et}_{25}$ ), poly(diphenyl-co-dimethyl)siloxane (M~12 500, 22 mol% diphenyl, Gelest PDV-2331,  ${}^VD_{98}D^{Ph}_{27}$ ) and poly(phenylmethyl)siloxane (M~3000, Gelest PMV-9925,  ${}^VD^{Ph-Me}_{22}$ ). Vinyl-terminated

dimethylsiloxane was prepared by equilibrium ring-opening polymerization of cyclic diethylsiloxane oligomers (Gelest) using tetramethylammonium hydroxide as catalyst and divinyltetramethyldisiloxane end-capping. The product has a molecular weight of 6000 ( $\text{VDEt}_{58}$ ). 30 mol% hydridomethyl copolymer (Gelest HMS-301,  $\text{D}_{18}\text{D}^{\text{H}}_8$ ) was used as crosslinker.

#### 4.2.2 Sample Preparation

*Linear Silicones.* Trimethylsilyl-terminated, linear silicone-MWCNT nanocomposite preparation depends on the neat silicone viscosity. High viscosity ( $\eta > 5 \text{ Pa}\cdot\text{s}$ ) silicones are prepared with the Flacktek Speedmixer (3000 RPM, 2 minutes). Lower viscosity silicones ( $\eta < 5 \text{ Pa}\cdot\text{s}$ ) require ultrasonic treatment (Branson 250 Digital Sonifier- 35% power, 5 sec pulse, 25 second rest, 1 minute total pulse time). In these studies, all silicones with viscosities less than  $5 \text{ Pa}\cdot\text{s}$  were prepared using sonication.

*Elastomers.* Vinyl-terminated, linear silicone-MWCNT composites were prepared in the same manner as linear trimethylsilyl-terminated silicone composites. The vinyl-terminated composite was then mixed with poly(hydridomethyl-co-dimethyl)siloxane (30 mol% hydridomethyl, HMS-301) to a Si-H:Vinyl ratio of 2:1. Karstedt's catalyst was added (20 ppm) and the mixture was cured into a solid elastomer at  $80 \text{ }^\circ\text{C}$  for 4 hours. Gelest OE41 polydimethylsiloxane (D) based, unfilled elastomer was used as received according to manufacturer instructions (1:1 ratio of part A and B, cured at  $80 \text{ }^\circ\text{C}$  for 4 hours).

#### 4.2.3 Characterization

*Optical Microscopy.* Dispersions were qualitatively studied with optical microscopy (Zeiss Axiovert 200). Samples for imaging were prepared by depositing a drop of silicone-



CNT composite onto a gridded microscope slide (Electron Microscopy Sciences) using a capillary tube.

*Rheology.* Silicone rheology was studied using a TA AR2000 Rheometer with 40 mm aluminum parallel plates. The high aspect ratio of CNTs can result in dramatic shear thinning from CNT alignment and the ability of CNTs to form elastic networks can be probed by measuring the viscoelastic properties of CNT reinforced composites. We use rheology as a means of quantifying the effect of dispersion quality on the viscoelasticity of PDMS-CNT composites.

Steady flow experiments of silicone and silicone-MWCNT fluids were run by ramping torque from  $0.1 \mu\text{N}\cdot\text{m}$  to  $10000 \mu\text{N}\cdot\text{m}$  (logarithmic ramp, 10 points per decade) and measuring shear rate. Viscosity was measured at each point and was then plotted as a function of shear rate. The steady flow viscosity was calculated from the average of three consecutive measurements per torque value. A 5% tolerance between points was used to determine if steady flow had been reached. Sampling time for each measurement is 15 seconds and point time is 3 minutes. The relationship between viscosity and shear rate was used to determine the zero shear viscosity and shear thinning behavior of silicone-MWCNT fluid composites.

Oscillatory shear experiments were used to probe the formation and elasticity of the MWCNT network within the silicones. Oscillatory stress sweeps from  $0.1$  to  $10\ 000 \mu\text{N}\cdot\text{m}$  were run at 1 Hz. Oscillatory frequency sweeps from  $0.01$  to  $10$  Hz were run within the linear viscoelastic region determined from stress sweeps ( $\sim 1\%$  strain). For both experiments, points were distributed logarithmically with 10 points per decade. All experiments were run at room temperature. Frequency sweeps are useful for analyzing

polymer dynamics. The low frequency domain corresponds to slow relaxations which may be associated with chain center-of-mass diffusion or reptation. High frequencies correspond to fast relaxations associated with segmental mobility. Because the glass transition in silicones ( $-125\text{ }^{\circ}\text{C}$  and  $-135\text{ }^{\circ}\text{C}$  for D and  $D^{\text{Et}}$ , respectively) is far below room temperature, it is unlikely that segmental relaxations will be detected, but diffusive processes and larger scale relaxations can be analyzed.

*Surface Resistivity.* The surface resistivity of composite elastomers was measured using a DESCO Concentric Ring Surface Conductivity Meter. 3-5 mm thick composites were prepared in 90 mm petri dishes. Above 3 mm, there is no observable change in the measured surface resistivity in these samples. Three measurements are made for each composite.

### 4.3 Results and Discussion

#### 4.3.1 Polydimethylsiloxane ( $D_n$ ): Processing, Dispersions and Viscoelastic Reinforcement in high ( $M > M_{\text{ent}}$ ) and low ( $M < M_{\text{ent}}$ ) molecular weight linear D polymers

Qualitatively homogeneous dispersions of Nanocomp CNT powder in polydimethylsiloxane are remarkably easy to achieve. With high viscosity  $D_{1570}$ , shear mixing of CNTs into the polymer melt using a Dual Assymmetric Centrifuge (Speedmixer) results in dispersions of CNT bundles that could be observed by optical microscopy. Some large aggregates are visible by eye in thin samples. Figure 4.1a shows a representative 20x optical micrograph of the 0.1 wt% CNT filled  $D_{1570}$  composite which exhibits wormlike CNT bundles. At loadings of 0.5 wt% CNT or higher,  $D_{1570}$  becomes a semi-solid pasty material. Flow rheology shown in Figure 4.1b illustrates a dramatic 1000x increase in zero shear viscosity upon addition of 1 wt% CNTs to  $D_{1570}$ . The composites exhibit extreme shear thinning, returning to the unfilled polymer viscosity at high shear rates. This indicates

that the CNTs align in the shear field generated during flow. This has been reported previously<sup>24, 25, 31</sup> and is expected for high aspect ratio fillers. The thixotropic loops in Figure 4.1c indicate that after alignment and shear thinning at high shear rates, the composites still retain the CNT reinforcement at low shear rates. Due to their size and the viscosity of the matrix, it is unlikely that the CNTs can rearrange from an aligned state to the initial random state on the time scale of the experiment. That the zero shear viscosity is retained in the aligned composite indicates that the interactions of the aligned CNT network are able to retard flow similar to the random network. These flow responses are schematically illustrated in Figure 4.2. The hysteresis observed at intermediate shear rates arises from the difference between flow during the process of aligning CNTs in the increasing shear rate step (up step) and the flow of aligned CNTs in the decreasing shear rate step (down step).

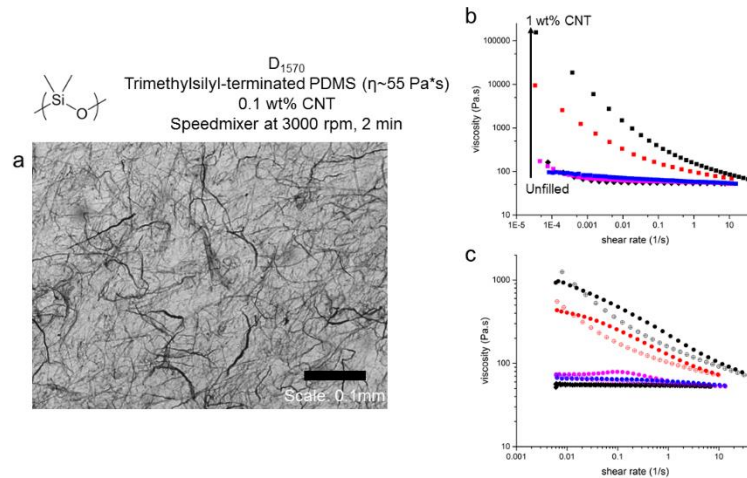


Figure 4.1. (a) Optical micrograph (20x) of 0.1 wt% - D<sub>1570</sub> composite. (b) Steady-state flow experiment of CNT- D<sub>1570</sub> composites and control showing dramatic shear thinning. (c) Thixotropic loops where filled symbols are for the increasing shear rate step (Up step) and crossed open symbols are for the decreasing shear rate step (Down step). For (b) squares and (c) circles: black = 1.0 wt% CNT, red = 0.5 wt% CNT, pink = 0.1 wt% CNT, 0.05 wt% = blue, control = black diamond. Note the hysteresis between up and down steps observed in (c) at higher loadings.



Figure 4.2: Alignment of CNTs during shear flow. The initially random CNT network aligns in the direction of flow as shearing forces are applied (Up step in thixotropic loop). At the highest shear rates the CNTs are aligned in the direction of flow and the viscosity of the fluid is low. On the Down step in the thixotropic loop, the CNTs are still roughly aligned in the direction of flow but they are able to interact as shear rate decreases, thus reinforcing the composite and raising viscosity.

Figure 4.3 further exhibits the effect of shear-induced structuring of the CNTs by comparing oscillatory rheology of unsheared and sheared composite fluids. In the unsheared state, the CNTs form a random network. The arrangement of CNTs in this network could be imagined as a stack of hay with interpenetrating silicone polymer chains (Figure 4.2). This random, physical network is elastic as indicated by the low phase shift ( $\delta$ ) measured in stress and frequency sweeps. Shearing of the physical CNT network during flow breaks it down and the CNTs align in the flow direction as previously discussed (and illustrated in Figure 4.2). After the CNT network is broken down and the CNTs are aligned, they are no longer as effective at reinforcing the silicone fluid (as indicated by the lower elasticity) in the range of stresses and frequencies tests. The decreased elasticity is exhibited by the decrease in  $G'$  and increased phase shift of the sheared composites as well as the decreased viscosity in the intermediate shear rates of the thixotropic loops (Figure 4.1c). Network elasticity can likely be returned by remixing the composite or over time if the CNTs are capable of rearranging back into a random physical network.<sup>29</sup>

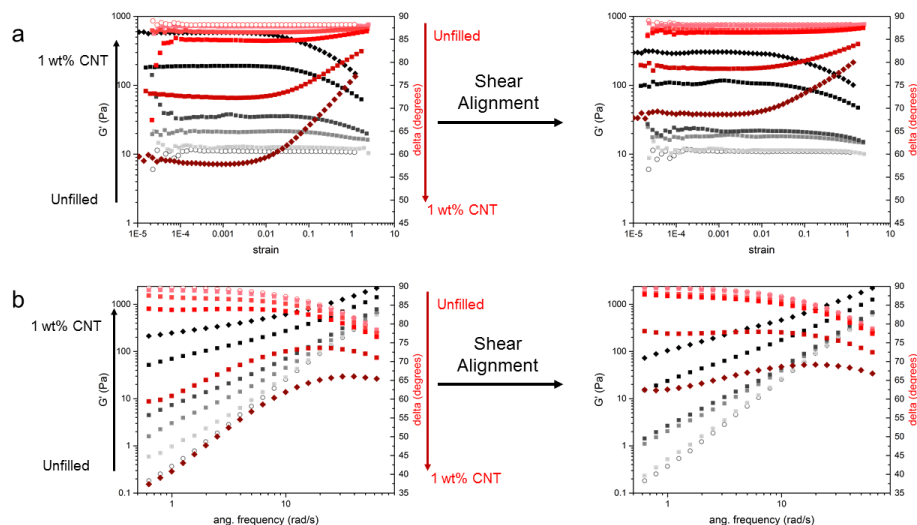


Figure 4.3. Breakdown of elastic CNT network by shear alignment in CNT-D<sub>1570</sub> composites. (a) Oscillatory stress sweeps and (b) oscillatory frequency sweeps show reductions in elasticity after shear alignment accomplished by a preshear conditioning step. Black symbols are G' and red symbols are delta. Unfilled controls are hollow circles. CNT loadings are 0, 0.01, 0.05, 0.1, 0.5 and 1 wt% and increase in the directions shown by the arrows. Generally G' increases and delta decreases with CNT loading. All experiments are run at room temperature. Frequency sweeps are run in the linear viscoelastic region.

The dispersions of CNTs in D<sub>1570</sub> are stable for long periods of time: no additional aggregation or sedimentation was observed over periods of months. This is due to kinetic trapping of the CNTs in the high viscosity matrix. The diffusion of the high aspect ratio CNTs in the entangled D<sub>1570</sub> is slow and would require long times for CNTs to aggregate by diffusion. The high viscosity of the D<sub>1570</sub> not only aids in stability but also in processing. The Speedmixer is a dual asymmetric centrifugal mixer that generates high shear forces in the polymer melt that depend on polymer melt viscosity. The shear energy put into the system is evident in the case of the D<sub>1570</sub> composites by the heat generated during the short mixing process. After 2-3 minutes of mixing at 3000 rpm, the D<sub>1570</sub> is warm to the touch.

With lower viscosity  $D_{230}$ , shear mixing in the Speedmixer is not capable of dispersing nanotubes. The low viscosity of the matrix does not generate and transmit the shear energy required to break up the nanotube aggregates in the same way that the high viscosity matrix can. For  $D_{230}$  and other low viscosity matrices that cannot produce the required shear energy in the Speedmixer, sonication must be used to disperse the nanotubes. GPC analysis of polymers subjected to sonication showed that the process does not cleave polymer chains. No test was conducted to test if CNTs are broken under these conditions, but based on discussions with personnel at Nanocomp, it is unlikely that the CNTs would break under the relatively low sonication power used. Figure 4.4 shows that sonication of CNTs in  $D_{230}$  resulted in dispersions of the same qualitative state as those prepared by Speedmixing  $D_{1570}$ . Some aggregates are observable by eye and optical micrographs exhibited bundles. The  $D_{230}$  dispersions are not as stable against sedimentation. Sedimentation is observed in periods of approximately weeks to one month; however, simply stirring the fluid can disperse the CNT sediment with no signs of additional aggregation.

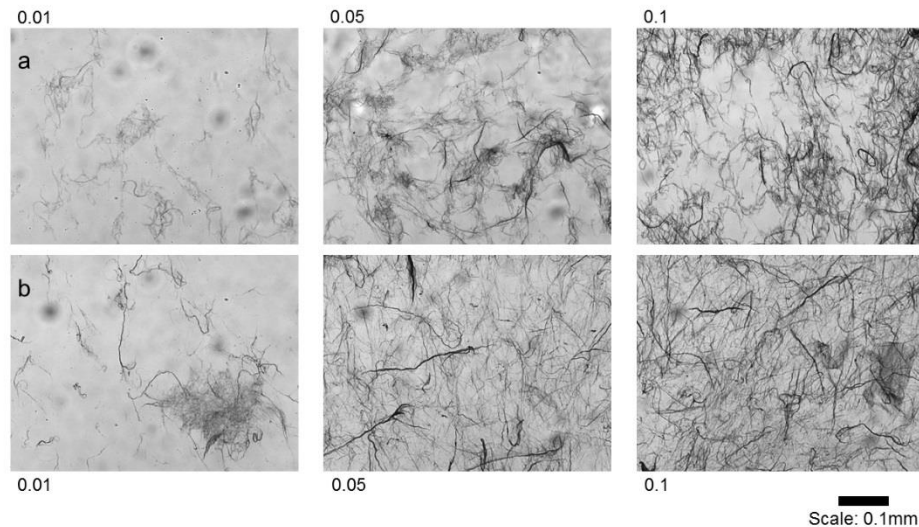


Figure 4.4. (a)  $D_{230}$  and (b)  $D_{1570}$  linear silicone-CNT composite micrographs (20x). Numbers indicate wt% CNT in silicone

The qualitative microscopy in Figure 4.4 indicates similar dispersion states in the two PDMS fluids, yet obvious quantitative differences are observed by the rheology shown in Figure 4.5. In the  $D_{230}$  composite processed by sonication, the elastic modulus ( $G'$ ) increases by 1000 times with 0.1 wt% CNT and the phase shift (delta) demonstrates the formation of an elastic CNT network at 0.025 wt% CNTs. In the case of  $D_{1570}$ , processed by shear mixing, a similar increase in  $G'$  occurs but only with the addition of 0.5 wt% CNTs and the elastic network becomes apparent at 0.05 wt%. Comparing phase shift in the two composites highlights that the elastic contribution of the CNT network in the  $D_{1570}$  composite is much lower than that of the  $D_{230}$  composite. Differences in the composite fluid's rheology clearly indicate that although the dispersions appear similar by microscopy, the CNT network that forms in these silicones is much different. Sonication in the  $D_{230}$  silicone composites can break up the nanotube bundles enabling the formation of a CNT network at remarkably low CNT loadings. This is exhibited by the 0.1 wt% CNT- $D_{230}$  composite, which behaves like a physical CNT gel swollen with PDMS chains as indicated by its highly elastic character (delta  $\sim 15^\circ$ ).

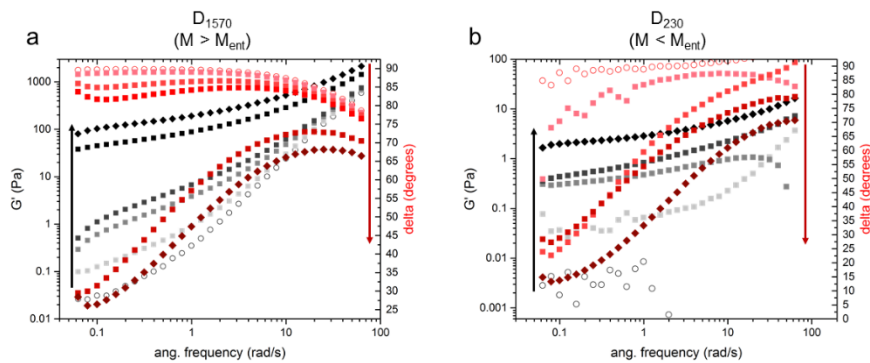


Figure 4.5. Oscillatory frequency sweeps at room temperature of (a)  $D_{1570}$  composites and (b)  $D_{230}$  composites. Arrows indicate increasing CNT concentration. Unfilled control samples are unfilled circles. In (a) increasing color intensity corresponds to loadings of 0.01, 0.05, 0.1, 0.5, and 1.0 wt% CNT. In (b) increasing color intensity corresponds to loadings of 0.01, 0.025, 0.05 and 0.1 wt% CNT. In general,  $G'$  increases and delta decreases with CNT loading. All experiments were run the linear viscoelastic region.

Across the tested frequencies (at room temperature), the shape of the responses for the two silicones and their composites is similar. The only noticeable difference arises in the higher frequency domain because of entanglements present in  $D_{1570}$  and not in  $D_{230}$ . The increase in  $G'$  and elasticity in  $D_{1570}$  at high frequency comes from entanglements in the polymer acting as physical crosslinks. With the incorporation of 0.5 wt% or more CNTs we see that  $G'$  and elasticity in this region begin to increase suggesting that the entangled silicone network is being constrained by the CNT network. The formation of an interpenetrating entanglement-CNT network has interesting implications for polymer dynamics. The  $D_{230}$  samples do not show this change in behavior:  $G'$  and elasticity increase steadily in all frequency regions as CNT loading increases.

Based on the above measurements, sonication proved to be a superior method of dispersing CNTs in neat silicones. One downside of the sonication method is that it was only found to be useful in lower viscosity fluids. At high viscosities, the sonication is locally confined to the tip of the ultrasonic probe due to the inability of the silicone to flow during the short sonic pulses, whereas flow occurs in low viscosity fluids to allow complete mixing of samples. Luckily, the viscosity of silicone polymers can be controlled by adjusting molecular weight. Addition of solvent is not required to prepare silicone composites as long as their viscosity (molecular weight) is low enough to enable sample mixing during sonication. If a higher molecular weight silicone composite was desired, addition of plasticizing solvent would be required to adequately utilize sonication. This was not studied, as an objective of this work was to achieve dispersions in neat silicones without addition of solvent, surfactant or chemical modification. Future work on the differences between the effects of CNT reinforcement in matrices above and below the entanglement threshold could provide insight into chain dynamics and relaxations in silicone polymer nanocomposites.



#### 4.3.2 Effect of siloxane polymer chemistry on CNT dispersion

Having determined the optimal processing conditions for achieving dispersions in silicones, the next step was to determine how the chemistry of the silicone polymer affects the dispersion. Changes in the organic substituents attached to the silicone backbone change the polymer-nanotube interactions. Increasing the strength of polymer-nanotube interactions can improve CNT dispersability in the silicone matrix. An obvious choice of side group to improve polymer-nanotube interactions is phenyl rings which introduce attractive  $\pi$ - $\pi$  interactions between the polymer chain and the nanotube. Diethylsiloxane was also chosen because it has been shown to be effective at dispersing pigments in silicone cosmetic formulations.<sup>49</sup> All of the linear silicones were purchased from Gelest and have comparable room temperature viscosities of approximately 0.5 Pa\*s and are below the entanglement molecular weight. Their molecular weights vary since the molecular weight-viscosity relationship depends on the side group composition of the silicone. All composites were prepared using the same sonication procedure. The difference between these silicone-CNT composites therefore arises solely from the chemistry of the backbone. Figure 4.6 exhibits representative micrographics of three homopolymer composites: D<sub>230</sub>, D<sup>Me-Ph</sup><sub>20</sub> and D<sup>Et</sup><sub>20</sub>.

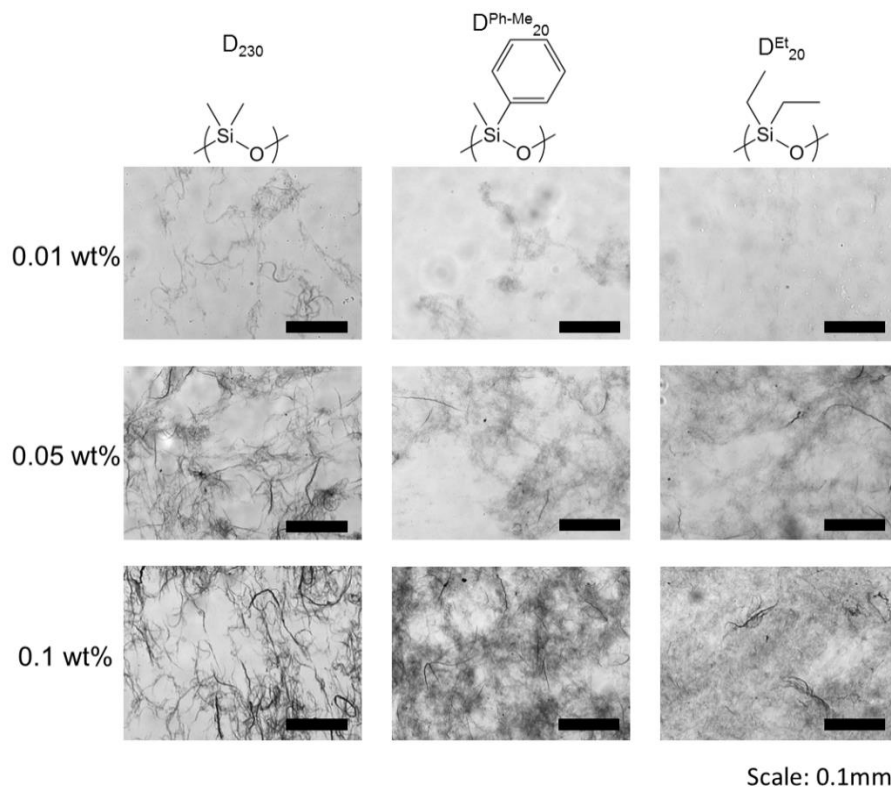


Figure 4.6. Optical micrographs (20x) of linear siloxane homopolymer – CNT composites.

There are obvious qualitative differences in the CNT dispersions in the homopolymer composites. The incorporation of phenyl and ethyl groups improves the dispersion as indicated by the reduction in the size and number of large CNT bundles. In the phenylmethylsiloxane homopolymer micrographs, dark CNT ‘clouds’ are apparent in a lighter background. In diethylsiloxane homopolymer, the CNTs appear to be dispersed homogeneously with some bundling.

Dimethylsiloxane copolymers containing phenyl groups were also investigated:  $D_{112}D^{Ph-Me}_{13}$  and  $D_{19}D^{Ph}_5$ . Optical micrographs of CNT dispersions are exhibited in Figure 4.7. The  $D_{112}D^{Ph-Me}_{13}$  copolymer has very similar properties to  $D_{230}$  homopolymer. With only 10 mol% phenylmethyl comonomer present, there are too few phenyl groups to significantly improve the dispersions. Incorporating 20 mol% diphenyl comonomer did

improve dispersion. This suggests a systematically study for future work to investigate the change in dispersion quality with increasing phenyl content on the backbone. Such a study would enable optimization of matrix properties and dispersion quality.

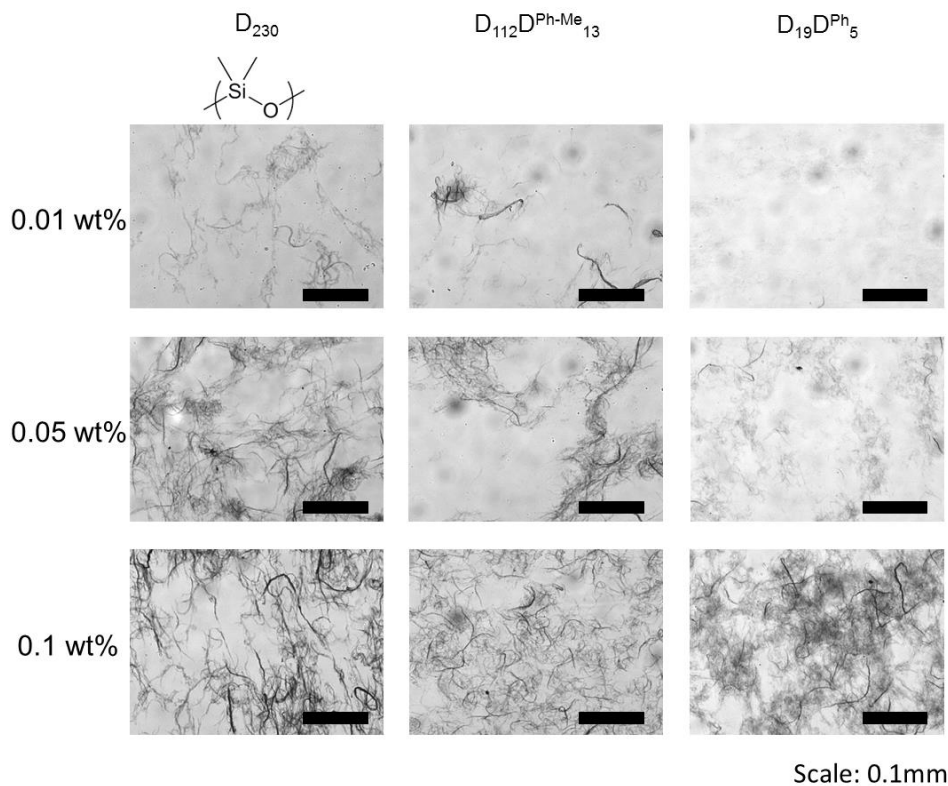


Figure 4.7. Optical micrographs (20x) of linear dimethylsiloxane copolymer – CNT composites.

Rheology of the composite fluids demonstrates that the qualitative improvements in dispersion do translate to improved reinforcement and CNT network formation. Figure 4.8 shows oscillatory frequency sweeps for each silicone chemistry with CNT loadings of 0 (control), 0.01, 0.025, 0.05 and 0.1 wt%. In all cases, as the concentration of CNTs increases, storage modulus ( $G'$ ) increases and phase shift ( $\delta$ ) decreases. The shapes of the curves are similar: across all samples  $G'$  and phase shift increases with frequency. The reinforcement of the siloxane fluids by CNTs is greatest in the phenylmethyl

homopolymer which shows a  $\sim 10\,000\times$  increase in  $G'$ . The phenylmethyl homopolymer also shows the most efficient reinforcement as indicated by the large decrease in delta at 0.01 wt% CNTs. This indicates that the CNTs form an elastic network at remarkably low loadings in this siloxane polymer.

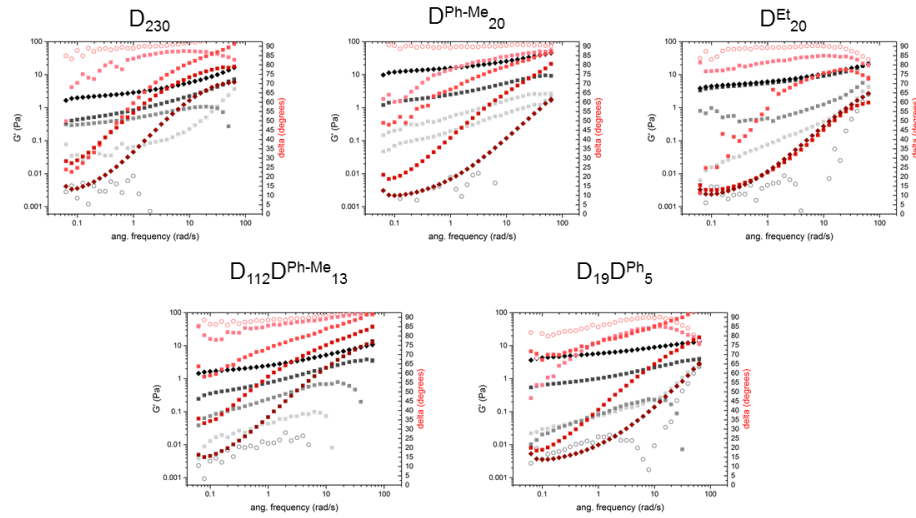


Figure 4.8. Oscillatory frequency sweeps at room temperature of siloxane polymer – CNT composites. CNT loadings are 0, 0.01, 0.025, 0.05 and 0.1 wt%. Black symbols are  $G'$  and red symbols are phase shift (delta). Empty circles are unfilled controls. Color intensity indicates loading from lightest (0.01 wt%) to darkest (0.1 wt%). Generally,  $G'$  increases and delta decreases with CNT loading. All experiments were run the linear viscoelastic region.

Figure 4.9a shows comparative steady flow viscosity measurements of control and 0.1 wt% CNT composites. The unfilled silicones display shear rate - independent viscosity meaning that in the accessible shear rates, they are Newtonian. The composites, on the other hand, demonstrate dramatic shear thinning: the zero-shear viscosity is  $10^4$ - $10^5$  times greater than unfilled controls, but at high shear rates the viscosity decreases to that of the unfilled controls. These same observations were made in the  $D_{1570}$  sample and the same mechanism is responsible. The ranking of zero-shear viscosity in silicone-CNT composites is:  $D^{Ph-Me} > D^{Et} > DD^{Ph} > DD^{Ph-Me} > D$ . At 0.1 wt% these composites are paste-like. This

dramatic increases in zero shear viscosity at only 0.1 wt% CNTs is unprecedented. The remarkable reinforcement is due to the unique high aspect ratio of the Nanocomp CNTs. If we assume that nanotubes have an average number of interactions per length, as nanotube length increases the number of nanotube-nanotube interactions per nanotube increases. The longer the nanotubes, the more interactions, the stronger the physical network that forms from these interactions, and thus the greater the reinforcing effect.

Figure 4.9b shows comparative oscillatory frequency sweep measurements of control and 0.1 wt% CNT composite fluids. At 0.1 wt% CNT, all composites have predominantly elastic behavior (phase shifts less than  $45^\circ$ ) at low frequencies. The similarity in the elastic contribution of the CNT network at low frequencies, for all the siloxanes, indicates that under these conditions we are probing the CNT network. The CNT network appears to constrain diffusive relaxations of siloxane chains, resulting in the observed elastic bulk properties. At the highest tested frequencies,  $\delta$  increases and all the composites exhibit viscous behavior. The elasticity at these frequencies is still greater than the unfilled controls (which have phase shifts of  $90^\circ$  indicating completely viscous behavior) which indicates that the CNT network is constraining the polymer chains to some degree. This region corresponds to where the effect of entanglements is observed in  $D_{1570}$  which suggests that the constraints of the CNT network are of a similar length and time scale as entangled polymer relaxations. It is unlikely that the segmental motions of the chains are restricted, but these frequencies were not accessed in these experiments. This could be detected using time-temperature superposition methods or with differential scanning calorimetry measurements of glass transitions in these polymers. Instrumentation limitations in our labs did not allow these measurements. If such experiments were to be run, a small or absence of shift in glass transition would be expected. At intermediate frequencies, better dispersed samples are more elastic than the

lower quality dispersions. The  $D^{\text{Ph-Me}}$  composite has the most elasticity in this region. This shows that the CNT network is more robust in the better dispersed samples, creating a gel-like material where the siloxane polymer chain mobility and freedom is constrained to a greater extent.

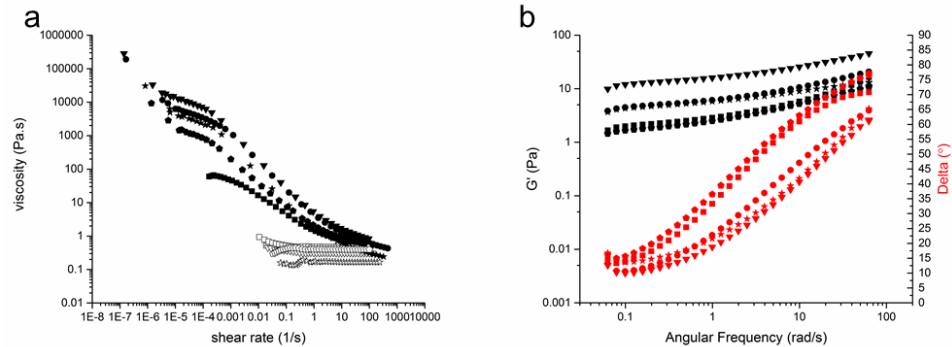


Figure 4.9. (a) Steady state flow and (b) oscillatory frequency sweeps of siloxane-CNT composites. In (a) filled symbols are 0.1 wt% CNT composites and open symbols are unfilled controls. In (b) black,  $G'$ , and red,  $\Delta$ , plots are for 0.1 wt% CNT samples.

Symbol Key:  $D^{\text{Ph-Me}}$  = Down Triangle,  $D^{\text{Et}}$  = circle,  $DD^{\text{Ph}}$  = star,  $DD^{\text{Ph-Me}}$  = pentagon,  $D$  = square.

The best mechanical reinforcement (by oscillatory shear) occurred in the  $D^{\text{Ph-Me}}$  composites, with the  $DD^{\text{Ph}}$  copolymer composite a close second. This is contradictory to the dispersion quality observed in optical microscopy. These phenyl containing silicones composites exhibit cloudy, heterogeneous CNT-rich domains. How is it that the CNT reinforcement is better in this heterogeneous dispersion than in the homogenous  $D^{\text{Et}}$  silicone composite? My hypothesis is that the mechanisms of load bearing in the CNT network and load transfer between CNT network and silicone matrix are enhanced by the heterogeneity. Too heterogeneous a mixture leads to inefficient use of the CNTs (like in the  $D$  composites) or, in the worst case, aggregates that act as defects that have a negative impact on properties. Too homogenous a mixture leads to weaker nanotube-nanotube

interactions and a weaker CNT network. With just the right amount of heterogeneity, the CNT network is strong but also well dispersed through the composite. This could be imagined as a percolated CNT superstructure.

#### 4.3.3 Conductivity in Silicone-CNT Elastomer Composites

Silicone elastomers were prepared that mimicked the backbone chemistry of the silicone fluids. Vinyl-terminated siloxane polymers were crosslinked using an oligomeric hydridomethyl crosslinker and Pt catalyst. An additional entry is a PDMS-based elastomer from Gelest, OE41. Surface resistivity measurements are shown in Table 4.1. Conductivity in the elastomers increases from:  $D^{Et} > DD^{Et} > DD^{Ph} > D$ . A  $D^{Ph-Me}$  elastomer was attempted but phase separation occurred between the crosslinker and the polymer and no apparent crosslinking occurred. The most conductive silicone,  $D^{Et}$ , is also the silicone with the most homogeneous dispersion in microscopy. Electrical conductivity requires a continuous path for electrons through a material and a more homogeneous dispersion of conductive CNTs provides the greatest number of such continuous paths. For this reason the  $D^{Et}$  silicones were the most conductive of the materials tested. Unfortunately, the  $D^{Ph-Me}$  system does not cure and could not be compared.

Table 4.1. Surface Resistivity of Silicone-CNT Elastomers ( $\Omega/\square$ )

Siloxane Matrix	wt % CNT			
	0.01	0.025	0.05	0.1
${}^V D_{230}$	3.77E+08	1.31E+06	1.10E+05	4.58E+03
${}^V D_{380}$	-	8.90E+07	1.65E+06	6.95E+04
OE41 ( $D_n$ )	-	1.60E+12	7.56E+08	4.58E+04
${}^V D_{98} D_{27}^{Ph}$	5.13E+09	7.00E+06	1.39E+06	1.20E+05
${}^V D_{100} D_{25}^{Et}$	8.00E+05	1.14E+06	8.00E+04	2.40E+03
${}^V D_{58}^{Et}$	4.87E+04	1.53E+05	4.07E+03	1.50E+03

#### 4.4 Conclusions

The results clearly show that CNTs can be dispersed into silicones with ease and that small amounts of CNT filler can go a long way toward improving mechanical properties and electrical conductivity. The processing methods depend on the silicone molecular weight (or viscosity) and sonication of low molecular weight (low viscosity) silicones proved to be optimal over shear mixing of high molecular weight (high viscosity) silicones. Silicone chemistry allows dispersion quality to be tuned without the use of cosolvents, surfactants or CNT modification. As expected, the lowest quality dispersions in D polymers had the lowest mechanical reinforcement and electrical conductivity. However, in the other silicones, interesting differences occur in the rheology and conductivity performance. Qualitative microscopy of the composites showed that  $D^{Et}$  had the most homogenous appearing dispersions. The  $D^{Et}$  elastomers also have the lowest surface resistivity (highest conductivity). But, in the case of mechanical properties, the  $D^{Ph-Me}$  composites perform best even though they have less 'optimal', homogenous dispersions. Qualitatively the  $D^{Ph-Me}$  and  $DD^{Ph}$  polymers have intermediate dispersion but rheology shows that the CNT network that forms is stronger and more elastic. Figure 4.10 illustrates three dispersion states of CNT filler: heterogeneous (D), homogeneous ( $D^{Et}$ ) and intermediate ( $D^{Ph}$ ). The heterogeneous case contains CNT bundles that limit the interconnectedness of the CNT network thus reducing the ability to conduct or reinforce. The homogeneous case contains no large bundles. The uniform dispersion of CNTs allows electron transport for high conductivity but does not have a strong network structure that transfers load thus reinforcement is limited. The intermediate case has an elastic, percolated CNT superstructure that supports load but reduces the number of electron conducting paths. This results in good reinforcement but reduced electrical conductivity.



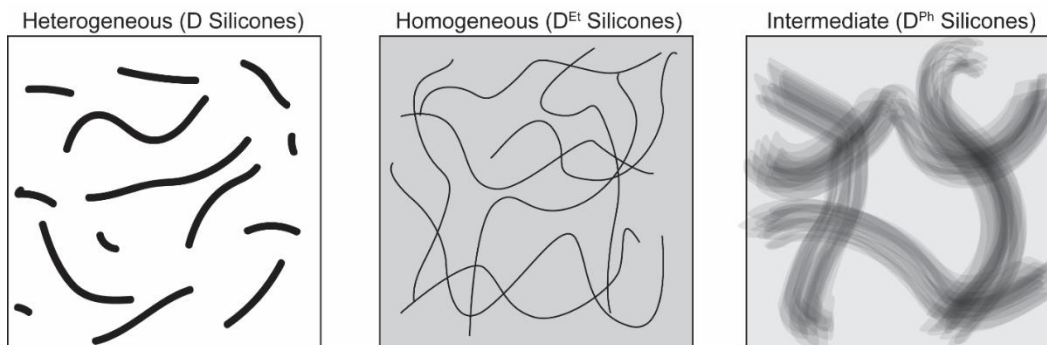


Figure 4.10: Schematic representations of heterogeneous, homogeneous and intermediate CNT dispersions.

This presents an important lesson when deciding what is ‘optimal.’ The optimal dispersion depends on the application. A perfectly homogeneous dispersion is advantageous for transport of electricity or heat. A degree of heterogeneity is advantageous for the formation of a strong CNT network with adequate load bearing and transfer to result in improved mechanical properties. The effect of different dispersion qualities on different properties illustrates that each property has a unique mechanism of action that requires specific filler-matrix or filler-filler interactions. This work shows that with silicones, the dispersion quality can be tuned and the tuning of the dispersion enables engineering of composite properties. The chemistry of the silicone polymer becomes the knob for engineering CNT structures that are reflected in silicone-CNT composite properties.

#### 4.5 References

1. Kumar, S. K.; Benicewicz, D. B.; Vaia, R. A.; Winey, K. I. Are Polymer Nanocomposites Practical for applications. *Macromolecules* **2017**, *50*, 714-731.
2. Spahr, M. E.; Rothon, R. Carbon black as a polymer filler. *Fillers for Polymer Applications* **2017**, 261-291.
3. Davenport, M. Much ado about small things. *C&EN* **2015**, *June 8<sup>th</sup>*, 10-15.
4. Noorden, R. V. The Trails of New Carbon. *Nature* **2011**, *469*, 14-16.

5. Tennent, H. G. Carbon Fibrils, Method For Producing Same and Compositions Containing Same. US Pat. 4,663,230, May 5, 1987.
6. Iijima, S. Helical microtubules of graphitic carbon. *Nature* **1991**, *354*, 56-58.
7. Georgakilas, V.; Perman, J. A.; Tucek, J.; Zboril, R. Broad Family of Carbon Nanoallotropes: Classification, Chemistry, and Applications of Fullerenes, Carbon Dots, Nanotubes, Graphene, Nanodiamonds, and Combined Superstructures. *Chem. Rev.* **2015**, *115*, 4744-4822.
8. Tasis, D.; Tagmatarchis, N.; Bianco, A.; Prato, M. Chemistry of Carbon Nanotubes. *Chem. Rev.* **2006**, *106*, 1105-1136.
9. Moniruzzaman, Mohammad; Winey, Karen I. Polymer Nanocomposites Containing Carbon Nanotubes. *Macromolecules* **2006**, *39*, 5194-5205.
10. Kota, A. K.; Cipriano, B. H.; Duesterberg, M. K.; Gershon, A. L.; Powell, D.; Raghavan, S. R.; Bruck, H. A. Electrical and Rheological Percolation in Polystyrene/MWCNT Nanocomposites. *Macromolecules* **2007**, *40*, 7400-7406.
11. Bauhofer, W.; Kovacs, J.Z. A Review and Analysis of Electrical Percolation in Carbon Nanotube Polymer Composites. *Comp. Sci. Tech.* **2009**, *69*, 1486-1498.
12. Zhang, Q.; Huang, J. Q.; Qian, W. Z.; Zhang, Y. Y.; Wei, F. The road for nanomaterials industry: a review of carbon nanotube production, post-treatment, and bulk applications for composites and energy storage. *Small* **2013**, *9*, 1237-1265.
13. De Volder, M. F. L.; Tawfick, S. H.; Baughman, R. H.; Hart, A. J. Carbon Nanotubes: Present and Future Commercial Applications. *Science* **2013**, *339*, 535-539.
14. Breuer, O.; Sundararaj, U. Big Returns From Small Fibers: A Review of Polymer/Carbon Nanotube Composites. *Polym. Comp.* **2004**, *25*, 630-645.
15. Winey, K. I.; Vaia, R. A. Polymer Nanocomposites. *MRS Bulletin* **2007**, *32*, 314-319.
16. Coleman, J. N.; Khan, U.; Blau, W. J.; Gun'ko, Y. K. Small but strong: A review of the mechanical properties of carbon nanotube-polymer composites. *Carbon* **2006**, *44*, 1624-1652.
17. Spitalsky, Z.; Tasis, D.; Papagelis, K.; Galotis, C. Carbon nanotube-polymer composites: Chemistry, processing, mechanical and electrical properties. *Prog. Polym. Sci.* **2010**, *35*, 357-401.
18. Vilatela, J.; Marcilla, R. Tough Electrodes: Carbon Nanotube Fibers as the Ultimate Current Collectors/Active Material for Energy Management Devices. *Chem. Mater.* **2015**, *27*, 6901-6917.
19. Ma, Peng-Cheng; Siddiqui, Naveed A.; Marom, Gad; Kim, Jang-Kyo. Dispersion and functionalization of carbon nanotubes for polymer-based nanocomposites: A review. *Composites: Part A* **2010**, *41*, 1245-1367.
20. Grossiord, N.; Loos, J.; Regev, O.; Koning, C. E. Toolbox for Dispersing Carbon Nanotubes into Polymers to get Conductive Nanocomposites. *Chem. Mater.* **2006**, *18*, 1089-1099.

21. Ausman, K. D.; Piner, R.; Lourie, O.; Ruoff, R. S. Organic Solvent Dispersions of Single-Walled Carbon Nanotubes: Toward Solutions of Pristine Nanotubes. *J. Phys. Chem. B.* **2000**, *104*, 1811-1815.
22. Krishnamoorti, Ramanan. Strategies for Dispersing Nanoparticles into Polymers. *MRS Bulletin.* **2007**, *32*, 341-347.
23. Du, F.; Scogna, R. C.; Zhou, W.; Brand, S.; Fischer, J. E.; Winey, K. I. Nanotube Networks in Polymer Nanocomposites: Rheology and Electrical Conductivity. *Macromolecules.* **2004**, *37*, 9048-9055.
24. Kharchenko, S. B; Douglas, J. F.; Obrzut, J.; Grulke, E. A.; Migler, K. B. Flow-induced properties of nanotube-filled polymer materials. *Nature Materials* **2004**, *3*, 564-568.
25. Niu, R.; Gong, J.; Xu, D.; Tang, T.; Sun, Z. Flow-induced structure and rheological properties of multiwall carbon nanotube/polydimethylsiloxane composites. *RSC Adv.* **2014**, *4*, 62759-62768.
26. Huang, Y. Y.; Ahir, S. V.; Terentjev, E .M. Dispersion rheology of carbon nanotubes in a polymer matrix. *Phys. Rev. B.* **2006**, *73*, 125422.
27. Marceau, S.; Dubois, P.; Fulchiron, R.; Cassagnau, P. Viscoelasticity of Brownian Carbon Nanotubes in PDMS Semidilute Regime. *Macromolecules* **2009**, *42*, 1433-1438.
28. Pötschke, P.; Abdel-Goad, M.; Alig, I.; Dudkin, S.; Lellinger, D. Rheological and dielectric characterization of melt mixed polycarbonate-multiwalled carbon nanotube composites. *Polymer* **2004**, *45*, 8863-8870.
29. Alig, I.; Skipa, T.; Lellinger, D.; Pötschke, P. Destruction and formation of a carbon nanotube network in polymer melts: Rheology and conductivity spectroscopy. *Polymer* **2008**, *49*, 3524-3532
30. Kashiwagi, T.; Fagan, J.; Douglas, J. F.; Yamamoto, K.; Heckert, A. N.; Leigh, S. D.; Obrzut, J.; Du, F.; Lin-Gibson, S.; Mu, M.; Winey, K. I.; Haggemueller, R. Relationship between dispersion metric and properties of PMMA/SWNT nanocomposites. *Polymer* **2007**, *48*, 4855-4866.
31. Lin-Gibson, S.; Pathak, J. A.; Grulke, E. A.; Wang, H.; Hobbie, E. K. Elastic Flow Instability in Nanotube Suspensions. *Phys. Rev. Lett.* **2004**, *92*, 048302.
32. Schaefer, D. W.; Justice, R. S. How Nano Are Nanocomposites? *Macromolecules* **2007**, *40*, 8501-8517.
33. Du, F.; Fischer, J. E.; Winey, K. I. Coagulation Method for Preparing Single-Walled Carbon Nanotube/Poly(methyl methacrylate) Composites and Their Modulus, Electrical Conductivity, and Thermal Stability. *J. Polym. Sci. B: Polym. Phys.* **2003**, *41*, 3333-3338.
34. Gong, X.; Liu, J.; Baskaran, S.; Voise, R. D.; Young, J .S. Surfactant-Assisted Processing of Carbon Nanotube/Polymer Composites. *Chem. Mater.* **2000**, *12*, 1049-1052.

35. Chadwick, R. C.; Grande, J. B.; Brook, M. A.; Adronov, A. Functionalization of Single-Walled Carbon Nanotubes via the Piers-Rubinsztajn Reaction. *Macromolecules*. **2014**, *47*, 6527-6530.
36. Tour, J. M.; Dyke, C. A. Covalent Functionalization of Single-Walled Carbon Nanotubes for Materials Applications. *J. Phys. Chem. A*. **2004**, *108*, 11151-11159.
37. Saalwächter, K. Proton multiple-quantum NMR for the study of chain dynamics and structural constraints in polymeric soft materials. *Prog. Nucl. Magn. Reson. Spectrosc.* **2007**, *51*, 1-35.
38. Papon, A.; Saalwächter, K.; Schäler, K.; Guy, L.; Lequeux, F.; Montes, H. Low field NMR Investigations of Nanocomposites: Polymer Dynamics and Network Effects. *Macromolecules* **2011**, *44*, 913-922.
39. Cheng, Q.; Bao, J.; Park, J.; Liang, Z.; Wang, B. High Mechanical Performance Composite Conductor: Multi-walled Carbon Nanotube Sheet/Bismaleimide Nanocomposites. *Adv. Funct. Mater.* **2009**, *19*, 1-7.
40. Downes, R. D.; Hao, A.; Park, J. G.; Su, Y.; Liang, R.; Jensen, B. D.; Siochi, E. J.; Wise, K. E. Geometrically constrained self-assembly and crystal packing of flattened and aligned carbon nanotubes. *Carbon* **2015**, *93*, 953-966.
41. Cheng, Q.; Wang, B.; Zhang, C.; Liang, Z. Functionalized Carbon-Nanotube Sheet/Bismaleimide Nanocomposites: Mechanical and Electrical Performance Beyond Carbon-Fiber Composites. *Small* **2010**, *6*, 763-767.
42. Benson, J.; Kovalenko, I.; Boukhalfa, S.; Lashmore, D.; Sanghadasa, M.; Yushin, G. Multifunctional CNT-Polymer Composites for Ultra-Tough Structural Supercapacitors and Desalination Devices. *Adv. Mater.* **2013**, *25*, 6625-6632.
43. Beigbeder, A.; Linares, M.; Devalckenaere, M.; Degée, P.; Claes, M.; Beljonne, D.; Lazzaroni, R.; Dubois, P. CH- $\pi$  Interactions as the Driving Force for Silicone-Based Nanocomposites with Exceptional Properties. *Adv. Mater.* **2008**, *20*, 1003-1007.
44. Bai, L.; Bai, Y.; Zheng, J. Improving the filler dispersion and performance of silicone rubber/multi-walled carbon nanotube composites by noncovalent functionalization of polymethylphenylsiloxane. *J. Mater. Sci.* **2017**, *52*, 7516-7529.
45. Sonnier, R.; Bokobza, L.; Concha-Lozano, N. Influence of multiwall carbon nanotube (MWCNT) dispersion on ignition of poly(dimethylsiloxane)-MWCNT composites. *Polym. Adv. Technol.* **2015**, *26*, 277-286.
46. Sagar, S.; Iqbal, N.; Maqsood, A.; Shahid, M.; Shah, N. A.; Jamil, T.; Bassyouni, M. I. Fabrication and thermal characteristics of functionalized carbon nanotubes impregnated polydimethylsiloxane nanocomposites. *J. Compos. Mater.* **2015**, *49*, 995-1006.
47. Kim, T. A.; Kim, H. S.; Lee, S. S.; Park, M. Single-walled carbon nanotube/silicone rubber composites for compliant electrodes. *Carbon* **2012**, *50*, 444-449.
48. Yao, S.; Zhu, Y. Nanomaterial-Enabled Stretchable Conductors: Strategies, Materials and Devices. *Adv. Mater.* **2015**, *27*, 1480-1511.
49. Personal communications with B. Arkles.

## CHAPTER 5

### SILICONE CARBON NANOTUBE COMPOSITES: THERMAL STABILITY

#### ENHANCEMENTS AND DECOMPOSITION MECHANISM

##### 5.1 Introduction

##### 5.1.1 Background

In Chapter 4 and a recent publication<sup>1</sup>, silicone polymers have been recognized for their special interactions with carbon nanotubes. Carbon nanotubes (CNTs) have generated tremendous interest as polymer additives<sup>2</sup> to enhance electrical<sup>3</sup>, thermal<sup>4</sup> and mechanical properties<sup>5</sup>. A major challenge in the effective utilization of CNTs in polymers is achieving homogeneous and/or controlled filler dispersion.<sup>6-10</sup> Typically, CNTs require chemical modifications<sup>11-13</sup>, solution processing<sup>14,15</sup>, surfactants<sup>16,17</sup>, intense mechanical mixing, such as high power sonication, or combinations of processes to be dispersed. Unfortunately, these processes can introduce defects or fracture nanotubes, hindering performance in composites. Due to their size, nanotubes and other nanoparticles have high surface area-to-volume ratios in comparison to conventional microscale fillers. In polymer nanocomposites, such high surface area-to-volume ratios make the polymer-nanotube interface critical. Our approach to nanocomposite preparation comes from the perspective of polymer adsorption to and wetting of nanotube surfaces. A multi-walled carbon nanotube (MWCNT) with 50 nm diameter has dimensions of a similar scale to a high molecular weight polymer coil but is much larger than the segments that make up the polymer. Should the segments of the polymer favor adsorption, spontaneous adsorption will occur on the nanotube surface. This disrupts the nanotube-nanotube interactions that promote aggregation and has been recognized as a non-covalent method to functionalize CNTs and improve dispersion and stability.<sup>11</sup>

Silicones are a family of polymers based on the siloxane backbone that have very different properties than carbon-based polymers. Owing to the structure of the backbone and the mobility of the methyl groups attached to the silicon atom, poly(dimethyl siloxane) (PDMS, Figure 5.1) has an anomalously low glass transition temperature ( $T_g \sim -125^\circ\text{C}$ ), low surface energy (21.6 mN/m), high vapor permeability and high thermal stability (Si-O bond strength of  $\sim 800$  kJ/mol).<sup>18,19</sup> In considering matrix polymers for the wetting and adsorption to CNTs, methylsilicones seemed like an obvious choice. The mobility of the methyl groups allows favorable segmental interactions with CNTs and the backbone is flexible enough to allow conformations that maximize the number of segmental interactions between polymer and nanotube. The ability to melt process PDMS at room temperature is an additional preparative advantage in terms of ease and energy requirements. The advantages of PDMS as a matrix for CNT nanocomposites has been observed previously in the work of Beigbeder *et. al.*<sup>1</sup> and was attributed by molecular dynamics simulations to CH- $\pi$  interactions between PDMS segments and CNTs. In their work, the authors mechanically dispersed MWCNTs into Dow Corning Sylgard 184, a commercially available, filled PDMS-based elastomer, and observed dramatic increases in zero shear viscosity. Molecular dynamics simulations showed that PDMS chains completely wrap the nanotube with strong CH- $\pi$  interactions between one methyl group of each repeat unit.

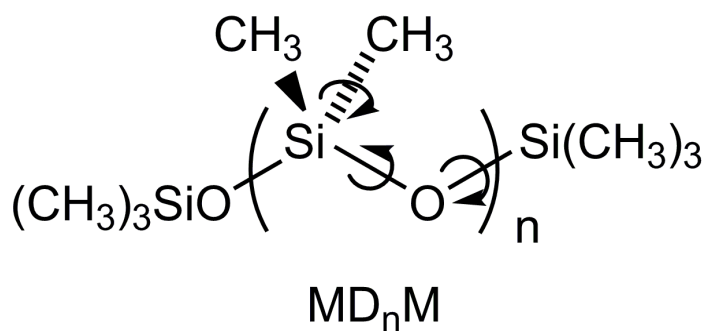


Figure 5.1. Structure and mobility of PDMS (MD<sub>n</sub>M in GE nomenclature<sup>20</sup>)

## 5.2 Objective

I began investigating the properties of various silicone-CNT composites with the goal of creating composites that take advantage of the unique properties of methylsilicones and carbon nanotubes. This first required the development of processing methods to overcome the dispersion challenges facing CNT nanocomposites. In the course of these studies, it was unexpectedly discovered that small additions of CNTs to PDMS-based elastomers dramatically increase their thermal stability. In this work, stable dispersions of MWCNTs are incorporated into polydimethylsiloxanes (PDMS) without chemical modification using a simple shear melt mixing process. These dispersions are characterized using optical microscopy, rheology and electrical surface resistivity. Thermogravimetric Analysis (TGA) of the PDMS-MWCNT composites shows an increase in thermal stability. Kinetic analysis and Pyrolysis Gas Chromatography – Mass Spectroscopy (Py GC-MS) of the composites indicate that the mechanism of decomposition changes upon addition of MWCNTs. The impact on thermal properties we discover from adding fractions of a percent of MWCNTs to PDMS materials is unprecedented and suggests a special synergy between silicone and carbon nanotubes.

## 5.2 Experimental Section

### 5.2.1 Materials

Unfilled PDMS-based two-part silicone elastomer (Gelest OE 41 Optical Encapsulant) and trimethylsilyl-terminated PDMS (MW = 17 250, 116 500) were purchased from Gelest and used as received. Multi-walled carbon nanotubes (MWCNTs) were provided by Nanocomp Technologies, Inc.

### 5.2.2 Sample Preparation

OE41 PDMS elastomer was prepared by mixing a 1:1 ratio of Part A and Part B as recommended by the manufacturer. PDMS-MWCNT composites were prepared by mixing MWCNTs into OE41 Part A in a Flacktek Speedmixer (3000 RPM, 2 minutes). OE41 Part B was added and mixed. All samples were cured at 80 °C for 4 hours.

Trimethylsilyl-terminated linear PDMS-MWCNT composites were prepared in a similar manner. High viscosity ( $\eta > 5 \text{ Pa}\cdot\text{s}$ ) PDMS fluids could be prepared with the Flacktek Speedmixer in the same manner as the OE41 Part A fluid (3000 RPM, 2 minutes). Lower viscosity PDMS fluids ( $\eta < 5 \text{ Pa}\cdot\text{s}$ ) required ultrasonic treatment (Branson 250 Digital Sonifier- 35% power, 5 sec pulse, 25 second rest, 1 minute total pulse time).

### 5.2.3 Characterization

*Optical Microscopy.* Dispersions were qualitatively studied with optical microscopy (Zeiss Axiovert 200). Samples for imaging were prepared by depositing a drop of liquid PDMS or PDMS-MWCNT onto a gridded microscope slide (Electron Microscopy Sciences) using a capillary tube.

*Rheology.* PDMS fluid rheology was studied using a TA AR2000 Rheometer with 40 mm aluminum parallel plates. The high aspect ratio of CNTs can result in dramatic shear thinning from CNT alignment and the ability of CNTs to form elastic networks can be probed by measuring the viscoelastic properties of CNT reinforced fluids.<sup>14,21-24</sup> We used rheology as a means of quantifying the dispersion quality of PDMS-CNT composites, since better dispersions provide more efficient improvement in properties.



Steady flow experiments of PDMS and PDMS-MWCNT fluids were run by ramping torque from 0.1  $\mu\text{N}\cdot\text{m}$  to 10000  $\mu\text{N}\cdot\text{m}$  (logarithmic ramp, 10 points per decade) and measuring shear rate. The steady flow viscosity was calculated from the average of three consecutive measurements per torque value. A 5% tolerance between points was used to determine if steady flow had been reached. Sampling time for each measurement was 15 seconds and point time was 3 minutes. The relationship between viscosity and shear rate is used to determine the zero shear viscosity and shear thinning behavior of PDMS-MWCNT fluid composites.

Oscillatory shear experiments were used to probe the formation and elasticity of the MWCNT network within the PDMS liquid. Oscillatory stress sweeps from 0.1 to 10 000  $\mu\text{N}\cdot\text{m}$  were run at 1 Hz. Oscillatory frequency sweeps from 0.01 to 10 Hz were run within the linear viscoelastic region (strain  $\sim$  1%) determined from stress sweeps. For both experiments, points were distributed logarithmically with 10 points per decade.

*Surface Resistivity.* The surface resistivity of PDMS-MWCNT composites was measured using a DESCO Concentric Ring Surface Conductivity Meter. 3-5 mm thick PDMS-MWCNT composites were prepared in 90 mm petri dishes. Above 3 mm, there was no observable change in the measured surface resistivity in these samples. Three measurements were made for each composite.

*Thermogravimetric Analysis.* A TA TGA Q50 was used to study the thermal decomposition of PDMS and PDMS-MWCNT composites. Samples (2-3 mg) were heated in a nitrogen atmosphere from 30  $^{\circ}\text{C}$  to 900  $^{\circ}\text{C}$  at a rate of 10  $^{\circ}\text{C}/\text{min}$ . Kinetics were studied using an isoconversion method (Kissinger-Akahira-Sunose)<sup>25</sup> with heating rates of 1, 2.5, 5, 10 and 20  $^{\circ}\text{C}/\text{min}$ . Stepwise isothermal experiments were run with a heating rate of 5

°C/min and a weight loss rate threshold of 1%/min. Isothermal experiments at 300 °C were conducted for 180 minutes.

*Pyrolysis Combustion Flow Calorimetry.* PCFC measurements were made on a Microscale Combustion Calorimeter (MCC, FAA). A sample is heated from 80 to 800 °C at a heating rate of 1 °C/min under a stream of nitrogen. Gas decomposition byproducts enter the combustion furnace where they are mixed with 20% O<sub>2</sub>/80% N<sub>2</sub> atmosphere at 900 °C. Oxygen consumption during byproduct combustion is measured and used to calculate energy/heat release (Reference 26 details all aspects of PCFC measurement and is provided for the interested reader).

*Pyrolysis Gas Chromatography – Mass Spectrometry.* Pyrolysis was conducted with a CDS Analytical Pyroprobe 2000. Samples were pyrolyzed in quartz tubes surrounded by a platinum wire coil that was heated to 900 °C at a rate of 1 °C/ms and held at 900 °C for 10 seconds. Pyrolyzed samples were injected into a Hewlett-Packard 5890 Series II Gas Chromatograph with helium carrier gas. The GC oven temperature was set to 50 °C for 1 minute and ramped at 8 °C/min to 240 °C. Pyrolysis products separated by GC were detected by a Hewlett-Packard 5972 Series mass spectrometer.

## 5.3 Results and Discussion

### 5.3.1 Sample preparation and dispersion of MWCNTs in PDMS

It has previously been observed that MWCNTs can be easily dispersed into a PDMS-based elastomer (Dow Corning Sylgard 184).<sup>1</sup> We confirmed these findings using an unfilled PDMS elastomer as well as in linear trimethylsilyl-terminated PDMS fluids. We chose these systems to avoid effects from other fillers or additives in the Sylgard 184 formula. By using 'neat' PDMS elastomers we aimed to isolate the effects of carbon

nanotubes on the silicone properties. Processing methods for dispersions depend on the viscosity of the PDMS (see Experimental section). Stable CNT dispersions can be prepared in one step in high viscosity silicones using a Dual Assymmetric Centrifuge (Flacktek Speedmixer). No aggregation or sedimentation is observed in the dispersions for up to a month of storage, but no longer term study was conducted. Figure 5.2a, shows heterogeneities that can be observed by eye in thin elastomer samples and optical microscopy (Figure 5.2b) of the PDMS-MWCNT composite fluid shows that the CNTs are bundled into long fibers. These long fibers are further aggregated to form the larger heterogeneities observed by eye. Longer mixing times and ultrasonic treatment does not improve the quality of these dispersions. We did not pursue solvent or surfactant assisted dispersion or chemical modification of the nanotubes. Our goal was to prepare silicone nanocomposites without damaging the nanotubes and to use the simplest methods possible. It must be emphasized that these dispersions, while still containing MWCNT bundles and aggregates, are achieved in only a single, simple, 2 minute mixing procedure. Further characterization of these dispersions demonstrates the efficient use of CNT filler even without achieving “optimal” dispersion states: electrical percolation is reached at 0.025 wt% CNT (Figure 5.2e), zero shear viscosity increases by ~100 times at 0.5 wt% CNT and ~10 000 times at 1.0 wt% (Figure 5.2c), and signs of elastic MWCNT network formation can be detected at 0.05 wt% (Figure 5.2d).

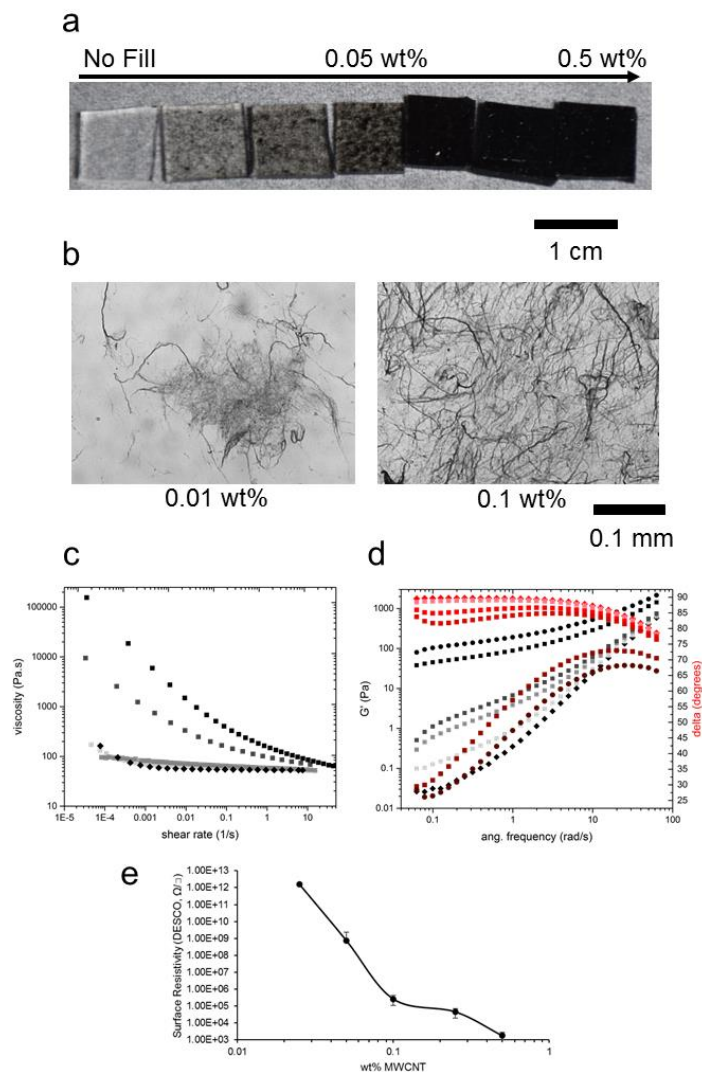


Figure 5.2. (a) Photos of 1 cm x 1 cm x 1 mm PDMS-MWCNT elastomer samples with MWCNT loadings from left to right of 0, 0.01, 0.025, 0.05, 0.1, 0.25 and 0.5 wt%. (b) Optical micrographs of 0.01 wt% and 0.1 wt% MWCNTs dispersed in linear PDMS<sup>116k</sup>. (c) Steady flow and (d) oscillatory frequency sweeps of PDMS<sup>116k</sup>-MWCNT composite fluids. In (c) square symbols represent composite samples of 1.0, 0.5, 0.1 and 0.05 wt% MWCNTs from black to light gray. Black diamonds are the unfilled control. Shear thinning is observed by the large reduction in viscosity with increasing shear rate. In (d) black and maroon circles are for 1.0 wt% MWCNTs and black and red diamonds are the unfilled controls. Composites of 0.01, 0.05, 0.1 and 0.5 wt% are squares from light gray to dark gray and light red to red. G' increases with CNT loading and delta decreases. (e) Surface resistivity as a function of MWCNT loading. Measured using DESCO surface conductivity meter.

### 5.3.2 Thermogravimetric Analysis

Improvements in electrical and viscoelastic properties of PDMS-MWCNT composites are expected. Unexpected is the observed increase in thermal stability of MWCNT-reinforced PDMS elastomers. TGA weight loss and derivative weight loss plots are shown in Figure 5.3 for composites containing 0, 0.05, 0.1, 0.25 and 0.5 wt% MWCNTs. The first signs of increased thermal stability appear in the 0.05 wt% MWCNT composite, where there is a 10 °C increase in the peak decomposition temperature. Increasing the MWCNT loading to 0.5 wt% leads to a 54 °C increase in peak decomposition temperature from 446 °C to 500 °C and a 5% weight loss increase of 20 °C. Char formation increases by a factor of two from ~20% to ~40% with 0.5 wt% CNTs. Similar increases in the thermal stability of silicone-CNT composites have been observed but only at higher loadings<sup>27</sup>, in the presence of other nanofillers<sup>28,29</sup> or with modified nanotubes<sup>30</sup>. These finding at such low CNT loadings have been verified internally with numerous reruns and externally by Nanocomp Technologies Inc.

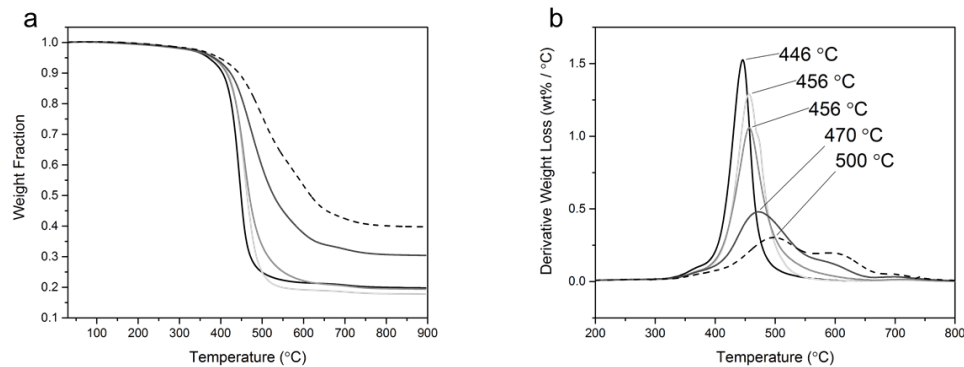


Figure 5.3. TGA (a) weight loss and (b) derivative weight loss of PDMS-MWCNT elastomer composites in nitrogen atmosphere. Results for unfilled control (solid black), 0.05 (light gray), 0.1 (gray), 0.25 (dark gray) and 0.5 wt% (dashed black) are shown. Peak degradation temperatures are labeled in (b)

Figure 5.4 exhibits studies into the kinetics of decomposition of the control elastomer and the 0.5 wt% MWCNT composite elastomer. Kinetics are studied using a

variable heating rate isoconversion method (KAS)<sup>25</sup> (Figure 5.4 a-d) along with an isothermal method (Figure 5.4e) and a stepwise isothermal method (Figure 5.4f). Isoconversion analysis with heating rates of 1, 2.5, 5, 10 and 20 °C/min shows an increase in activation energy of the primary decomposition process when carbon nanotubes are incorporated. For the unfilled silicone elastomer, an activation energy of 158 kJ/mol is calculated for the first 30% of decomposition. When 0.5 wt% MWCNTs is added to the silicone elastomer, the activation energy of the first 30% of the decomposition process increases to 233 kJ/mol. No heating rate dependence on the estimated activation energy of the primary decomposition process is observed, as has been reported previously.<sup>31</sup> This may be due to the smaller sample masses we use or due to differences in the network structures of the silicone elastomers under investigation. Increasing the activation energy for decomposition should practically manifest in the ability of the composite to function at higher operating temperatures. To verify that the composites have increased high temperature stability, isothermal experiments are carried out where a 0.5 wt% composite sample and an unfilled control are held at 300 °C for 180 minutes. The 10% difference in weight loss (95% versus 85%) and the difference in the weight loss rates (0.008 %/min versus 0.047 %/min) clearly indicate the improved thermal stability of the composite. A step isothermal experiment also reinforces the improved stability with the primary decomposition process starting at 373 °C for the unfilled control and 430 °C for the 0.5 wt% MWCNT composite.

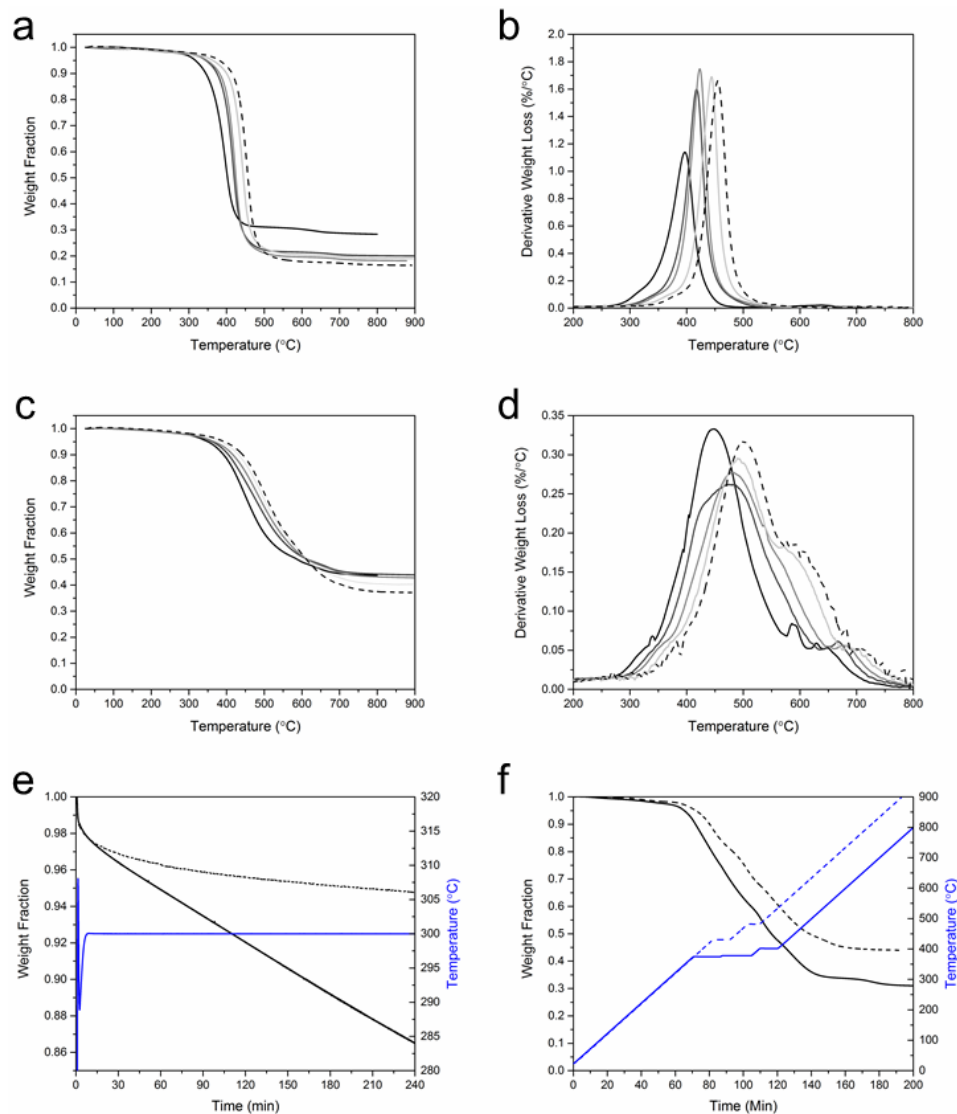


Figure 5.4. Decomposition kinetics studied by TGA. (a) Weight loss and (b) derivative weight loss curves of unfilled PDMS elastomer (Gelest OE41) at heating rates of 1 (black), 2.5 (dark gray), 5 (gray), 10 (light gray) and 20 (dashed black) °C/min. (c) Weight loss and (d) derivative weight loss curves of 0.5 wt% MWCNT in PDMS elastomer at heating rates of 1 (black), 2.5 (dark gray), 5 (gray), 10 (light gray) and 20 (dashed black) °C/min. (e) 300 °C isothermal weight loss of unfilled (solid line) and 0.5 wt% MWCNT filled (dashed line) PDMS elastomers. (f) Stepwise isothermal analysis of unfilled PDMS elastomer (solid lines) and 0.5 wt% MWCNT filled PDMS elastomer (dashed lines). Black curves are for weight loss and blue curves show the temperature profile of the experiment.

In addition to the increased onset and peak temperature of decomposition and additional char in the PDMS-MWCNT composites, there is a higher temperature

decomposition process evident in derivative weight loss curves. The first, larger weight loss peak is considered the primary decomposition process as the majority of the weight loss occurs in this step. The primary process alone is observed in the unfilled PMDS elastomer. The second peak is considered a secondary process and is detected at CNT loadings greater than 0.1 wt%. In 0.5 wt% MWCNT composites, the weight loss that occurs from each process also appears to be dependent on the heating rate. The shape of the second weight loss peak changes from a well-defined peak at heating rates greater than 5 °C/min, to a weak shoulder at heating rates less than or equal to 5 °C/min. Two defined decomposition processes are also detected in stepwise isothermal experiments. To determine how each process contributes to the overall weight loss, TGA derivative weight loss curves are deconvoluted into Gaussian expressions. Figure 5.5 shows example results of the overall fit of derivative weight loss (TGA) at 10 °C/min from the sum of Gaussians for the 0.5 wt% composite and the unfilled control. All unfilled control samples can be fit using a single Gaussian representing the primary decomposition process. Composite samples are fit using three Gaussians representing the primary and secondary processes discussed above, as well as a third small, high temperature peak. The third peak has a similar contribution of about 10% of the total degradation for all the samples and is detected in unfilled controls; it will not be further analyzed here since it is a minor contributor to the total decomposition process, has similar contributions at all rates and for all PDMS elastomers and composites, and does not seem unique to the weight loss process in composites. By integration of the total curve fit and determining the contribution of each Gaussian to that curve, it is possible to estimate the contribution of each process to the overall process. The fitting results for the composite elastomers are exhibited in Table 5.1. For heating rates of 1, 2.5 and 5 °C/min the primary process contributes 86% of the total weight loss and the secondary process accounts for only 3%. At heating rates of 10 and 20 °C/min the contribution of the primary process decreases to 78% and 75%



with an increase in the secondary process to 10% and 13%. Along with these changes in the degradation processes that occur in the composites, char formation also depends on the heating rate. Similar char residues of about 43% form at heating rates of 1, 2.5 and 5 °C/min but the char residue decreases to 40% and 37% at rates of 10 and 20 °C/min. The increased contribution of the second decomposition process and the decrease in char formation at higher heating rates suggests that there are kinetic limitations in decomposition that arise from rates of decomposition reactions or rates of adsorption-desorption of decomposition products.

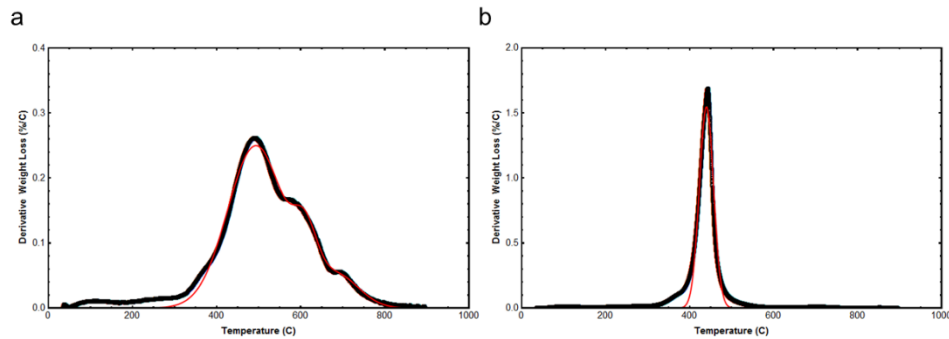


Figure 5.5. Derivative weight loss (black) and total curve fit (red) from deconvolution into Gaussian functions for (a) 0.5 wt% MWCNT composite and (b) unfilled control at a heating rate of 10 °C/min.

Table 5.1. Contributions of degradation processes calculated from Gaussian deconvolution for 0.5 wt% PDMS-MWCNT Composite

Heating Rate, °C/min	Peak 1, %	Peak 2, %	Peak 3, %	Total Area, wt%	Char, wt%
1	86	4	10	53	43.7
2.5	89	2	9	53.5	44
5	87	3	10	54	42.8
10	78	10	12	54	40
20	75	13	12	59	37

### 5.3.3 Pyrolysis Combustion Flow Calorimetry

The increased degradation temperature and char formation suggest that the silicone-CNT nanocomposites may have promising flame retardant properties. Pyrolysis Combustion Flow Calorimetry (PCFC) results are summarized in Table 5.2 and Figure 5.6. Addition of 0.5 wt% CNTs led to a total heat release decrease from 18.8 kJ/g (for unfilled elastomer) to 14.8 kJ/g (for 0.5 wt% composite) and a heat release capacity decrease from 538 J/g\*K to 188 J/g\*K. Figure 5.6 shows the fitted heat release rates from PCFC experiments conducted at a heating rate of 1 °C/sec for an unfilled control sample and composites containing 0.1, 0.25, and 0.5 wt% CNTs. These data mimic the derivative weight loss curves from TGA indicating that the degradation byproducts act as fuel for combustion. CNTs have previously been recognized as char forming and char stabilizing flame retardants<sup>32-34</sup>, and these experiments demonstrate that self-extinguishing silicone elastomers can be prepared by adding small amounts of CNT fillers.

Table 5.2. PCFC results for PDMS-MWCNT Composites

	Peak Temp (TGA, °C)	Char (TGA, 900 °C)	Total HR (kJ/g)	HRC (J/g*K)	Peak Temp (PCFC, °C)
Control	445	0.19	18.8	538	466
0.1 wt% CNT	456	0.2	18.8	411	479
0.25 wt% CNT	470	0.3	17.8	207	493
0.5 wt% CNT	500	0.4	14.8	188	515

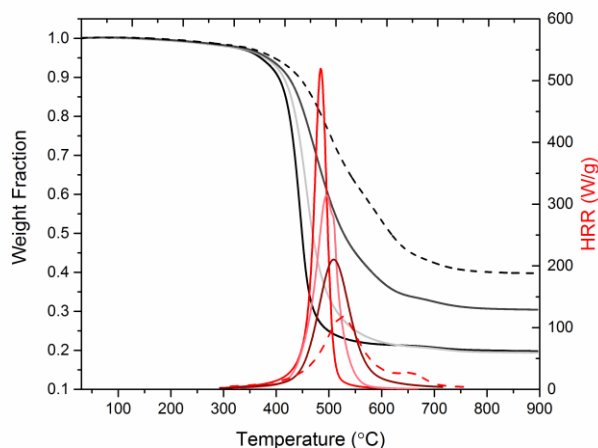


Figure 5.6. PCFC HRR (reds) with TGA weight loss (blacks) results for unfilled control (solid) and 0.1 (light gray/pink), 0.25 (gray/maroon), and 0.5 wt% (dash) PDMS-MWCNT Composites.

#### 5.3.4 Differential Scanning Calorimetry of Elastomer Composites

DSC of PMDS elastomers allowed for the detection of  $T_g$ , as well as any changes in crystallization behavior in MWCNT composite samples. Differences detected by DSC were minor and are presented in Figure 5.7, which compares the unfilled control with a 0.5 wt% MWCNT composite, Table 5.3 exhibits results for composites of MWCNT loadings from 0.01 wt% to 0.5 wt% and Table 5.4 shows calculations from crystallization and melting peaks in unfilled and 0.5 wt% CNT composites.

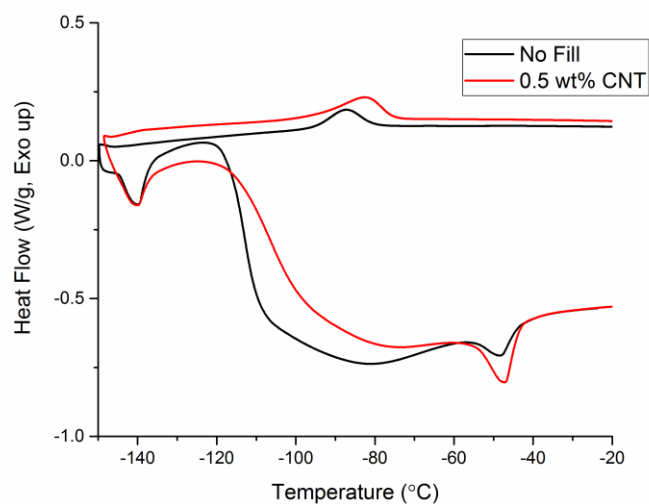


Figure 5.7. DSC (exotherm up) of unfilled and 0.5 wt% MWCNT composite elastomers. Crystallization is observed in the cooling step (top curve) and melting is observed in the heating step (bottom curve). The glass transition is detected in the heating step (bottom curve) by the shift of the baseline indicating a change in heat capacity.

Table 5.3. Glass Transition measurements from DSC of PDMS-MWCNT elastomers

Sample	Onset	Inflection	End
Control- Unfilled	-121.0 ± 6.30	-117.27 ± 5.84	-111.47 ± 4.60
0.01%	-118.92	-113.50	-103.81
0.025%	-117.08	-115.87	-105.27
0.05%	-118.39	-112.19	-104.33
0.1%	-120.47	-114.92	-106.6
0.25%	-125.09	-119.46	-110.47
0.5%	-115.26± 1.63	-109.39±3.94	-98.85±4.48

Table 5.4. DSC Glass Transition and Crystallization Data for 0.5 wt% MWCNT in PDMS Elastomer

	$T_g$	$T_{c, heating}$	$T_{c, cooling}$	$H_{c, heating}$	$H_{c, cooling}$
No Filler	-121	-47.6	-86.1	10.18	14.27
0.5 wt% CNT	-112	-47.1	-82.6	8.877	12.46

### 5.3.5 Decomposition Products in Elastomer Composites

To investigate how the decomposition mechanism of PDMS-MWCNT composites might be changing, Py GC-MS was used to analyze decomposition products. Typically, clean, end-terminated PDMS decomposes in inert atmosphere by an intramolecular backbiting mechanism shown in Figure 5.8 in which cyclic trimer (hexamethylcyclotrisiloxane,  $D_3$ ) is the primary byproduct.<sup>35-37</sup> Silicone elastomers degrade by a similar backbiting mechanism but with a range of cyclic byproducts, the distribution of which depends on network structure.<sup>38,39</sup> The degradation products of the unfilled elastomer and the 0.5 wt% composite are summarized in Figure 5.9 and Table 5.4. The incorporation of 0.5 wt% MWCNTs into the PDMS elastomer leads to an 8% increase in  $D_3$  formation with a 7% decrease in  $D_4$  and a 1% decrease higher cyclic formation. No significant differences in the relative distribution of higher cyclic byproducts is detected: in both unfilled and composite elastomers, cyclic products greater than  $D_4$  are composed of approximately 40% $D_5$ , 30%  $D_6$ , 24%  $D_7$  and 6%  $D_n$ . Based on these experiments, it appears the decomposition products in the composites do not change dramatically from the control. The similarity in cyclic byproducts greater than  $D_4$  suggests that the chemical structure of the silicone network is not significantly altered by the presence of MWCNTs.<sup>38</sup> The higher  $D_3$  production could reflect the higher temperature at which degradation occurs. Degradation into  $D_3$  leads to a greater entropy than degradation into larger cyclics but requires additional enthalpy to form the strained ring. At higher temperatures, entropy overcomes this enthalpic penalty and free energy is minimized by  $D_3$  production.

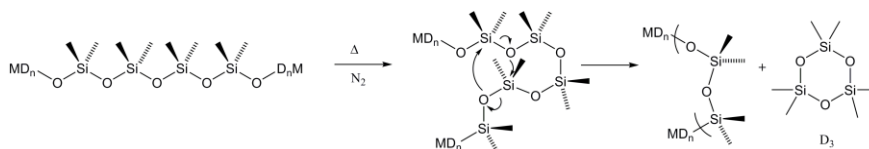


Figure 5.8. Intramolecular depolymerization of PMDS to cyclic trimer

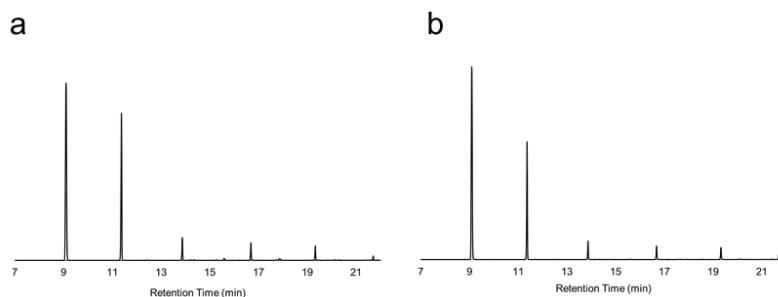


Figure 5.9. Pyrolysis GC-MS chromatograms of (a) unfilled PDMS elastomer and (b) 0.5 wt% CNT PDMS composite. Pyrolysis conducted at 900 °C in helium atmosphere.

Table 5.5. Py GC-MS Results of Elastomers and Linear PDMS Model

	D <sub>3</sub> (%)	D <sub>4</sub> (%)	Higher Cyclics (%)	D <sub>3</sub> :D <sub>4</sub>
OE41	55	33.4	11.6	1.65
	56	33	11	1.70
OE41-0.5 wt% MWCNT	64	26	10.0	2.46
	63.8	26.1	10.1	2.44
PDMS	86.0	13.8	<0.5	6.23
	91.5	8.4	<0.5	10.90
MWCNT enriched PDMS	58.6	24.9	16.5	2.35
	65.5	25.2	9.3	2.60

### 5.3.6 Decomposition in Linear PDMS Models

From the study of PDMS and PDMS-MWCNT composite elastomers it was clear that the presence of MWCNTs was increasing thermal stability, increasing char, increasing the activation energy of decomposition and altering decomposition products. How the mechanism of decomposition could be changing in these composites to produce such changes remains unclear from these experiments alone. To gain more insight, linear trimethylsilyl-terminated PDMS is used as a model in which the constraints and contributions of the elastomer network can be removed.

Two linear PDMS samples were studied: one above the entanglement molecular weight (PDMS<sup>116k</sup>) and one below (PDMS<sup>17k</sup>). TGA of the fluids, presented in Figure 5.10, shows very similar decomposition processes and a slightly higher thermal stability in the PDMS<sup>116k</sup>. Py GC-MS analysis of PDMS<sup>17k</sup> shows the expected cyclic oligomer products: 90% D<sub>3</sub> and 10% D<sub>4</sub> (Figure 5.10c and Table 5.4). The decomposition products of trimethylsilyl-terminated PDMS do not depend on molecular weight<sup>36</sup> so similar products would be expected from PDMS<sup>116k</sup>. Compounding the fluids with 0.1 and 1.0 wt% MWCNTs exhibits only a slight increase in thermal stability but a significant difference in weight loss behavior. In the composite fluids, the decomposition process shifts to higher temperatures and a second sharp degradation peak appears similar to what is observed in the composite elastomers. To attempt to isolate this process, a PDMS<sup>17k</sup> sample containing 1 wt% MWCNT was drained of excess PDMS by squeezing between filter paper. The composition of the resulting paste was not determined. TGA of the MWCNT enriched PDMS shows a small primary weight loss peak similar to the neat PDMS and a large sharp weight loss peak at higher temperatures. Py GC-MS of the MWCNT-enriched PDMS illustrates a dramatic change in degradation products (Figure 5.10d and Table 5.4) that is closer in composition to the elastomer networks than the linear polymers. D<sub>3</sub> yield decreases from 90% to 60%, D<sub>4</sub> yield increases by roughly 2 times to 25% and higher cyclic species which are not observed in the neat PDMS make up the remaining 15% of the degradation products. The second degradation process observed in the model linear composites presumably arises from polymer that interacts strongly with MWCNTs through adsorption to increase the activation energy of decomposition. Adsorption of linear polymer onto the physical network formed by the MWCNTs not only leads to the second decomposition peak, but also to the generation of larger cyclic decomposition products that appear similar to those observed in covalent elastomer networks.

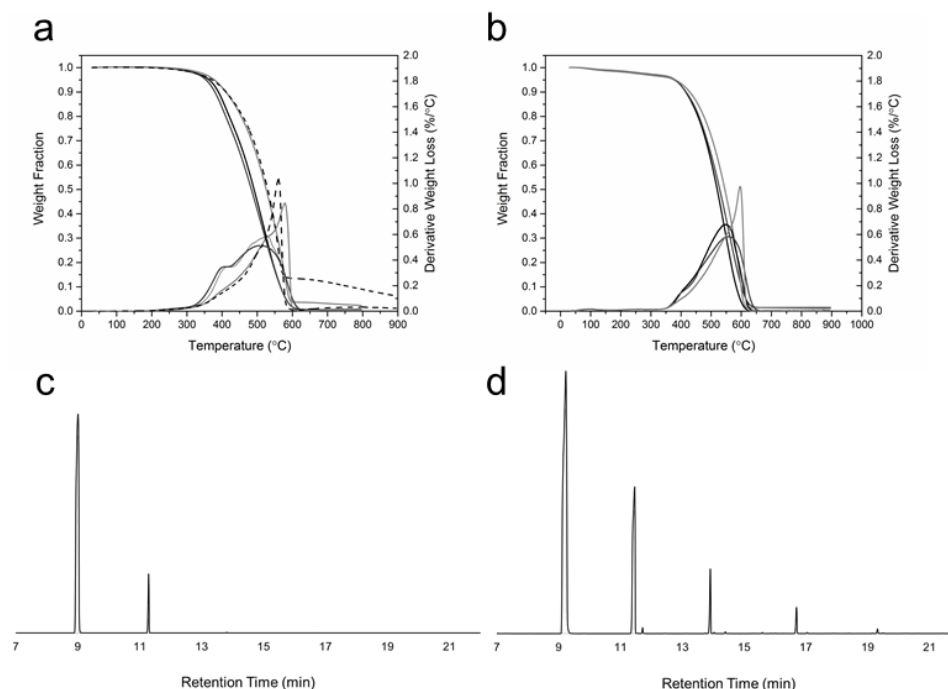


Figure 5.10. TGA of (a) PDMS<sup>17k</sup> and (b) PDMS<sup>116k</sup>. Black lines are unfilled controls, dark gray are 0.1 wt% MWCNTs and light gray lines are 1 wt% MWCNTs. The dashed line in (a) is the MWCNT enriched PDMS<sup>17k</sup> sample prepared by pressing and draining the 1 wt% MWCNT-PDMS<sup>17k</sup> sample. Py GC chromatographs of (c) neat PDMS<sup>17k</sup> and (d) PDMS<sup>17k</sup> saturated MWCNTs. All pyrolysis experiments were conducted at 900 °C in helium atmosphere.

### 5.3.7 Proposed mechanism of Thermal Decomposition in PDMS-CNT composites.

A mechanism to describe the effect of MWCNTs on the decomposition of PDMS must account for numerous changes: (1) increased activation energy of primary decomposition, (2) the appearance of a high temperature secondary decomposition process, (3) increased char formation, (4) heating rate dependence of secondary decomposition and char formation and (5) dramatic changes in decomposition products in linear models.

The increased activation energy of decomposition, the second decomposition process, and the changes in decomposition products can be explained by adsorption of PDMS onto the MWCNT network. The adsorption energy of PDMS segments onto the



surface of MWCNTs has been calculated to be approximately 10.9 kJ/mol.<sup>1</sup> This strong adsorption results in a bound layer of PDMS on MWCNTs. The cooperative adsorption of PDMS segments must be overcome in the composite before decomposition of the bound chains can occur. The desorption is important not only in the ability of PDMS to form cyclic intermediates during decomposition, but also in the ability of high molecular weight byproducts to vaporize. The bound layer that forms from adsorption accounts for the second decomposition process. Acting synergistically with the direct adsorption of PDMS chains to form a bound polymer layer, the MWCNTs themselves form a three-dimensional physical network that imparts constraints on the bulk PDMS that is not part of the bound layer. Rheology of the PDMS composite fluids exhibits an increase in storage modulus in low frequencies that is attributed to the reduced diffusional mobility of the polymer that results from the formation of a PDMS-MWCNT network. The shift of the primary decomposition process to higher temperatures and the increased activation energy of the primary decomposition arise from the constraints imposed by the PDMS-MWCNT network. The effect of the physical constraints on degradation byproducts is most apparent in the linear PDMS model. In linear, uncrosslinked PDMS composites, polymer chains that are not part of the adsorbed layer cannot freely diffuse around the physical junctions formed by the PDMS-MWCNT physical network; Py GC-MS results indicate that this physical network is capable of constraining these PDMS chains to create a dramatic difference in the structure of cyclic transition states that is reflected in cyclic decomposition products. Restricting the motion of individual PDMS chains hinders their ability to form intramolecular cyclic transition states and pushes them towards the formation of intermolecular cyclic transition states between adjacent network strands. This intermolecular decomposition mechanism enables the formation of larger cyclic transition states and products, like those observed in the linear PDMS model. It also increases the

apparent activation energy and alters reaction kinetics since two reactions must occur to form the cyclic product (Figure 5.11).

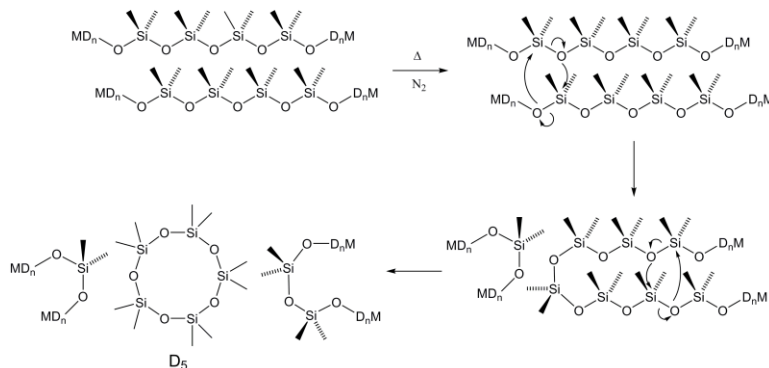


Figure 5.11. Intramolecular depolymerization of PDMS to cyclic pentamer (D<sub>5</sub>)

Adsorption and physical constraint of PDMS chains in MWCNT composites can account for the differences in activation energy, the second decomposition process and the change in cyclic decomposition products, but do not provide a good explanation for increased char formation. MWCNTs contain numerous reactive defects in form of edges, dangling bonds, vacancies, dislocations, kinks and 5,7 rings.<sup>11,40-42</sup> It is plausible that at elevated temperatures, oxidized defects on CNT surfaces may react with physisorbed PDMS chains or cyclic decomposition byproducts. These thermally activated 'grafting' reactions immobilize PDMS that would otherwise escape during decomposition and ultimately increase the residual mass. CNTs are also reactive towards radicals and are commonly functionalized using radical chemistries.<sup>11,13,42</sup> Radicals generated during PDMS decomposition would be expected to react with nanotubes. Greater generation of radical decomposition products will occur at the higher decomposition temperatures of the composites and reactions of these radicals with nanotube surfaces would increase the residual mass in the same way that the 'grafting' reactions described above do. These

hypothesizes are purely speculative and we have not been able to identify if these reactions are occurring. It remains unclear why char formation or the secondary decomposition process depend on heating rate.

### 5.3.8 Are Nanocomp CNTs Unique?

To determine if the Nanocomp Technologies, Inc. MWCNTs are unique in their ability to increase thermal stability of PDMS elastomer, various other nanocarbon fillers were incorporated into Gelest OE41 elastomer at 0.5 wt% using the same sample preparation procedures. TGA results shown in Figure 5.12, show that the dramatic increase in thermal stability from Nanocomp MWCNTs is unique. This may be attributed to the high aspect ratio of Nanocomp MWCNTs that arises from their preparation method.

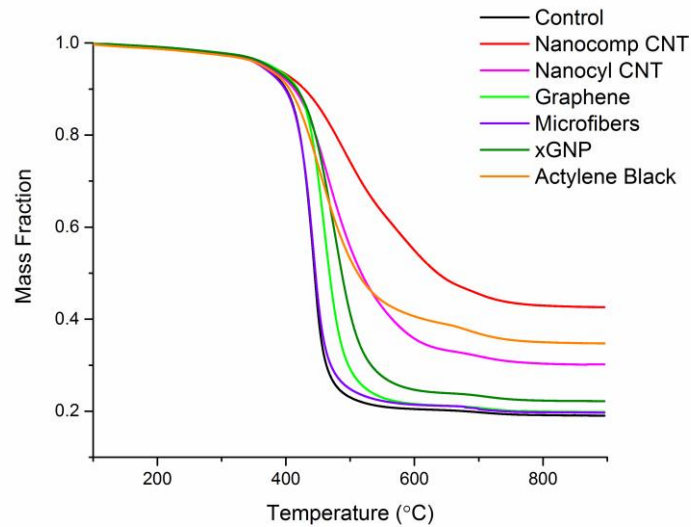


Figure 5.12. Effect of nanocarbon fillers at 0.5 wt% on thermal stability of Gelest OE41 PDMS elastomer

In addition to the carbon nanofillers tested, Boron Nitride Nanotubes (BNNTs) and Boron nanopowders were provided by Nanocomp and tested. The results in Figure 5.13

illustrate a remarkable increase in thermal stability that exceeds that of the CNTs. The reason for this dramatic improvement is not known.

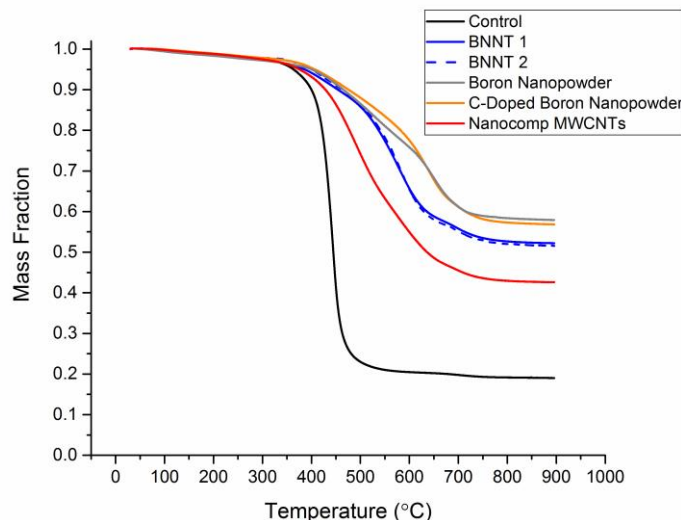


Figure 5.13. Effect of Boron Nitride Nanotube (BNNT) and Boron Nanopowder fillers at 0.5 wt% on thermal stability of Gelest OE41 PDMS elastomer. Nanocomp MWCNTs and control provided as reference.

### 5.3.9 Is the Thermal Stabilization by CNTs Universal to All Silicones?

The effect of CNTs on thermal decomposition was investigated in other silicone elastomers and model silicone fluids. TGA was conducted on 3 additional elastomers: Dow Corning Sylgard 184, Gelest D200, and Gelest HV22. The results in Figure 5.14 demonstrate that the effect of MWCNTs on thermal stability are different in each elastomer. The differences between these silicones is a result of their compositions. In Sylgard 184, there is no change in the initial degradation steps but there is a decrease in degradation at higher temperatures (greater than 500 °C) and slightly higher char formation. We are unsure of the exact composition of Sylgard 184 but know that it is PDMS-based and contains fillers. Addition of CNTs to Sylgard 184 does not appear to constrain the polymer chains beyond what is already done by the other fillers in Sylgard 184. The additional high temperature stability in Sylgard 184 could be due to radical

scavenging by the CNTs as discussed in the case of OE41. In Gelest D200 and HV22 elastomers there is evidence of thermal stabilization during the first degradation process but there is greater weight loss at high temperatures and decreased char. Gelest D200 is PDMS-based and we do not know its composition, however the high char suggests that there is filler present. HV22 contains *only* linear PDMS (or silica in the dashed data): it is a unique elastomer in that it is composed solely of ultra-high molecular weight linear polymer that is highly entangled. The stabilization at intermediate temperatures in the D200 and neat HV22 elastomers suggests constraints on polymer mobility by the CNT network. At higher temperatures (greater than 600 °C), a second decomposition process is accelerated with the addition of CNTs. While this opposes the hypothesis that CNTs act as radical scavengers during high temperature decomposition of PDMS, it may be an indication that these reactions are less efficient in these composites at these temperatures. In the silica-filled HV22 there is no change in decomposition with the addition of CNT's suggesting that the high silica content (15 wt%) overrides any benefits of the CNTs.

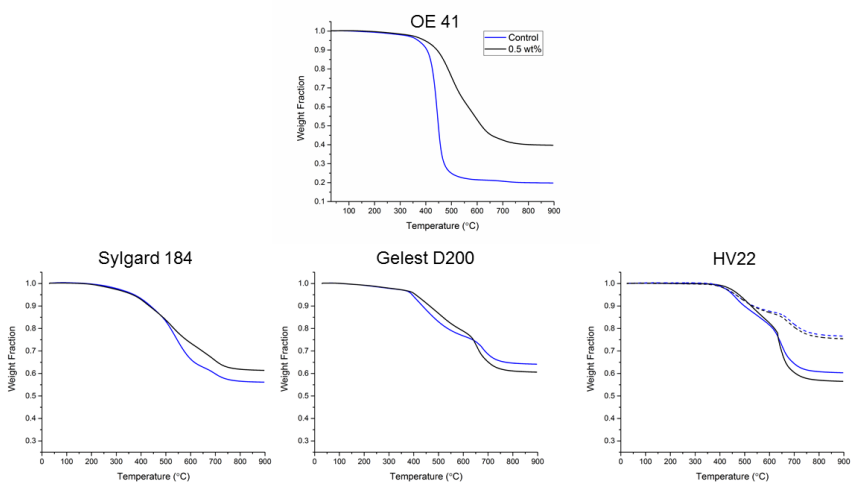


Figure 5.14. TGA of silicone elastomers and composites containing 0.5 wt% MWCNTs. Blue lines are unfilled controls and black lines are composites. Dashed curves for the HV22 elastomer are filled with an additional 15 wt% hexamethyldisilazane-treated silica.

TGA was also conducted on 6 model silicone fluids: PDMS<sup>17.5k</sup>, PDMS<sup>116k</sup>, poly(diethylsiloxane), poly(phenylmethyl)siloxane, poly(phenylmethyl-co-dimethyl)siloxane and poly(diphenyl-co-dimethyl)siloxane. These composite fluids and their preparation are reported in Chapter 4. Results shown in Figure 5.15 indicate that at loadings of up to 1 wt% MWCNT, there is only evidence of slight thermal stabilization in the PDMS models, as discussed above. The other silicones do not show any significant change in degradation behavior. This could be due to differences in degradation mechanisms in phenyl and ethyl siloxanes.<sup>31</sup> Interestingly, char formation is seen to decrease in phenyl siloxanes as CNT loading is increased. Char in phenyl containing siloxane polymers is typically attributed to radical crosslinking that occurs with scission of phenyl groups at temperatures above 450 °C. CNTs appear to effect this reaction in a manner that leads to less crosslinking and less char.

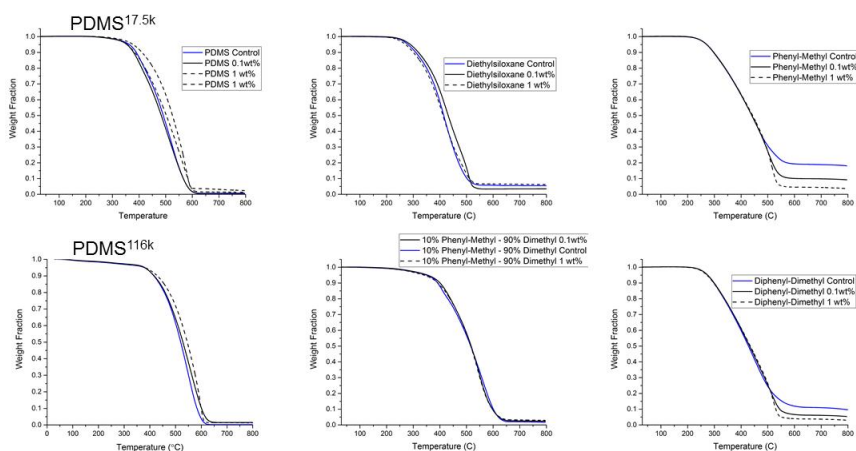


Figure 5.15. TGA of linear model silicone composites of varied chemistry. Blue curves are control samples, black solid curves are 0.1 wt% CNT composites and black dashed curves are 1 wt% CNT composites.

## 5.4 Conclusions

This work on PDMS-MWCNT nanocomposites has confirmed the facile preparation of stable MWCNT dispersions. It supports the hypothesis that the favorable

wetting and adsorption of PDMS chains onto MWCNTs is responsible for this. Along with the expected improvements in electrical conductivity and viscoelastic properties, it is unexpectedly found that the thermal stability of PDMS elastomers is dramatically improved by the addition of fractions of a wt% of MWCNT filler. Experimental evidence suggest that: (1) the adsorption of PDMS onto MWCNTs creates a bound polymer layer that results in a second decomposition process, (2) the formation of a physical MWCNT network results in a constrained PDMS-MWCNT network resulting in increases activation energy of decomposition and a change in cyclic oligomer decomposition products, and (3) reactions with defects on MWCNTs or with radical decomposition products results in increased char formation. The increase in thermal stability of PDMS by fractions of a wt% of filler is unprecedented. It is suggestive of the untapped potential of PDMS nanocomposites and of new routes for the effective utilization of nanotube fillers.

## 5.5 References

1. Beigbeder, A.; Linares, M.; Devalckenaere, M.; Degée, P.; Claes, M.; Beljonne, D.; Lazzaroni, R.; Dubois, P. CH- $\pi$  Interactions as the Driving Force for Silicone-Based Nanocomposites with Exceptional Properties. *Adv. Mater.* **2008**, *20*, 1003-1007.
2. Moniruzzaman, Mohammad; Winey, Karen I. Polymer Nanocomposites Containing Carbon Nanotubes. *Macromolecules.* **2006**, *39*, 5194-5205.
3. Winey, Karen I.; Kashiwagi, T; Mu, Minfang. Improving Electrical Conductivity and Thermal Properties of Polymers by the Addition of Carbon Nanotubes as Fillers. *MRS Bulletin.* **2007**, *32*, 348-353.
4. Huang, H.; Liu, C.; Wu, Y.; Fan, S. Aligned Carbon Nanotube Composite Films for Thermal Management. *Adv. Mater.* **2005**, *17*, 1652-1656.
5. Coleman, Jonathan N.; Khan, Umar; Blau, Werner J.; Gun'ko, Yurii K. Small but strong: A review of the mechanical properties of carbon nanotube-polymer composites. *Carbon.* **2006**, *44*, 1624-1652.
6. Kumar, S. K; Benicewicz, B. C.; Vaia, R. A.; Winey, K. I. 50<sup>th</sup> Anniversary Perspective: Are Polymer Nanocomposites Practical for Applications? *Macromolecules* **2017**, *50*, 714-731.

7. Ma, Peng-Cheng; Siddiqui, Naveed A.; Marom, Gad; Kim, Jang-Kyo. Dispersion and functionalization of carbon nanotubes for polymer-based nanocomposites: A review. *Composites: Part A*. **2010**, *41*, 1245-1367.
8. Grossiord, N.; Loos, J.; Regev, O.; Koning, C. E. Toolbox for Dispersing Carbon Nanotubes into Polymers to get Conductive Nanocomposites. *Chem. Mater.* **2006**, *18*, 1089-1099.
9. Spitalsky, Z.; Tasis, D.; Papagelis, K.; Galiotis, C. Carbon nanotube-polymer composites: Chemistry, processing, mechanical and electrical properties. *Prog. Polym. Sci.* **2010**, *35*, 357-401.
10. Krishnamoorti, Ramanan. Strategies for Dispersing Nanoparticles into Polymers. *MRS Bulletin*. **2007**, *32*, 341-347.
11. Tasis, D.; Tagmatarchis, N.; Bianco, A.; Prato, M. Chemistry of Carbon Nanotubes. *Chem. Rev.* **2006**, *106*, 1105-1136.
12. Chadwick, R. C.; Grande, J. B.; Brook, M. A.; Adronov, A. Functionalization of Single-Walled Carbon Nanotubes via the Piers-Rubinsztajn Reaction. *Macromolecules*. **2014**, *47*, 6527-6530.
13. Tour, J. M.; Dyke, C. A. Covalent Functionalization of Single-Walled Carbon Nanotubes for Materials Applications. *J. Phys. Chem. A*. **2004**, *108*, 11151-11159.
14. Du, F.; Scogna, R. C.; Zhou, W.; Brand, S.; Fischer, J. E.; Winey, K. I. Nanotube Networks in Polymer Nanocomposites: Rheology and Electrical Conductivity. *Macromolecules*. **2004**, *37*, 9048-9055.
15. Kim, T. A.; Kim, H. S.; Lee, S. S.; Park, M. Single-walled carbon nanotube/silicone rubber composites for compliant electrodes. *Carbon* **2012**, *50*, 444-449.
16. Gong, X.; Liu, J.; Baskaran, S.; Voise, R. D.; Young, J. S. Surfactant-Assisted Processing of Carbon Nanotube/Polymer Composites. *Chem. Mater.* **2000**, *12*, 1049-1052.
17. Sonnier, R.; Bokobza, L.; Chocha-Lozano, N. Influence of multiwall carbon nanotube (MWCNT) dispersion on ignition of poly(dimethylsiloxane)-MWCNT composites. *Polym. Adv. Technol.* **2015**, *26*, 277-286.
18. Mark, J. E. Some Interesting Things about Polysiloxanes. *Acc. Chem. Res.* **2004**, *37*, 946-953.
19. Kuo, A. C. M. Poly(dimethylsiloxane). *Polymer Data Handbook*. **1999**
20. Hurd, C. B. Studies on Siloxanes. I. The Specific Volume and Viscosity in Relation to Temperature and Constitution. *J. Am. Chem. Soc.* **1946**, *68*, 364-370.
21. Kharchenko, S. B.; Douglas, J. F.; Obrzut, J.; Grulke, E. A.; Migler, K. B. Flow-induced properties of nanotube-filled polymer materials. *Nature Materials* **2004**, *3*, 564-568.
22. Niu, R.; Gong, J.; Xu, D.; Tang, T.; Sun, Z. Flow-induced structure and rheological properties of multiwall carbon nanotube/polydimethylsiloxane composites. *RSC Adv.* **2014**, *4*, 62759-62768.



23. Huang, Y. Y.; Ahir, S. V.; Terentjev, E. M. Dispersion rheology of carbon nanotubes in a polymer matrix. *Phys. Rev. B* **2006**, *73*, 125422.
24. Marceau, S.; Dubois, P.; Fulchiron, R.; Cassagnau, P. Viscoelasticity of Brownian Carbon Nanotubes in PDMS Semidilute Regime. *Macromolecules* **2009**, *42*, 1433-1438.
25. Vyazovkin, Sergey et.al. ICTAC Kinetic Committee recommendations for performing kinetic computations on thermal analysis data. *Thermochimica Acta*. **2011**, *520*, 1-19.
26. Lyon R. E.; Walters R. N. Pyrolysis combustion flow calorimetry. *J. Anal. Appl. Pyrolysis* **2004**, *71*, 27-46.
27. Kong, K. T. S.; Mariatti, M.; Rashid, A. A.; Busfield, J. J. C. Effect of processing methods and functional groups on the properties of multi-walled carbon nanotube filled poly(dimethyl siloxane) composites. *Polym. Bull.* **2012**, *69*, 937-953.
28. Bai, L.; Wang, X.; Tan, J.; Li, H.; Zheng, J. Study of distinctions in the synergistic effects between carbon nanotubes and different metal oxide nanoparticles on enhancing thermal oxidative stability of silicone rubber. *J. Mater. Sci.* **2016**, *51*, 7130-7144.
29. Pradhan, B.; Srivastava, S. K. Synergistic effect of three-dimensional multi-walled carbon nanotube-graphene nanofiller in enhancing the mechanical and thermal properties of high-performance silicone rubber. *Polym. Int.* **2014**, *63*, 1219-1228.
30. Sagar, S.; Iqbal, N.; Maqsood, A.; Shahid, M.; Shah, N. A.; Jamil, T.; Bassyouni, M. I. Fabrication and thermal characteristics of functionalized carbon nanotubes impregnated polydimethylsiloxane nanocomposites. *J. Compos. Mater.* **2015**, *49*, 995-1006.
31. Camino, G.; Lomakin, S. M.; Lazzari, M. Polydimethylsiloxane thermal degradation Part 1. Kinetic aspects. *Polymer* **2001**, *42*, 2395-2402.
32. Kashiwagi T.; Du F.; Douglas J. F.; Winey K. I.; Harris Jr. R. H.; Shields J. R. Nanoparticle networks reduce the flammability of polymer nanocomposites. *Nature Materials* **2005**, *4*, 928-933.
33. Mateos A. J.; Cain A. A.; Grunlan J. C. Large-Scale Continuous Immersion System for Layer-by-Layer Deposition of Flame Retardant and Conductive Nanocoatings on Fabric. *Ind. Eng. Chem. Res.* **2014**, *53*, 6409-6416.
34. Sonnier R.; Bokobza L.; Chocha-Lozano N. Influence of multiwall carbon nanotube (MWCNT) dispersion on ignition of poly(dimethylsiloxane)-MWCNT composites. *Polym. Adv. Technol.* **2015**, *26*, 277-286.
35. Dvornic, Petar R.; Lenz, Robert W. High Temperature Siloxane Elastomers. **1990**.
36. Kleinert, J. C.; Weschler, C. J. Pyrolysis Gas Chromatographic-Mass Spectrometric Identification of Polydimethylsiloxanes. *Anal. Chem.* **1980**, *52*, 1245-1248.
37. Camino, G.; Lomakin, S.M.; Lageard, M. Thermal polydimethylsiloxane degradation. Part 2. The degradation mechanisms. *Polymer* **2002**, *43*, 2011-2015.

38. Lewicki, J.P.; Mayer, B.P.; Alviso, C.T. et.al. Thermal Degradation Behavior and Product Speciation in Model Poly(dimethylsiloxane) Networks. *J. Inorg Organomet. Polym.* **2012**, *22*, 636-645.
39. Lewicki, J. P.; Albo, R. L. F.; Alviso, C. T.; Maxwell, R. S. Pyrolysis-gas chromatography/mass spectrometry for the forensic fingerprinting of silicone engineering elastomers. *J. Anal. Appl. Pyrol.* **2013**, *99*, 85-91.
40. Georgakilas, V.; Perman, J. A.; Tucek, J.; Zboril, R. Broad Family of Carbon Nanoallotropes: Classification, Chemistry, and Applications of Fullerenes, Carbon Dots, Nanotubes, Graphene, Nanodiamonds, and Combined Superstructures. *Chem. Rev.* **2015**, *115*, 4744-4822.
41. Bom, D.; Andrews, R.; Jacques, D.; Anthony, J.; Chen, B.; Meier, M. S.; Selegue, J. P. Thermogravimetric Analysis of the Oxidation of Multiwalled Carbon Nanotubes: Evidence for the Role of Defect Sites in Carbon Nanotube Chemistry. *Nano Lett.* **2002**, *2*, 615-619.
42. Balasubramanian, K.; Burghard, M. Chemically Functionalized Carbon Nanotubes. *Small* **2005**, *1*, 2, 180-192.

## CHAPTER 6

### RAPID AND CLEAN COVALENT ATTACHMENT OF METHYLSILOXANE POLYMERS AND OLIGOMERS TO SILICA USING $B(C_6F_5)_3$ CATALYSIS

#### 6.1 Introduction

##### 6.1.1 Background

Silica and silicates are the most common materials in which silicon exists on Earth. The importance of silica to modern technologies cannot be understated and with all the ways we use silica, it is important that we are able to modify its surface to optimize performance in different environments. Chemical modification through covalent attachment is preferred since it will result in the most stable linkage between the silica surface and the desired modifier. Such chemical modification of silica surfaces through the covalent attachment most often utilizes alkylsilanes.<sup>1-5</sup> Typically, the attachment is achieved through the reaction of surface silanols (Si-OH) with reactive chloro-, amino- or alkoxy- silanes either in solution or from the vapor. Molecular monolayers can be prepared through random attachment of functional silanes<sup>6,7</sup> or self-assembly of trifunctional *n*-alkyl silanes.<sup>8,9</sup> Polymerized grafted structures can also be formed from di- and tri- functional silanes, but control of structure is challenging or impossible due to the sensitivities of the hydrolysis and condensation reactions to the experimental/environmental conditions.<sup>7</sup> These silane modifications typically require long reaction times (>24 hours) at elevated temperatures (>70 °C) to form complete monolayers, making this a time and energy intensive process. Moreover, their hydrolysis byproducts may damage substrates, competitively adsorb during reaction (which can negatively affect monolayer structure), catalyze restructuring the monolayer, and need to be removed.

It would be advantageous to use hydrosilanes to modify silica surfaces for two major reasons: (1) the byproduct of the condensation of a hydrosilane with a silanol, H<sub>2</sub>



the formation of 'highly stable self-assembled monolayers.' Quantum mechanical calculations are consistent with a mechanism similar to the Piers-Rubinsztajn reaction that involves the formation of a borane-hydridosilane adduct followed by nucleophilic attack of the electron deficient Si atom by a surface silanol. Following hydride transfer from silicon to boron, a siloxane bond forms with the surface, molecular hydrogen is formed by acid-base chemistry between the borohydride and protonated surface siloxane, and finally the BCF catalyst is regenerated. This work demonstrates the versatility of the reaction by chemically patterning a surface using microcontact printing and the rapid preparation of superhydrophobic hydridosilane-functionalized silicon nanowires.

Prior to this work, Moitra *et al.*<sup>2</sup> reported the modification of amorphous silica with a variety hydridosilanes using BCF catalysis. These authors also noted that the reaction proceeds rapidly (<5 minutes) at room temperature with 1 mol% catalyst concentration and produces only H<sub>2</sub> as a byproduct and proposed a mechanism essentially identical to the one discussed above. The synthetic versatility of hydridosilanes and functional group tolerance of the modification method was demonstrated through the preparation and purification of numerous (23) functional hydridosilanes that were successfully attached to silica. Sweetman *et al.*<sup>3</sup> used this method to prepare phenyl-modified porous silicon surfaces for surface-assisted laser desorption/ionization mass spectrometry.

The previous research<sup>1-3</sup> illustrates advantages in speed, chemical versatility and technological applicability for this BCF-catalyzed surface modification reaction. In this work, monolayers of several trialkylsilanes are prepared to compare with samples derived from analogous trialkylchlorosilanes and to those recently reported.<sup>1</sup> Dynamic contact angle analysis is used to study these reactions, with particular regard to the density of *n*-alkyl groups and the time required to achieve maximum bonding density. The importance

of reporting both advancing ( $\theta_A$ ) and receding ( $\theta_R$ ) contact angle values has been discussed earlier but it deserves restating: the static angles most often reported in the literature are merely one value in between these two. No other researchers who used this reaction have measured advancing and receding angles making a complete understanding of this reaction impossible.

Additionally, I wanted to show that this reaction is also useful for preparing poly(dimethylsiloxane) (PDMS) grafts on silica surfaces. Low molecular weight model hydridomethylsiloxanes are first investigated to provide insight into both the steric issues of this surface modification reaction and the structure-wetting relationships for methylsiloxanes. I have particular interest in the wetting behavior of PDMS-grafted surfaces, which is special and in some ways unique with regard to water repellency. As described in the introductory chapter, repellency can be quantified by contact angle hysteresis - the difference between  $\theta_A$  and  $\theta_R$ . PDMS-grafted silica can be prepared by a number of approaches and some of these are summarized along with conditions and contact angle data in Figure 6.1. The literature contains numerous reports of surfaces of this (silica/PDMS) structure; those in Figure 6.1 were chosen because of their reported contact angle data. Two others that deserve attention are the first report<sup>13</sup> (1947) of the wetting of PDMS-grafted silica and a more recent paper<sup>14</sup> that claims "laterally chemisorbed" PDMS is a highly robust surface modifier. In route **a**, a silicon wafer was simply wet with PDMS oil ( $M_n \sim 9000$  g/mol) and heated at 100 °C for 24 h. Water contact angles of  $\theta_A/\theta_R = 104^\circ/102^\circ$  and a thickness of  $\sim 1.2$  nm were observed.<sup>15</sup> The PDMS thin film structure and wetting properties depend on temperature, reaction time and polymer molecular weight in nontrivial ways. No details of the bonding structure are known. In route **b**, a silicon wafer was treated with dimethyldichlorosilane in the vapor phase at 70 °C for 72 h.<sup>16</sup> Hydrolysis by water in the hydrated silica and condensation rendered a covalently

attached PDMS layer that was 2.5 nm thick and exhibited water contact angles of  $\theta_A/\theta_R = 104^\circ/103^\circ$ . Again, no details of the bonding, structure or molecular weight are known. Indistinguishable (identical contact angles and thicknesses) grafted layers can also be formed from the three oligomers,  $\text{Cl}(\text{SiMe}_2\text{O})_n\text{SiMe}_2\text{Cl}$ , where  $n = 1-3$ . In route **c**, the wafer was treated with dimethylsilanediol in the vapor phase at  $150^\circ\text{C}$ .<sup>17</sup> Ellipsometry indicated the thickness was  $\sim 2.5$  nm and water contact angles were  $\theta_A/\theta_R = 106^\circ/96^\circ$ . Although  $\text{Me}_2\text{Si}(\text{OH})_2$  is the presumed intermediate in the reaction with  $\text{Me}_2\text{SiCl}_2$ , the wetting behavior suggests a different structured monolayer. Route **d** involved the sulfuric acid-catalyzed hydrolysis and condensation of dimethyldimethoxysilane in isopropanol.<sup>18</sup> A step growth graft polymerization from the silicon surface occurred and the thickness depended on time and reaction temperature. Reaction for 30 min at  $21^\circ\text{C}$  yielded minimum hysteresis and a surface with a thickness of 4.7 nm and water contact angles of  $\theta_A/\theta_R = 103^\circ/102^\circ$ . Many other silica-PDMS surfaces and wetting data are reported in this paper and the wetting behavior depends on every variable. This "grafting from" method produces chains that are "vertically oriented" as opposed to the "laterally chemisorbed" chains described as robust.<sup>14</sup> These vertically oriented monolayers exhibit better hydrolytic stability than samples prepared from routes **a**, **b** and **c**. Route **e** entailed the platinum-catalyzed hydrosilylation of vinyl-terminated PDMS ( $^V\text{PDMS}^V$ ,  $M_n \sim 6000$  g/mol) with a silicon wafer that contained Si-H bonds, introduced by reaction with 1,3,5,7-tetramethylcyclotetrasiloxane ( $\text{D}_4^H$ ).<sup>19</sup> The thickness of this PDMS layer was 3.0 nm and water contact angles were  $\theta_A/\theta_R = 109^\circ/104^\circ$ .

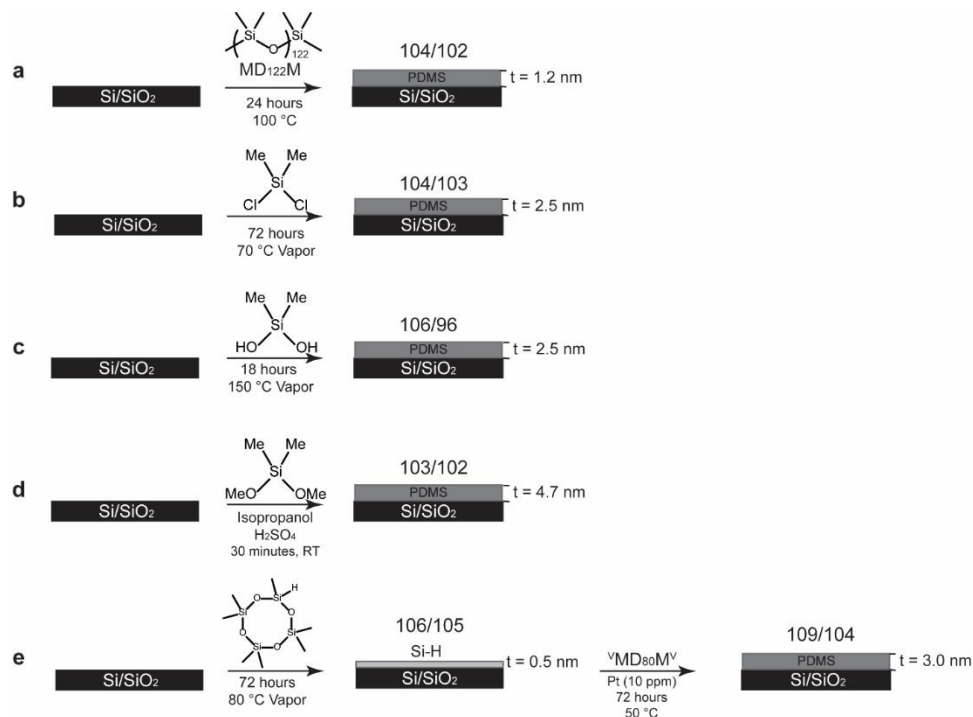


Figure 6.1. Five reported<sup>15-19</sup> methods for the preparation of covalently attached monolayers of PDMS on silicon wafers along with ellipsometric thickness and water contact angle data.

Although Figure 6.1 and the associated references<sup>15-20</sup> indicate that there are multiple routes to PDMS-grafted silica surfaces and that a few of these yield surfaces with low contact angle hysteresis, there is little known concerning the molecular weight of the attached chains, and nothing known about how bonding density or grafted chain architecture affect wetting. Why some surfaces exhibit almost no hysteresis while others, that are indistinguishable by every other technique, exhibit significant hysteresis is not understood. The BCF-catalyzed reaction between surface silanols and hydrosilane groups placed in controlled position(s) in the PDMS chains should in principle permit control of grafted chain architecture and correlations with wetting behavior; this was the major impetus of these studies.



### 6.1.2 Objectives

The objectives of this work were to (1) develop a more complete understanding of the BCF-catalyzed modification of silica surfaces by measuring and analyzing dynamic contact angle of trialkylsilane monolayers, (2) prepare model methylsiloxane surfaces and (3) prepare precise methylsiloxane polymer grafts. Preparations of methylsiloxane model and polymer surfaces provides insight into the unique water repellency of 'PDMS' surfaces and allows the formulation of structure-dynamic wetting relationships. Understanding the wetting of methylsiloxane polymer grafts is considered the primary objective of this work.

## 6.2 Experimental Section

### 6.2.1 Materials.

Solvents were purchased from Fisher Scientific and used as received. Alkylsilanes, monohydridomethylsiloxanes, hydride-terminated poly(dimethylsiloxane)s, monohydride/butyl-terminated poly(dimethylsiloxane)s, monohydride/vinyl-terminated poly(dimethylsiloxane)s, poly(hydridomethyl-co-dimethylsiloxane)s, poly(hydridomethylsiloxane), and BCF/toluene solution were obtained from Gelest and used as received. Silicon wafers (100 mm diameter, ~500  $\mu\text{m}$  thickness, 100 orientation, resistivity from 20 to 40  $\Omega\cdot\text{cm}$ ) were obtained from International Wafer Service and cut into ~1 cm square sections. Wafer sections were sonicated in toluene, ethanol and deionized water, rinsed with additional deionized water and dried under nitrogen. Wafer sections were then cleaned in a Harrick oxygen plasma cleaner at an oxygen pressure ~250 mtorr for 15 minutes.

Hydride/methyl terminated poly(dimethylsiloxane)s were prepared using lithium trimethylsilanolate-initiated anionic polymerization of hexamethylcyclotrisiloxane ( $\text{D}_3$ ) followed by termination with dimethylchlorosilane.  $\text{D}_3$  was dissolved in hexane and dried

overnight with calcium hydride. The dry D<sub>3</sub>-hexane mixture was distilled under reduced pressure into a liquid nitrogen - cooled trap and transferred via cannula to a flame-dried round bottom flask. Lithium trimethylsilanolate initiator was generated *in situ* by the addition of methyllithium by syringe. Following initiator generation, anhydrous dimethylformamide was added to promote polymerization. Polymerization was followed using <sup>1</sup>H NMR until 90-95% conversion was achieved and terminated by the addition of a 2 mol% excess (over methyllithium) of dimethylchlorosilane. For higher molecular weights, the end-capping reaction was run overnight to ensure complete reaction. The reaction was worked up with an aqueous rinse, neutralization with aqueous sodium bicarbonate, drying of the organic phase with magnesium sulfate, filtration, and solvent removal by rotary evaporation. Number average molecular weights were calculated from <sup>1</sup>H NMR and polydispersity was determined by gel permeation chromatography.

#### 6.2.2 General Reaction Information.

Reactions were carried out in Fisher septum-sealed 20 mL scintillation vials. Cleaned wafers were introduced to vials followed by capping, nitrogen purging and the addition via syringe of anhydrous toluene (99.8% ARCOS), siloxane, silane or polysiloxane, and then BCF catalyst solution - in that order. All reactions were carried out at room temperature. Following reaction, wafers were removed from the reaction vial and rinsed with toluene, ethanol, and deionized water (MilliQ 18.2 MΩ) and dried with a stream of nitrogen. Wafers were stored in a vacuum desiccator prior to analysis. Silane concentrations, catalyst concentrations and reaction times were varied as indicated.

*Control reactions of silanes and siloxanes.* Control reactions of hexamethyldisiloxane, octamethylcyclotetrasiloxane (D<sub>4</sub>) and trimethyl-terminated poly(dimethylsiloxane) (PDMS) were carried out under equivalent conditions as BCF-

catalyzed reactions. Additional control reactions were carried out using hydride-containing silanes and polysiloxanes under equivalent conditions but with no BCF catalyst. For these control experiments, wafers that were removed from the reaction solution and rinsed exhibited contact angle data that was indistinguishable from data on wafers that were stored in toluene, removed and rinsed.

*Vinyltetramethyldisiloxane surfaces.* Vinyltetramethyldisiloxane (VTMDS) surfaces were prepared by immersion of silicon wafers into a 0.1 M solution of VTMDS in dry toluene. 0.5 mol% BCF catalyst was added and the reaction proceeded at room temperature for 60 minutes. Wafers were then removed from the reaction solution and rinsed with toluene, ethanol and water. After drying under nitrogen, contact angle and ellipsometric thicknesses were measured.

*Platinum-catalyzed hydrosilylation of vinyl surfaces.* Vinyl functional surfaces were immersed in 0.1 M Bis(nonafluorohexyldimethylsiloxy)methylsilane in dry toluene. 1 drop (~3 $\mu$ L) of 2% Pt catalyst (Karstedt's catalyst in xylene, Gelest) was added and the solution was heated to 60 °C for 1 hour. Wafers were then rinsing with toluene, ethanol and water, dried with nitrogen, and stored under vacuum.

*UV-initiated thiol-ene reactions of vinyl surfaces.* Vinyl functional surfaces were immersed in 0.2 M mercaptopropionic acid in dry THF. 1 mol % ERGACURE 2959 UV-initiator was added and the solution was exposed to UV irradiation (Newport Flood Exposure Source, Hg(Xe) Lamp, 300 W) for 2 minutes. Wafers were then rinsing with toluene, ethanol and water, dried with nitrogen, and stored under vacuum.

*<sup>1</sup>H NMR Kinetics of D<sub>4</sub><sup>H</sup>*. To study the previously reported<sup>21</sup> oligomerization of D<sub>4</sub><sup>H</sup> under the reaction conditions used for surface modifications, a 0.1 M Si-H (0.025 M D<sub>4</sub><sup>H</sup>) toluene-d<sub>8</sub> solution was prepared in a septum-sealed NMR tube. At t = 0, a spectrum was recorded before the addition of BCF catalyst. Catalyst (0.5 mol% BCF, 40 mg/ml in toluene) was added and spectra were recorded every 3 minutes for 2 hours.

### 6.2.3 Characterization.

Advancing and receding contact angles of water were measured using a Ramé-Hart telescopic goniometer. Smooth (no stick-slip) motion of the contact line during advancing and receding events indicated the absence of macroscopic pinning defects on the smooth substrates. The reported contact angle values are one of 3-5 measurements made at different locations on the wafer surface. In general, variations in advancing and receding angles for a sample are less than 2°. Ellipsometry measurements were made with a Gaertner LSE Stokes Ellipsometer with a 6328 Å laser. The oxide was modeled with a thickness of 10 Å and refractive index of n = 1.46. The refractive index of silanes and siloxanes was estimated as n = 1.4. Reported thicknesses are the average of 5 measurements per modified wafer section. Angle-resolved X-ray photoelectron spectroscopy (XPS) was performed using a Physical Electronics Quantum 2000 at take-off angles of 15°, 45° and 75°.

## 6.3 Results and Discussion

All of the experiments described in this work involve reactions of the native oxide of silicon wafers that were manufactured to expose the (100) face of silicon. Wafer sections were diced to be ~1 cm x ~1 cm and were cleaned by methods consistent with those historically used in our group to prepare thousands of supported monolayers<sup>6,7,10,11,15-18</sup> from (mostly) alkyldimethylchlorosilanes. The reaction conditions

chosen were influenced by those reported by Escorihuela *et al.*,<sup>1</sup> but differ in subtle but significant ways. These researchers used Si(111) wafers and dichloromethane as solvent. This work used the more available, less expensive Si(100) wafers and toluene as a solvent. As stated above, the principal objective involved PDMS-grafted surfaces, but research began with the study the BCF-catalyzed surface modifications with trialkylsilanes and low molecular weight model hydridosiloxanes. These studies permitted comparisons with monolayers of identical alkylsilane structure that were prepared from chlorosilanes in toluene as well as with samples described in the recent report.<sup>1</sup> They also gave insight into steric effects on reaction kinetics.

### 6.3.1 Alkylsilane Monolayers

Four comments concerning silicon-supported trialkylsilane monolayers prepared from chlorosilanes are warranted. (1) *n*-Alkyldimethylsilane monolayers do not form on silica by self-assembly, as is the case for certain *n*-alkyltrichlorosilanes and *n*-alkylthiols on gold. The density of groups in *n*-alkyldimethylsilane monolayers is ~2.5 groups/nm<sup>2</sup> as opposed to the 4.5-5 groups/nm<sup>2</sup> observed in self-assembled monolayers prepared from *n*-alkyltrichlorosilanes and *n*-alkylthiols.<sup>7</sup> The two methyl groups on silicon require a larger "footprint" for the silane resulting in *n*-alkyl groups that are further apart and disordered rather than arrayed in the nearly vertical, all-trans configuration of self-assembled trifunctional silanes. (2) The reaction of chlorosilanes proceeds by hydrolysis and random covalent attachment (condensation) with the surface, thus the kinetics of reactions is unusual. In the initial stages the reaction is very fast, but as the surface fills and surface silanols become less accessible, the reaction slows considerably. The kinetics of formation of a trimethylsilyl monolayer illustrates this:<sup>6</sup> water contact angles increase from  $\theta_A/\theta_R = 0^\circ/0^\circ$  (wets) to  $\theta_A/\theta_R = 80^\circ/35^\circ$  after 6 min,  $\theta_A/\theta_R = 99^\circ/93^\circ$  after 60 min and  $\theta_A/\theta_R = 100^\circ/97^\circ$  after 150 min, but the reaction is not complete ( $\theta_A/\theta_R = 105^\circ/96^\circ$ ) until a time

in between 24 and 48 h. Hysteresis is minimized at 150 min reaction time and this is explained by the rotational mobility of trimethylsilyl groups in this non-close-packed monolayer. This mobility is inhibited by the greater bonding density that occurs during the later stages of the reaction. The reaction is not limited by lack of surface silanols; these are present in excess and completely reacted monolayers still contain ~2 surface silanols per nm<sup>2</sup> that can impact the wetting behavior.<sup>6</sup> (3) The yield of reactions of chlorosilanes with surfaces and the structure of the resulting monolayers are dependent on multiple variables in the reaction conditions. Much denser monolayers are formed using toluene as the solvent than when benzene is used. Ethyldiisopropylamine is a catalyst (and reagent to neutralize HCl) that increases bonding density over uncatalyzed reactions, but pyridine and triethylamine both decrease bonding density. The most dense monolayers are formed using vapor phase reactions with no base. The reactions and resulting bonding density are affected by competitive adsorption/desorption equilibria of reagents, solvents, catalysts and byproducts. (4) The reactions of chlorosilanes are thermally activated and proceed faster at elevated temperatures, but more dense monolayers are most often formed at lower temperatures.

These points concerning chlorosilane-derived monolayers, which the McCarthy group has developed over years of wrestling with surface preparation and contact angle data, are mentioned to advocate that the BCF-catalyzed reaction of silica with hydridosilanes is most certainly also condition-dependent and warrants study beyond what has been reported.<sup>1-3</sup> Table 6.1 shows water contact angle and XPS atomic composition data for nine monolayer surfaces prepared by reaction with 1 M silane and 0.5 mole% BCF in toluene at room temperature for 2, 16 and 72 hours. In all cases the wafer was sealed in a reaction vial that was subsequently purged with nitrogen before anhydrous toluene, silane and then a toluene solution of BCF was added by syringe (in this order).

Careful kinetics studies were not performed, but longer and shorter reaction times were studied to determine insight into the time required for maximum bonding density. All reactions exhibited rapid hydrogen evolution upon catalyst introduction and samples isolated at times of 15 min or less exhibited dramatic increases in advancing contact angle. Only the phenyldimethyl monolayer was complete as assessed by receding contact angle after 2 h. The results for triisopropylsilane and *tert*-butyldimethylsilane implicate sterics as an important criterion in this reaction as these reagents react much more slowly than less hindered silanes. Neither of these reactions is complete after 16 h. Although the BCF catalyst clearly functions with these sterically demanding reagents, the bonding density on the surface is much lower than that observed with *n*-alkyl groups. XPS atomic composition data show the expected trend of increasing carbon content as a function of the number of carbon atoms in the silane.

Water contact angle data for monolayers prepared from chlorosilanes with identical alkyl group structure are available<sup>6</sup> for 7 of the entries in Table 6.1. These data are reproduced in Table 6.2 for comparison. The triisopropyl- and *tert*-butyl- dimethylsilyl monolayers prepared from the chlorosilanes in the vapor phase exhibit water contact angles of  $\theta_A/\theta_R = 80^\circ/63^\circ$  and  $104^\circ/98^\circ$ , respectively, indicating higher bonding density than those prepared from hydridosilanes with BCF catalysis ( $\theta_A/\theta_R = 58^\circ/42^\circ$  and  $90^\circ/76^\circ$  - 72 h reactions). This suggests that steric congestion at the interface during BCF-catalyzed silylation limits bonding density. Data for surfaces modified with these chlorosilanes in solution are not reported, but the experiments were carried out and it is noted<sup>6</sup> that much lower contact angles were observed and that bonding density increased with increasing reaction temperature. These observations suggest that steric requirements of the BCF-catalyzed silylation are not as great as those for the ethyldiisopropylamine-catalyzed reaction of chlorosilanes with silica. Significant amounts

of reaction occur at room temperature with BCF-catalysis, but it was not determined if more dense monolayers will form at elevated temperatures. The ethyldimethylsilyl monolayers prepared from the chlorosilane under all three conditions exhibit higher contact angles ( $\theta_A/\theta_R = 104\text{-}110^\circ/91\text{-}98^\circ$ ) than the monolayer prepared from the hydridosilane ( $\theta_A/\theta_R = 96^\circ/90^\circ$ ), indicating higher bonding density. Monolayers prepared from chlorosilanes also have higher hysteresis than those prepared from hydridosilanes ( $12\text{-}13^\circ$  versus  $6^\circ$ ). This suggests that the lower bonding density monolayer produced by BCF-catalysis is smoother and/or more flexible than the chlorosilane-derived monolayers. The same effect appears to be operative in the cases of the *n*-butyl, *n*-octyl and *n*-octadecyl surfaces. Lower contact angles, but also lower hysteresis values are observed for BCF-catalyzed hydridosilane modifications. These contact angle values of  $\theta_A/\theta_R = 100^\circ/97^\circ$ ,  $104^\circ/101^\circ$  and  $103^\circ/97^\circ$  suggest very smooth/flexible, liquid-like surfaces. These hysteresis values are anomalously low for *n*-alkyl monolayers and this can be considered an advantage of BCF-catalyzed silylation over traditional methods. The steric requirements of the BCF-catalyzed silylation controls bonding density to fortuitously yield low hysteresis surfaces. A comparison to the work of Escorihuela *et al.*<sup>1</sup> can be made for the *n*-octyl- and *n*-octadecyl-dimethylsilane surfaces. The authors report a static contact angle of  $103^\circ$  for the *n*-octyldimethylsilane monolayer, that is consistent with this data, and a value of  $111^\circ$  for the *n*-octadecyldimethylsilane monolayer, that is much higher than any we observed and suggests roughness (molecular topography). Without  $\theta_A$  and  $\theta_R$  values, further comparison is not possible.



Table 6.1 Water Contact Angle and XPS Data (15° take-off angle) for Alkylsilane Monolayers (1 M Silane, anhydrous toluene, 0.5 mol% BCF)

Silane	Reaction Time (h)	$\theta_A/\theta_R$	%C	%O	%Si	%F
ethyltrimethyl	2	94°/83°				
	16	96°/90°	13.5	48.3	38.1	
	72	96°/90°				
isopropyltrimethyl	2	93°/86°				
	16	96°/89°	14.9	47.5	37.6	
	72	95°/89°				
triisopropyl	2	48°/35°				
	16	50°/32°	14.6	49.6	35.8	
	72	58°/42°				
<i>n</i> -butyltrimethyl	2	98°/92°				
	16	100°/97°	22.8	43.1	34	
	72	101°/98°				
<i>tert</i> -butyltrimethyl	2	42°/28°				
	16	50°/37°	18.2	47.1	34.6	
	72	90°/76°				
<i>n</i> -octyltrimethyl	2	103°/100°				
	16	104°/101°	26	40.5	33.5	
	72	101°/92°				
<i>n</i> -octadecyltrimethyl	2	100°/92°				
	16	103°/97°	41.4	31.7	26.9	
	72	104°/96°				
phenyltrimethyl	2	89°/82°				
	16	90°/83°	26.1	40.2	26.9	
	72	90°/84°				
Bis(nonafluorohexyldimethylsiloxy)-methylsilane	2	84°/73°				
	16	91°/80°	17.2	40.2	30.6	12.0
	72	93°/84°				

Table 6.2. Water Contact Angle for Alkylsilane Monolayers Prepared from Chlorosilanes for Comparison.

Alkylsilane	Solution 60-70 °C	Solution RT	Vapor, 60-70 °C	BCF- Catalyzed RT, 16 h
ethyldimethyl	104°/91°	108°/96°	110°/98°	96°/90°
isopropyldimethyl			108°/96°	96°/89°
triisopropyl			80°/63°	52°/32°
<i>n</i> -butyldimethyl	104°/92°	105°/93°	105°/93°	100°/97°
<i>tert</i> -butyldimethyl			104°/98°	50°/37°
<i>n</i> -octyldimethyl	103°/91°	106°/93°	106°/99°	104°/101°
<i>n</i> -octadecyldimethyl	103°/91°	107°/95°		103°/97°

### 6.3.2 Model Methylsiloxane Monolayers

To optimize reaction conditions, investigate steric issues for BCF-catalyzed surface modifications and begin to understand structure-wetting properties of methylsiloxanes, model low molecular weight monohydridomethylsiloxanes were studied. These are better model reagents for PDMS copolymer attachment reactions than the alkyldimethylsilane reagents. It should also be emphasized that these monolayers would be very difficult to prepare by conventional techniques as most of the discrete chlorosilanes are not available; this is yet another advantage of the BCF-catalyzed modification method. Pentamethyldisiloxane,  $\text{Me}_3\text{SiOSiMe}_2\text{H}$  ( $\text{MM}^{\text{H}}$ ), both isomers of heptamethyltrisiloxane,  $\text{Me}_3\text{SiOSiMe}_2\text{OSiMe}_2\text{H}$  ( $\text{MDM}^{\text{H}}$ ) and  $\text{Me}_3\text{SiOSi(H)MeOSiMe}_3$  ( $\text{MD}^{\text{H}}\text{M}$ ), tris(trimethylsiloxy)silane,  $(\text{Me}_3\text{SiO})_3\text{SiH}$  ( $\text{M}_3\text{T}^{\text{H}}$ ), and heptamethylcyclotetrasiloxane ( $\text{D}_4^{\text{H}}$ ) were studied. The convenient General Electric nomenclature (M, D, T, Q)<sup>22</sup> is used to abbreviate silicone reagents and the superscripts, V, H and Bu to represent that one methyl group is replaced with one vinyl, hydro or *n*-butyl group.

Many reactions were run with MM<sup>H</sup>, which reacts faster than any of the alkylsilanes discussed above, to test and optimize conditions and procedures. It was found that the order of addition of the hydridosiloxane/BCF/toluene/wafer has a pronounced effect on monolayer structure as evidenced by contact angle analysis (Table A6.1). The preferred method is to purge the reaction vial containing a silicon wafer section with nitrogen, add toluene, then hydridosiloxane, and finally BCF catalyst. If the BCF catalyst is added before the hydridosiloxane, or if the wafer is submerged as the final step, significantly lower advancing and receding contact angles result. The reaction is extremely fast and attempts to determine kinetics at 0.1 M Si-H and 0.5 mol% BCF yielded the data shown in Table 6.3. The reaction is complete (statistically) within 1 minute as evidenced by both contact angle and ellipsometric thickness data. Although Table 6.3 shows practically nothing concerning the kinetics of the reaction, it is included as representative data describing a well-behaved random covalent attachment reaction. The scatter in the contact angle data is real and expected from slightly different, completely modified surfaces. These surfaces contain "holes" between randomly attached disiloxane groups that are smaller than the disiloxane, contain surface silanols, and cannot be filled by further reaction (at least at this temperature). The residual silanols present in these "holes" on the silicon wafer are shrouded to a high degree by the disiloxane, but can be accessed by the water probe fluid resulting in the observed hysteresis. It might be argued that the reaction is not complete after 1 or 5 min and is after 10 or 15 min, based on the 1° contact angle differences, but this is not significant other than that it suggests reactions be run for 15 min or more. No deleterious effects of longer reaction times, up to 2 h, are observed. The sample prepared with 90 min reaction has slightly higher contact angles. These differences are real, but indicate only that smaller "holes" or different disiloxane group random placement occurred in this particular reaction; there is nothing special about the 90 min reaction time.

Table 6.3. Contact Angle and Ellipsometric Thickness Values for the BCF-Catalyzed Reaction of Pentamethyldisiloxane with Si(100).

Time, min	$\theta_A$	$\theta_R$	Hysteresis	Thickness (Å)
1	96°	89°	7°	2.66
5	96°	89°	7°	3.72
10	97°	90°	7°	2.76
15	97°	90°	7°	2.6
30	97°	90°	7°	3.03
60	97°	90°	7°	2.92
90	99°	92°	7°	1.95
120	97°	90°	7°	2.8

Decreasing the BCF catalyst concentration by two orders of magnitude decreases the rate of reaction, but monolayer formation still occurs. Table A6.2 shows data for 1, 0.5, 0.1, 0.05 and 0.01 mol% BCF. Higher contact angles were observed more often at 0.5 mol% than at 1 mol% concentration, perhaps due to the competing adsorption of BCF. Decreasing MM<sup>H</sup> concentration from 0.1M to 0.05M and 0.01M also decreased the reaction rate (Table A6.3), but monolayers were still formed. It must be emphasized that 0.01M MM<sup>H</sup> and 0.00001M BCF in toluene (extremely dilute conditions) formed hydrophobic monolayers with  $\theta_A/\theta_R = 92^\circ/87^\circ$  in 15 min (longer times were not studied). That monolayers form under such dilute conditions indicates (1) that there is some adsorption affinity of the silane to the silica surface such that silane molecules form an enriched layer, and (2) the important fact that in 2D surface modifications in solutions, there is always a large excess of reagent present. The conditions chosen for further studies were 0.1 M hydridosiloxane and 0.0005M BCF (0.5 mol%).

The rates of reaction for other model hydridomethylsiloxanes were determined in similar fashion and the kinetics data for MDM<sup>H</sup> (Table A6.4), MD<sup>H</sup>M (Table A6.5), (M<sub>3</sub>T<sup>H</sup>) (Table A6.6), and D<sub>4</sub><sup>1H</sup> (Table A6.7) are included in the appendix following this chapter.

Figure 6.2 summarizes the results of these experiments with regard to reaction time required for maximum bonding density. MDM<sup>H</sup> reacts rapidly, but more slowly than MM<sup>H</sup>. Significant hydrophobization is evident after 15 min reaction, but the reaction is not complete until ~2 h. The contact angles are higher than those of the MM<sup>H</sup>-derived monolayer indicating more complete coverage of surface silanol groups. The hysteresis is lower with the trisiloxane than the disiloxane suggesting a smoother and/or more flexible surface. More complete shrouding of surface silanols by the trisiloxane may also explain the longer reaction times required to reach completion. MD<sup>H</sup>M reacts more slowly and contact angles did not level until ~16 h reaction. The lower contact angles and higher hysteresis observed in comparison with the end-functional isomer, MDM<sup>H</sup>, suggest that the steric issues observed with the *tert*-butyldimethylsilane and triisopropylsilane (Table 6.1) monolayers are operative. The same steric issues are more evident with M<sub>3</sub>T<sup>H</sup>; even lower contact angles and higher hysteresis are observed, indicating significant contributions of surface silanols to the wetting behavior. These observations suggest that terminal silanes (M<sup>H</sup>) are more reactive than internal silanes (D<sup>H</sup>, T<sup>H</sup>) under these conditions. The cyclic hydridomethylsiloxane, D<sub>4</sub><sup>1H</sup>, reacts somewhat anomalously and reaction is complete in ~10 min to yield a surface that exhibits silanols to water as a contact angle probe fluid, but that are unreactive to further modification by D<sub>4</sub><sup>1H</sup>/BCF under these conditions. Apparently, the ring structure increases the rate of reaction of this internal silane. These hydridomethylsiloxanes form an interesting and perhaps useful series of surfaces with a range of water contact angles:  $\theta_A/\theta_R = 101^\circ/97^\circ, 97^\circ/90^\circ, 90^\circ/81^\circ, 84^\circ/70^\circ, 73^\circ/47^\circ$ . This is a convenient, reproducible, clean (no byproducts to remove), room temperature surface modification reaction that is worked up by simple solvent rinsing. BCF is a very effective catalyst that is removed completely upon rinsing and can be used in very low concentration. No fluorine (or boron) was observed in XPS spectra of any of the surfaces reported here.

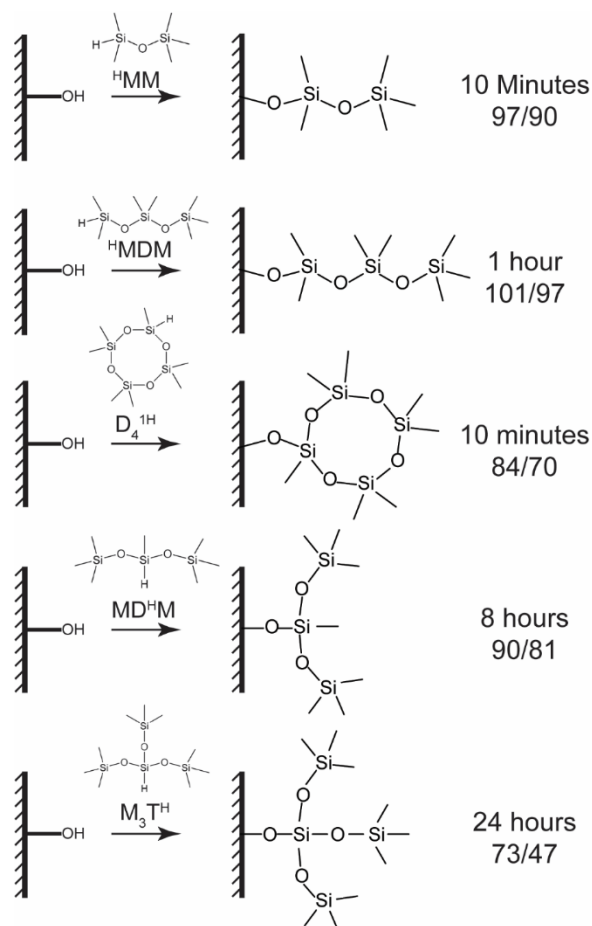


Figure 6.2. Conditions for maximum bonding density for BCF-catalyzed reactions of Si(100) with model hydridomethylsiloxanes (toluene, room temperature, 0.1 M hydridomethylsiloxane and 0.0005M BCF (0.5 mol%).

Surfaces prepared from the reaction of tetramethylcyclotetrasiloxane ( $\text{D}_4^{\text{H}}$ ) demonstrate behavior very different than the model hydridomethylsiloxanes that contain only one hydride, specifically  $\text{D}_4^{\text{1H}}$ . The results of kinetics studies at 0.1 M and 1.0 M Si-H solutions with 0.5 mol% BCF catalyst are presented in Table 6.4. The special behavior of  $\text{D}_4^{\text{H}}$  in comparison to  $\text{D}_4^{\text{1H}}$  is the result of (1) the variety of surfaces that may arise from a mixture of  $\text{D}_4^{\text{H}}$  isomers and (2) the hydride transfer oligomerization of  $\text{D}_4^{\text{H}}$  in the presence of BCF catalysis.<sup>21</sup> Unlike  $\text{D}_4^{\text{1H}}$  which may react only once in one configuration with surface silanols,  $\text{D}_4^{\text{H}}$  may react more than once with exposed silanols and will do so in a manner

that depends on the configuration of hydrides on the ring. For example, an all-*cis* configuration of hydrides where all the hydrides are on the same side of the ring could be expected to react more than once and to lie down on the surface. In cases where the hydrides are on different sides of the ring, a molecule may react only once and stick out from the surface. The randomness of this attachment will yield a heterogeneous hydridomethylsiloxane surface which is evidenced by the  $\theta_A/\theta_R = 90^\circ/80^\circ$  in the initial monolayer that forms at short reaction times. These initial monolayers are similar to those formed from  $D_4^H$  but the increased contact angles indicate that silanols are more shrouded by the randomly attached mixture of  $D_4^H$  isomers. The additional complication of oligomerization arises once a  $D_4^H$  molecule is attached. Hydride transfer oligomerization will occur from surface bound  $D_4^H$  to form polycyclic grafts. Oligomerization is observed directly by the increase in thickness with reaction time and in  $^1H$  NMR kinetics shown in Figure A6.10. Graft thickness increases faster in higher concentrations of  $D_4^H$ . It is shown in Table 6.4 that graft growth directly corresponds to increased advancing contact angles and greater contact angle hysteresis. Like the other silanes reported, adsorption of  $D_4^H$  will lead to a high local concentration of  $D_4^H$  at the surface. Under such conditions, the surface adsorbed layer is likely to form a highly branched, polycyclic, network structure similar to the solid materials reported<sup>21</sup> when BCF is added to neat  $D_4^H$ . This surface layer contains methylsiloxane groups responsible for the high advancing contact angles, but is heterogeneous and rigid on the molecular scale resulting in high contact angle hysteresis.

Vinyl group - containing monolayers were prepared using  $^VMM^H$ . The reactivity is similar to  $MM^H$  and complete monolayers were formed within 15 minutes ( $\theta_A/\theta_R = 96^\circ/90^\circ$ ). Samples containing this monolayer were further modified by Pt-catalyzed hydrosilylation with bis(nonafluorohexyldimethylsiloxy)methylsilane and UV-initiated thiol-ene addition with mercaptopropionic acid. Table 6.5 exhibits XPS, contact angle and ellipsometry data

that are consistent with further modification of the vinyl groups. Yields estimated by XPS were low, but these reactions were not optimized.

Table 6.4 Kinetics of BCF-catalyzed modification of Si(100) with D<sub>4</sub>H at indicated Si-H concentration. (toluene, 0.5 mol% BCF, room temperature)

[Si-H]	time, min	$\theta_A$	$\theta_R$	Hysteresis	Thickness (Å)
<b>1.0 M</b>	10	90	80	10	2.72
	30	91	80	11	1.37
	60	94	83	11	3.97
	120	101	90	11	3.82
	960	104	88	16	8.55
	1440	105	89	15	10.04
<b>0.1 M</b>	1	82	66	16	4.68
	10	84	73	11	4.28
	30	91	78	13	3.7
	60	91.5	81	10.5	3.3
	90	92.5	82	10.5	4.64
	120	94	82	12	4.27
	960	93	82	11	6.32
	4320	96	76	20	9.03

Table 6.5. Thickness, Contact Angles and XPS (15° ToA) of Vinyltetramethyldisiloxane surfaces and derivatives

	Thickness, Å	$\theta_A$	$\theta_R$	$\Delta$	%C	%S	%F
Vinyltetramethyldisiloxane	0.76	96°	90°	6°	14.3		<0.1
Bis(nonafluorohexyl) methylsilane Pt-Catalyzed Hydrosilylation	6.06	106°	97°	9°	19		6
Mercaptopropionic Acid Thiol-ene	2.91	77°	63°	14°	20.2	1.6	



### 6.3.3 Covalently Attached Polymeric Methylsiloxane Monolayers

Three types of hydridosilane-containing methylsiloxane polymer were studied: PDMS containing one terminal hydridosilane,  ${}^R\text{MD}_n\text{M}^H$  ( $R = \text{Me, vinyl, } n\text{-butyl}$ ), PDMS containing two terminal hydridosilanes,  ${}^H\text{MD}_n\text{M}^H$ , PDMS containing different concentrations of randomly placed hydridomethylsiloxane comonomer,  $\text{MD}_x\text{D}^H_y\text{M}$ . Samples of different molecular weight  ${}^H\text{MD}_n\text{M}^H$ ,  ${}^{\text{Bu}}\text{MD}_n\text{M}^H$  and  ${}^V\text{MD}_n\text{M}^H$  and samples of  $\text{MD}_x\text{D}^H_y\text{M}$  that contained 3-100 mol% hydridomethylsiloxane backbone units were obtained commercially (Gelest); their molecular weight data were determined using  ${}^1\text{H-NMR}$ .  $\text{MD}_n\text{M}^H$  samples ( $M = \text{trimethylsilyl}$ ) were prepared by methyllithium-initiated ring-opening polymerization of  $\text{D}_3$  and termination with dimethylchlorosilane.

Surface modification experiments were carried out using the conditions and procedure optimized for the model methylsiloxane monolayers discussed above: anhydrous toluene, 0.1 M Si-H, 0.5 mol% (0.0005 M) BCF. Toluene and then the hydridomethylsiloxane polymer, sufficient to generate 0.1 M Si-H, were added to the nitrogen-purged wafer-containing reaction vial followed by addition of BCF. The polymer concentration in solution varied significantly in terms of g/mL; Si-H and BCF concentrations remained constant. After reaction, the wafer was removed, rinsed with a series of solvents and dried with a stream of nitrogen.

Table 6.6 exhibits ellipsometric thickness, water contact angle and angle-dependent XPS data for  ${}^R\text{MD}_n\text{M}^H$  and  ${}^H\text{MD}_n\text{M}^H$  samples. Sufficient kinetics data were obtained to indicate that these data are reproducible and that reactions are complete after 2h. These reactions were rapid and often complete within minutes. Scatter in the data was

minimal. Although toluene was used as the solvent for all of these preparations, other solvents were investigated for their compatibility. Table A6.10 shows contact angle and ellipsometry data for BCF-catalyzed reactions of  ${}^{\text{Bu}}\text{MD}_{20}\text{M}^{\text{H}}$  with silica surfaces in seven additional solvents. We note that higher contact angles and lower hysteresis were observed with heptane and cyclohexane. These may be better solvents (render more repellent surfaces) for this reaction than toluene.

Table 6.6. Ellipsometric Thickness, Water Contact Angle and Angle-Dependent XPS Data for  ${}^{\text{R}}\text{MD}_n\text{M}^{\text{H}}$  and  ${}^{\text{H}}\text{MD}_n\text{M}^{\text{H}}$  - Derived Monolayers.

Silicone	Thickness (Å)	$\theta_{\text{A}}/\theta_{\text{R}}$	%C (15° ToA)	%C (45° ToA)	%C (75° ToA)
$\text{MD}_{15}\text{M}^{\text{H}}$ (M=1070)	9.16	103°/98°	33.0	18.1	15.7
$\text{MD}_{28}\text{M}^{\text{H}}$ (M=2070)	17.44	104°/101°	33.0	19.5	15.5
$\text{MD}_{36}\text{M}^{\text{H}}$ (M=2664)	24.71	104°/100°	34.9	23.5	19.8
$\text{MD}_{68}\text{M}^{\text{H}}$ (M=5000)	31.68	104°/102°	41.0	30.5	24.1
$\text{MD}_{112}\text{M}^{\text{H}}$ (M=8280)	39.90	104°/101°	45.6	33.8	29.0
$\text{MD}_{117}\text{M}^{\text{H}}$ (M=8660)	50.81	104°/101°	44.0	35.9	33.1
$\text{MD}_{423}\text{M}^{\text{H}}$ (M=31 300)	122.61	111°/92°	49.4	45.3	42.9
${}^{\text{Bu}}\text{MD}_{15}\text{M}^{\text{H}}$ (M=1080)	13.54	104°/100°	21.6	12.1	8.9
${}^{\text{Bu}}\text{MD}_{20}\text{M}^{\text{H}}$ (M=1450)	15.40	106°/103°	27.5	14.5	10.3
${}^{\text{Bu}}\text{MD}_{97}\text{M}^{\text{H}}$ (M=7150)	44.66	105°/100°	45.1	32.8	27.2
${}^{\text{V}}\text{MD}_{53}\text{M}^{\text{H}}$ (M=3920)	26.16	105°/102°	40.0	27.5	23.6
${}^{\text{V}}\text{MD}_{270}\text{M}^{\text{H}}$ (M=19 980)	67.02	107°/93°	46.9	40.5	37.2
${}^{\text{H}}\text{MD}_{10}\text{M}^{\text{H}}$ (M=740)	5.58	101°/95°	18.7	9.1	6.5
${}^{\text{H}}\text{MD}_{17}\text{M}^{\text{H}}$ (M=1260)	10.28	103°/98°	30.3	17.1	13.0
${}^{\text{H}}\text{MD}_{60}\text{M}^{\text{H}}$ (M=4440)	25.92	105°/102°	41.0	26.0	21.4
${}^{\text{H}}\text{MD}_{195}\text{M}^{\text{H}}$ (M=14 400)	56.70	108°/101°	46.3	41.7	35.7
${}^{\text{H}}\text{MD}_{283}\text{M}^{\text{H}}$ (M=20 900)	86.70	109°/99°	47.7	46.7	43.1

A cursory look at the water contact angle data in Table 6.6 suggests that all of these modification reactions produce rather similar highly hydrophobic PDMS-grafted surfaces. This is indeed the case, however several trends give insight into the structure-wetting behavior of the PDMS-grafted surfaces. Figure 6.3 shows the scaling of measured ellipsometric thickness with  $N$ , the number of repeat units in the end-functional polymers. The scaling exponent for these surfaces in the dry state is 0.71, which is close to the predicted 0.66 scaling exponent of a dry/'melt' brush in Alexander-de Gennes brush theory. This indicated that the PDMS grafts have an extended brush-like conformation and that in the solvent swollen state thickness would scale linearly with  $N$ . As a more visually intuitive depiction, Figure 6.4 shows the shape of individual grafted chains for all samples analyzed. The rectangles are drawn (based on molecular weight, bulk density and measured ellipsometric thickness) to represent the calculated shape (degree of stretching) and packing density of individual chains as though they were monodisperse, close-packed, non-penetrating arrays of square prisms with their long axis perpendicular to the surface. Of course, the chains penetrate, are stretched to different extents and the PDMS samples are polydisperse, but the rectangles in the Figure represent averages and are insightful. Evident in both Figure 6.4 and Table 6.6 is that grafted layer thickness and degree of chain stretching increase with molecular weight for both  $^R\text{MD}_n\text{M}^H$  and  $^H\text{MD}_n\text{M}^H$  polymers. The series of samples on the left in the blue box in Figure 6.4,  $\text{MD}_n\text{M}^H$  with  $n = 15, 28, 36, 68, 112, 117$  and  $423$ , contain grafted polymers with average aspect ratios of 0.63, 1.2, 1.7, 1.9, 2.1, 3.0 and 5.9, respectively. Data used in similar calculations for all samples are in Table A6.11. The other  $^R\text{MD}_n\text{M}^H$  polymers (vinyl dimethylsilyl- and *n*-butyldimethylsilyl-terminated) in the blue box and the  $^H\text{MD}_n\text{M}^H$  polymers (pink box) show similar (indistinguishable) molecular weight - dependent chemisorption/chain stretching tendencies. Having two chain end anchors, or *n*-butyl or vinyl groups rather than methyl

groups, has little or no effect on chain density. The measured thickness value of  ${}^{\text{H}}\text{MD}_{60}\text{M}^{\text{H}}$  (26 Å) is similar to those of  ${}^{\text{V}}\text{MD}_{53}\text{M}^{\text{H}}$  (26 Å) and  $\text{MD}_{68}\text{M}^{\text{H}}$  (32 Å). Based on the rapid BCF-catalyzed reaction discussed above, it is expected that both chain ends of  ${}^{\text{H}}\text{MD}_n\text{M}^{\text{H}}$  polymers have reacted, but this apparently does not significantly affect thickness. Toluene is a good solvent for these polymers and the adsorption and attachment steps of the reaction occur in toluene-swollen adsorbed chains. As previously mentioned with regard to scaling, the swollen chains have higher aspect ratios than those calculated from the ellipsometric thickness data of dry samples. The carbon content in XPS data reflects this molecular weight / thickness correlation as well, and the take-off angle dependence of the carbon content is consistent with carbon-containing layers of the thicknesses measured by ellipsometry on silicon/silica (non-carbon-containing) substrates. This is obvious in the sharp take-off angle dependence in thinner films: carbon content in the  $\sim 9$  Å thick  $\text{MD}_{15}\text{M}^{\text{H}}$ -derived monolayer is 33.0% (15°), 18.1% (45°) and 15.7% (75°), while those values for the  $\sim 123$  Å thick  $\text{MD}_{423}\text{M}^{\text{H}}$  sample are 49.4% (15°), 45.3% (45°) and 42.9% (75°).

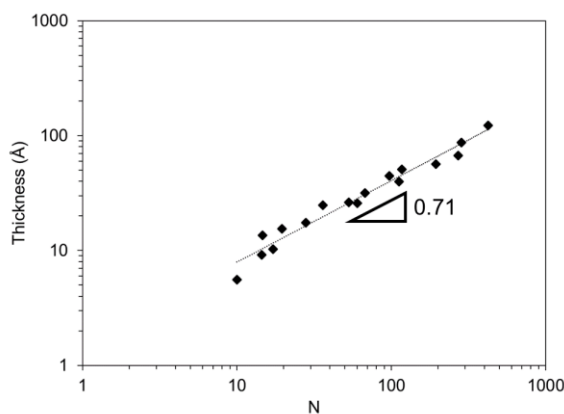


Figure 6.3: Log-Log plot of ellipsometric thickness versus the number of repeat units,  $N$ , of  ${}^{\text{x}}\text{MDM}^{\text{H}}$  polymer grafts from BCF catalysis on Si(100) surface. The slope of the fitted data indicates the scaling exponent for the relationship of thickness and  $N$ .

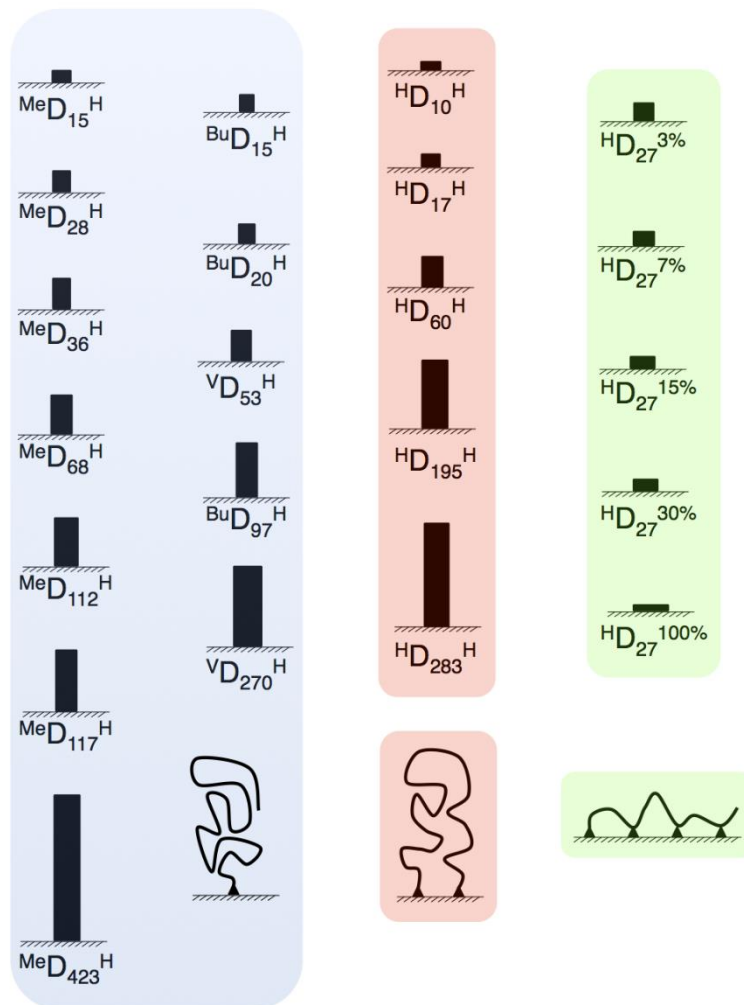


Figure 6.4. Graphic depictions the average degree of stretching of individual grafted chains based on molecular weight and ellipsometric thickness values. The abbreviations are abridged in the figure, leaving out the terminal M groups, thus  ${}^V D_{53}^H$  represents  ${}^V M_{D_{53}} M^H$ .

There are subtle differences in the water contact angle data that confirm very similar tendencies observed in other methods of grafting PDMS onto silica, in particular Methods **a**, **d** and **e** in Figure 6.1.<sup>15,18,19</sup> For both  ${}^R M D_n M^H$  and  ${}^H M D_n M^H$  (end grafted) polymers, contact angles increase with molecular weight in the low molecular weight range while hysteresis decreases. This is consistent with the arguments that were made above for the differences between  $MM^H$  and  $MDM^H$  monolayers - silanols are more completely shrouded by the additional dimethylsiloxane groups. Contact angles for  $MM^H$ ,  $MDM^H$ ,

$MD_{15}M^H$ , and  $MD_{28}M^H$  are  $\theta_A/\theta_R = 97^\circ/90^\circ$ ,  $101^\circ/97^\circ$ ,  $103^\circ/98^\circ$  and  $104^\circ/101^\circ$ . Contact angles of surfaces prepared from polymers ranging from  $M_n \sim 2000$  g/mol ( $MD_{28}M^H$ ) to  $\sim 8000$  g/mol ( $MD_{117}M^H$ ) show indistinguishable contact angles with low hysteresis, but surfaces prepared from higher molecular weight polymers show pronounced hysteresis:  $\theta_A/\theta_R = 111^\circ/92^\circ$  for  $MD_{423}M^H$  ( $M_n \sim 30\,000$ ). The same differences are observed between  ${}^VMD_{53}M^H$  ( $\theta_A/\theta_R = 105^\circ/102^\circ$ ,  $M_n \sim 4000$ ) and  ${}^VMD_{270}M^H$  ( $\theta_A/\theta_R = 107^\circ/93^\circ$ ,  $M_n \sim 20\,000$ ), as well as in the series of difunctional  ${}^HMD_nM^H$  polymers. Contact angle data for  ${}^HMD_{10}M^H$ ,  ${}^HMD_{17}M^H$ ,  ${}^HMD_{60}M^H$ ,  ${}^HMD_{195}M^H$  and  ${}^HMD_{283}M^H$  are  $\theta_A/\theta_R = 101^\circ/95^\circ$ ,  $103^\circ/98^\circ$ ,  $105^\circ/102^\circ$ ,  $108^\circ/101^\circ$  and  $109^\circ/99^\circ$ . Samples prepared by Method **a** in Figure 6.1 (thermal equilibration of PDMS oils with silicon wafers) exhibited contact angles of  $\theta_A/\theta_R = 93^\circ/79^\circ$ ,  $104^\circ/102^\circ$ ,  $106^\circ/105^\circ$ , and  $113^\circ/94^\circ$  with PDMS samples of  $M_n = 770$ , 2000, 9430 and 116 000 g/mol, respectively. The ellipsometric thickness values are consistent with molecular weight for all of these samples and surfaces exhibiting low hysteresis all have thickness values of 5 nm or less. The thickness values for  $MD_{423}M^H$ ,  ${}^VMD_{270}M^H$ ,  ${}^HMD_{195}M^H$ ,  ${}^HMD_{283}M^H$  and  $PDMS^{116K}$  that exhibit significant hysteresis are  $\sim 12.3$ , 6.7, 5.7, 8.7 and 12.5 nm, respectively. Samples prepared by Method **e** in Figure 6.1 (hydrosilylation of vinyl-terminated PDMS to  $D_4^H$  modified wafers) exhibited contact angles of  $\sim \theta_A/\theta_R = 108^\circ/104^\circ$ ,  $112^\circ/99^\circ$ ,  $115^\circ/98^\circ$ ,  $117^\circ/97^\circ$ ,  $116^\circ/94^\circ$  and  $117^\circ/95^\circ$  with  ${}^VMD_nM^V$  samples of  $M_n = 6000$ , 17 200, 28 000, 49 500, 72 000, and 117 000 g/mol, respectively. The measured thickness values of these surfaces fall between 3 and 8 nm making them thinner than what would be expected from these molecular weights: this may be due to several factors including but low reaction yields for surface hydrosilylation or polymer degradation resulting from long reaction times. Regardless, the same trend of increasing hysteresis in high molecular weight/thick PDMS grafts is observed. Data for samples prepared using Method **d** in Figure 6.1 are also consistent with this thickness-wettability behavior (the molecular weight values of these grafted chains are not known).<sup>17</sup>

Two explanations are presented in Figure 6.5 for why the thicker (~10 nm) films of higher molecular weight end-grafted polymer exhibit significantly greater hysteresis ( $\theta_A - \theta_R = 14-19^\circ$ ) than the thinner (1-5 nm) ones of lower molecular weight polymer ( $\theta_A - \theta_R = 1-3^\circ$ ). Difunctional end-grafted polymers,  ${}^H\text{MD}_n\text{M}^H$ , show intermediate contact angle disparities,  $\theta_A - \theta_R = 3-6^\circ$  for the 0.6-2.6 nm thick layers and  $\theta_A - \theta_R = 7$  and  $10^\circ$  for the 5.7 and 8.7 nm thick layers. All of these surfaces contain covalently attached liquid PDMS ( $T_g \sim -125^\circ\text{C}$ ) and the rotational motions of these chains at room temperature ( $\sim 150^\circ\text{C}$  above  $T_g$ ) should be sufficient to negate contact line pinning and eliminate hysteresis. PDMS, however, spontaneously spreads on the air-water interface; Langmuir films can be prepared.<sup>23,24</sup> Grafted chains at the 3-phase PDMS/water/air contact line should spread onto the liquid surface (Figure 6.5a). During motion of a drop (contact line) on a surface, either through sliding or in a contact angle measurement, this spreading of PDMS chains has to be occurring reversibly. Evidently the lower molecular weight chains can spread/despread (or adsorb/desorb or wet/dewet) on the water surface rapidly enough (at rates in nanometers per millisecond) so that they do not impede the mm/sec (identical units as nm/msec) motions of the contact line; in fact, they move the contact line. This motion of the contact line on methylsiloxane surfaces can visually depicted using molecular umbrellas.<sup>25</sup> The higher molecular weight chains, however, can spread further from the 3-phase contact line up onto the water drop surface and their spreading/despreading, adsorption/desorption or wetting/dewetting kinetics impedes the contact line motion. It could be argued that chains in monolayers composed of samples grafted at both ends,  ${}^H\text{MD}_n\text{M}^H$ , are slightly less mobile at low molecular weight and cannot spread as far onto the drop at high molecular weight to rationalize the intermediate hysteresis values. This mechanism is consistent with the data, but is also probably over-analysis of very small differences. A second, less molecular and more continuum

explanation (Figure 6.5b) is that the three phase contact line changes from one that behaves as a solid/liquid/vapor interface to one of a liquid/liquid/vapor interface with increasing PDMS layer thickness. With sufficient attached liquid film thickness, the interface is deformed at the contact line to a degree that the liquid (PDMS) motion required to advance and recede is a significant component of the activation barrier between metastable contact line states. The events depicted in both of these explanations may be occurring together and they may, in fact, be two different perspectives of the same events.

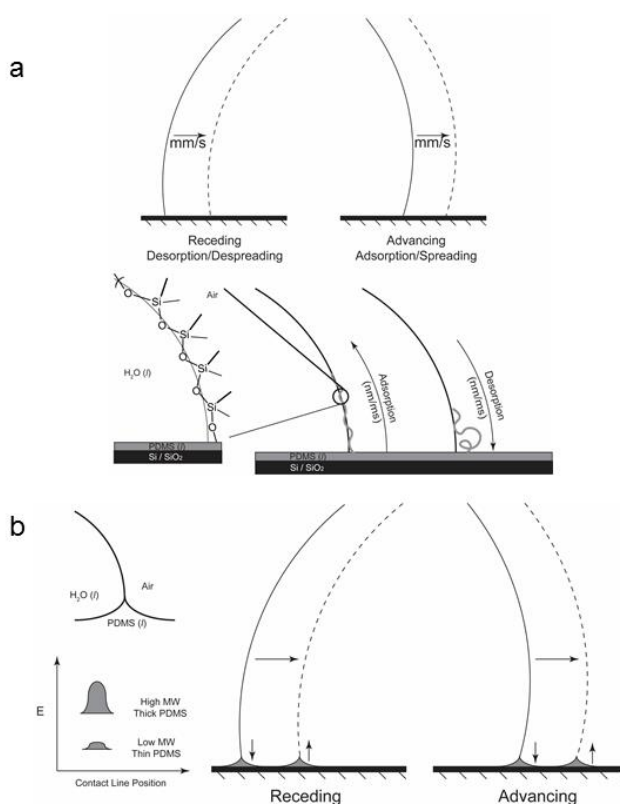


Figure 6.5. Two explanations for why thicker (~10 nm) films of higher molecular weight end-grafted PDMS exhibit greater contact angle hysteresis. In **a**, polymer chains spread onto the water drop and impede advancing and retreating events. In **b**, the liquid PDMS interface distorts at the contact line forming a liquid/liquid/air interface that must restructure for advancing and retreating events to occur.

Surface modification reactions with the poly(hydridomethyl-co-dimethyl)siloxane polymers were less well behaved and kinetics data are included in Tables A6.12-16 for



MD<sub>26</sub>D<sup>H</sup><sub>1</sub>M, MD<sub>25</sub>D<sup>H</sup><sub>2</sub>M, MD<sub>23</sub>D<sup>H</sup><sub>4</sub>M, MD<sub>18</sub>D<sup>H</sup><sub>8</sub>M, and MD<sup>H</sup><sub>27</sub>M, respectively. The hydride content varies from 3 to 100 mol% (at a constant molecular weight of M<sub>n</sub>~2000) and increasing hydride content leads to a decrease in thickness, a decrease in contact angle and an increase in contact angle hysteresis (Table 6.7, Figure 6.4, green box). The two copolymers with the lowest hydride content exhibit wetting behavior that is very similar to the end-grafted polymers. As hydride content in the polymer increases, the number of surface attachments per chain increases and the average molecular weight between surface attachments decreases. With a lower molecular weight between attachments, the average thickness decreases and the effective mobility of the siloxane decreases.

Table 6.7. Ellipsometric Thickness, Water Contact Angle and XPS Data for MD<sub>x</sub>D<sub>y</sub><sup>H</sup>M - Derived Monolayers.

Silicone	Thickness (Å)	$\theta_A / \theta_R$	%C (15° ToA)	%C (45° ToA)	%C (75° ToA)
MD <sub>26</sub> D <sup>H</sup> <sub>1</sub> M	13.88	103°/99°	27.4	15.0	11.2
MD <sub>25</sub> D <sup>H</sup> <sub>2</sub> M	11.38	104°/99°	24.7	14.5	10.9
MD <sub>23</sub> D <sup>H</sup> <sub>4</sub> M	8.77	102°/92°	19.5	9.4	7.7
MD <sub>18</sub> D <sup>H</sup> <sub>8</sub> M	8.73	100°/90°	19.1	8.8	7.3
MD <sup>H</sup> <sub>27</sub> M	3.61	98°/88°	15.9	8.7	6.7

There are additional complexities involved in the reactions of MD<sub>x</sub>D<sub>y</sub><sup>H</sup>M with surface silanols as evidenced by the time required to reach reaction completion (24 hours as compared to 2 hours for end-terminated siloxanes). The model hydridomethylsiloxanes illustrate that the internal hydridosilanes are less reactive, but that alone does not explain

the differences. Additional disparities are: (1) The siloxane polymers are polydisperse not only in molecular weight but also in backbone hydridosilane content (the end-functional polymers do not have this issue). The Si-H mol% determined by NMR is an average of the entire sample and some chains contain greater or fewer Si-H groups. Each molecule thus has an Si-H content - dependent probability of reaction as well as a molecular weight - dependent physical adsorption-desorption equilibrium constant. (2) Physical adsorption and desorption are simultaneous with grafting reactions. Polymers with a greater number of Si-H groups per chain are more likely to react with a surface upon adsorption and be kinetically trapped in non-equilibrium states. (3) Polymers that are grafted covalently are still mobile. Their conformations can fluctuate to both cover and uncover reactive silanols on the surface. The high hysteresis values for these samples are likely due to unreacted surface silanols that are covered from additional grafting reactions by toluene-swollen oligodimethylsiloxane chains, but are accessible to the water probe fluid in the dry state.

#### 6.3.4 Mechanism of BCF Catalysis of Hydridosilanes on Silica

Escorihuela *et al.*<sup>1</sup> and Moitra *et al.*<sup>2</sup> propose a mechanism for the BCF-catalyzed silylation of silica with alkylhydridosilanes, the skeleton of which is consistent with results that are reported here. The experiments presented here had preparative goals and were not designed as mechanistic studies, but some of these results suggest details of the mechanism that warrant comment and hypotheses, particularly with regard to the polymeric monolayers. Three arguments first need outlined: (1) All of the hydridosilanes studied here- the alkylhydridosilanes, the model methylhydridosiloxanes and polymethylhydridosiloxanes- adsorb (physisorb) from toluene to silica (meaning that their concentration at the interface is greater than the solution concentration). There are no data on adsorption isotherms for any of these materials from any solvent to any surface, however this is self-evident in that the alkylhydridosiloxanes can be purified by column

chromatography on silica and that PDMS (with no Si-H bonds) adsorbs to silica from toluene solution at room temperature as evidenced by thin layer chromatography. The low dependence of the reaction rate on concentration for  $MM^H$  (Table A6.3) suggests a high affinity isotherm for the smallest methylhydrosiloxane. The polymers must adsorb to an appreciably greater extent. (2) The BCF catalyst is extremely reactive and effective at much lower concentrations than have been previously reported. The catalyst likely adsorbs to silica from toluene as well, as it is less effective when added to the reaction prior to addition of  $MM^H$  (Table A6.1), but extremely effective when added to preadsorbed (from 0.01 M solution)  $MM^H$  at a BCF concentration of 0.00001 M (Table A6.3). The ratio of Si-H:BCF in the reaction vial is 1000:1 and likely significantly higher than this at the interface during reaction. (3) Arguments 1 and 2 suggest that the reaction takes place at a physisorbed layer of hydrosilane and is catalyzed by BCF that adsorbs to the Si-H-rich physisorbed layer and reacts many times without adsorption to silica. Figure 6.6 shows a mechanism using an end-functional PDMS,  $MD_nM^H$ , that details this perspective of the process. This is similar to the mechanism reported by Escorihuela *et al.*<sup>1</sup> and Moitra *et al.*<sup>2</sup> with the details of a pre-adsorbed hydrosilane that reacts with catalytic BCF (that is moving from surface site-to-site) rather than a hydrosilane-BCF adduct that competes with adsorbed species to react with silica, and oxidative addition of silanol followed by reductive elimination of  $H_2$  from a 6-coordinate silicon rather than acid-base chemistry between a discrete borohydride and protonated silanol. Hexavalent silicon is known and this method of hydride transfer avoids the formation of highly reactive intermediates. The very flexible siloxane bonds, Si-O-Si - that adsorb to the air-water interface, most certainly adsorb to hydrated silica from toluene. Due to the mobility of the siloxane backbone, it is expected that the  $M^H$  group is rotating freely at the chain end until BCF interacts with the silicon bound hydride.

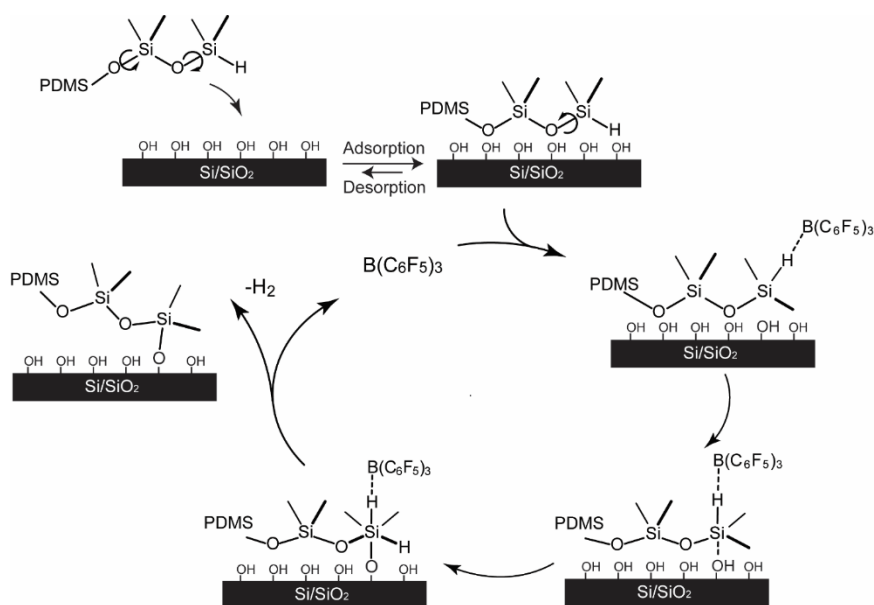


Figure 6.6. Proposed mechanism (after Escorihuela *et al.*<sup>1</sup>) for BCF-catalyzed reaction of Si(100) with hydride-terminated PDMS. OA and RE abbreviate oxidative addition and reductive elimination.

#### 6.4 Conclusions

This work confirms and further explores the recent reports<sup>1-3</sup> of the useful catalysis of the  $\text{Si-OH} + \text{H-Si} \rightarrow \text{Si-O-Si} + \text{H}_2$  reaction by tris(pentafluorophenyl)borane ( $\text{B}(\text{C}_6\text{F}_5)_3$ , BCF) and demonstrates that for at least certain hydridosilanes under certain conditions, BCF functions well at 2 orders of magnitude lower concentration than that used in previous reports. This is a very rapid, effective and simple surface modification procedure that should be considered along with conventional methods to functionalize silica surfaces. Indeed, this reaction offers routes to certain monolayers that are not accessible by conventional techniques. Kinetics of the modification reactions, followed by dynamic contact angle measurements of modified silicon wafer surfaces, suggest that the reaction occurs by a random covalent attachment mechanism that is reminiscent of reactions of monochlorosilanes and silica. Rapid, close-to-complete monolayer formation occurs in minutes, but complete monolayer formation, as assessed by minimization of contact angle

hysteresis, does not occur until ~2 h of reaction at room temperature. The density of attached trialkylsilanes in monolayers is lower than in monolayers prepared from trialkylchlorosilanes and this lower density permits rotational mobility that results in lower contact angle hysteresis.

BCF catalysis works very well to prepare both oligomeric and polymeric methylsiloxane monolayers and offers chemical structural control that is not possible with conventional reactive silanes. Model monolayers from  $\text{MM}^{\text{H}}$ ,  $\text{M}_2\text{MDM}^{\text{H}}$ ,  $\text{MD}^{\text{H}}\text{M}$ ,  $\text{M}_3\text{T}^{\text{H}}$  and  $\text{D}_4^{\text{H}}$  as well as numerous polymer (PDMS) monolayers from series of  $\text{MD}_n\text{M}^{\text{H}}$ ,  $\text{HMD}_n\text{M}^{\text{H}}$  and  $\text{MD}_x\text{D}_y^{\text{H}}\text{M}$  samples were prepared and studied by contact angle analysis. These surfaces provide insight into structure-wetting relationships of methylsiloxane surfaces that permit cogent arguments concerning events at 3-phase contact lines that contribute to contact angle hysteresis. In particular, well-defined polymer monolayers prepared from linear hydride-terminated PDMS exhibit decreasing contact angle hysteresis with increasing molecular weight until the thickness of the monolayer reaches ~5 nm. Above this value of molecular weight hysteresis becomes much greater. A thin, low molecular weight covalently attached PDMS film contribute to mobile 3-phase contact lines and thicker attached liquid films behave as liquids that pin contact lines.

## 6.5 References

1. Escorihuela, J.; Pujari S. P.; Zuilhof H. Organic Monolayers by  $\text{B}(\text{C}_6\text{F}_3)_3$ -Catalyzed Siloxanation of Oxidized Silicon Surfaces. *Langmuir* **2017**, *33*, 2185-2193.
2. Moitra, N.; Ichii, S.; Kamei, T.; Kanamori, K.; Zhu, Y.; Takeda, K.; Nakanishi, K.; Shimada, T. Surface Functionalization of Silica by Si-H Activation of Hydrosilanes. *J. Am. Chem. Soc.* **2014**, *136*, 11570-11573.

3. Sweetman M. J.; McInnes, S. J. P.; Vasani, R. B.; Guinan, T.; Blencowe, A.; Voelcker, N. H. Rapid, metal-free hydrosilanisation chemistry for porous silicon surface modification. *Chem. Commun.* **2015**, *51*, 10640-10643.
4. Plueddemann, E. P. *Silane Coupling Agents*, 2nd ed.; Plenum: New York, 1991.
5. Ulman, A. Formation and Structure of Self-Assembled Monolayers. *Chem. Rev.* **1996**, *96*, 1533-1554.
6. Fadeev A. Y.; McCarthy, T. J. Trialkylsilane Monolayers Covalently Attached to Silicon Surfaces: Wettability Studies Indicating that Molecular Topography Contributes to Contact Angle Hysteresis. *Langmuir* **1999**, *15*, 3759-3766.
7. Fadeev, A. Y.; McCarthy, T. J. Self-Assembly Is Not the Only Reaction Possible between Alkyltrichlorosilanes and Surfaces: Monomolecular and Oligomeric Covalently Attached Layers of Dichloro- and Trichloroalkylsilanes on Silicon. *Langmuir* **2000**, *16*, 7268-7274.
8. Maoz, R.; Sagiv, J. On the Formation and Structure of Self-Assembling Monolayers. 1. Comparative ATR-Wettability Study of Langmuir-Blodgett and Adsorbed Films on Flat Substrates and Glass Microbeads. *J. Coll. Interface Sci.* **1984**, *100*, 465-496.
9. Wasserman, S. R.; Tao, Y.-T.; Whitesides, G. M. Structure and Reactivity of Alkylsiloxane Monolayers Formed by Reaction of Alkyltrichlorosilanes on Silicon Substrates. *Langmuir* **1989**, *5*, 1074-1087.
10. Fadeev, A. Y.; McCarthy, T. J. A New Route to Covalently Attached Monolayers: Reaction of Hydrosilanes with Titanium and Other Metal Surfaces. *J. Am. Chem. Soc.* **1999**, *121*, 12184-12185.
11. Gao, L.; McCarthy, T. J. Teflon is Hydrophilic. Comments on Definitions of Hydrophobic, Shear versus Tensile Hydrophobicity, and Wettability Characterization. *Langmuir* **2008**, *24*, 9183-9188.
12. Furmidge, C. G. L. Studies at Phase Interfaces. I. The Sliding of Liquid Drops on Solid Surfaces and A Theory for Spray Retention. *J. Colloid Sci.* **1962**, *17*, 309-324.
13. Hunter, M. J.; Gordon, M. S.; Barry, A. J.; Hyde, J. F.; Heidenreich, R. D. Properties of Organopolysiloxanes on Glass. *Ind. Eng. Chem.* **1947**, *39*, 1389-1395.
14. Chae, S. S.; Oh, J. Y.; Park, J. H.; Choi, W. J.; Han, J. H.; Lee, J.-O.; Baik, H. K.; Lee, T. I. Strong Hydrophobizer: Laterally Chemisorbed Low-Molecular-Weight Polydimethylsiloxane. *Chem. Commun.* **2015**, *51*, 5844-5847.
15. Krumpfer, J. W.; McCarthy, T. J. Rediscovering Silicones: "Unreactive" Silicones React with Inorganic Surfaces. *Langmuir* **2011**, *27*, 11514-11519.
16. Chen, W.; Fadeev, A. Y.; Hsieh, M. C.; Öner, D.; Youngblood, J. McCarthy, T. J. Ultrahydrophobic and Ultralyophobic Surfaces: Some Comments and Examples. *Langmuir* **1999**, *15*, 3395-3399.
17. Lin, Y.; Wang, L. Krumpfer, J. W.; McCarthy, T. J. Hydrophobization of Inorganic Oxide Surfaces Using Dimethylsilanediol. *Langmuir* **2013**, *29*, 1329-1332.
18. Wang, L.; McCarthy, T. J. Covalently Attached Liquids: Instant Omniphobic Surfaces with Unprecedented Repellency. *Angew. Chem. Int. Ed.* **2016**, *55*, 244-248.

19. Cheng, D. F.; Urata, C.; Yagihashi, M.; Hozumi, A. A Statically Oleophilic but Dynamically Oleophobic Smooth Nonperfluorinated Surface. *Angew. Chem. Int. Ed.* **2012**, *51*, 2956-2959.
20. Cheng, D. F.; Urata, C.; Masheder, B.; Hozumi, A. A Physical Approach To Specifically Improve the Mobility of Alkane Liquid Drops. *J. Am. Chem. Soc.* **2012**, *134*, 10191-10199.
21. Chojnowski, J.; Jurjata, J.; Fortuniak, W.; Rubinsztajn, S.; Trzebicka, B. Hydride Transfer Ring-Opening Polymerization of a Cyclic Oligomethylhydrosiloxane. Route to a Polymer of Closed Multicyclic Structure. *Macromolecules* **2012**, *45*, 2654-2661.
22. Hurd, C. B. Studies on Siloxanes. I. The Specific Volume and Viscosity in Relation to Temperature and Constitution. *J. Am. Chem. Soc.* **1946**, *68*, 364-370.
23. Fox, H. W.; Taylor, P. W.; Zisman, W. A. Polyorganosiloxanes...Surface Active Properties. *Ind. Eng. Chem.* **1947**, *39*, 1401-1409.
24. Mann, E. K.; Langevin, D. Poly(dimethylsiloxane) Molecular Layers at the Surface of Water and of Aqueous Surfactant Solutions. *Langmuir* **1991**, *7*, 1112-1117.
25. Gao, L.; McCarthy, T. J. Contact Angle Hysteresis Explained. *Langmuir* **2006**, *22*, 6234-6237.

A6 Chapter 6 Data Appendix

MD<sub>n</sub>M<sup>H</sup> Characterization

Size exclusion chromatography was conducted on an Agilent 1260 GPC equipped with two PLgel Mixed-C and one PLgel Mixed-D columns (Polymer Laboratories) and a refractive index detector. Tetrahydrofuran (THF) at a flow rate of 1 mL/min was the mobile phase. Attenuated Total Reflection-Infrared spectra (FT ATR-IR) were recorded using a PerkinElmer Spectrum 100 spectrometer. NMR analysis was performed on a Bruker Avance III HD 500 MHz spectrometer in CDCl<sub>3</sub>. Number average molecular weights were calculated from <sup>1</sup>H NMR spectra by end-group analysis.

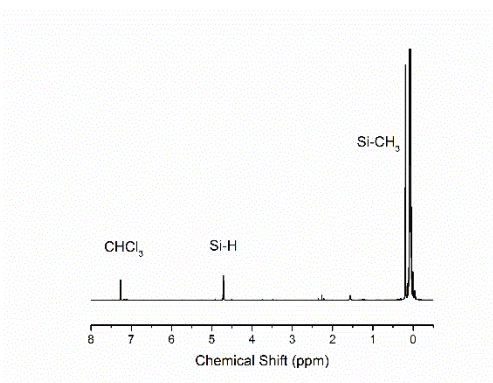


Figure A6.1: MD<sub>12</sub>M<sup>H</sup> (M=880) (GPC: Very low signal intensity did not allow analysis)

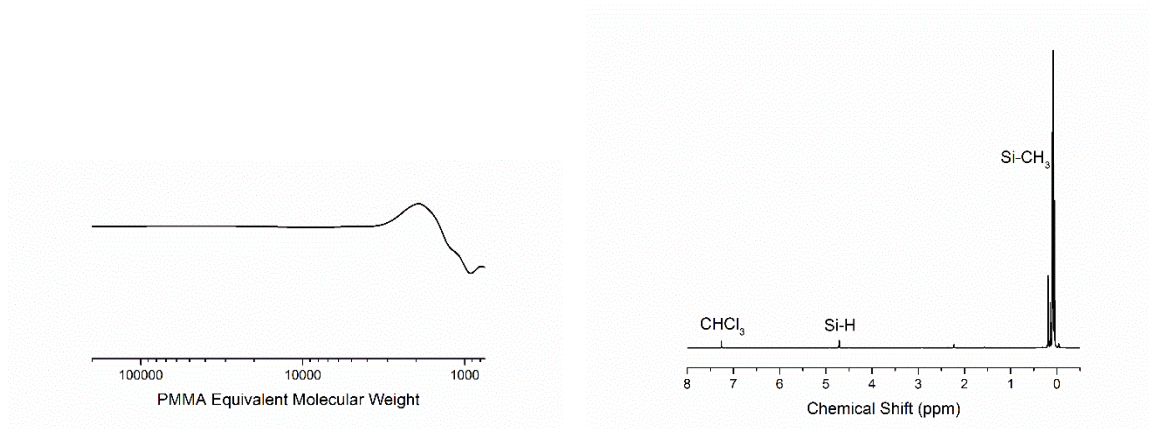


Figure A6.2: MD<sub>15</sub>M<sup>H</sup> (M=1070)



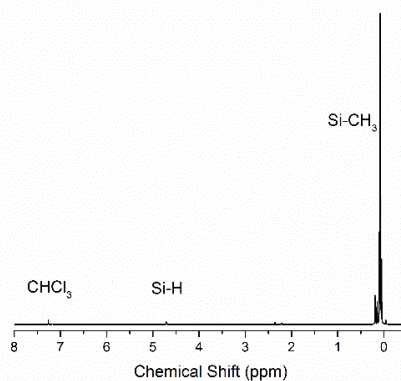
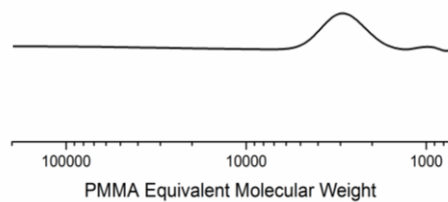


Figure A6.3:  $\text{MD}_{28}\text{M}^{\text{H}}$  ( $M=2070$ )

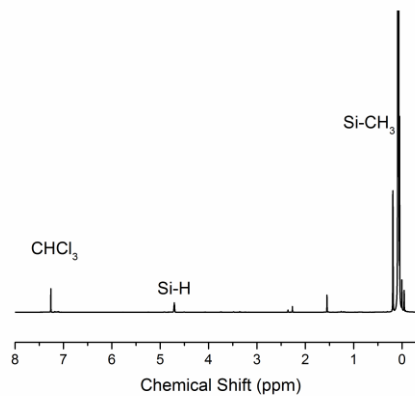
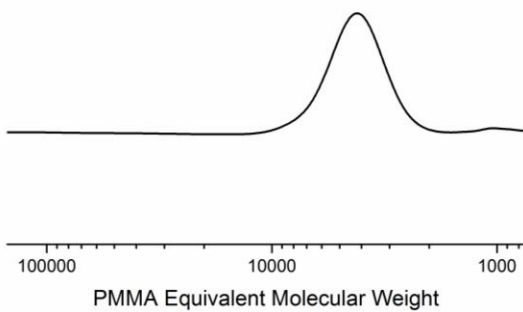


Figure A6.4:  $\text{MD}_{36}\text{M}^{\text{H}}$  ( $M=2664$ )

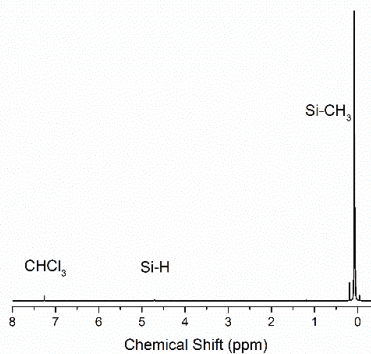
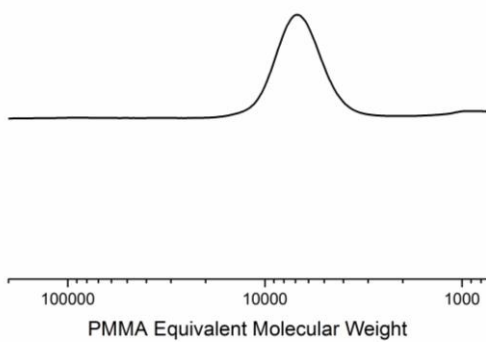


Figure A6.5:  $\text{MD}_{68}\text{M}^{\text{H}}$  ( $M=5000$ )

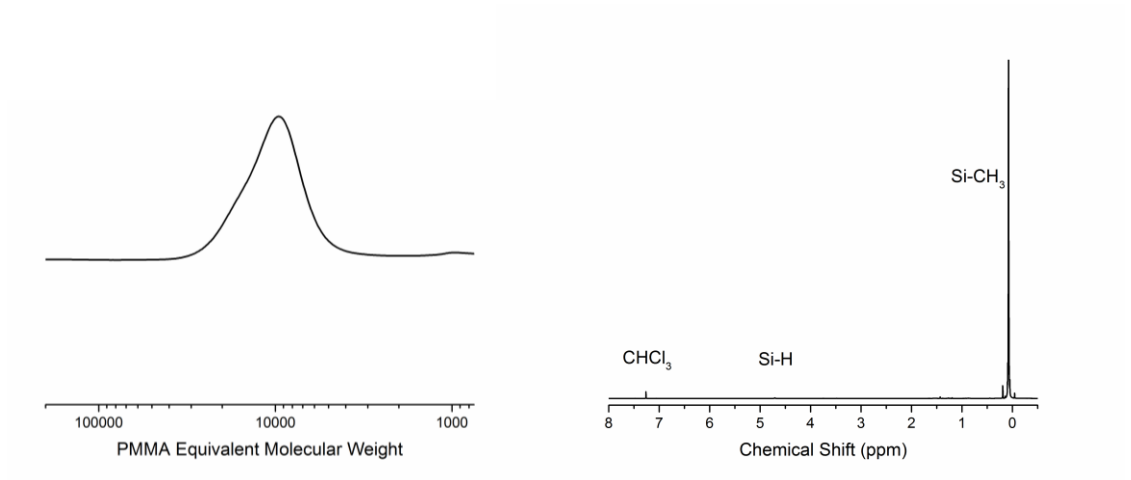


Figure A6.6: MD<sub>112</sub>M<sup>H</sup> (M=8280)

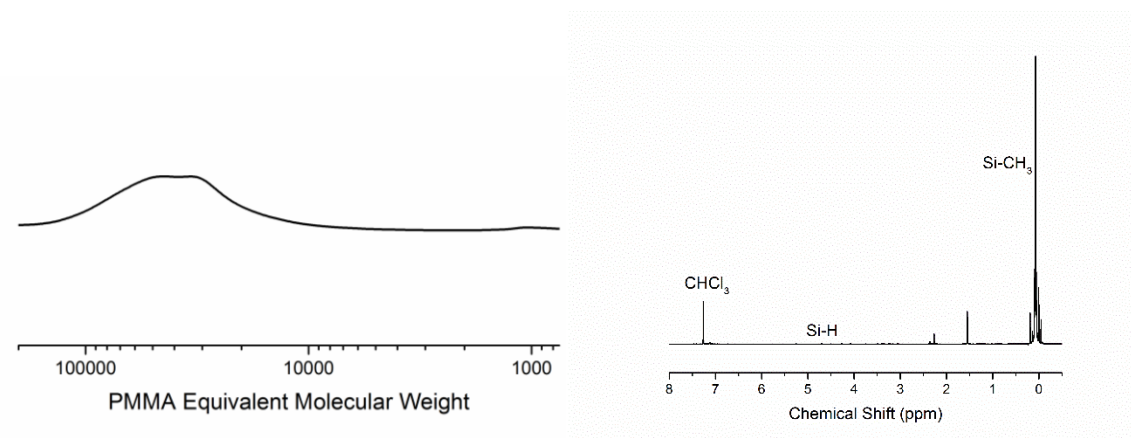


Figure A6.7: MD<sub>423</sub>M<sup>H</sup> (M=31 300)

## Infrared Spectroscopy of methylsiloxane polymers

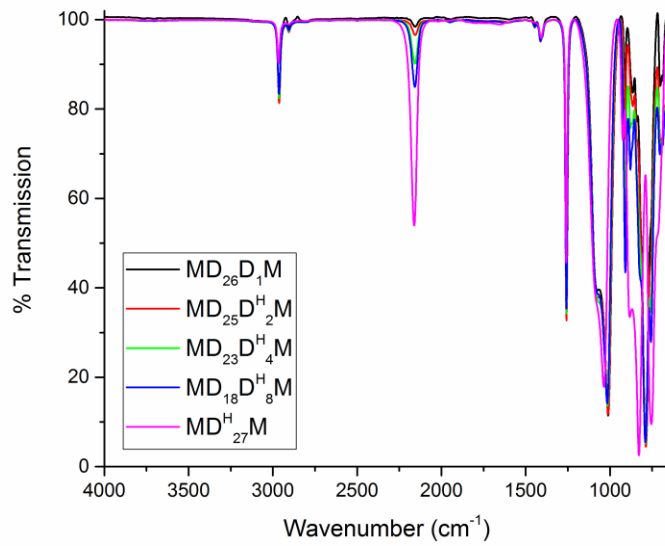


Figure A6.8: Stacked IR spectra of poly(methylhydro-co-dimethyl)siloxane (MD<sub>x</sub>D<sup>H</sup><sub>y</sub>M) random copolymers

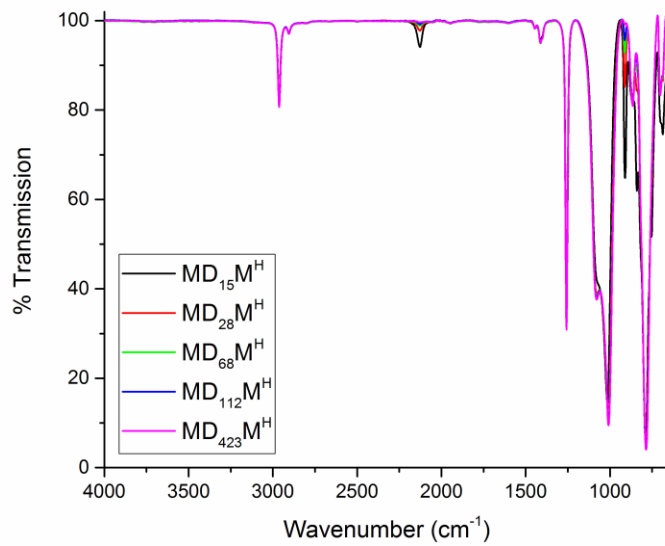


Figure A6.9: Stacked IR spectra of MD<sub>x</sub>M<sup>H</sup>

Methylsiloxane model contact angle kinetics

Table A6.1. Pentamethyldisiloxane Kinetics- Order of Addition (0.1 M Silane, 1 mol% BCF)

Order of Addition	$\theta_A$	$\theta_R$
1-Wafer 2-Toluene 3-Silane 4-Catalyst	96°	89°
1- Toluene 2- Silane 3- Catalyst 4- Wafer	91°	82°
1-Wafer 2-Toluene 3- Catalyst 4- Silane	91°	82°

Table A6.2. Pentamethyldisiloxane Kinetics- [BCF], 0.1 M Silane

Reaction Time, min	[BCF], mol%				
	0.01	0.05	0.1	0.5	1
1	50°/30°	48°/30°	74°/66°	91°/85°	96°/89°
2	91°/83°	90°/78°	94°/88°	97°/91°	
3	92°/86°	90°/79°	93°/87°	97°/86°	
5	92°/86°	95°/85°	95°/88°	97°/87°	96°/89°
10	92°/85°	93°/82°	96°/89°	98°/92°	97°/90°
15	94°/88°	93°/83°	96°/89°	99°/95°	97°/90°

Table A6.3. Pentamethyldisiloxane Kinetics- [Si-H] (0.1 mol% BCF)

Reaction Time, min	[PMDS], M		
	0.01	0.05	0.1
1	55°/32°	93°/87°	90°/82°
2	85°/80°	93°/88°	
3	80°/75°	93°/89°	
5	61°/45°	94°/88°	
10	92°/86°	95°/89°	
15	92°/87°	86°/88°	97°/90°, 98°/92°

Table A6.4. Heptamethyltrisiloxane (MDM<sup>H</sup>) Kinetics

Time, h	Thickness, Å	$\theta_A$	$\theta_R$
0.25	2.28	101°	91°
0.5	1.24	102°	95°
1	2.9	101°	97°
2	2.8	102°	99°
8	1.8	102°	98°
24	2.86	100°	96°
72	3.9	103°	98°

Table A6.5. bis(trimethylsiloxy)methylsilane (MD<sup>HM</sup>) Kinetics

Time, h	Thickness, Å	$\theta_A$	$\theta_R$
0.5	1.34	83°	72°
1		87°	79°
2		90°	79°
4		90°	79°
8		90°	81°
16		91°	82°
24	1.15	91°	81°

Table A6.6. tris(trimethylsiloxy)silane (M<sub>3</sub>T<sup>H</sup>) Kinetics

Time, h	Thickness, Å	$\theta_A$	$\theta_R$
1	4.01	63°	46°
2	3.59	64°	45°
4	4.75	65°	46°
16	5.15	66°	45°
24	6.32	73°	47°
72		72°	49°

Table A6.7. Heptamethylcyclotetrasiloxane (D<sub>4</sub><sup>1H</sup>) Kinetics

Time, min	Thickness, Å	$\theta_A$	$\theta_R$
1	3.15	65°	49°
10	3.95	84°	70°
30	3.27	82°	71°
60	3.48	83°	71°
90	3.74	82°	70°
120	3.74	83°	71°
960	3.14	84°	71°
4320	4.18	84°	71°

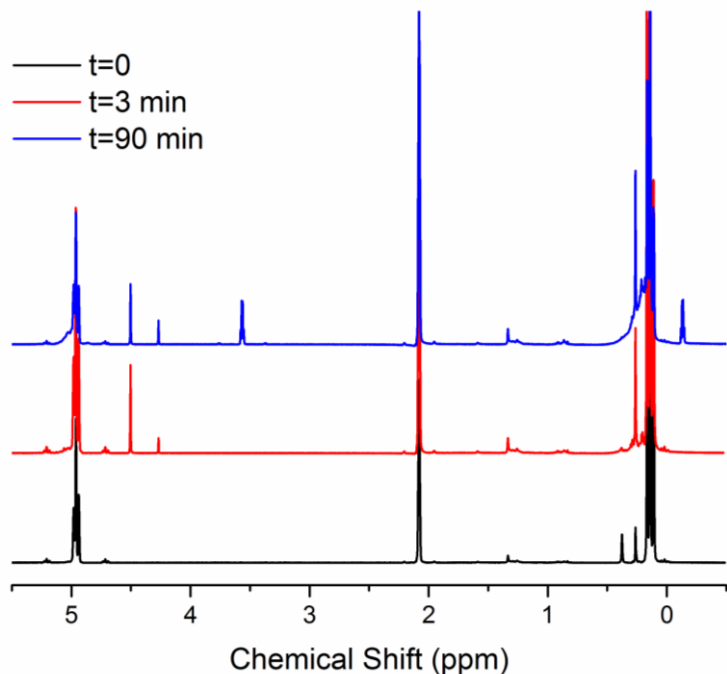


Figure A6.10.  $^1\text{H}$ NMR Kinetics of  $\text{D}_4^{\text{H}}$  (0.1 M Si-H, 0.5 mol% BCF, anhydrous toluene- $d_8$ ). Hydride transfer oligomerization is evident by the broadening of the Si- $\text{CH}_3$  peaks ( $\delta \sim 0.4$  ppm) and the appearance of the peaks at  $\delta \sim 3.5$  ppm corresponding to  $\text{CH}_3\text{SiH}_3$  byproduct.<sup>21</sup>

#### Methylsiloxane polymer surfaces and contact angle kinetics

Table A6.8.  $^{\text{H}}\text{MD}_{17}\text{M}^{\text{H}}$  ( $M_n$  1260)

Time, min	$\theta_A$	$\theta_R$	$\Delta$	Thickness, Å
1	104°	93°	11°	14.99
10	105°	100°	5°	16.18
10	104°	95°	9°	16.5
30	105°	99°	6°	16.84
60	106°	102°	4°	16.51
90	105°	101°	4°	17.51
120	105°	102°	3°	19.14
960	105°	102°	3°	13.2

Table A6.9. <sup>Bu</sup>MD<sub>20</sub>M<sup>H</sup> (M<sub>n</sub> 1450)

Time, min	$\theta_A$	$\theta_R$	$\Delta$	Thickness, Å
10	105°	102°	3°	25.5
960	107°	103°	4°	19.85
1	104°	100°	4°	26.15
10	105°	101°	4°	23.08
30	105°	101°	4°	25.26
60	106°	101°	5°	24.47
90	105°	101°	4°	26.45
120	105°	101°	4°	26.3

Table A6.10.

Solvent effects (<sup>Bu</sup>MD<sub>20</sub>M<sup>H</sup> (M=1450), 0.1 M Si-H, 0.5 mol% BCF, 2 h reactions at RT)

Solvent	$\theta_A$	$\theta_R$	Thickness, Å
Heptane	106°	104°	17.9
Hexane	105°	102°	17.4
Cyclohexane	106°	105°	16.5
Toluene	106°	103°	16.3
o-xylene	106°	104°	16.5
Ethyl Acetate	98°	81°	9.66
Chloroform	50°	33°	2.55
Methylene Chloride	105°	100°	12.5

Table A6.11. Polydimethylsiloxane graft thicknesses (t) and graft density

	Mn	N	t (nm)	chains/nm <sup>2</sup>	nm <sup>2</sup> per chain
<sup>Bu</sup> MD <sub>15</sub> M <sup>H</sup>	1080	14.6	1.35	0.70	1.42
<sup>Bu</sup> MD <sub>20</sub> M <sup>H</sup>	1450	19.6	1.54	0.60	1.67
<sup>Bu</sup> MD <sub>97</sub> M <sup>H</sup>	7150	96.7	4.47	0.36	2.75
MD <sub>15</sub> M <sup>H</sup>	1070	14.5	0.92	0.48	2.09
MD <sub>28</sub> M <sup>H</sup>	2070	28	1.74	0.48	2.07
MD <sub>68</sub> M <sup>H</sup>	5000	67.6	3.17	0.37	2.72
MD <sub>112</sub> M <sup>H</sup>	8280	111.9	3.99	0.28	3.56
MD <sub>36</sub> M <sup>H</sup>	2664	36	2.47	0.53	1.87
MD <sub>117</sub> M <sup>H</sup>	8658	117	5.09	0.34	2.92
MD <sub>423</sub> M <sup>H</sup>	31302	423	12.26	0.23	4.37
<sup>V</sup> MD <sub>53</sub> M <sup>H</sup>	3920	53	2.62	0.39	2.59
<sup>V</sup> MD <sub>270</sub> M <sup>H</sup>	19980	270	6.70	0.20	5.10
<sup>H</sup> MD <sub>10</sub> M <sup>H</sup>	740	10	0.56	0.41	2.45
<sup>H</sup> MD <sub>17</sub> M <sup>H</sup>	1260	17	1.03	0.46	2.19
<sup>H</sup> MD <sub>60</sub> M <sup>H</sup>	4440	60	2.59	0.34	2.93
<sup>H</sup> MD <sub>195</sub> M <sup>H</sup>	14000	195	5.67	0.23	4.35
<sup>H</sup> MD <sub>283</sub> M <sup>H</sup>	20960	283	8.67	0.24	4.14
MD <sub>26</sub> D <sup>H</sup> <sub>1</sub> M	2000	~27	1.39	0.41	2.47
MD <sub>25</sub> D <sup>H</sup> <sub>2</sub> M	2000	~27	1.14	0.33	3.01
MD <sub>23</sub> D <sup>H</sup> <sub>4</sub> M	2000	~27	0.88	0.26	3.90
MD <sub>18</sub> D <sup>H</sup> <sub>8</sub> M	2000	~27	0.87	0.25	3.92
MD <sup>H</sup> <sub>27</sub> M	1800	27	0.36	0.12	8.54



Table A6.12. MD<sub>26</sub>D<sup>H</sup><sub>1</sub>M kinetics

Time, min	$\theta_A$	$\theta_R$	$\Delta$	Thickness, Å
1	40°	30°	10°	4.19
10	100°	81°	19°	11.65
10	100°	83°	17°	11.81
30	102°	84°	18°	14.37
60	102°	89°	13°	10.52
60	102°	90°	12°	14.05
90	102°	89°	13°	10.09
120	103°	90°	13°	14.09
120	104°	89°	15°	13.88
120	102°	96°	6°	16.07
960	102°	89°	13°	8.39
960	104°	87°	17°	13.26
1440	104°	98°	6°	9.99
10080	103°	99°	4°	10.77

Table A6.13. MD<sub>25</sub>D<sup>H</sup><sub>2</sub>M kinetics

Time, min	$\theta_A$	$\theta_R$	$\Delta$	Thickness, Å
30	102°	90°	12°	12.46
60	103°	89°	14°	13.43
120	105°	91°	14°	11.38
120	105°	99°	6°	15.25
960	104°	88°	16°	14.26
1440	105°	99°	6°	10.07
10080	104°	99°	5°	11.69
10080	104°	99°	5°	13.18

Table A6.14. MD<sub>23</sub>D<sup>H</sup><sub>4</sub>M kinetics

Time, min	$\theta_A$	$\theta_R$	$\Delta$	Thickness, Å
30	100°	91°	9°	8.3
60	103°	93°	10°	9.6
120	103°	90°	13°	8.77
120	100°	93°	7°	9.56
960	102°	91°	11°	6.91
1440	102°	95°	7°	6.33
10080	102°	92°	10°	8.31
10080	103°	92°	11°	9.18

Table A6.15. MD<sub>18</sub>D<sup>H</sup><sub>8</sub>M kinetics

Time, min	$\theta_A$	$\theta_R$	$\Delta$	Thickness, Å
1	42°	30°	12°	3.54
10	93°	78°	15°	8.26
30	97°	84°	13°	7.69
30	102°	89°	13°	6.95
60	98°	86°	12°	8.56
60	94°	80°	14°	5.97
90	99°	85°	14°	8.51
120	98°	85°	13°	7.52
120	102°	91°	11°	7.38
120	103°	90°	13°	8.73
120	99°	91°	8°	7.11
960	98°	85°	13°	5.2
960	102°	90°	12°	6.26
1440	102°	93°	9°	4.87
10080	100°	90°	10°	5.75
10080	100°	89°	11°	7.37

Table A6.16. poly(hydromethylsiloxane) (MD<sup>H</sup><sub>27</sub>M) kinetics

Time, min	$\theta_A$	$\theta_R$	$\Delta$	Thickness, Å
1	46°	31°	15°	3.32
10	92°	77°	15°	7.28
10	91°	75°	16°	5.32
30	93°	81°	12°	4.14
30	96°	86°	10°	4.68
60	92°	79°	13°	6.9
60	96°	89°	7°	5.02
90	93°	80°	13°	4.44
120	91°	79°	12°	4.81
120	99°	86°	13°	4.86
120	98°	88°	10°	3.61
120	93°	80°	13°	9.22
960	95°	83°	12°	4.87
960	99°	79°	20°	8.95
1440	98°	88°	10°	3.42

## X-Ray Photoelectron Spectra

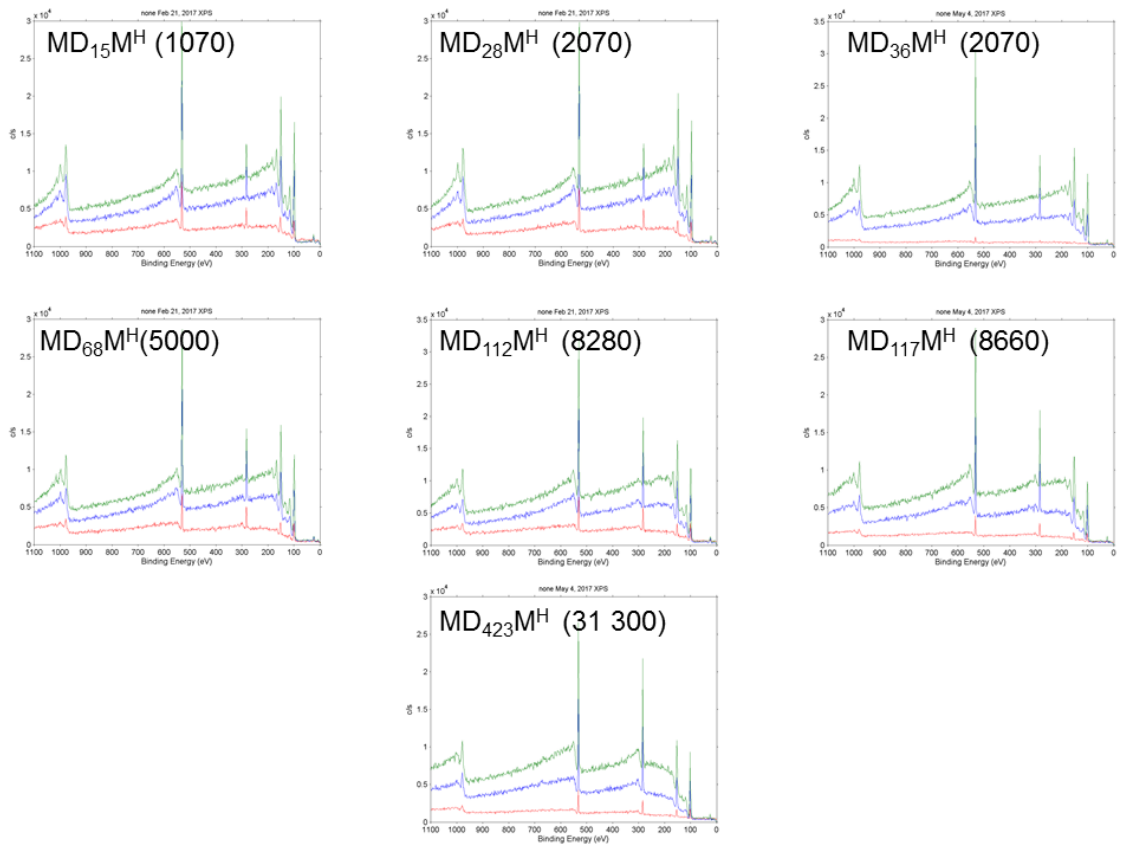


Figure A6.11. XPS Spectra of MeMD<sub>x</sub>M<sup>H</sup> grafts

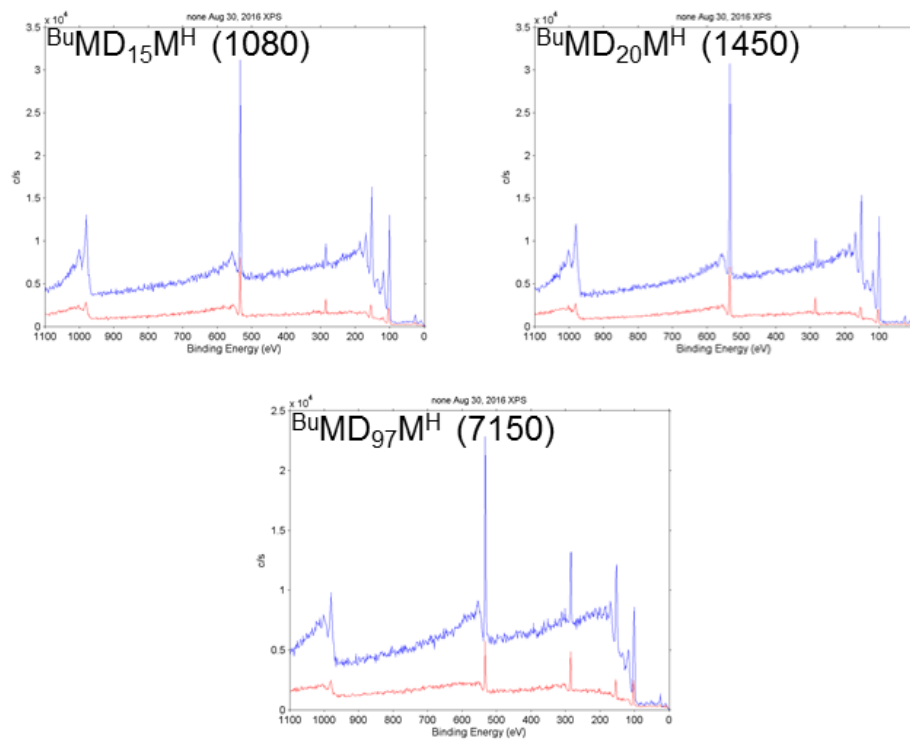


Figure A6.12. XPS Spectra of BuMD<sub>x</sub>M<sup>H</sup> grafts

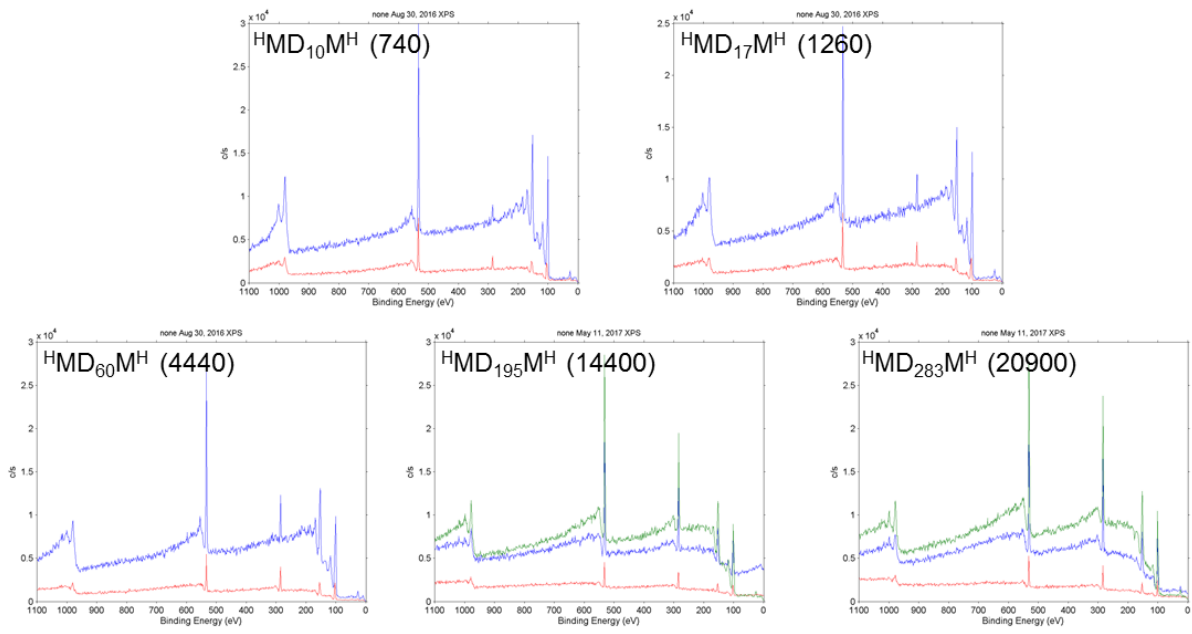


Figure A6.13. XPS Spectra of  $\text{HMD}_x\text{D}^{\text{H}}$  grafts

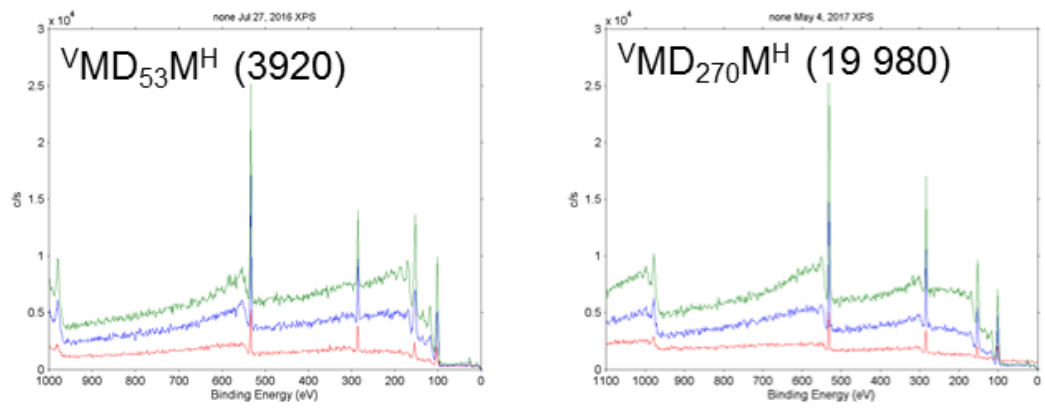


Figure A6.14. XPS Spectra of  $\text{VMD}_x\text{M}^{\text{H}}$  grafts

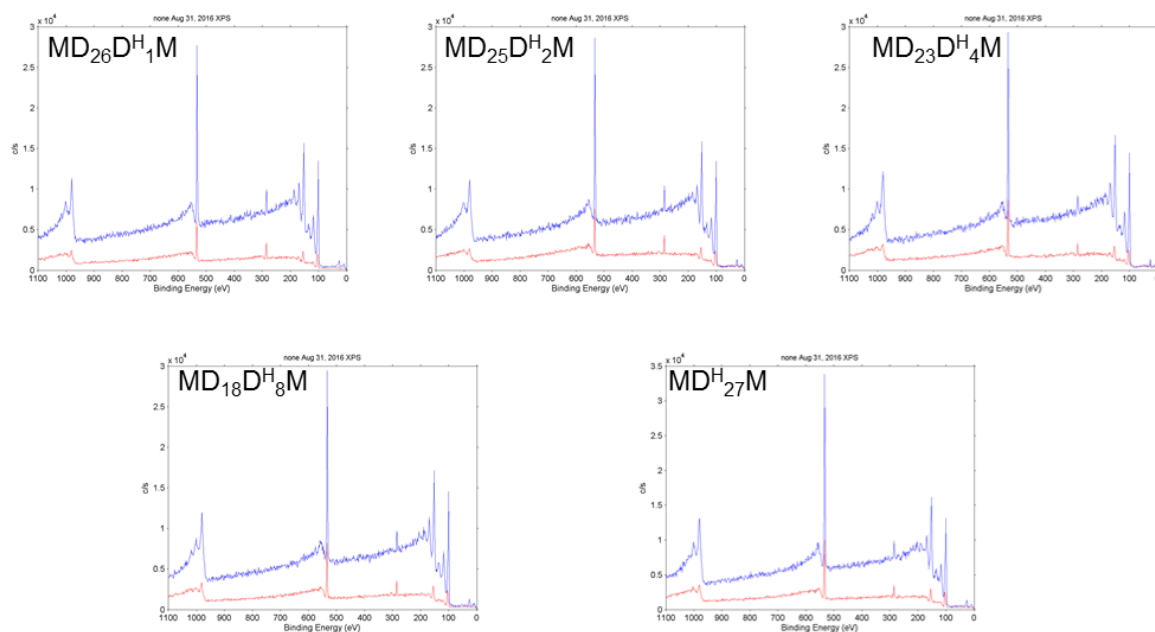


Figure A6.15. XPS Spectra of poly(hydromethyl-co-dimethyl)siloxane ( $MD_xD^H_y$ ) grafts

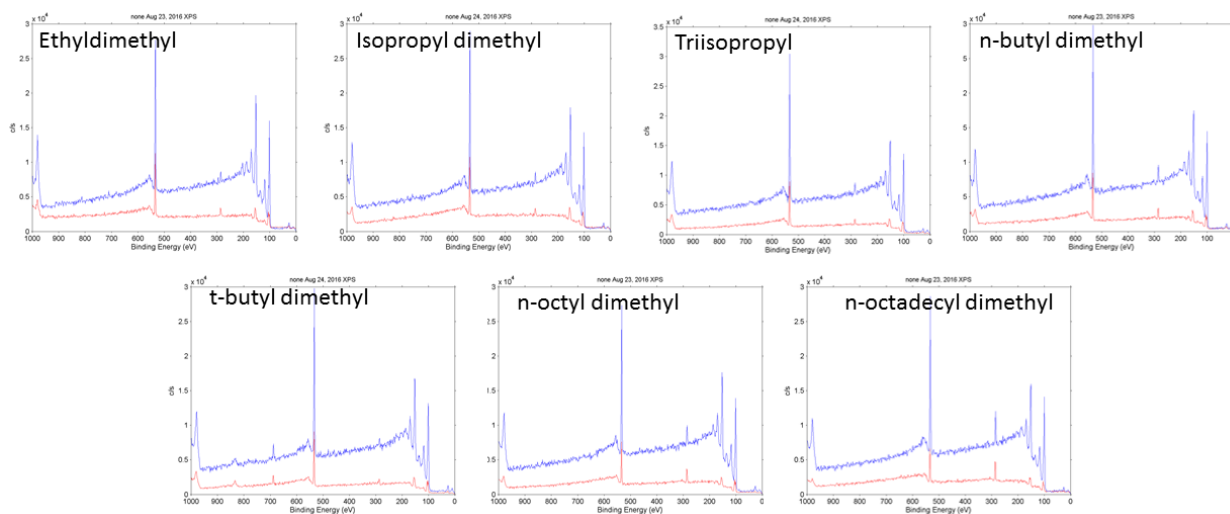
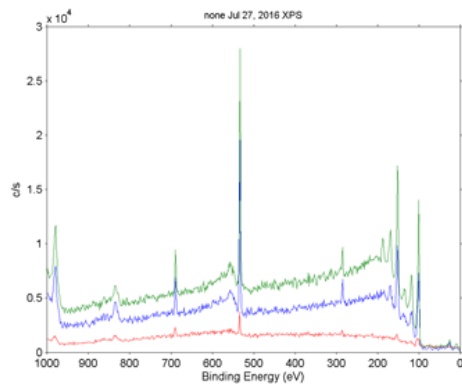
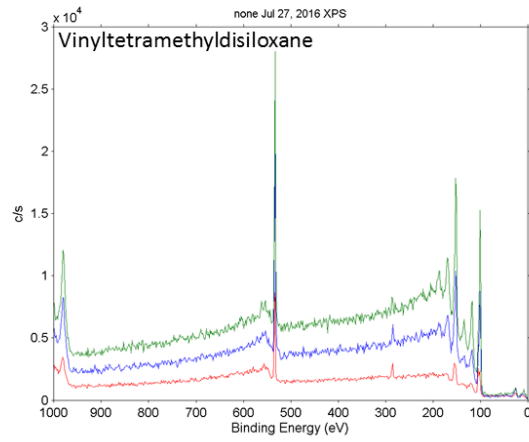
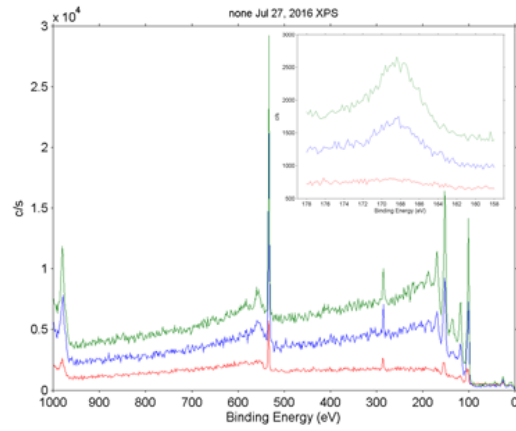


Figure A6.16. XPS Spectra of Alkyldimethylsilane grafts



Pt-catalyzed hydrosilylation of bis(nonafluorohexyl)methylsilane



Thiol-ene addition of mercaptopropionic acid

Figure A6.17. XPS Spectra of vinyl surfaces and derivatives

## CHAPTER 7

### DISCOVERING SILICONES

The insight gained over the last decade of research in the McCarthy group has established a foundation from which new silicone materials will be prepared, studied and applied. For example, developing our understanding of MQ copolymers and their synthesis through hydrolysis and condensation, has enabled us to prepare MQ-based materials and to extend MQ chemistry to the preparation of T and MT silicones. The growing toolbox of organosiloxane polymers and materials opens up numerous avenues of research (see Appendix A for an example). With each addition to the silicone family, more questions regarding silicone chemistry, physics and engineering will need addressing. In this final chapter, I would like to discuss open questions and opportunities that relate to the work in this thesis.

#### 7.1 MQ Silicones

One of my primary objectives when starting work on MQ copolymers did not involve their synthesis or interfacial activity. In fact, I wrongly assumed that the preparation of MQ would be the easy part. Instead, my interest in MQ was in its physical structure. There are no open literature reports that give an absolute molecular weight or a radius of gyration for any MQ. Static light scattering seemed like the answer but trimethylsilyl-terminated MQ copolymers had inadequate contrast in all the solvents I tried. These challenges were discussed in Chapter 2. To overcome this problem in the future, one could incorporate phenyl groups to increase the refractive index of the MQ and provide scattering contrast. Studying the scattering of MQ copolymers would provide an absolute weight average molecular weight, a radius of gyration and the second virial coefficient. Comparisons of the radius of gyration to the hydrodynamic radius will provide insight into



the physical shape of MQ in solution. One other experiment that would provide a number average absolute molecular weight is osmotic pressure measurements, but there are currently no membrane osmometers at UMass. Having an absolute molecular weight and a full understanding of the solvated shape of MQ can allow more complete chemistry-structure-property relationships to be developed.

At interfaces there are a few studies remaining that would best be carried out by fractionating a highly disperse MQ. Once well-defined fractions had been collected in adequate yield, the studies at the Air-Water and Oil-Water interfaces should be repeated to eliminate any complications from polydispersity in molecular weight; although dispersity in structure, M:Q ratio and silanol content will persist. At the Air-Water interface, studying fractions of MQ would provide a precise transition from soft, collapsing monolayers to rigid, elastic monolayers. Studying MQ at the Air-Water interface would also be aided by using Brewster Angle Microscopy to visualize the structure of MQ monolayers. At the Oil-Water interface, determination of the critical concentration, maximal reduction in interfacial tension, and kinetics of surface tension reduction at each molecular weight would grant useful structure-property relations for MQ surfactants.

Beyond fundamental studies of the molecular characteristics of MQ there are a variety of studies that can be done on MQ materials and composites. Preparation of MQ-PDMS composites is one direction. The most appropriate method for studying these composites would be rheology. First, the relationship between MQ molecular weight and loading on viscoelasticity in composite fluids would be investigated. From there, the effect of PDMS matrix molecular weight would need to be tested. Finally, the effects of the same MQ-PDMS composites should be tested in a cured state. MQ has been shown to be a plasticizer and a reinforcer in PDMS fluids depending on the molecular weights of the MQ

and the PDMS. This was shown in Dow Corning MQ1600 fractions in PDMS. How do the MQ copolymers prepared with the method presented in Chapter 2 compare? How do the properties of the uncured fluid compare to the cured elastomer? I hypothesize that an advantage of MQ formulations is their ability to plasticize a melt and reinforce in a cured state, but this hypothesis requires testing.

Similar to the above experiments, MQ pressure sensitive adhesives (PSAs) can be investigated. This would again be studied mainly by rheology, but would also involve tack and adhesion measurements. Typical formulations of MQ PSAs involve silanol-containing MQ and silanol-terminated PDMS that will condense at high temperature or with addition of catalyst. Other methods use hydrosilylation reactions to accomplish the same. The preparation of PSAs is an art and at this moment we have no experience in the formulation of such materials. This would be a challenging direction but would provide fruitful research opportunities. The ability to tailor MQ properties and chemistry would lead to an infinite number of PSA compositions. This could open up additional avenues to other silicone-based PSAs; for example, PSAs that contain no problematic D units.

Our group has pursued the creation of 'PDMS' elastomers containing no D units. This is an obvious goal to any silicones chemist since D units in PDMS form an equilibrium concentration of cyclic oligomers that will leach out during a product's lifetime. This is an issue in 'PDMS' elastomers used for contact printing, imprint lithography and electronics. D units are also responsible for hydrophobic recovery of hydrophilic silicones. MQ copolymers could be a useful component in a formulation of PDMS with no D.

Extensions of MQ chemistry are being carried out by Dr. Pei Bain. His work on T and MT silicones is leading to the creation of new silicone materials in our labs. Of

additional interest is the preparation of MQ' materials where Q' is some other metal oxide. Such MQ' materials may include titanium, boron or aluminum. Some preliminary studies using titanium isopropoxide were started but not pursued. I believe a route through  $\text{Ti}(\text{acac})_2$  is promising but complete removal of acac ligands was difficult.

## 7.2 Silicone-Carbon Nanotube Composites

Silicone-carbon nanotube composites have interesting opportunities for fundamental and applied research. On the applied side, making functional composites that address specific needs/requirements is going to require well defined performance metrics and objectives that can be addressed with materials engineering. Until goals are established, it will be impossible to design and optimize composites. Currently, much of the work involves adding CNTs to silicones and seeing what happens. This fundamental work is required to understand the Silicone-CNT materials system but does not necessarily result in applicable outcomes.

Two fundamental questions regarding Silicone-CNT composites stand out to me. One involves optimizing the balance between dispersion and material properties by incorporating phenyl groups into PDMS. At what phenyl substituent concentration do copolymers achieve improved dispersions over PDMS with the most PDMS-like properties? PDMS is special even for silicones and many applications call specifically for its properties. By minimizing phenyl substitution, the properties of the polymer should be changed only slightly while maximizing dispersion quality. The second question involves polymer dynamics in CNT composites. I have hypothesized that the dynamics of PDMS chains and network strands is constrained by a CNT network. The rheology supports this but was done in a narrow range of frequencies at room temperature. Additional experiments would provide deeper insights. These could include multiple quantum NMR,

low field NMR, differential scanning calorimetry (DSC) and expanding the frequency range in rheological experiments by time-temperature superposition (TTSP). All could in principle be set up here at UMass, although DSC and TTSP would require some changes and improvements to current instrumentation. These experiments would directly show how chain mobility and dynamics at different length scales (segmental to whole chain) are effected by the CNT filler.

### 7.3 Tris(pentafluorophenyl)borane-catalyzed modifications of silanols

There is much to be done regarding the  $B(C_6F_5)_3$ -catalyzed modification of silica presented in Chapter 6. Investigating solvent effects, temperature effects and precise kinetic studies are warranted. Mixed and functional monolayers are open for further investigation. The  $D_4^H$  surface should also be investigated in a thorough, multivariable manner. I suspect it will provide a technique to engineer surfaces of dramatically different properties by changing the reaction conditions (concentration, solvent, time, temperature, etc.) but using only one reagent. The structural complexity of the  $D_4^H$  surfaces invites academic consideration. Fundamentally, this reaction has been studied very little in comparison to chlorosilane and alkoxy silane modifications, so there is much to be done before our understanding of BCF-catalyzed monolayer formation catches up.

Practically, there is the question of scaling this reaction to modify silica which would mean optimizing and engineering a new reaction system. The application of this method as a replacement or substitute for traditional modification methods requires investigation in a more applied sense. This would involve demonstrating not only feasibility but performance.

#### 7.4 Discovering Silicones

Work along the lines of rediscovering silicones must continue to be pursued. These objectives have not only reminded the scientific community of silicones but have also provided the scientific community with new insights into silicones. However, now is the time to discover silicones. The process of discovery is certainly more challenging but the silicone alphabet offers an infinite number of possibilities. In my opinion, the future of silicones involves developing chemistries that allow control over the placement of M, D, T and Q units. Precisely structured silicones can then be engineered for specific properties. Creating a toolbox of silicones will enable materials scientists to tackle challenges were carbon-based polymers and current silicone materials fail.

Silicone tell a unique story of industrial research and development. They are a material class that was invented for a specific need, but through dedicated science became much more. Throughout their history, silicones have been technology enablers and this will continue due to their special properties and excellent performance in environments and applications where other materials fail. There is an exciting future in silicone materials for industry and academics. I am glad to have made a contribution to the story of silicones.

## APPENDIX A

### SULFOLANE-FUNCTIONALIZED SILICONES FOR LITHIUM ION CONDUCTION

#### A.1 Introduction

There are a variety of functional silicone polymers, all with useful properties inherited from the organic groups which are incorporated as side chains, end groups or as a part backbone.<sup>1</sup> Hybrid organic-inorganic silicones are often utilized to create materials which take advantage of each component's properties. To see the variety of commercially available functional silicones, one has to look no further than the Gelest catalog,<sup>2</sup> which contains amine, epoxy, methacrylate, mercapto, isocyanate, fluoro, ethylene oxide, cyanopropyl, N-pyrrolidonepropyl, and many other functional silicone polymers. Perhaps the greatest advantage of the attachment of organic compounds onto a linear silicone is the mobility that the siloxane backbone grants. At all molecular weights, linear PDMS is a fluid ( $T_g \approx -125$  °C) which argues that organic groups attached to the siloxane backbone have liquid-like mobility.

Of all the various functional groups that have been attached to silicones, sulfones are rare; there are only a few examples of sulfone containing silicones in patent literature.<sup>3-5</sup> I am interested in adding sulfolane, the most abundant sulfone, to silicones to study its properties and application as a lithium ion conducting polymer.

#### A.1.1 Polymer Electrolytes and Ion Conductors

We use lithium ion batteries everyday in our laptops, phones and portable electronic devices. As the need for energy storage increases, we need to continue developing cheap, efficient, and safe battery technologies. Current lithium battery technology is based on a 1991 Sony patent<sup>6</sup> and consists of a graphitic carbon anode and

a lithium metal cathode separated by a liquid electrolyte. There are five general classifications for electrolytes: (I) classical electrolytes that are small molecule solvents, (II) gel electrolytes that are polymer networks swollen by a classical electrolyte, (III) dry polymer electrolytes that are polymer without solvent, (IV) dry single-ion conductors where one ion is bound to the polymer and (V) solvated single-ion conductors where a single-ion conducting polymer is mixed with solvent.<sup>7</sup> Before discussing specific polymer-based electrolytes, it is important to first discuss ion transport in polymers.

The transport of ions in polymer electrolytes is characterized by three transport properties: conductivity( $\sigma$ ), salt diffusion coefficient ( $D$ ) and cation transference number ( $t^+$ ).<sup>7,8</sup> These quantities are measured for a given electrolyte via impedance spectroscopy, diffusion experiments (either NMR based or bulk diffusion measurements) and electrochemical current-interrupt and open circuit potential measurements. These properties can be measured to predict the performance of an electrolyte in a battery. Alternatively, one can prepare an actual battery using coin cells and test performance directly.<sup>9</sup> The mechanisms of salt diffusion depends on molecular weight and can either be dominated by segmental motions or whole polymer diffusion. Whole polymer diffusion mechanisms are only observed for very low molecular weight polymers, therefore segmental dynamics are often targeted to increase salt diffusion in high polymers.<sup>10</sup> Cation transference number refers to the ratio of charge transported by lithium cation compared to the total charge transported and is effected by the salt dissociation in the electrolyte.

Reference 7 includes transport properties for examples of each type of electrolyte. The highest performing polymer electrolytes are gel-type (type II) and solvated single-ion conductors (type V). There is currently interest in removing classical electrolytes and small molecules from batteries and thus moving toward dry systems. These dry solids systems

have advantages in cost, processability and safety. Dry solid polymer electrolytes (type III) based on poly(ethyleneoxide) (PEO) have found commercial use.<sup>11,12</sup> However, these electrolytes require elevated operating temperatures to achieve adequate conductivity due to their high crystallinity and low cation transference number. To overcome these obstacles, researchers have attached PEO side chains to siloxane backbones<sup>11,13</sup> or fabricated networks from PDMS and PEO.<sup>14</sup> In these systems, the flexibility of PDMS is utilized to lower  $T_g$  and facilitate segmental motions for better ion conduction. Dry single-ion conducting polymer electrolytes (type IV) have not yet attained the conductivity values of other polymer electrolytes but research into this class of electrolyte is ongoing. In a similar manner to dry polymer electrolytes, siloxanes are being used to improve the performance of single-ion conducting polymers and extensive work has been done by Colby and coworkers to design a materials system based on siloxane copolymers.<sup>15-17</sup> This system is based on siloxane backbones with pendant borates which weakly bind lithium ions and cyclic carbonate side chains which increase the dielectric constant of the polymer to reduce ion interactions.<sup>15</sup> While these copolymers alone did not have high conductivities ( $\sigma \approx 10^{-7}$  S/cm @ 25°C), oligomeric siloxane plasticizers with carbonate and PEO pendant groups were shown to improve performance ( $\sigma \approx 5 \cdot 10^{-7}$  S/cm @ 20°C).<sup>16</sup> Challenges of this system are the dramatic increase in  $T_g$  with increasing carbonate content and phase separation of perfluorophenyl borate pendant groups.

#### A.1.2 Sulfolane

Sulfur has an interesting role in organic chemistry due to its many oxidation states.<sup>18</sup> Sulfones are the most oxidized form of sulfides and possess interesting chemical and physical properties.<sup>19</sup> Sulfolane is the most abundant sulfone small molecule due to its extensive use in separations of aromatic compounds from crude hydrocarbon



mixtures.<sup>20,21</sup> It is synthesized by the hydrogenation of sulfolene using Raney Ni catalyst. Sulfolene is prepared by the reaction of butadiene with sulfur dioxide.

Sulfolane is a useful solvent for a wide range of reactions<sup>22</sup> and as an electrolyte for high voltage lithium batteries.<sup>23,24</sup> The advantageous properties of sulfolane as a solvent come from its high temperature stability, its inertness toward acid, base, and oxidation, its high boiling point, and its polarity. As an electrolyte, sulfolane is able to solubilize lithium salts and has a high dielectric constant. When mixed with dimethylsulfite as cosolvent, sulfolane electrolytes can be prepared with oxidation potentials >5V and conductivities around 3 mS/cm.<sup>24</sup> One notable disadvantage of sulfolane is its high toxicity, however its low skin penetration limits its harm.<sup>22</sup> Table A.1 compares the properties of sulfolane to other dipolar aprotic solvents. Sulfolane is attractive not only for its advantageous properties but also because of its abundance and low cost.

Very little research in polymer science has been devoted to sulfolane. It has been used as a solvent in ATRP<sup>25</sup> and in cationic ring opening polymerizations.<sup>26</sup> Additionally, it has received interest as a solvent in gel type polymer electrolytes.<sup>27</sup> Recent research in the McCarthy group incorporated sulfolane into methacrylate polymers.<sup>28</sup> These homopolymers had a glass transition ( $T_g$ ) of 183°C, significantly greater than ~105°C of poly(methylmethacrylate).<sup>29</sup> Films of these polymers showed both good hydrophilicity and oleophilicity in comparison to methyl and ethyl sulfone methacrylate polymers. Incorporation of sulfolane into polymers has not been thoroughly explored and any progress in this field would lead to new polymers which may exhibit useful solubility or conductivity.

Table A.1: Physical properties of sulfolane and four related, commonly used dipolar aprotic solvents<sup>22,30</sup>

Property	Sulfolane	Ethylene Carbonate	Dimethyl sulfoxide	N-methyl-2-pyrrolidone	Dimethyl-formamide
Boiling Point (°C)	287.3	243.0	189.1	201.9	153.1
Relative Permittivity	43.4 (30°C)	90.5 (40°C)	46.7 (25°C)	32.2 (25°C)	36.7 (25°C)
Dipole Moment	4.69	4.81	3.96	4.09	3.8
Viscosity	10.35		2	1.67	0.9
Flash Point(°C)	177	150	89	86	58
Autoignition Point (°C)	528	465	302	270	445
Vapor Pressure (kPa)	0.0091 (30°C)		0.06 (25°C)	0.05 (25°C)	0.37 (25°C)

### A.1.3 Objective

Methyl silicones have a low dielectric constant and are unable to dissolve lithium salts. Poly(dimethylsiloxane-co-ethylene oxide) polymers were first shown to dissolve and conduct lithium perchlorate by Nagaoka et.al.<sup>31</sup> Other solubilizing modifications including carbonate and carbamate pendant groups have been demonstrated since.<sup>32-34</sup> The performance of PEO-PDMS copolymers, or PDMS containing PEO side chains, is limited by their inability to effectively dissociate lithium salts. PDMS containing carbonate pendant groups made a silicone with the highest dielectric constant known ( $\epsilon=44$ ), however this polymer was a poor conductor due to the restricted mobility and strong dipole-dipole interactions of the carbonate groups.<sup>32</sup> The best performing siloxanes electrolytes contain both PEO and carbonate side chains.<sup>34</sup> Incorporating sulfolane as a solubilizing and lithium conducting functional group onto a siloxane has not been investigated. Sulfolane has a lower dielectric constant and lower dipole moment than ethylene carbonate and has

shown promise as a classical lithium electrolyte. Attaching sulfolane to the PDMS backbone can enable the silicone to dissociate the lithium salts and allow conduction without overly restricting the motion of the polymer from pendant group dipole-dipole interactions (as occurs in more polar carbonates pendant groups). The high mobility of the siloxane backbone will aid lithium conduction by segmental motion mechanisms. Taken together, this new class of sulfone-containing silicones has promise for polymer electrolyte applications.

I have incorporated sulfolane into siloxane backbones as pendant groups. I hope, but have not determined, that addition of sulfolane onto silicone will allow the polymer to dissolve lithium salts to make a dry polymer electrolyte. I believe that the versatility of silicone chemistry means that these polymers could be prepared as high molecular weight liquid electrolytes or as solid electrolytes.

## A.2 Results and Discussion

The most common method of functionalizing silicones is through hydrosilylation reactions of hydrosiloxanes and unsaturated organic molecules.<sup>13,15,35,36</sup> Pentamethyldisiloxane (<sup>1</sup>HMM) is a useful substrate to study hydrosilylation reactions due to its low cost and volatility (easing removal of excess/unreacted reagent). Hydrosilylation of <sup>1</sup>HMM and sulfolene was attempted using 2-5 excesses of <sup>1</sup>HMM. Platinum and radical catalysis was attempted but no reaction occurred. A search of chemical abstracts shows no radical reactions with sulfolene and no hydrogenation reactions of sulfolene outside of that catalyzed by Rainey Ni to produce sulfolane.

The lack of reactivity of the sulfolene meant that a different unsaturated sulfolene substrate would need to be synthesized. Luckily, the synthesis of allyloxysulfolene (Figure A.1)

is simple: 1 EQ sulfolene is cooled to 0 °C in a round bottom flask. 0.1 EQ Potassium Hydroxide is dissolved into 2 EQ Allyl alcohol which is cooled to 0 °C and added to the sulfolene. The mixture is warmed to room temperature. After 24 hours, the reaction is neutralized with hydrochloric acid. Allyloxysulfolane is purified by column chromatography (3:1 Hexanes:Acetone). The pure product is a clear viscous liquid. Yield: 95+ %.  $^1\text{H}$  NMR (500 MHz,  $\text{CDCl}_3$ ):  $\delta$  (ppm) = 2.34 (s, 2H), 3.01 (m, 1H), 3.14 (m, 1H), 3.21 (m, 2H), 3.97 (s, 2H), 4.30 (s, 1H), 5.17-5.19 (d, 1H), 5.25-5.27 (d, 1H), 5.77-5.89 (m, 1H).  $^{13}\text{C}$  NMR (500 MHz,  $\text{CDCl}_3$ ):  $\delta$  (ppm) = 29.0, 49.5, 56.4, 69.9, 73.9, 117.7, 133.5.

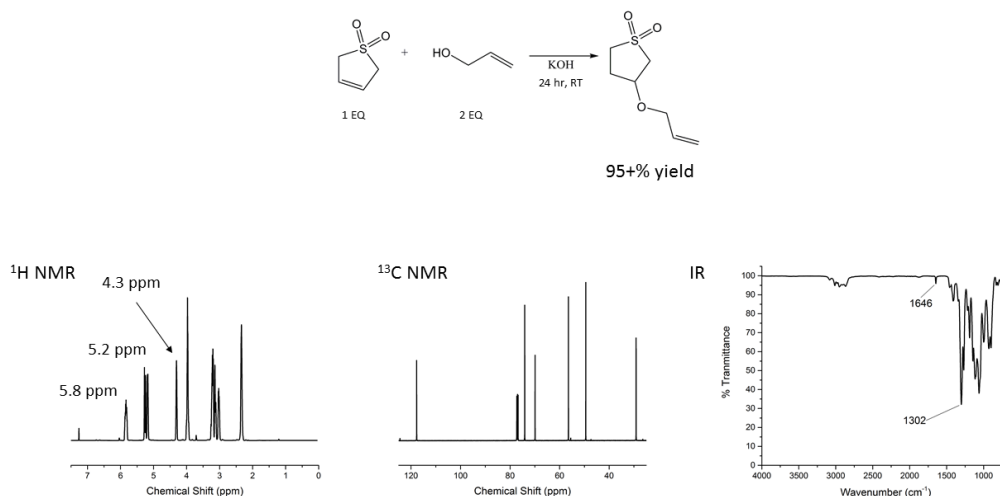


Figure A.1. Preparation and characterization of allyloxysulfolane

Hydrosilylation of allyloxysulfolane (AS) with  $^{\text{H}}\text{MM}$  was successful as shown by the disappearance of allyl protons in  $^1\text{H}$  NMR. Reactions of excess  $^{\text{H}}\text{MM}$  (1.1-2 EQ) were run in toluene solutions at 60 °C for 4 hours using 20 ppm Karstedt's catalyst (Gelest, 2% Pt in xylene). Figure A.2 shows  $^1\text{H}$  NMR and IR characterization. The product, propoxysulfolane-pentamethyldisiloxane ( $^{\text{POS}}\text{MM}$ ), was a clear, viscous liquid.  $^1\text{H}$  NMR

(500 MHz, CDCl<sub>3</sub>):  $\delta$  (ppm) = 0.062 (s, 15H), 0.49 (m, 2H), 1.58 (m, 2H), 2.37 (m, 2), 3.05 (m, 1H), 3.13-3.19 (m, 1H), 3.21-3.31 (m, 2H), 3.39 (m, 2H), **4.26** (m, 1H).

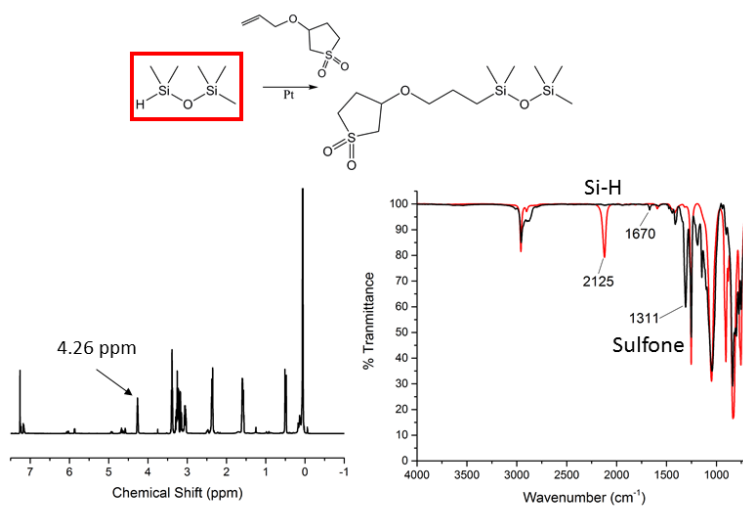


Figure A.2. <sup>1</sup>H NMR and IR of <sup>H</sup>M<sub>27</sub>AS Pt-catalyzed hydrosilylation product, <sup>POS</sup>M<sub>27</sub>

Having determined successful conditions for the Pt-catalyzed hydrosilylation of <sup>H</sup>M<sub>27</sub> and AS, I next began to prepare propoxysulfonate (POS) grafts on methylsiloxane polymers using AS. Six methylsiloxane polymers were modified: <sup>H</sup>MD<sub>50</sub>M<sup>H</sup> (Gelest DMS-Hm15), MD<sup>H</sup><sub>27</sub>M (Gelest HMS-991), and MD<sub>x</sub>D<sup>H</sup><sub>y</sub>M (Gelest HMS – 031 (y=1), 071 (y=2), 151 (y=4) and 301 (y=8), x+y = 27). Figure A.3 shows the three target methylsiloxane polymers

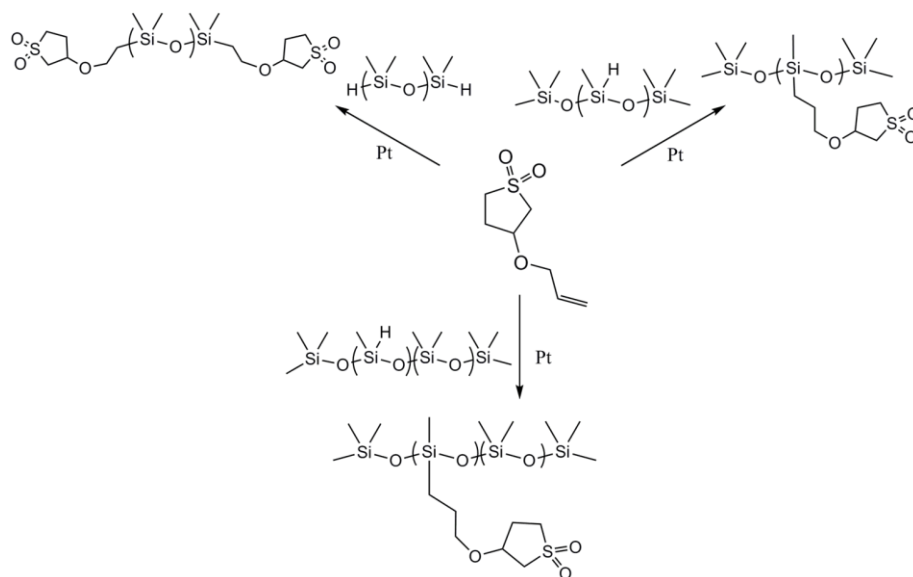


Figure A.3. Target propoxysulfolane-methylsiloxane polymers

The modification of  ${}^{\text{H}}\text{MD}_{50}\text{M}^{\text{H}}$  proceeds smoothly with 2 EQ of AS and 20 ppm Pt as shown by the disappearance of Si-H and allyl protons in  ${}^1\text{H}$  NMR (Figure A.4). To ensure complete end-capping reaction in the polymer sample, reactions were run at  $60\text{ }^{\circ}\text{C}$  for 16 hours. The work up procedure is important for obtaining pure product. First, Pt residue is removed by stirring over activated carbon for 1 hour. Following filtration, the toluene-siloxane solution is rinsed 5x with water to remove excess AS. If the solution is not rinsed, residual AS will be present. The toluene-siloxane solution is dried over magnesium sulfate, filtered and stripped by rotary evaporation.  ${}^1\text{H}$  NMR shows no signs of residual Si-H or AS and the appearance of a peak at  $\delta = 4.26\text{ ppm}$ .

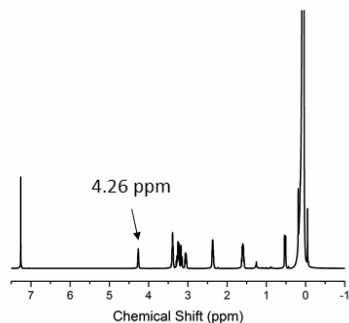


Figure A.4.  $^1\text{H}$  NMR of propoxysulfone-terminated PDMS,  $^{\text{POS}}\text{MDM}^{\text{POS}}$

Hydrosilylation of  $\text{MD}_{27}^{\text{H}}\text{M}$  polymers was unsuccessful and in all cases led to the formation of insoluble gels and solids.

$\text{MD}_x\text{D}_y^{\text{H}}\text{M}$  polymers could be modified but with low efficiency. Reaction conditions that yielded the greatest grafting efficiency were 2 EQ AS and 20 ppm Pt carried out at 80 °C for 72 hours. These conditions yielded modifications of 38%, 48%, 65% and 78% for  $\text{MD}_{26}\text{D}_1^{\text{H}}\text{M}$ ,  $\text{MD}_{25}\text{D}_2^{\text{H}}\text{M}$ ,  $\text{MD}_{23}\text{D}_4^{\text{H}}\text{M}$  and  $\text{MD}_{19}\text{D}_8^{\text{H}}\text{M}$ , respectively. Figure A.5 exhibits  $^1\text{H}$  NMR for the purified polymers that shows residual Si-H signals at  $\delta = 4.7$  ppm and grafting signals at  $\delta = 4.27$  ppm. The ratio of these was used to determine yield. IR shows residual Si-H at  $2155\text{ cm}^{-1}$  and grafted sulfone at  $1312\text{ cm}^{-1}$ . GPC also showed a broadening in molecular weight for the  $\text{MD}_{19}\text{D}_8^{\text{H}}\text{M}$  polymer indicating coupling of polymers through condensation side reactions. The aqueous rinsing procedure used to purify the  $^{\text{H}}\text{MDM}^{\text{H}}$  polymers was also important in the purification of these polymers as shown in Figure A.6. The AS proton at  $\delta = 4.34$  ppm is eliminated after rinsing. As POS content in the methylsiloxane polymers increases, separation of the organic and aqueous phases became more difficult due to the formation of emulsions. This suggests that the polar sulfone groups are providing amphiphilic character.

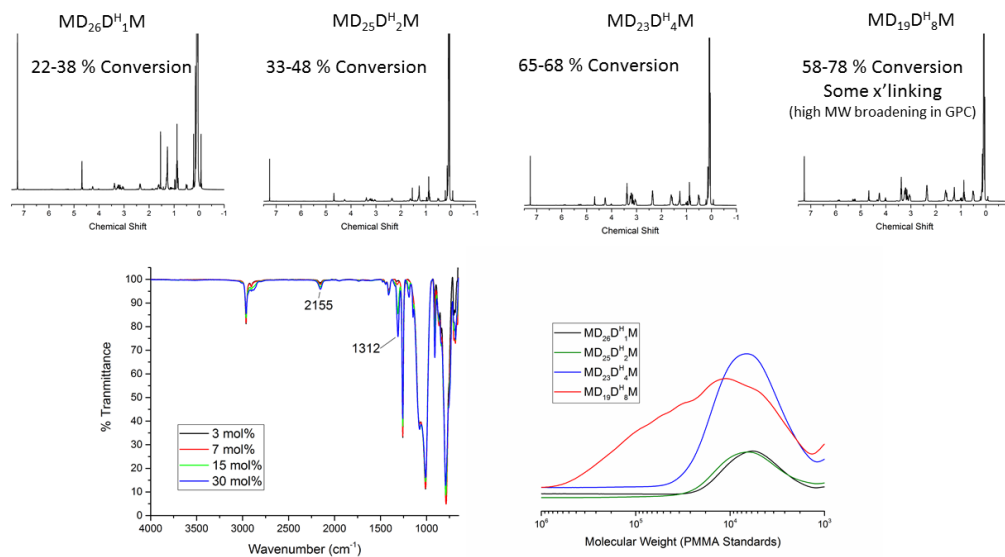


Figure A.5.  $^1\text{H}$ NMR, IR and GPC of AS- $\text{MD}_x\text{D}_y\text{M}$  Pt-catalyzed hydrosilylation products.

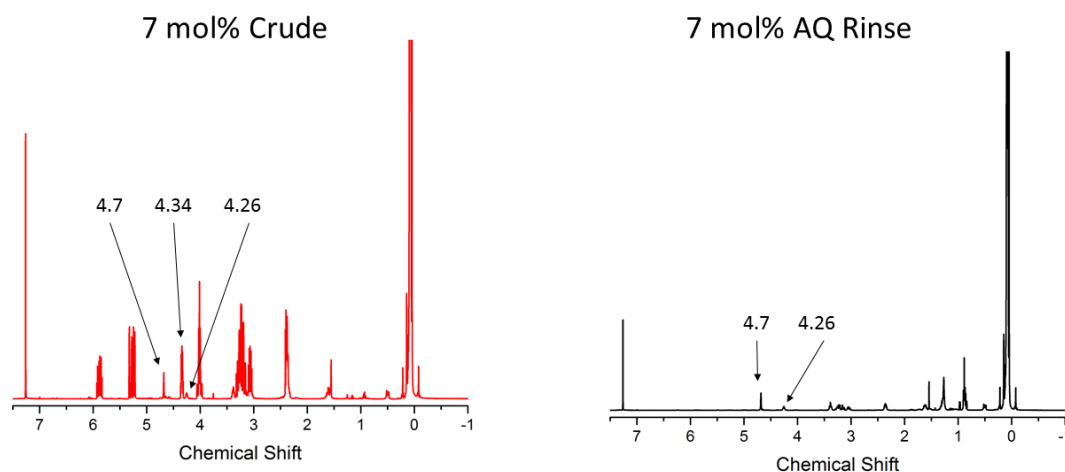


Figure A.6.  $^1\text{H}$ NMR of crude and rinsed  $\text{MD}_{25}\text{D}_2\text{M}$ -AS hydrosilylation. The conversion in this sample was 22% (2 EQ AS, 20 ppm Pt, 80 °C, 16 hours)

The low efficiency of AS incorporation into  $\text{MD}_x\text{D}_y\text{M}$  copolymers led me to the synthesis of a cyclic POS-methylsiloxane monomer that could be polymerized by ring-opening. I chose  $\text{D}_4^{\text{H}}$  as the methylsiloxane substrate. It is available from Gelest, would be easy to remove by stripping of the crude product and it produces one product as opposed to the mixture of products that results from the hydrosilylation of  $\text{D}_4^{\text{H}}$ . The



downside of using  $D_4^{1H}$  is that it only affords polymers with a maximum of 25 mol% POS. Lower POS contents can be prepared by ROP of mixtures of  $D_4^{1POS}$  with  $D_4$ . Hydrosilylation of  $D_4^{1H}$  was successful and yielded  $D_4^{1POS}$  (Figure A.7).  $^1H$ NMR (500 MHz,  $CDCl_3$ ) = 0.08 (s, 21H), 0.52 (m, 2H), 1.6 (m, 2H), 2.37 (m, 2H), 3.04 (m, 1H), 3.12-3.17 (m, 1H), 3.20-3.35 (m, 2H), 3.39 (m, 2H), 4.26 (s, 1H).

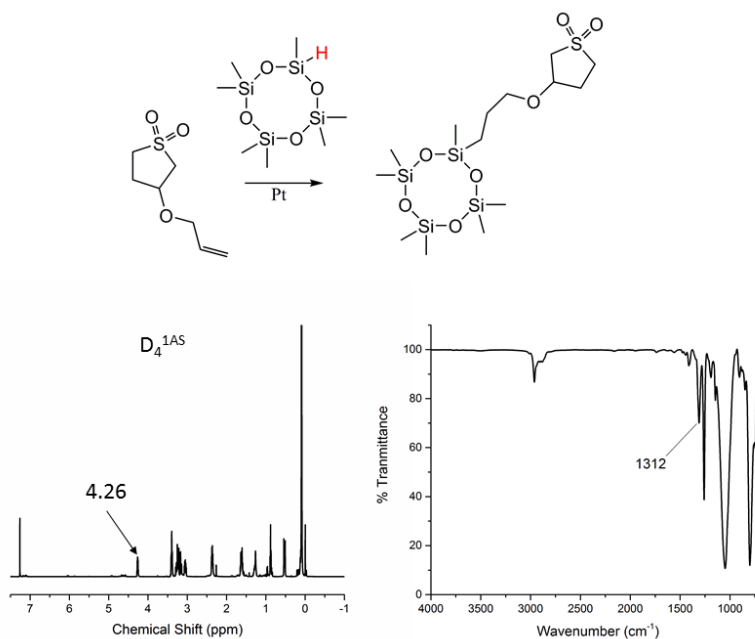


Figure A.7.  $^1H$ NMR and IR of  $D_4^{1H}$ -AS Pt-catalyzed hydrosilylation product,  $D_4^{1POS}$ .

Ring-opening of the neat  $D_4^{1POS}$  monomer and toluene solutions of  $D_4^{1POS}$  monomer were attempted with sulfuric acid and tetramethylammonium hydroxide catalyst. In all cases, insoluble solids and gels were obtained. These solids swell in toluene and tetrahydrofuran (THF). Mixtures of  $D_4^{1POS}$  and  $D_4$  produced solids as well.

### A.3 Project Outlook and Future Directions

So far, this project has demonstrated that sulfolane can be incorporated into methylsilicone polymers, however there is a lot of room for optimization of the chemistry, and complete characterization of the products. The most promising method of achieving a linear oxysulfolane-methylsiloxane polymer is through the ring-opening of oxysulfolane-methylsiloxane cyclic oligomer ( $D_4^{1\text{POS}}$ ). The low efficiency of hydrosilylation, extensive rinsing procedure and residual reactivity of Si-H groups in hydridomethyl copolymers suggest that this is not a good route. Synthesis of  $D_4^{1\text{POS}}$ , however was efficient and it is easily purified. Determining the ROP conditions for this monomer remains as the challenge, as my experiments yielded insoluble solids.

Once  $D_4^{1\text{POS}}$  can be used effectively to yield linear polymer, characterization of a series of POS-methylsiloxane polymers with different POS contents must be carried out to determine structure-property relationships in this linear model system. The most important characterization will involve determining the effect of POS incorporation on glass transition, wettability/water solubility, and solubility and conductivity of  $\text{Li}^+$  ions as specific characterization for electrolyte applications.

The creation of solid polymer electrolytes, the original motivation of this work, requires a crosslinking chemistry to be incorporated into the linear polymers. In this case, the residual Si-H groups in the  $\text{MD}_x\text{D}_y\text{M}$  polymers may be useful. Another, yet to be explored route could be through thiol-ene chemistry. Mercaptopropyl-methylsiloxane polymers can be purchased from Gelest. Thiol-ene chemistry with AS and a difunctional crosslinker ( $^V\text{MDM}^V$  for example) could be used to make AS-methylsiloxane networks. Structure-property relationships developed from the linear models will be useful in

establishing a starting point and guiding further optimization of POS incorporation into methylsiloxane networks.

There are numerous pathways through which the goal of this work may be achieved. A small portion of those was explored in limited depth; however, there are no reports in the open literature of sulfolane-containing silicones making this a worthwhile pursuit. If the history of silicone polymers has shown us anything, combining the properties of silicones with sulfolane (and other sulfones) will make materials with properties that will at least be interesting, but have the potential to be revolutionary.

#### A.4 References

- (1) Jones, R. G.; Ando, W.; Chojnowski, J. *Silicon-Containing Polymers*; 2000.
- (2) Arkles, B.; Larson, G. L. *Gelest Silicon Compounds: Silanes and Silicones*. 2013.
- (3) Kantor, S. W. Sulfone-Containing Organopolysiloxanes. US Pat 2,997,457, 1961.
- (4) Wu, T. C. Sulfone-Containing Organocyclotrisiloxanes. US Pat 3,487,098, 1969.
- (5) Arkles, B.; Pan, Y. Sulfolane Functional Silanes, Compositions, and Methods of Use of the Same. US Pat 68,818,454 B2, 2005.
- (6) Anzai, M.; Yamahira, T.; Kato, H. Nonaqueous Electrolyte Secondary Battery. US Pat 5,053,297, 1991.
- (7) Hallinan Jr., D. T.; Balsara, N. P. Polymer Electrolytes. *Annu. Rev. Mater. Res.* **2013**, *43*, 503–525.
- (8) Webb, M. A.; Jung, Y.; Pesko, D. M.; Savoie, B. M.; Yamamoto, U.; Coates, W.; Balsara, N. P.; Wang, Z.; Iij, T. F. M. Systematic Computational and Experimental Investigation of Lithium-Ion Transport Mechanisms in Polyester-Based Polymer Electrolytes. *ACS Cent. Sci.* **2015**, *1*, 198–205.
- (9) Kayyar, A.; Huang, J.; Samiee, M.; Luo, J. Construction and Testing of Coin Cells of Lithium Ion Batteries. *J. Vis. Exp.* **2012**.
- (10) Ratner, M. A.; Shriver, D. F. Ion Transport in Solvent-Free Polymers. *Chem. Rev.* **1988**, *88*, 109–124.
- (11) Meyer, W. H. Polymer Electrolytes for Lithium-Ion Batteries. *Adv. Eng. Mater.* **1998**, *10* (6), 439–448.
- (12) Armand, M.; Tarascon, J. Building Better Batteries. *Nature* **2008**, *451*, 652–657.

- (13) Oh, B.; Vissers, D.; Zhang, Z.; West, R.; Tsukamoto, H.; Amine, K. New Interpenetrating Network Type Poly ( Siloxane- G -Ethylene Oxide ) Polymer Electrolyte for Lithium Battery. *Power Sources* **2003**, *121*, 442–447.
- (14) Walker, C. N.; Versek, C.; Touminen, M.; Tew, G. N. Tunable Networks from Thiolene Chemistry for Lithium Ion Conduction. *ACS Macro Lett.* **2012**, *1*, 737–741.
- (15) Liang, S.; Choi, U. H.; Liu, W.; Runt, J.; Colby, R. H. Synthesis and Lithium Ion Conduction of Polysiloxane Single-Ion Conductors Containing Novel Weak-Binding Borates. *Chem. Mater.* **2012**, *24*, 2316–2323.
- (16) Liang, S.; Chen, Q.; Choi, U. H.; Bartels, J.; Bao, N.; Runt, J.; Colby, R. H. Plasticizing Li Single-Ion Conductors with Low-Volatility Siloxane Copolymers and Oligomers Containing Ethylene Oxide and Cyclic Carbonates †. *J. Mater. Chem. A* **2015**, *3* (1), 21269–21276.
- (17) Choi, U. H.; Liang, S.; Chen, Q.; Runt, J.; Colby, R. H. Segmental Dynamics and Dielectric Constant of Polysiloxane Polar Copolymers as Plasticizers for Polymer Electrolytes. *ACS Appl. Mater. Interfaces* **2016**, *8*, 3215–3225.
- (18) Reusch, W. Sulfur and Phosphorus Compounds  
<https://www2.chemistry.msu.edu/faculty/reusch/virttxtjml/special2.htm> (accessed May 27, 2016).
- (19) Roy, K.-M. Sulfones and Sulfoxides. *Ullmann's Encyclopedia of Industrial Chemistry*, 2012.
- (20) Morris, R. C.; Evans, T. W. Solvent Extraction Process. US Pat 2,360,859, 1944.
- (21) Clark, E. Sulfolane and Sulfones. *Kirk-Othmer Encyclopedia of Chemical Technology*, 2000.
- (22) Tilstam, U. Sulfolane: A Versatile Dipolar Aprotic Solvent. *Org. Process Res. Dev.* **2012**, *16*, 1273–1278.
- (23) Xu, K.; Angell, C. A. Sulfone-Based Electrolytes for Lithium-Ion Batteries. *J. Electrochem. Soc.* **2002**, *149*, 920–926
- (24) Wu, F.; Zhou, H.; Bai, Y.; Wang, H.; Wu, C. Toward 5 V Li-Ion Batteries : Quantum Chemical Calculation and Electrochemical Characterization of Sulfone-Based High-Voltage Electrolytes. *ACS Appl. Mater. Interfaces* **2015**, *7*, 15098–15107
- (25) Mendes, J. P.; Branco, F.; Abreu, C. M. R.; Mendonc, V. Sulfolane: An Efficient and Universal Solvent for Copper-Mediated Atom Transfer Radical (co)Polymerization of Acrylates, Methacrylates, Styrene, and Vinyl Chloride. *ACS Macro Lett.* **2014**, *3*, 18–21.
- (26) Vergaelen, M.; Verbraeken, B.; Monnery, B. D.; Hoogenboom, R. Sulfolane as Common Rate Accelerating Solvent for the Cationic Ring-Opening Polymerization of 2-Oxazolines. *ACS Macro Lett.* **2015**, *4*, 825–282
- (27) Lewandowski, A.; Ste, I. Polyacrylonitrile – Sulfolane – CuX<sub>2</sub> Solid Polymer Electrolyte. *Solid State Ionics* **2001**, *140*, 361–367.

- (28) Fujii, S.; Mccarthy, T. J. Sulfone-Containing Methacrylate Homopolymers: Wetting and Thermal Properties. *Langmuir* **2015**, *32*, 765–771.
- (29) Mark, J. E. *Polymer Data Handbook*; Oxford University Press, 1999.
- (30) Chernyak, Y. Dielectric Constant, Dipole Moment, and Solubility Parameters of Some Cyclic Acid Esters. *J. Chem. Eng. Data* **2006**, *51*, 416–418.
- (31) Nagaoka, K.; Naruse, H.; Shinohara, I. High Ionic Conductivity in Poly(dimethyl Siloxane-Co- Ethylene Oxide) Dissolving Lithium Perchlorate. *J. Polym. Sci. Polym. Lett. Ed.* **1984**, *22*, 659–663.
- (32) Zhu, Z.; Einset, A. G.; Yang, C.; Chen, W.; Wnek, G. E. Polysiloxanes Bearing Cyclic Carbonate Side Chains. Dielectric Properties and Ionic Conductivities of Lithium Triflate Complexes. *Macromolecules* **1994**, *27*, 4076–4079.
- (33) Jeschke, S.; Gentshev, A.-C.; Wiemhofer, H.-D. Disiloxanes with Cyclic or Non-Cyclic Carbamate Moieties as Electrolytes for Lithium-Ion Batteries. *Chem. Commun.* **2013**, *49*, 1190–1192.
- (34) Rossi, N.; West, R. Silicon-Containing Liquid Polymer Electrolytes for Application in Lithium Ion Batteries. *Polym. Int.* **2009**, *58*, 267–272.
- (35) Liang, S.; Reilly, M. V. O.; Choi, U. H.; Shiau, H.; Bartels, J.; Chen, Q.; Runt, J.; Winey, K. I.; Colby, R. H. High Ion Content Siloxane Phosphonium Ionomers with Very Low Tg. *Macromolecules* **2014**, *47*, 4428–4437.
- (36) Zhang, Z. C.; Jin, J. J.; Bautista, F.; Lyons, L. J.; Shariatzadeh, N.; Sherlock, D. Ion Conductive Characteristics of Cross-Linked Network Polysiloxane-Based Solid Polymer Electrolytes. *Solid State Ionics* **2004**, *170*, 233–238.

**APPENDIX B**

**CLIMBING OF SUPERHYDROPHOBIC MICROPARTICLES ON WATER WETTED SURFACES**

B.1. Introduction

For about two decades there has been extensive use of scintillation vials in the McCarthy group. They have proven useful as reaction vessels and were reported as the only container in which perfectly hydrophobic ( $\theta_A/\theta_R = 180^\circ/180^\circ$ ) surfaces could be prepared. A fascinating phenomenon occurs when superhydrophobic powders are shaken in clean scintillation vials with a few milliliters of clean water: a continuous, elastic particle film forms on the walls of the vial. Figure B.1 is a photo of a vial containing 1  $\mu\text{m}$  PTFE powder (Sigma-Aldrich) that has been vigorously shaken with 5 mL water. This is a solid stabilized air bubble surrounded by water wetted glass, or an “inverse liquid marble.” The particle film shows elasticity through wrinkling, folding, and the ability to support load (excess particles, sand or even a toothpick placed into or onto the film). If the vial is shaken and the particle film is rinsed off the walls, it will spontaneously and rapidly climb the walls to reform a continuous particle film. The particle film can move independent of the vial: if the vial is rotated on its side, the film may remain stationary. Having played with this phenomenon in the lab, I wanted to run some of my own experiments to gain insight into what was happening.

To study the climbing particle films formed in scintillation vials I asked a few questions:

1. What hydrophobic particles form the best films?
2. What is the structure of the particle film?
3. Why does this happen?
4. Is there good science here or is this simply a parlor trick?



Figure B.1. 1  $\mu\text{m}$  PTFE powder that has been vigorously shaken with 5 mL water in a Fisher scintillation vial. The opaque particle film coats the wetted walls of the glass. This film exhibits elastic behavior and will climb the walls if it is rinsed down.

## B.2. Experiments, Results and Discussion

*What hydrophobic particles perform best?* The qualification ‘best’ must first be defined. Performance criteria for particle films in scintillation vials were qualitative in nature and selection was subjective but differences in performance were obvious. These criteria were: particle availability, particle stability, reproducibility of film formation, insolubility in water (no signs of dispersion or clumps of particle in water) and elasticity of the film. Numerous particles were found to form films, including hydrophobized silica (hexamethyldisilazane treated silica, Gelest and Cab-o-sil treated fumed silica, Cabot), Stöber particles treated with perfluorochlorosilane (tridecafluorotetrahydrooctyldimethylchlorosilane), Tospearl (Momentive), freeze-dried MQ copolymer and all sizes of PTFE (1, 12, 35  $\mu\text{m}$ , Sigma-Aldrich). Of these, 1  $\mu\text{m}$  PTFE was determined to perform best. It forms the most robust films that are extremely reproducible. The films climb rinsed vials rapidly and do not puncture or fracture when poked with a clean spatula. It is available from Sigma-Aldrich for about \$10 per gram and was the particle that initially sparked our interest. Last, it is inert to water, air and glass and will not undergo chemical changes over time in these experiments.

*What is the structure of the particle film?* To investigate the structure of the rafts, I first examined the structure of the particles using Scanning Electron Microscopy with Dr. Alex Ribbe. Micrographs in Figure B.2 show that the ‘particles’ have a large dispersity in size and appear to be highly structured aggregates of roughly 100 nm particles. Structure is apparent on multiple length scales: from single particle (100 nm) to the entire aggregate (1-5  $\mu\text{m}$ ). The hierarchical structure of the hydrophobic PTFE is responsible for the “superhydrophobic” properties but the large-scale roughness also ensures that contact line pinning occurs. This contact line pinning fixes the particles to a water interface, thus enabling the formation of stable films on water in the form of liquid marbles or the inverse liquid marbles discussed here. In this text, I will refer to the microscopic aggregates of primary particles that are seen in SEM as ‘particles’ and to macroscopic collections of particles as ‘aggregates.’

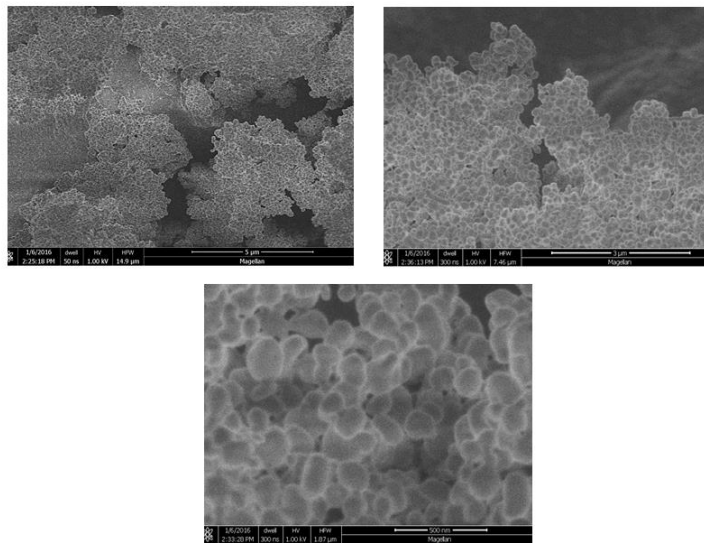


Figure B.2. SEM micrographs of 1  $\mu\text{m}$  PTFE particles. Increasing the magnification shows that the particles have structure on multiple length scales.

The morphology of the particles indicates that their ability to form robust, elastic films on water is due to contact line pinning of a superhydrophobic object. Now I wanted



to determine the structure of the particle film. To do so I isolated two films: one directly from a vial from which the supporting water film had been evaporated in a clean oven and one deposited onto wetted glass using the Langmuir-Blodgett technique. Use of the Langmuir trough also enabled me to study pressure-area isotherms of the particles at the air-water interface.

First, let's consider the Langmuir monolayer and the film deposited onto glass from this monolayer. These monolayers were prepared by dispersing PTFE powders into chloroform (1 mg/ml) using an ultrasonic bath. This dispersion was immediately deposited onto the water surface using a syringe. After deposition and solvent evaporation, freely diffusing, isolated particle 'islands' were visible. Upon compression, the islands merge and a uniform particle raft forms that wrinkles, folds, and buckles. When the surface pressure is relieved (trough area expanded), the particle raft breaks back into islands. The raft can be reformed with compression, indicating the reversibility of the process. The pressure-area isotherm is shown in Figure B.3 and displays a sharp, solid-like response in surface pressure. Hysteresis experiments, also in Figure B.3, show that the film does not collapse and is elastic at surface pressures of 10 mN/m. Based on the lift-off area, 1 mg of the PTFE particles covers 2000 mm<sup>2</sup> which corresponds to 4.5 million spherical, 1 μm PTFE spheres per mm<sup>2</sup>. A close-packed monolayer of 1 μm spheres is estimated to consist of 1.5 million particles per mm<sup>2</sup>. While these estimates are of the same order of magnitude, it is likely that the film formed on the Langmuir trough is a multilayered structure or contains many aggregated structures.

To probe the structure of the PTFE Langmuir film, films were driven up wetted glass slides for characterization. This was accomplished by compressing films to a stable, constant surface pressure (in this case 30 mN/m was sufficient) and touching film surfaces

with the wetted glass slides. At the moment the wet glass touched a particle film, the film jumped up the sides of the glass and the measured surface pressure was relieved due to the increase in water interface area provided by the water film on glass. Once the particle film stopped climbing the glass slide due to relaxation of surface pressure, the slide was removed from the interface and dried. The result is shown in a photo and optical micrograph in Figure B.4. The isolated film appears homogenous by eye but shows many aggregate structures at 20x magnification.

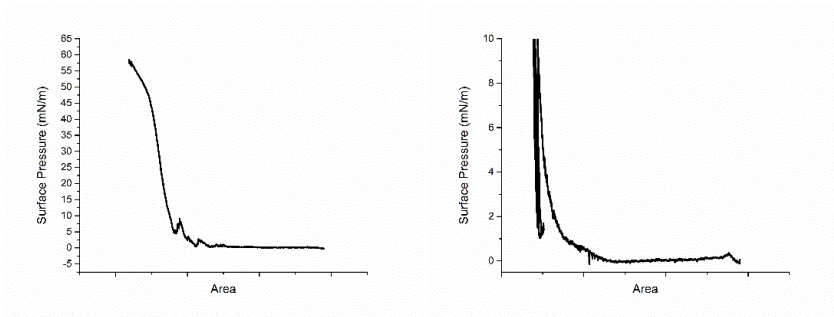


Figure B.3. Pressure-area isotherm (left) and hysteresis of 1  $\mu\text{m}$  PTFE particles at the air-water interface.

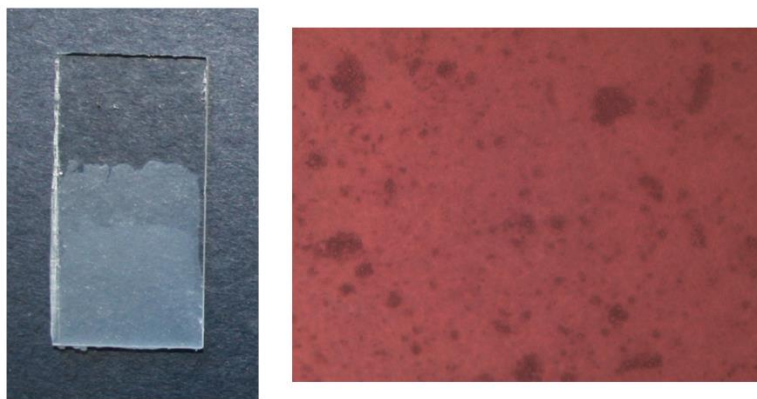


Figure B.4. Photograph and 20x optical micrograph of 1  $\mu\text{m}$  PTFE film isolated from the air-water interface of a Langmuir monolayer

A film was isolated from the vial by preparing a particle film in a vial and evaporation of the water subphase in a warm oven (65  $^{\circ}\text{C}$ ). A 20x optical micrograph of

the vial wall is shown in Figure B.5. The structure appears homogenous to the naked eye, with only a few large particle aggregates standing out. The micrograph similarly shows a homogenous film made up of aggregated particles. Compared to the film isolated by Blodgett deposition, the film from the vial is more opaque and appears to be thicker either due to multilayer formation or more aggregated particles. That the particles are more aggregated suggests that the mechanical agitation that occurs during shaking does not break up the particles as well as ultrasound in an organic solvent, which is to be expected.

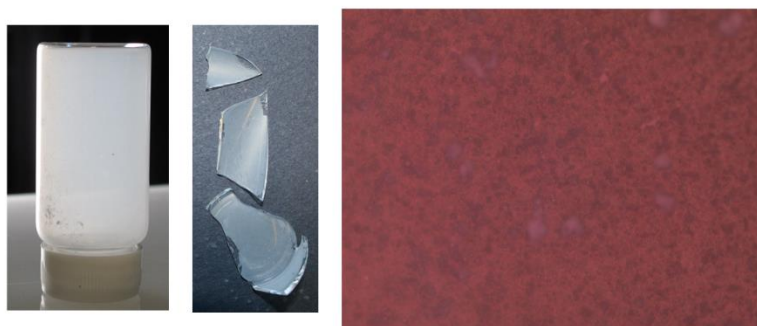


Figure B.5. Photograph and 20x optical micrograph of 1  $\mu\text{m}$  PTFE film isolated from the air-water interface within a scintillation vial

*Why does this happen?* Other experiments were run to test the effects of liquid subphase viscosity and surface tension. As viscosity increases, by addition of glycerol, the climbing of the raft slows, but the elasticity remains. Increasing viscosity slows the motion of the liquid and thus slows the apparent motion of the particles at the interface. A particle pinned to the fluid surface can only move up the walls as fast as the liquid it is pinned to. Decreasing the surface tension of the subphase, by addition of methanol, leads to no particle film formation and eventually to the dispersion of the particles.

Surface pressure is responsible for the climbing of PTFE particles up the wet glass walls of scintillation vials. This is most obvious from the Blodgett depositions where a film

under pressure spontaneously climbs wet glass. The surface pressure comes from excess particles. Shaking breaks up aggregated particles, which explains the need to shake vials vigorously before a stable film forms: in the aggregated state the effective particle concentration is low and the aggregates are less effective at forming films than the separated particles. With only a few mg's of particles in a vial, there is a large excess over what is needed to form a monolayer over the vial's inner surface area. During shaking, particles form films over air-water interfaces (droplets surfaces and whatever other water surfaces are available during shaking). When the shaking stops, the water settles into a configuration with the minimum surface area but the particles which covered the larger shaken area are still pinned to the air-water interface. This leads to a large excess of particles at the interface. This excess concentration at the air-water interface creates a surface pressure that drives the film up the wet walls of the vial. The pressure is relieved by the increase in film area/decrease in surface concentration. The film climbs until (1) no more excess particles are present to create the required surface pressure or (2) the pressure is too low to drive the film higher due to the weight of the film. The second case might be observed in a very long tube but it not seen in the short vials. In the case of the scintillation vials, there is often still a large excess of particles present. While I was unable to directly measure this, I suspect that this creates a high surface pressure at the interface. Figure B.6 is a schematic representation of the process.

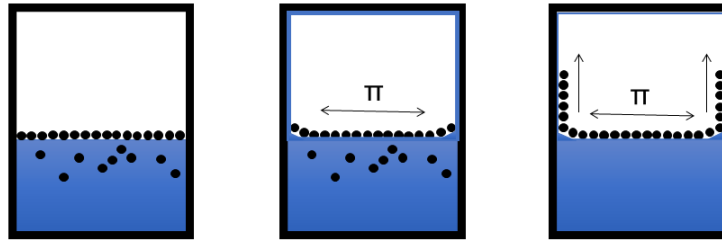


Figure B.6. Surface pressure - driven climbing of hydrophobic particles. In the first image, the walls of the vessel are dry and no climbing will occur: there is no water surface for the excess particles to expand onto. In the second image, the walls of the vessel are wet and excess particles are trapped (this could be in the form of bubbles or agglomerates that form from the collapse of the high surface area of the water during shaking). In the final image, the excess particles are merging with the film, creating a surface excess of particles. This exerts a surface pressure that drives the film up the wet walls of the vessel. Climbing continues until all excess particles have merged, the entire water interface has been covered or the surface pressure cannot overcome the weight of the climbing film.

It is important to mention that the cleanliness of the vials is critical. A water film on the walls of the glass is required for the observed climbing and film formation to occur. This film forms during the shaking process in clean glass vials. In dirty vials, a stable water film does not form and the particle film will not climb.

Elasticity in the particle raft comes from contact line pinning and capillary interactions of the superhydrophobic powders, which are the same forces that hold liquid marbles and dry water together. These are manifestations of the high surface tension of water.

*Is there good science here or is this simply a parlor trick?* The climbing of PTFE particle films on wetted substrates contains interesting scientific questions and might be a useful model for other surface pressure driven phenomena. There might even be practical applications of this lab curiosity.

Numerous researchers are interested in colloidal arrays and self-assembly of colloidal particles. The surface pressure - driven climbing of hydrophobic objects might be a way to transfer 2-dimensional particle assemblies or to form such assemblies. In one experiment, water was removed from a vial containing a particle film using a syringe. As the water level dropped, the particle film coated the walls of the vial. This is a way to create particle coatings.

Scientifically, I believe that the behaviors observed for these pinned hydrophobic powders are macroscopic analogs to what occurs in insoluble monolayers of molecules (like fatty acids at the air-water interface). The similarities to spreading, film elasticity and surface pressure - driven climbing onto wetted substrates is striking. However, the colloidal system presents new problems and opportunities. The most interesting of these new challenges is the kinetics of assembly of colloidal particles. Is it possible to create a true equilibrium state or are the particles always kinetically trapped? If the particles are always trapped, how can kinetics be used to create specific particle assemblies? What are the effects of particle dispersity in both size and structure? I am sure these are questions that colloid scientists are working on and perhaps this system and phenomenon could be useful.

Ultimately, there is more to be done in studying the climbing of PTFE particle films in wet scintillation vials experimentally, theoretically and practically.

## BIBLIOGRAPHY

- Alig, I.; Skipa, T.; Lellinger, D.; Pötschke, P. Destruction and formation of a carbon nanotube network in polymer melts: Rheology and conductivity spectroscopy. *Polymer* **2008**, *49*, 3524-3532
- Amouroux, N.; Petit, J.; Léger, L. Role of Interfacial Resistance to Shear Stress on Adhesive Peel Strength. *Langmuir* **2011**, *17*, 6510-6517.
- Araud, C. Polydimethylsiloxane/MQ resin antifoaming compositions. US Pat. 5,082,590 Jan. 21, 1992.
- Arkles, B. Future Developments in Silicon Chemistry - An Industrial Perspective. *Main Group Chem. News*, **1994**, *2(2)*, 4-10.
- Arkles, B.; Larson, G. L. Silicon Compounds: Silanes and Silicones, 3rd Edition; Gelest, Inc.: Morrisville, PA., 2013, p. 535.
- Ausman, K. D.; Piner, R.; Lourie, O.; Ruoff, R. S. Organic Solvent Dispersions of Single-Walled Carbon Nanotubes: Toward Solutions of Pristine Nanotubes. *J. Phys. Chem. B*. **2000**, *104*, 1811-1815.
- Aveyard, R.; Binks, B. P.; Clint, J. H. Emulsions stabilized solely by colloidal particles. *Adv. Colloid Interface Sci.* **2003**, *100*, 503-546.
- Bai, L.; Bai, Y.; Zheng, J. Improving the filler dispersion and performance of silicone rubber/multi-walled carbon nanotube composites by noncovalent functionalization of polymethylphenylsiloxane. *J. Mater. Sci.* **2017**, *52*, 7516-7529.
- Bai, L.; Wang, X.; Tan, J.; Li, H.; Zheng, J. Study of distinctions in the synergistic effects between carbon nanotubes and different metal oxide nanoparticles on enhancing thermal oxidative stability of silicone rubber. *J. Mater. Sci.* **2016**, *51*, 7130-7144.
- Balasubramanian, K.; Burghard, M. Chemically Functionalized Carbon Nanotubes. *Small* **2005**, *1*, 2, 180-192.
- Bauhofer, W.; Kovacs, J.Z. A Review and Analysis of Electrical Percolation in Carbon Nanotube Polymer Composites. *Comp. Sci. Tech.* **2009**, *69*, 1486-1498.
- Beigbeder, A.; Linares, M.; Devalckenaere, M.; Degée, P.; Claes, M.; Beljonne, D.; Lazzaroni, R.; Dubois, P. CH- $\pi$  Interactions as the Driving Force for Silicone-Based Nanocomposites with Exceptional Properties. *Adv. Mater.* **2008**, *20*, 1003-1007.
- Benson, J.; Kovalenko, I.; Boukhalfa, S.; Lashmore, D.; Sanghadasa, M.; Yushin, G. Multifunctional CNT-Polymer Composites for Ultra-Tough Structural Supercapacitors and Desalination Devices. *Adv. Mater.* **2013**, *25*, 6625-6632.
- Bernardini, C.; Stoyanov, S. D.; Cohen Stuart, M. A.; Arnaudov, L. N.; Leermakers, F. A. M. PMMA Highlights the Layering Transition of PDMS in Langmuir Films. *Langmuir* **2011**, *27*, 2501-2508.
- Berzelius, J. J. *Ann. Phys. Chem.* **1824**, *1*, 169.

- Binks, B. P. Particles as Surfactants-Similarities and Differences. *Curr. Opin. Colloid Interface Sci.* **2002**, *7*, 21–41.
- Binks, B. P.; Whitby, C. P. Silica Particle-Stabilized Emulsions of Silicone Oil and Water: Aspects of Emulsification. *Langmuir* **2004**, *20*, 1130–1137.
- Blodgett, K. B. Films built by depositing successive monomolecular layers on a solid surface. *J. Am. Chem. Soc.* **1935**, *57*, 1007-1022.
- Blodgett, K. B. Monomolecular films of fatty acids on glass. *J. Am. Chem. Soc.* **1934**, *56*, 495-495.
- Blodgett, K. B.; Langmuir, I. Built-up films of barium stearate and their optical properties. *Phys. Rev.* **1937**, *51*, 0964-0982.
- Boker, A.; He, J.; Emrick, T.; Russell, T. P. Self-assembly of nanoparticles at interfaces. *Soft Matter* **2007**, *3*, 1231–1248.
- Bom, D.; Andrews, R.; Jacques, D.; Anthony, J.; Chen, B.; Meier, M. S.; Selegue, J. P. Thermogravimetric Analysis of the Oxidation of Multiwalled Carbon Nanotubes: Evidence for the Role of Defect Sites in Carbon Nanotube Chemistry. *Nano Lett.* **2002**, *2*, 615-619.
- Bordács, S.; Agod, A.; Hórvölgyi, Z. Compression of Langmuir Films Composed of Fine Particles: Collapse Mechanism and Wettability. *Langmuir* **2006**, *22*, 6944–6950.
- Breuer, O.; Sundararaj, U. Big Returns From Small Fibers: A Review of Polymer/Carbon Nanotube Composites. *Polym. Comp.* **2004**, *25*, 630-645.
- Brinker, C. J.; Scherer, G. W. *Sol-Gel Science: The Physics and Chemistry of Sol-Gel Processing*. Academic Press: Boston **1990**.
- Brook, M. A. *Silicon in Organic, Organometallic, and Polymer Chemistry*. Wiley-Interscience, John Wiley & Sons: New York, **2000**.
- Butts, M.; Cella, J.; Wood, C. D.; Gillette, G.; Kerboua, R.; Leman, J.; Lewis, L.; Rubinsztajn, S.; Schattenmann, F.; Stein, J.; Wicht, D.; Rajaraman, S.; Wengrovius, J. Silicones. In *Encyclopedia of Polymer Science and Technology*, 2nd ed.; Wiley & Sons: New York, 2003, vol. 11, pp. 765-841.
- Butts, M.; Cella, J.; Wood, C. D.; Gillette, G.; Kerboua, R.; Leman, J.; Lewis, L.; Rubinsztajn, S.; Schattenmann, F.; Stein, J.; Wicht, D.; Rajaraman, S.; Wengrovius, J. Silicones. In *Kirk-Othmer Encyclopedia of Chemical Technology*, Wiley & Sons: New York, 2006, vol. 22, pp. 547-626.
- Camino, G.; Lomakin, S. M.; Lazzari, M. Polydimethylsiloxane thermal degradation Part 1. Kinetic aspects. *Polymer* **2001**, *42*, 2395-2402.
- Camino, G.; Lomakin, S.M.; Lageard, M. Thermal polydimethylsiloxane degradation. Part 2. The degradation mechanisms. *Polymer* **2002**, *43*, 2011-2015.
- Carter, C. B.; Norton, M. G. *Ceramic Materials Science and Engineering*. Springer: New York. **2007**.
- Chadwick, R. C.; Grande, J. B.; Brook, M. A.; Adronov, A. Functionalization of Single-Walled Carbon Nanotubes via the Piers-Rubinsztajn Reaction. *Macromolecules* **2014**, *47*, 6527-6530.



Chae, S. S.; Oh, J. Y.; Park, J. H.; Choi, W. J.; Han, J. H.; Lee, J.-O.; Baik, H. K.; Lee, T. I. Strong Hydrophobizer: Laterally Chemisorbed Low-Molecular-Weight Polydimethylsiloxane. *Chem. Commun.* **2015**, *51*, 5844-5847.

Chalk, A. J.; Harrod, J. F. Homogeneous Catalysis. II. The Mechanism of the Hydrosilation of Olefins Catalyzed by Group VIII Metal Complexes. *J. Am. Chem. Soc.* **1965**, *87*, 16-21.

Chen D.; Chen F.; Hu X.; Zhang H.; Yin X.; Zhou. Thermal stability, mechanical and optical properties of novel addition cured PDMS composites with nano-silica sol and MQ silicone resin. *Compos. Sci. Technol.* **2015**, *117*, 307-314.

Chen, W.; Fadeev A. Y.; Hsieh, M. C.; Öner, D.; Youngblood, J.; McCarthy, T. J. Ultrahydrophobic and Ultralyophobic Surfaces: Some Comments and Examples. *Langmuir* **1999**, *15*, 3395-3399.

Cheng, D. F.; Urata C.; Mashed B.; Hozumi A. A Physical Approach To Specifically Improve the Mobility of Alkane Liquid Drops. *J. Am. Chem. Soc.* **2012**, *134*, 10191-10199.

Cheng, D. F.; Urata, C.; Yagihashi, M.; Hozumi, A. A Statically Oleophilic but Dynamically Oleophobic Smooth Nonperfluorinated Surface. *Angew. Chemie Int. Ed.* **2012**, *51*, 2956-2959.

Cheng, Q.; Bao, J.; Park, J.; Liang, Z.; Wang, B. High Mechanical Performance Composite Conductor: Multi-walled Carbon Nanotube Sheet/Bismaleimide Nanocomposites. *Adv. Funct. Mater.* **2009**, *19*, 1-7.

Cheng, Q.; Wang, B.; Zhang, C.; Liang, Z. Functionalized Carbon-Nanotube Sheet/Bismaleimide Nanocomposites: Mechanical and Electrical Performance Beyond Carbon-Fiber Composites. *Small* **2010**, *6*, 763-767.

Chojnowski J.; Jurjata J.; Fortuniak W.; Rubinsztajn S.; Trzebicka B. Hydride Transfer Ring-Opening Polymerization of a Cyclic Oligomethylhydrosiloxane. Route to a Polymer of Closed Multicyclic Structure. *Macromolecules* **2012**, *45*, 2654-2661.

Chojnowski, J. Ring-opening Polymerization of Cyclosiloxanes in *Silicon Compounds: Silanes and Silicones*. 3<sup>rd</sup> ed. Gelest, Inc.

Chojnowski, J.; Cypryk, M. in *Silicon-containing polymers*, Jones, R. G.; Ando, W.; Chojnowski, J.; Kluwer Acad. Publ.: Dordrecht, **2000**.

Chojnowski, J.; Fortuniak, W.; Kurjata, J. Oligomerization of Hydrosiloxanes in the Presence of Tris(pentafluorophenyl)borane. *Macromolecules* **2006**, *39*, 3802-3807.

Chojnowski, J.; Rubinsztajn, S.; Cella, J. A.; Fortuniak, W.; Cypryk, M.; Kurjata, J.; Kaźmierski, K. Mechanism of the B(C<sub>6</sub>F<sub>5</sub>)<sub>3</sub>-Catalyzed Reaction of Silyl Hydrides with Alkoxysilanes. Kinetic and Spectroscopic Studies. *Organometallics* **2005**, *24*, 6077-6084.

Churaev, N. V.; Esipova, N. E.; Hill, R. M.; Sobolev V. D.; Starov, V. M.; Zorin Z. M. The Suprespreading Effect of Trisiloxane Surfactant Solutions. *Langmuir* **2001**, *17*, 1338-1348.

Clarson, S. J.; Semlyen, J. A. *Siloxane Polymers*. Prentice Hall: Englewood Cliffs, **1993**.

Coleman, J. N.; Khan, U.; Blau, W. J.; Gun'ko, Y. K. Small but strong: A review of the mechanical properties of carbon nanotube-polymer composites. *Carbon* **2006**, *44*, 1624-1652.

Cosgrove T.; Roberts C.; Choi Y.; Schmidt R. G.; Gordon G. V.; Goodwin A. J.; Kretschmer A. Relaxation Studies of High Molecular Weight Poly(dimethylsiloxane)s Blended with Polysilicate Nanoparticles. *Langmuir* **2002**, *18*, 10075-10079.

Cosgrove T.; Roberts C.; Garasanin T.; Schmidt R. G.; Gordon G. V. NMR Spin-Spin Relaxation Studied of Silicate-Filled Low Molecular Weight Poly(dimethylsiloxane)s. *Langmuir* **2002**, *18*, 10080-10085.

Currie, C. C.; Kell, J. W. Organopolysiloxane Adhesive and Pressure-Sensitive Adhesive Tape Containing Same. US Pat. 2,814,601, Nov. 26, 1957.

Daudt, W. H.; Tyler, L. J. Copolymeric Siloxanes and Methods of Preparing Them. U.S. Patent 2,676,182, Apr. 20, 1954.

Davenport, M. Much ado about small things. *C&EN* **2015**, *June 8<sup>th</sup>*, 10-15.

De Volder, M. F. L.; Tawfick, S. H.; Baughman, R. H.; Hart, A. J. Carbon Nanotubes: Present and Future Commercial Applications. *Science* **2013**, *339*, 535-539.

Deng, J.; Polidan, J. T.; Hottle, J. R.; Farmer-Creely, C. E.; Viers, B. D.; Esker, A. R. Polyhedral Oligomeric Silsesquioxanes: A New Class of Amphiphiles at the Air/Water Interface. *J. Am. Chem. Soc.* **2002**, *124*, 15194–15195.

Deng, J.; Viers, B. D.; Esker, A. R.; Anseth, J. W.; Fuller, G. G. Phase Behavior and Viscoelastic Properties of Trisilanolcyclohexyl-POSS at the Air/Water Interface. *Langmuir* **2005**, *21*, 2375–2385.

Di. M.; He S.; Li R.; Yang D. Radiation effect of 150 keV protons on methyl silicone rubber reinforced with MQ silicone resin. *Nucl. Instrum. Methods. Phys. Res., Sect. B.* **2006**, *248*, 31-36.

Downes, R. D.; Hao, A.; Park, J. G.; Su, Y.; Liang, R.; Jensen, B. D.; Siochi, E. J.; Wise, K. E. Geometrically constrained self-assembly and crystal packing of flattened and aligned carbon nanotubes. *Carbon* **2015**, *93*, 953-966.

Du, F.; Fischer, J. E.; Winey, K. I. Coagulation Method for Preparing Single-Walled Carbon Nanotube/Poly(methyl methacrylate) Composites and Their Modulus, Electrical Conductivity, and Thermal Stability. *J. Polym. Sci. B: Polym. Phys.* **2003**, *41*, 3333-3338.

Du, F.; Scogna, R. C.; Zhou, W.; Brand, S.; Fischer, J. E.; Winey, K. I. Nanotube Networks in Polymer Nanocomposites: Rheology and Electrical Conductivity. *Macromolecules.* **2004**, *37*, 9048-9055.

Du, K.; Glogowski, E.; Emrick, T.; Russell, T. P.; Dinsmore, A. D. Adsorption Energy of Nano- and Microparticles at Liquid-Liquid Interfaces. *Langmuir* **2010**, *26*, 12518–12522.

Dvornic, Petar R.; Lenz, Robert W. High Temperature Siloxane Elastomers. **1990**.

Escorihuela, J.; Pujari S. P.; Zuilhof H. Organic Monolayers by B(C<sub>6</sub>F<sub>3</sub>)<sub>3</sub>-Catalyzed Siloxanation of Oxidized Silicon Surfaces. *Langmuir* **2017**, *33*, 2185-2193.

- Fadeev A. Y.; McCarthy, T. J. Trialkylsilane Monolayers Covalently Attached to Silicon Surfaces: Wettability Studies Indicating that Molecular Topography Contributes to Contact Angle Hysteresis. *Langmuir* **1999**, *15*, 3759-3766.
- Fadeev, A. Y.; McCarthy, T. J. A New Route to Covalently Attached Monolayers: Reaction of Hydridosilanes with Titanium and Other Metal Surfaces. *J. Am. Chem. Soc.* **1999**, *121*, 12184-12185.
- Fadeev, A. Y.; McCarthy, T. J. Self-Assembly Is Not the Only Reaction Possible between Alkyltrichlorosilanes and Surfaces: Monomolecular and Oligomeric Covalently Attached Layers of Dichloro- and Trichloroalkylsilanes on Silicon. *Langmuir*, **2000**, *16*, 7268-7274.
- Flagg, D. H.; McCarthy, T. J. Rediscovering Silicones: MQ Copolymers *Macromolecules* **2016**, *49*, 8581–8592.
- Fox H. W.; Taylor P. W.; Zisman W. A. Polyorganosiloxanes...Surface Active Properties. *Ind. Enge. Chem.* **1947**, *39*, 1401-1409
- Friedel, C.; Crafts, J. M. *Ann.* **1863**, *127*, 28.
- Frye, C. L.; Salinger, R. M.; Fearon, F. W. G.; Klosowski, J. M.; DeYoung T. Reactions of Organolithium Reagents with Siloxane Substrates. *J. Org. Chem.* **1970**, *35*, 1308-1314.
- Furmidge, C. G. L. Studies at Phase Interfaces. I. The Sliding of Liquid Drops on Solid Surfaces and A Theory for Spray Retention. *J. Colloid Sci.* **1962**, *17*, 309-324.
- Gaines, G. L. Insoluble Monolayers at Liquid-Gas Interfaces. Interscience Publishers: New York, **1966**.
- Galeandro-Diamont, T.; Zanota, M.; Sayah, R.; Veyre, L.; Nikitine, C.; Bellefon, C.; Marrot, S.; Meille, V.; Thieduleux, C. Platinum nanoparticles in suspension are as efficient as Karstedt's complex for alkene hydrosilylation. *Chem. Commun.* **2015**, *51*, 16194-16196.
- Ganicz, T.; Pakula, T.; Stańczyk, W. A. Novel liquid crystalline resins based on MQ siloxanes. *J. Organomet. Chem.* **2006**, *691*, 5052–5055.
- Gao, L.; McCarthy, T. J. Contact Angle Hysteresis Explained. *Langmuir* **2006**, *22*, 6234-6237.
- Gao, L.; McCarthy, T. J. Teflon is Hydrophilic. Comments on Definitions of Hydrophobic, Shear versus Tensile Hydrophobicity, and Wettability Characterization. *Langmuir* **2008**, *24*, 9183-9188.
- Gao, L.; McCarthy, T. J. Wetting 101°. *Langmuir* **2009**, *25*, 14105-14115.
- Georgakilas, V.; Perman, J. A.; Tucek, J.; Zboril, R. Broad Family of Carbon Nanoallotropes: Classification, Chemistry, and Applications of Fullerenes, Carbon Dots, Nanotubes, Graphene, Nanodiamonds, and Combined Superstructures. *Chem. Rev.* **2015**, *115*, 4744-4822.
- Gilbert, A. R.; Kantor, S. W. Transient catalysts for the polymerization of organosiloxanes. *J. Polym. Sci.* **1959**, *40*, 35-58.

- Goff, J.; Sulaiman, S.; Arkles, B.; Lewicki, J. P. Soft materials with recoverable shape factors from extreme distortion states. *Adv. Mater.* **2016**, *28*, 2393-2398.
- Gong, X.; Liu, J.; Baskaran, S.; Voise, R. D.; Young, J. S. Surfactant-Assisted Processing of Carbon Nanotube/Polymer Composites. *Chem. Mater.* **2000**, *12*, 1049-1052.
- Goodwin, J. T. Organopolysiloxane Compositions Having Pressure-Sensitive Adhesive Properties. U.S. Patent 2,857,356, Oct. 21, 1958.
- Gordon, G. V.; Schmidt, R. G.; Quintero, M.; Benton, N. J.; Cosgrove, T.; Krukoni, V. J.; Williams, K.; Wetmore, P. M. Impact of Polymer Molecular Weight on the Dynamics of Poly(dimethylsiloxane)-Polysilicate Nanocomposites. *Macromolecules* **2010**, *43*, 10132-10142.
- Grande, G. B.; Gonzaga, F.; Brook, M. A. Rapid assembly of explicit, functional silicones. *Dalton Trans.* **2010**, *39*, 9369-9378.
- Grande, G. B.; Ulrich, T.; Dickie, T.; Brook, M. A. Silicone dendrons and dendrimers from orthogonal SiH coupling reactions. *Polym. Chem.* **2014**, *5*, 6728-6739.
- Grande, J. B.; Thompson, D. B.; Gonzaga, F.; Brook, M. A. Testing the functional tolerance of the Piers-Rubinsztajn reaction: a new strategy for functional silicones. *Chem. Commun.* **2010**, *46*, 4988-4990.
- Griswold, R. M.; Krencieski, M.; Wengrovius, J. Designing Silicone PSAs. *Adhesives Age* **2002**, *45(9)*, 35-40.
- Gromilov, S. A.; Basova, T. V.; Emel'yanov, D. Y.; Kuzmin, V.; Prokhorova, S. Layer Arrangement in the Structure of Octakis(trimethylsiloxy)octasilsesquioxane and Dodecakis(trimethylsiloxy)cyclohexasiloxane. *J. Structural Chem.* **2004**, *45*, 471-475.
- Grossiord, N.; Loos, J.; Regev, O.; Koning, C. E. Toolbox for Dispersing Carbon Nanotubes into Polymers to get Conductive Nanocomposites. *Chem. Mater.* **2006**, *18*, 1089-1099.
- Hahn, T. D.; Hsu, S. L.; Stidham, H. D. Reflectance Infrared Spectroscopic Analysis of Polymers at the Air-Water Interface. 4. Microstructure of Poly(dimethylsiloxane). *Macromolecules* **1997**, *30*, 87-92.
- Hildebrand, M. Diatoms, Biomineralization Processes, and Genomics. *Chem. Rev.* **2008**, *108*, 4855-4874.
- Hottle, J. R.; Deng, J.; Kim, H. J.; Farmer-Creely, C. E.; Viers, B. D.; Esker, A. R. Blends of Amphiphilic Poly(dimethylsiloxane) and Nonamphiphilic Octaisobutyl-POSS at the Air/Water Interface. *Langmuir* **2005**, *21*, 2250-2259.
- Hottle, J. R.; Kim, H. J.; Deng, J.; Farmer-Creely, C. E.; Viers, B. D.; Esker, A. R. Blends of Amphiphilic PDMS and Trisilanolisobutyl-POSS at the Air/Water Interface. *Macromolecules* **2004**, *37*, 4900-4908.
- Hua, X.; Bevan, M. A.; Frechette, J. Reversible Partitioning of Nanoparticles at an Oil-Water Interface. *Langmuir* **2016**, *32*, 11341-11352.
- Huang, H.; Liu, C.; Wu, Y.; Fan, S. Aligned Carbon Nanotube Composite Films for Thermal Management. *Adv. Mater.* **2005**, *17*, 1652-1656.

- Huang, W. E. I.; Huang, Y.; Yu, Y. Synthesis of MQ Silicone Resins through Hydrolytic Condensation of Ethyl Polysilicate and Hexamethyldisiloxane. *J. Appl. Polym. Sci.* **1998**, *70*, 1753–1757.
- Huang, W.; Huang, Y.; Yu, Y. The effect of the acid catalyst on the preparation of MQ silicone resins. *Chinese J. Polym. Sci.* **1999**, *17*, 429–433.
- Huang, Y. Y.; Ahir, S. V.; Terentjev, E. M. Dispersion rheology of carbon nanotubes in a polymer matrix. *Phys. Rev. B.* **2006**, *73*, 125422.
- Hunter, M. J.; Gordon, M. S.; Barry, A. J.; Hyde, J. F.; Heidenreich, R. D. Properties of Organopolysiloxanes on Glass. *Ind. Eng. Chem.* **1947**, *39*, 1389-1395.
- Hurd, C. B. Studies on Siloxanes. I. The Specific Volume and Viscosity in Relation to Temperature and Constitution. *J. Am. Chem. Soc.* **1946**, *68*, 364–370.
- Hyde J. F.; DeLong, R. C. Condensation Products of the Organo-silane Diols. *J. Am. Chem. Soc.* **1941**, *63*, 1194-1196.
- Iijima, S. Helical microtubules of graphitic carbon. *Nature* **1991**, *354*, 56-58.
- Iler, R. K. *The Chemistry of Silica*. John Wiley & Sons: New York, **1979**.
- Itoh, M.; Oka F.; Suto M.; Cook S.; Auner N. Characterization and Some Insights into the Reaction Chemistry of Polymethylsilsesquioxane or Methyl Silicone Resins. *Int. J. Polym. Sci.* **2012**.
- Johnson, D. H.; McLoughlin, J. R.; Tobolsky, A. V. Chemorheology of some specially prepared silicone rubbers. *J. Phys. Chem.* **1954**, *58*, 1073-1075.
- Juen, D. R.; Zhong B.; Diaz M.; Johnson T. Foam Control Compositions having Resin-Fillers. US Pat. 6,207,722 B1 Mar. 27, 2001.
- Kantor, S. W.; Grubb, W. T.; Osthoff, R. C. The Mechanism of the Acid- and Base-catalyzed equilibration of Siloxanes. *J. Am. Chem. Soc.* **1954**, *76*, 5190-5197.
- Kashiwagi T.; Du F.; Douglas J. F.; Winey K. I.; Harris Jr. R. H.; Shields J. R. Nanoparticle networks reduce the flammability of polymer nanocomposites. *Nature Materials* **2005**, *4*, 928-933.
- Kashiwagi, T.; Fagan, J.; Douglas, J. F.; Yamamoto, K.; Heckert, A. N.; Leigh, S. D.; Obrzut, J.; Du, F.; Lin-Gibson, S.; Mu, M.; Winey, K. I.; Haggmueller, R. Relationship between dispersion metric and properties of PMMA/SWNT nanocomposites. *Polymer* **2007**, *48*, 4855-4866.
- Kharchenko, S. B; Douglas, J. F.; Obrzut, J.; Grulke, E. A.; Migler, K. B. Flow-induced properties of nanotube-filled polymer materials. *Nature Materials* **2004**, *3*, 564-568.
- Kim, C.; Gurau, M. C.; Cremer, P. S.; Yu, H. Chain Conformation of Poly(dimethyl siloxane) at the Air/Water Interface by Sum Frequency Generation. *Langmuir* **2008**, *24*, 10155–10160.
- Kim, T. A.; Kim, H. S.; Lee, S. S.; Park, M. Single-walled carbon nanotube/silicone rubber composites for compliant electrodes. *Carbon* **2012**, *50*, 444-449.
- Kipping, F. S. Organic Derivatives of Silicon. *Proc. R. Soc. (London)* **1937**, *159*, 136-148.

- Kipping, F. S.; Lloyd, L. L. *J. Chem. Soc.*, **1901**, 79, 449-459.
- Kleinert, J. C.; Weschler, C. J. Pyrolysis Gas Chromatographic-Mass Spectrometric Identification of Polydimethylsiloxanes. *Anal. Chem.* **1980**, 52, 1245-1248.
- Kong, K. T. S.; Mariatti, M.; Rashid, A. A.; Busfield, J. J. C. Effect of processing methods and functional groups on the properties of multi-walled carbon nanotube filled poly(dimethyl siloxane) composites. *Polym. Bull.* **2012**, 69, 937-953.
- Kota, A. K.; Cipriano, B. H.; Duesterberg, M. K.; Gershon, A. L.; Powell, D.; Raghavan, S. R.; Bruck, H. A. Electrical and Rheological Percolation in Polystyrene/MWCNT Nanocomposites. *Macromolecules* **2007**, 40, 7400-7406.
- Krishnamoorti, Ramanan. Strategies for Dispersing Nanoparticles into Polymers. *MRS Bulletin.* **2007**, 32, 341-347.
- Krumpfer, J. W.; McCarthy, T. J. Contact angle hysteresis: a different view and a trivial recipe for low hysteresis hydrophobic surfaces. *Faraday Discuss.* **2010**, 146, 103-111.
- Krumpfer, J. W.; McCarthy, T. J. Rediscovering Silicones: "Unreactive" Silicones React with Inorganic Surfaces. *Langmuir* **2011**, 27, 11514-11519.
- Kumar, S. K; Benicewicz, B. C.; Vaia, R. A.; Winey, K. I. 50<sup>th</sup> Anniversary Perspective: Are Polymer Nanocomposites Practical for Applications? *Macromolecules* **2017**, 50, 714-731.
- Kuo, A. C. M. Poly(dimethylsiloxane). *Polymer Data Handbook.* **1999**
- Kuo, C. J.; Chen, J.; Shih, C.; Huang, C. Silicone Resin Synthesized by Tetraethoxysilane and Chlorotrimethylsilane Through Hydrolysis-Condensation Reaction. *J. Appl. Polym. Sci.* **2014**, 131, 40317.
- Kutuzov, S.; He, J.; Tangirala, R.; Emrick, T.; Russell, T. P.; Boker, A. On the kinetics of nanoparticle self-assembly at liquid/liquid interfaces. *Phys. Chem. Chem. Phys.* **2007**, 9, 6351-6358.
- Ladenburg, A. *Ann.* **1872**, 164, 390.
- Langley, N. R.; Mbah, G. C.; Freeman, H. A.; Huang, H.-H.; Siochi, E. J.; Ward, T. C.; Wilkes, G. Physical Structure of Polysilicate Particles in Organic Media. *J. Coll. Interfac. Sci.* **1991**, 143, 309-317.
- Langmuir, I. Composition of fatty acid films on water containing calcium or barium salts. *J. Am. Chem. Soc.* **1936**, 58, 284-287.
- Langmuir, I. Constitution and fundamental properties of solids and liquids. Part I. Solids. *J. Am. Chem. Soc.* **1916**, 38, 2221-2295.
- Langmuir, I. Constitution and fundamental properties of solids and liquids. Part II. Liquids. *J. Am. Chem. Soc.* **1917**, 39, 1848-1906.
- Langmuir, I. Oil Lenses on water and the nature of monomolecular expanded films. *J. Chem. Phys.* **1933**, 1, 756-776.
- Langmuir, I. Surface Chemistry. *Chem. Rev.* **1933**, 13, 147-191.
- Langmuir, I. *Surface Chemistry.* Nobel Lecture. **1932**.

- Langmuir, I. The adsorption of gases on plane surfaces of glass, mica, and platinum. *J. Am. Chem. Soc.* **1918**, *40*, 1361-1403.
- Langmuir, I.; Langmuir, D. B. The Effect of Monomolecular Films on the Evaporation of Ether Solutions. *J. Phys. Chem.* **1927**, *31*, 1719-1731.
- Larsen, R. G.; Diamond, H. Antifoaming Composition. US Pat. 2,375,007 May 1, 1945.
- Lenk, T. J.; Lee, D. H. T.; Koberstein, J. T. End Group Effects on Monolayers of Functionally-Terminated Poly(dimethylsiloxanes) at the Air-Water Interface. *Langmuir* **1994**, *10*, 1857-1864.
- Lewicki, J. P.; Albo, R. L. F.; Alviso, C. T.; Maxwell, R. S. Pyrolysis-gas chromatography/mass spectrometry for the forensic fingerprinting of silicone engineering elastomers. *J. Anal. Appl. Pyrol.* **2013**, *99*, 85-91.
- Lewicki, J.P.; Mayer, B.P.; Alviso, C.T. et.al. Thermal Degradation Behavior and Product Speciation in Model Poly(dimethylsiloxane) Networks. *J. Inorg Organomet. Polym.* **2012**, *22*, 636-645.
- Lewis, L. N.; Wengrovius, J. H.; Burnell, T. B.; Rich, J. D. *Chem. Mater.* **1997**, *9*, 761-765.
- Lewis, L. N.; Wengrovius, J. H.; Burnell, T. B.; Rich, J. D. Powdered MQ Resin - Platinum Complexes and Their Use as Silicone-Soluble Hydrosilylation Cure Catalysts. *Chem. Mater.* **1997**, *9*, 761-765.
- Li H.; Ujihira Y.; Yoshino T.; Yoshii K.; Yamishita T.; Horie K. Free volumes and their distribution in crosslinked polysiloxanes probed by positron annihilation lifetime technique. *Polymer* **1998**, *39*, 17, 4075-4079.
- Li Y.; Wang J.; Fan L.; Chen D. Feasible Fabrication of a Durable Superhydrophobic Coating on Polyester Fabrics for Oil-Water Separation. *Acta Phys.-Chim. Sin.* **2016**, *32*, 990-996.
- Liebhafsky, H. A. *Silicones Under the Monogram*. J. Wiley & Sons: New York, **1978**.
- Lin, S.B. Addition-Cured Silicone Adhesive Technology: Vinyl Silicone Crosslinker. *J. Appl. Polym. Sci.* **1994**, *54*, 2134-2145.
- Lin, Y.; Boker, A.; Skaff, H.; Cookson, D.; Dinsmore, A. D.; Emrick, T.; Russell, T. P. Nanoparticle Assembly at Fluid Interfaces: Structure and Dynamics. *Langmuir* **2005**, *21*, 191-194.
- Lin, Y.; Wang, L. Krumpfer, J. W.; McCarthy, T. J. Hydrophobization of Inorganic Oxide Surfaces Using Dimethylsilanediol. *Langmuir* **2013**, *29*, 1329-1332.
- Lin-Gibson, S.; Pathak, J. A.; Grulke, E. A.; Wang, H.; Hobbie, E. K. Elastic Flow Instability in Nanotube Suspensions. *Phys. Rev. Lett.* **2004**, *92*, 048302.
- Liu, J. J.; Wu, P.; Feng, B.; Ylitalo, D. A. Silicone Compositions and Related Methods. US Pat. 2015/0259495 A1 Sep. 17, 2015.
- Liu, Y. Method of Making Silicone Resin Emulsions. US Pat. 6,737,444 B1 May 18, 2004.

- Liu, Y. Silicone MQ resin reinforced silicone elastomer emulsions. US Pat. 8,012,544 B2 Sept. 6, 2011.
- Lyon R. E.; Walters R. N. Pyrolysis combustion flow calorimetry. *J. Anal. Appl. Pyrolysis* **2004**, *71*, 27-46.
- Ma, Peng-Cheng; Siddiqui, Naveed A.; Marom, Gad; Kim, Jang-Kyo. Dispersion and functionalization of carbon nanotubes for polymer-based nanocomposites: A review. *Composites: Part A*. **2010**, *41*, 1245-1367.
- Magee W. L.; Emerson A. W.; Joslyn W. G.; Odneal R. S. MQ resins from stable ethylsilicate polymer polymers. U.S. Patent Appl. 2011/0184142 A1, Jul. 28, 2011.
- Mann, E. K.; Langevin D. Poly(dimethylsiloxane) Molecular Layers at the Surface of Water and of Aqueous Surfactant Solutions. *Langmuir* **1991**, *7*, 1112-1117.
- Mansuri, E.; Zepeda-Velazquez, L.; Schmidt, R.; Brook, M. A.; DeWolf, C. E. Surface Behavior of Boronic Acid-Terminated Silicones. *Langmuir*, **2015**, *31*, 9331-9339.
- Maoz, R.; Sagiv, J. On the Formation and Structure of Self-Assembling Monolayers. 1. Comparative ATR-Wettability Study of Langmuir-Blodgett and Adsorbed Films on Flat Substrates and Glass Microbeads. *J. Coll. Interface Sci.* **1984**, *100*, 465-496.
- Marceau, S.; Dubois, P.; Fulchiron, R.; Cassagnau, P. Viscoelasticity of Brownian Carbon Nanotubes in PDMS Semidilute Regime. *Macromolecules* **2009**, *42*, 1433-1438.
- Marciniec, B. Hydrosilylation: A Comprehensive Review on Recent Advances. Springer
- Marciniec, B.; Chojnowski, J. Progress in Organosilicon Chemistry; Overseas Publishers Association: Amsterdam, 1995, p. 575.
- Mark, J. E. Some Interesting Things About Polysiloxanes. *Acc. Chem. Res.* **2004**, *37*, 946-953.
- Maschke, U.; Wagner, T. Synthesis of high-molecular-weight poly(dimethylsiloxane) of uniform size by anionic polymerization, 1. Initiation by a monofunctional lithium siloxanolate. *Makromol. Chem.* **1992**, *193*, 2453-2466.
- Mateos A. J.; Cain A. A.; Grunlan J. C. Large-Scale Continuous Immersion System for Layer-by-Layer Deposition of Flame Retardant and Conductive Nanocoatings on Fabric. *Ind. Eng. Chem. Res.* **2014**, *53*, 6409-6416.
- McGregor, R. R.; Warrick, E. L. Organo-Silicon Polymers and Methods of Making Them. U.S. Patent 2,375,998, May 15, 1945.
- Min, H.; Qiuyu Z.; Jiying G. Synthesis and characterization of silicone based pressure sensitive adhesive. *Adv. Mtls. Res.* **2011**, *306*, 1773-1778.
- Mironova, M. V.; Tatarinova, E. A.; Meshkov, I. B.; Muzafarov, A. M.; Kulichikhin, V. G. Rheological and Relaxation Properties of MQ Copolymers. *Polym. Sci., Ser. A* **2012**, *54*, 177-186.
- Mitsuishi, M.; Zhao, F.; Kim, Y.; Watanabe, A.; Miyashita, T. Preparation of Ultrathin Silsequioxane Nanofilms via Polymer Langmuir-Blodgett Films. *Chem. Mater.* **2008**, *20*, 4310-4316.
- Moissan, H. *Bull. Soc. Chim. Fr.* **1895**, *13*, 972.



- Moitra, N.; Ichii, S.; Kamei, T.; Kanamori, K.; Zhu, Y.; Takeda, K.; Nakanishi, K.; Shimada, T. Surface Functionalization of Silica by Si-H Activation of Hydrosilanes. *J. Am. Chem. Soc.* **2014**, *136*, 11570-11573.
- Moniruzzaman, Mohammad; Winey, Karen I. Polymer Nanocomposites Containing Carbon Nanotubes. *Macromolecules.* **2006**, *39*, 5194-5205.
- Müller, R. *Chem. Tech.* **1950**, *2*, 41.
- Ng, L. V.; Thompson, P.; Sanchez, J. Macosko, C. W.; McCormick, A. V. Formation of Cagelike Intermediates from Nonrandom Cyclization during Acid-Catalyzed Sol-Gel Polymerization of Tetraethyl Orthosilicate. *Macromolecules* **1995**, *28*, 6471-6476.
- Nikolov, A.; Wasan, D. Current opinion in superspreading mechanisms. *Adv. Colloid Interface Sci.* **2015**, *222*, 517–529.
- Niu, R.; Gong, J.; Xu, D.; Tang, T.; Sun, Z. Flow-induced structure and rheological properties of multiwall carbon nanotube/polydimethylsiloxane composites. *RSC Adv.* **2014**, *4*, 62759-62768.
- Noll W. *Chemistry and Technology of Silicones*. Academic Press: New York; London, **1968**.
- Noorden, R. V. The Trails of New Carbon. *Nature* **2011**, *469*, 14-16.
- Norton, F. J. Production of Water-Repellent Materials. US Pat. 2,412,470, Dec. 10, 1946.
- Norton, F. J. Waterproofing Treatment of Materials. US Pat. 2,386,259 Dec. 10 1946.
- Odian, G. *Principles of Polymerization*. Wiley-Interscience: Hoboken, **2004**.
- Osthoff, R. C.; Bueche, A. M.; Grubb, W. T. Chemical stress-relaxation of polydimethylsiloxane elastomers. *J. Am. Chem. Soc.* **1954**, *76*, 4659-4663.
- Owen, M. J. Why Silicones Behave Funny. *Chemtech.* **1981**, *11*, 288-292.
- Paczesy, J.; Binkiewicz, I.; Janczuk, M.; Wybrańska, K.; Richter, Ł.; Hołyst, R. Langmuir and Langmuir-Blodgett Films of Unsymmetrical and Fully Condensed Polyhedral Oligomeric Silsesquioxanes (POSS). *J. Phys. Chem. C* **2015**, *119*, 27007–27017.
- Papon, A.; Saalwächter, K.; Schäler, K.; Guy, L.; Lequeux, F.; Montes, H. Low field NMR Investigations of Nanocomposites: Polymer Dynamics and Network Effects. *Macromolecules* **2011**, *44*, 913-922.
- Parks, D. J.; Blackwell J. M.; Piers W. A. Studies on the Mechanism of B(C<sub>6</sub>F<sub>5</sub>)<sub>3</sub>-Catalyzed Hydrosilation of Carbonyl Functions. *J. Org. Chem.* **2000**, *65*, 3090-3098.
- Parks, D. J.; Piers, W. E. Tris(pentafluorophenyl)boron-Catalyzed Hydrosilation of Aromatic Aldehydes, Ketones, and Esters. *J. Am. Chem. Soc.* **1996**, *118*, 9440-9441.
- Patnode, W. I. Method of Rendering Materials Water Repellent. US Pat. 2,306,222 Dec. 22, 1942.
- Pauling, L. The Nature of the Chemical Bond. IV. The Energy of Single Bonds and the Relative Electronegativity of Atoms. *J. Am. Chem. Soc.* **1932**, *54*, 3570-3582.

- Petroff, L.; Snow, S. A. *Silicone Surfactants in Silicone Surface Science*. Springer: Dordrecht, **2012**.
- Piers, W. E.; Marwitz, A. J. V.; Mercier, L. G. Mechanistic Aspects of Bond Activation with Perfluoroarylborananes. *Inorg. Chem.* **2011**, *50*, 12252-12262.
- Plueddemann, E. P. *Silane Coupling Agents*, 2nd ed.; Plenum: New York, **1991**.
- Post, H. W. *Silicones and Other Organosiloxane Compounds*. Reinhold: New York, **1949**.
- Pötschke, P.; Abdel-Goad, M.; Alig, I.; Dudkin, S.; Lellinger, D. Rheological and dielectric characterization of melt mixed polycarbonate-multiwalled carbon nanotube composites. *Polymer* **2004**, *45*, 8863-8870.
- Pradhan, B.; Srivastava, S. K. Synergistic effect of three-dimensional multi-walled carbon nanotube-graphene nanofiller in enhancing the mechanical and thermal properties of high-performance silicone rubber. *Polym. Int.* **2014**, *63*, 1219-1228.
- Ramdani, K.; Bossy H.; Lomel, S.; Durand N. Process for Preparing a Silicone Resin. U.S. Patent 7,951,895, May 31, 2011.
- Razavi, S.; Cao, K. D.; Lin, B.; Lee, K. Y. C.; Tu, R. S.; Kretzschmar, I. Collapse of Particle-Laden Interfaces under Compression: Buckling vs Particle Expulsion. *Langmuir* **2015**, *31*, 7764-7775.
- Roberts C.; Cosgrove T.; Schmidt R.G.; Gordon G.V. Diffusion of Poly(dimethylsiloxane) Mixtures with Silicate Nanoparticles. *Macromolecules* **2001**, *34*, 538-543.
- Rochow, E. G. Methyl Silicones and Related Products. U.S. Patent 2,258,218, October 7, 1941.
- Rochow, E. G. Preparation of Organosilicon Halides. US Pat. 2,380,995, Aug. 7, 1945.
- Rochow, E. G. *Silicon and Silicones*. Springer-Verlag: Berlin; New York, **1987**.
- Rochow, E. G. The Direct Synthesis of Organosilicon Compounds. *J. Am. Chem. Soc.* **1945**, *67*, 963-965.
- Rochow, E. G.; Gilliam, W. F. Polymeric Methyl Silicon Oxides. *J. Am. Chem. Soc.* **1941**, *63*, 798-800.
- Rubinsztajn, S.; Cella, J. A. A New Polycondensation Process for the Preparation of Polysiloxane Copolymers. *Macromolecules* **2005**, *38*, 1061-1063.
- Saalwächter, K. Proton multiple-quantum NMR for the study of chain dynamics and structural constraints in polymeric soft materials. *Prog. Nucl. Magn. Reson. Spectrosc.* **2007**, *51*, 1-35.
- Sagar, S.; Iqbal, N.; Maqsood, A.; Shahid, M.; Shah, N. A.; Jamil, T.; Bassyouni, M. I. Fabrication and thermal characteristics of functionalized carbon nanotubes impregnated polydimethylsiloxane nanocomposites. *J. Compos. Mater.* **2015**, *49*, 995-1006.
- Sainte-Claire Deville, H. E. *Compt. Rend. Acad. Sci.* **1854**, *39*, 321.
- Schaefer, D. W.; Justice, R. S. How Nano Are Nanocomposites? *Macromolecules* **2007**, *40*, 8501-8517.

- Schmidt, R. G.; Gordon, G. V.; Dreiss, C. A.; Cosgrove, T.; Krukonis, V. J.; Williams, K.; Wetmore, P. M. A Critical Size Ratio for Viscosity Reduction in Poly(dimethylsiloxane)-Polysilicate Nanocomposites. *Macromolecules* **2010**, *43*, 10143–10151.
- Seyferth D. Dimethyldichlorosilane and the Direct Synthesis of Methylchlorosilanes. The Key to the silicones Industry. *Organometallics* **2001**, *20*, 4978-4992.
- Shea, T. M. Durable Hydrophobic Surface Coatings using Silicone Resins. US Pat. 7,344,783 B2, Mar. 18, 2008.
- Shi X.; Chen Z.; Yang Y. Toughening of Poly(L-lactide) with Methyl MQ Silicone Resin. *Eur. Polym. J.* **2014**, *50*, 243-248.
- Sonnier, R.; Bokobza, L.; Chocha-Lozano, N. Influence of multiwall carbon nanotube (MWCNT) dispersion on ignition of poly(dimethylsiloxane)-MWCNT composites. *Polym. Adv. Technol.* **2015**, *26*, 277-286.
- Spahr, M. E.; Rothon, R. Carbon black as a polymer filler. *Fillers for Polymer Applications* **2017**, 261-291.
- Spitalsky, Z.; Tasis, D.; Papagelis, K.; Galiotis, C. Carbon nanotube-polymer composites: Chemistry, processing, mechanical and electrical properties. *Prog. Polym. Sci.* **2010**, *35*, 357-401.
- Stein, J.; Lewis, L. N.; Gao, Y.; Scott, R. A. In Situ Determination of the Active Catalyst in Hydrosilylation Reactions Using Highly Reactive Pt(0) Catalyst Precursors. *J. Am. Chem. Soc.* **1999**, *121*, 3693-3703.
- Stöber, W.; Fink, A. Controlled growth of monodisperse silica spheres in the micron size range. *J. Colloid Interface Sci.* **1968**, *26*, 62-69.
- Stock, A.; Somieski, C. *Ber. Dtsch. Chem. Ges.* **1919**, *52*, 695.
- Stoebe, T.; Lin, Z.; Hill, R. M.; Ward, M. D.; Ted David H. Surfactant-Enhanced Spreading. *Langmuir* **1996**, *12*, 337-344.
- Sun, F.; Hu, Y.; Du, H. Synthesis and Characterization of MQ Silicone Resins. *J. Appl. Polym. Sci.* **2012**, *125*, 3532-3536.
- Sweetman M. J.; McInnes, S. J. P.; Vasani, R. B.; Guinan, T.; Blencowe, A.; Voelcker, N. H. Rapid, metal-free hydrosilanisation chemistry for porous silicon surface modification. *Chem. Commun.* **2015**, *51*, 10640-10643.
- Tasis, D.; Tagmatarchis, N.; Bianco, A.; Prato, M. Chemistry of Carbon Nanotubes. *Chem. Rev.* **2006**, *106*, 1105-1136.
- Tennent, H. G. Carbon Fibrils, Method For Producing Same and Compositions Containing Same. US Pat. 4,663,230, May 5, 1987.
- Theodorakis, P. E.; Müller, E. A.; Craster, R. V.; Mater, O. K. Insights into surfactant-assisted superspreading. *Curr. Opin. Colloid Interface Sci.* **2014**, *19*, 283-289.
- Kuroda, K.; Kato, C. Synthesis of Polyorganosiloxane retaining SiO<sub>4</sub> Framework from Inosilicate Mineral by Trimethylsilylation. *Polymer* **1978**, *19*, 1300-1302.
- Tour, J. M.; Dyke, C. A. Covalent Functionalization of Single-Walled Carbon Nanotubes for Materials Applications. *J. Phys. Chem. A.* **2004**, *108*, 11151-11159.

- Tuteja, A.; Mabry, J. M. The Design of Non-wetting Surfaces with FluoroPOSS. In *Silicone Surface Science*; Springer: New York; **2012**; pp 179–193.
- Ulman, A. Formation and Structure of Self-Assembled Monolayers. *Chem. Rev.* **1996**, *96*, 1533-1554.
- Vasil'ev S. G.; Volkov V. I.; Tatarinova E. A.; Muzafarov A. M. A Solid-State NMR Investigation of MQ Silicone Copolymers. *Appl. Magn. Reson.* **2013**, *44*, 1015-1025.
- Vasil'ev S. G.; Volkov V. I.; Tatarinova E. A.; Muzafarov A. M. Study of Self-Diffusion of Silicone MQ Resins in Chloroform Solutions by Pulsed Field-Gradient NMR Spectroscopy. *Appl. Magn. Reson.* **2014**, *45*, 315-328.
- Vilatela, J.; Marcilla, R. Tough Electrodes: Carbon Nanotube Fibers as the Ultimate Current Collectors/Active Material for Energy Management Devices. *Chem. Mater.* **2015**, *27*, 6901-6917.
- Voronina, N. V.; Meshkov, I. B.; Myakushev, V. D.; Laptinskaya, T. V.; Papkov, V. S.; Buzin, M. I.; Il'ina, M. N.; Ozerin, A. N.; Muzafarov, A. M. Hybrid organo-inorganic globular nanospecies: Transitions from Macromolecule to Particle. *J. Polym. Sci., Part A: Polym. Chem.* **2010**, *48*, 4310–4322.
- Vyazovkin, Sergey et.al. ICTAC Kinetic Committee recommendations for performing kinetic computations on thermal analysis data. *Thermochimica Acta.* **2011**, *520*, 1-19.
- Wagner, H. L. The Mark–Houwink–Sakurada relation for poly(methyl methacrylate). *J. Phys. Chem. Ref. Data.* **1987**, *16*, 165-173.
- Wang, L.; McCarthy, T. J. Covalently Attached Liquids: Instant Omniphobic Surfaces with Unprecedented Repellency. *Angew. Chemie Int. Ed.* **2016**, *55*, 244–248.
- Wasserman, S. R.; Tao, Y.-T.; Whitesides, G. M. Structure and Reactivity of Alkylsiloxane Monolayers Formed by Reaction of Alkyltrichlorosilanes on Silicon Substrates. *Langmuir* **1989**, *5*, 1074-1087.
- Wengrovius, J. H.; Burnell T. B.; Zumburum M. A. Method for Making Substantially Silanol-Free Silicone Resin Powder, Product and Use. U.S. Patent 5,319,040, Jun. 7, 1994.
- Wengrovius, J. H.; Burnell T. B.; Zumburum M. A. 10th *International Symposium on Organosilicon Chemistry*, Poznan, Poland, August 1993.
- Wengrovius, J. H.; Green R. W.; Capuano, C. F. Continuous process for producing a silicon resin. European Patent 1,113,036, Dec. 21, 2005.
- Winey, K. I.; Vaia, R. A. Polymer Nanocomposites. *MRS Bulletin* **2007**, *32*, 314-319.
- Winey, Karen I.; Kashiwagi, T; Mu, Minfang. Improving Electrical Conductivity and Thermal Properties of Polymers by the Addition of Carbon Nanotubes as Fillers. *MRS Bulletin.* **2007**, *32*, 348-353.

- Xiang H.; Ge J.; Cheng S.; Han H.; Cui S. Synthesis and characterization of titania/MQ silicone resin hybrid nanocomposite via sol-gel process. *J. Sol-Gel Sci. Technol.* **2011**, *59*, 635-639.
- Xu, X.; Wu, C.; Zhang, B.; Dong, H. Preparation, structure characterization, and thermal performance of phenyl-modified MQ silicone resins. *J. Appl. Polym. Sci.* **2013**, *128*, 4189–4200.
- Yao, S.; Zhu, Y. Nanomaterial-Enabled Stretchable Conductors: Strategies, Materials and Devices. *Adv. Mater.* **2015**, *27*, 1480-1511.
- Yin, W.; Deng, J.; Esker, A. R. Surface Rheology of Trisilanolisobutyl-POSS at the Air/Water Interface. *Langmuir*, **2009**, *25*, 7181-7184.
- Yin, Y.; Chen X.; Lu J.; Liu Z.; Chen X. Influence of molar ratio of Si-H to Si-CH=CH<sub>2</sub> on mechanical and optical properties of silicone rubber. *J. Elastomers Plast.* **2016**, *48*, 206-216.
- Yoshii, K.; Yamashita, T.; Machida, S.; Horie, K.; Itoh, M.; Nishida, F.; Morino, S. Photo-probe study of siloxane polymers. I. Local free volume of an MQ-type silicone resin containing crosslinked nanoparticles probed by photoisomerization of azobenzene. *J. Non-Crystal. Solids* **1999**, *246*, 90-103.
- Zhan, H.; Lu, X.; Cao J. New Application and Technology of Silicone Pressure Sensitive Adhesives. *J. Polym. Eng.* **1997**, *17*, 339-344.
- Zhan, X.; Zhang J.; Cheng J.; Shi L.; Lin X. Synthesis, characterization, and cure kinetics analysis of high refractive index copolysiloxanes. *J. Therm. Anal. Calorim.* **2014**, *117*, 875-883.
- Zhang, J.; Chen, Y.; Brook, M. A. Reductive Degradation of Lignin and Model Compounds by Hydrosilanes. *ACS Sustainable Chem. Eng.* **2014**, *2*, 1983-1991.
- Zhang, J.; Chen, Y.; Sewell, P.; Brook, M. A. Utilization of softwood lignin as both crosslinker and reinforcing agent in silicone elastomers. *Green Chem.* **2015**, *17*, 1811-1819.
- Zhang, Q.; Huang, J. Q.; Qian, W. Z.; Zhang, Y. Y.; Wei, F. The road for nanomaterials industry: a review of carbon nanotube production, post-treatment, and bulk applications for composites and energy storage. *Small* **2013**, *9*, 1237-1265.
- Zhang, Y.; Wang, S.; Zhou, J.; Zhao, R.; Benz, G., Tcheimou, S.; Meredith, J. C.; Behrens, S. H. Interfacial Activity of Nonamphiphilic Particles in Fluid-Fluid Interfaces. *Langmuir* **2017**, *33*, 4511-4519.
- Zheng, P.; McCarthy T. J. A Surprise from 1954: Siloxane Equilibration is a Simple, Robust, and Obvious Polymer Self-Healing Mechanism. *J. Am. Chem. Soc.* **2012**, *134*, 2024-2027.
- Zheng, P.; McCarthy, T. J. Rediscovering Silicones: Molecularly Smooth, Low Surface Energy, Unfilled, UV/Vis-Transparent, Extremely Cross-Linked, Thermally Stable, Hard, Elastic PDMS. *Langmuir* **2010**, *26*, 18585-18590.